Development of Electrostatic and Piezoelectric Sensor Arrays for Determining the Velocity and Concentration Profiles and Size Distribution of Pneumatically Conveyed Bulk Solids

---

A Thesis Submitted to the
University of Kent
For the Degree of PhD in
Electronic Engineering

By
James Robert Coombes
August 2016

“I see now that the circumstances of one's birth are irrelevant; it is what you do with the gift of life that determines who you are.”

- Mewtwo, Pokemon the First Movie

Abstract

One way countries around the world are increasing the proportion of renewable fuels for electricity generation is to convert coal fired power stations to co-fired (biomass/coal fired) or converting coal fired power stations to burn only biomass fuels. This however has led to measurement challenges monitoring the complex multi-phase flow of the pulverised fuels entering the furnace due to the complex shape of biomass particles.

To meet these measurement challenges a novel electrostatic sensor array and piezoelectric sensor array have been developed. The electrostatic sensor array consists of an array of electrostatic electrodes pairs that span the diameter of the pipe. Consequently the electrostatic sensor array is capable of determining the particle velocity and concentration profiles as well as detecting specific flow regimes such as roping. The piezoelectric impact sensor array consists of an array of piezoelectric individual impact sensors that span the diameter of the pipe. The piezoelectric sensor array is capable of determining the particle concentration and size distribution profiles.

Experimentation has been carried out on laboratory scale pneumatic conveying systems using a variety of materials such as coal, biomass, coal/biomass blends and plastic shot. Experiments using the electrostatic sensor array have shown that it is indeed capable of determining the particle velocity and concentration profiles in both dilute developed and undeveloped flows. Analysis of the standard deviation of the velocity profiles as well as the correlation coefficient profiles have indicated that parts of the pipe cross section have a more stable flow compared to others. Data obtained through on-line and off-line experimentation using the piezoelectric sensor array has shown that through selective frequency filtering of the impact signal particle size can be determined assuming the particle velocity and the mechanical properties of the conveyed pulverised materials are known. By using a threshold voltage to determine when an impact has occurred on each element of the piezoelectric sensor array the particle concentration profile has been determined. The concentration profiles measured by the piezoelectric sensor array were verified using the electrostatic sensor array.

Acknowledgements

The author wishes to express his gratefulness and thanks to all the people who have, in numerous ways, contributed to this research.

Prof. Yong Yan my main supervisor who though his advice and mentoring has allowed me to conduct this research encouraging me to push the boundaries of what is possible.

Dr. Gang Lu my second supervisor who has always been there to offer support and advice in a wide range of engineering fields.

Clive Birch for his help in machining the impact waveguides on the piezoelectric sensor array as well as offering advice.

Tony Brazier for manufacturing the aluminium sensor blade housing for the electrostatic sensor array as well as his assistance in the construction of the positive pressure test rig and sensor mounting pipe spool.

Simon Jakes for all his assistance and advice in PCB manufacturing as well as the etching process for the custom piezoelectric film transducers.

David O'Connell for his advice in machining processes/practices as well as machining the sensor blade housing for the piezoelectric sensor array.

Robert Horne for always dispensing useful advice for microcontroller implementation as well as someone who was a laugh to have around in the lab.

Dr. Emily Coombes my sister for giving her time to proof-read my thesis as well as being totally awesome.

Carol Coombes my mother for always being there for me as well as the person who all those years ago pushed me to start a career in engineering.

University of Kent for providing research facilities as well as professional and supportive staff.

The author would also like to thank the University of Kent and EPSRC for awarding him the scholarship that has allowed this research to be completed.

Contents

Nomenclature

A	Area (m^2)
A_0	Gain
C	Value of capacitance of a capacitor (F)
D	Charge density developed in charge mode ($C\ m^{-1}$)
d_{3n}	Axis of the applied stress or strain in charge mode (m/m/V/m)
E	Young's modulus (N/m^2)
E*	Effective elastic modulus (N/m^2)
f_c	Cut-off frequency (Hz)
f_f	Frictional force (F)
f_H	Upper cut-off frequency (Hz)
f_L	Lower cut-off frequency (Hz)
F_{max}	Maximum impact force (N)
F_n	Applied stress in the specified direction in charge mode (N)
g_{3n}	Axis of the applied stress or strain in voltage mode ($V/m/N/m^2$)
I_{in}	Current input signal (A)
L	Spacing between the upstream and downstream electrostatic electrodes (m)
m	Mass (Kg)

m^*	Effective mass (Kg)
n	Sample number
N	Total number of samples for calculating the correlation coefficient
Q	Charge developed in charge mode (C)
R	Value of resistance for a resistor (Ω)
R	Radius (m)
R*	Median radius (m)
r.m.s	Root mean square of an electrostatic signal (V)
R_{xy}	Normalised correlation function
t	Time (S)
t_f	Thickness of the PVDF film (m)
t_m	Time difference between the upstream and downstream signals (S)
V_c	Particle velocity (m/s)
V_{DD}	Supply voltage (V)
V_{in}	Voltage input signal (V)
V_{out}	Voltage output signal (V)
V_{ref}	Reference voltage (V)
X[n]	Digitised signal from the upstream electrostatic sensor
X_n	Applied stress in the specified direction in voltage mode
Y[n]	Digitised signal from the downstream electrostatic sensor
ν	Poisson's ratio

List of Tables

List of Figures

Chapter 1

Introduction

1.1 Introduction

One of the most common and efficient ways granular and pulverised materials are transported is through the use of bulk solid pneumatic conveying systems. This chapter is an introduction to all aspects of bulk solid pneumatic conveying systems including: the principle of bulk solid pneumatic conveying systems; design challenges; flow characteristics; and specific particle flow regimes (such as dilute multi-phase flow). This chapter will likewise introduce the justification for this research; illustrating its importance in the power generation industry where the increasing use of pulverised biomass fuels is boosting the amount of renewable electricity being generated. The increasing use of biomass fuels in power generation is being used by governments around the world to fulfil their commitment to reduce greenhouse gas emissions. This use of biomass, however, has had the effect of increasing the complexity of the particle flow in pneumatic conveying systems which is presenting measurement challenges.

1.2 Pneumatic Bulk Solid Conveying Systems

One of the most common ways granular and pulverised materials are transported is through the use of bulk solid pneumatic conveying systems. Bulk solid pneumatic conveying systems use high velocity gas to convey pulverised and granular materials down a pipework system. Depending on the properties of the granular/pulverised material, the conveying gas can be air or an inert gas (for conveying explosive materials) [1].The conveying gas in the pneumatic conveying systems can be either positive or negative pressure (positive pressure blows the particles down the pipe work system where negative sucks the particles down the pipework system).

The bulk solid pneumatic conveying system is commonly but not limited to four main components illustrated in Fig. 1.1:

- Fan/Blower – the fan/blower is the method utilised to generate the high velocity gas used to convey the pulverised/granular material (in a positive pressure system). The most common system to generate the high velocity gas is to use a centrifugal fan which has the advantage that the gas velocity can be easily controlled by varying the centrifugal fan speed. For some applications (where high back pressure is required in the pipework system) compressed gas from a compressor or high pressure storage tank can be used.
- Particle Feeding System – in order to meter in the pulverised/granular material into the pneumatic conveying system some kind of feeding system needs to be employed. The two most common methods are to use either a venturi educator (which has the advantage of having no moving parts) or a rotary feeding system (which is capable of being used on systems with back pressure).
- Pipe Network – the pipe network is what is used to contain and direct the particle flow in the pneumatic conveying system. The Pipe network in pneumatic conveying systems can be either horizontal or vertical pipes consisting of straight and angled pipe sections. The bore of the pipe network is

dependent on the application of the pneumatic conveying system and can range from tens of millimetres to thousands of millimetres.

- Particle Output – once the particles have travelled through the pipe network they will reach their destination. Depending on the application of the system, this could be a sealed storage tank (where the particles will have to be decelerated and separated from the conveying gas using a cyclone chamber) or directly to a combustion chamber such as the furnace in a coal fired power station.

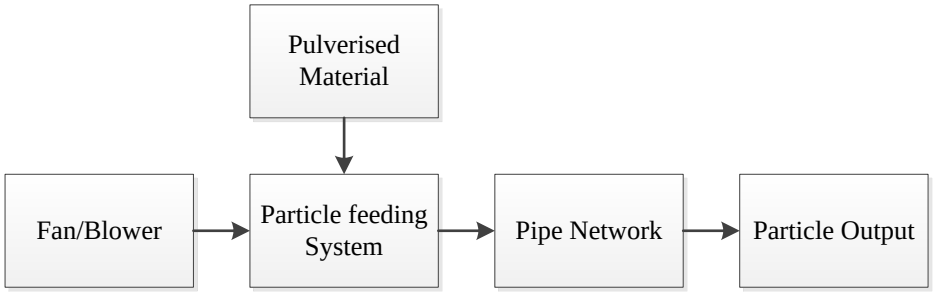

Fig. 1.1 Block diagram of a typical bulk solid pneumatic conveying system

1.2.1 Particle Flow Characteristics

Depending on the design of the bulk solid pneumatic conveying system different flow regimes occur inside the pipe line. These flow regimes create measurement challenges for measuring the mass flow rate of the pneumatically conveyed bulk solids.

1.2.2 Multiphase Flow

When a mono-pulverised/granular material (same material and particle size) is conveyed in a pneumatic conveying system the flow is regarded as a two-phase flow consisting of the conveying gas and the pulverised/granular material. When multiple pulverised/granular materials are conveyed at the same time in a pneumatic conveying system pipe line the flow is consequently regarded as multiphase flow [1].

1.2.3 Dilute-Phase Flow

Dilute-phase flow uses air velocity (either positive or negative pressure) to fully suspend the particles in the conveying gas. Using this method of conveyance almost any pulverised or granular material can be conveyed regardless of the particle size and shape

[1]. The particle concentration in dilute-phase flow is less than 0.1% by volume [2]. Due to the low particle concentration this creates measurement challenges. In order to suspend the particles in the conveying gas the gas velocity has to be in the region of 12 m/s for fine pulverised material and around 16 m/s for fine granular material [1]. If, however, the conveying gas velocity is not sufficient to fully suspend the particles saltation or choking occurs. This is where the particles will fall out of suspension and settle on the bottom of the pipe causing a build-up of pulverised material which will eventually lead to a blockage in the pipe line. Due to the high particle velocity some fragile materials cannot be transported in dilute phase systems since interaction between the high velocity particles and the pipe wall will result in damage to the conveyed material [1].

1.2.4 Dense Phase Flow

Dense phase flow differs from dilute phase flow in that, firstly the particle concentration in dense phase flow systems are much higher than in dilute phase flow systems. The reason for this is the method of conveying the pulverised materials differs since the pulverised material are not fully suspended in dense phase flow (dense phase flow is often referred to as non-suspended flow) [1]. In dense phase flow the particles are conveyed down the pipeline in the form of dunes along the bottom of the pipe; or as slugs/plugs that cover the whole bore of the pipe separated between each other by air gaps [1]. When dense phase flow particles are conveyed in dunes along the pipe bottom the system is only capable of conveying finely pulverised material (having a mean particle size of 40 – 70 μm) [1]. When plug/slug flow regime is employed in dense phase flow systems only materials that have a good permeability can be conveyed (mono-sized particles that allow the conveying gas to pass between the particles such as pellet type materials and seeds) [1]. The gas velocity in dense phase is much lower than in dilute phase (< 3 m/s) [1].

1.2.5 Developed Particle Flow

When the pulverised/granular material is inputted into a dilute phase pneumatic conveying system the particle velocity is zero. The high velocity air accelerates the particles to their maximum velocity (dictated by the particle size and the conveying air velocity). Once the conveyed particles are no longer accelerating the flow is developed. The distance along the pipe to create a developed flow is approximately 30 pipe diameters of straight pipe [3]. A developed particle flow, however, can become underdeveloped by obstructions in the pipe or different geometries of pipe section (such as right angle pipe bends). If this occurs then the particle flow will need to travel another 30 pipe diameters inside a straight pipe section to become developed again [3].

1.2.6 Particle Velocity

The particle velocity is primarily determined by the conveying gas velocity with the particle velocity typically being around 80% the velocity of the conveying gas velocity (however this ratio is dependent on the particle size, shape and density) [1]. Due to the interaction of the conveying gas and the pipe wall the conveying gas velocity will be different depending on how close it is to the pipe wall; the conveying gas velocity in the centre of the pipe moves faster than the conveying gas along the pipe wall, thus creating a velocity profile as shown in Fig. 1.2. Since the conveyed particles have a mass they are also affected by gravity. The effect of gravity can be seen in a developed flow in a horizontal pipe as shown in Fig. 1.2. This illustrates the particle velocity profile with the particles at the bottom of the pipe having a lower velocity compared to the particle velocity along the pipe wall in the top of the pipe. The reason for this is that the particles at the bottom of the pipe are interacting more with the pipe wall and are being slowed down due to friction. This increased interaction between the particles and pipe wall is caused by gravity pulling the particles towards the bottom of the pipe. Fig. 1.3 however demonstrates the expected velocity profile that is perpendicular to the profile shown in Fig. 1.2. The velocity profile in Fig. 1.3 is more symmetrical across the pipe

diameter compared to Fig. 1.2. The reason for this is that gravity is having a uniform effect on all the particles traveling inside the pipe.

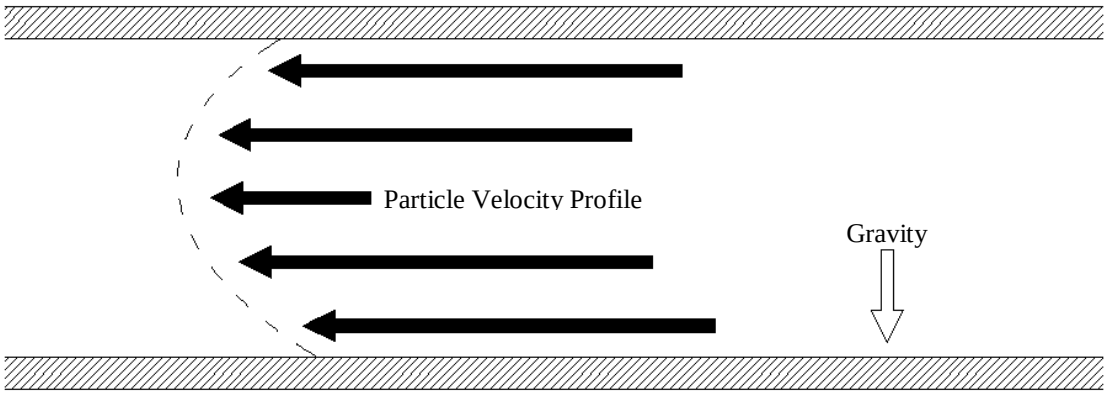

Fig. 1.2 Illustration of the expected particle velocity profile on a developed dilute phase flow on a horizontal pipe (side view)

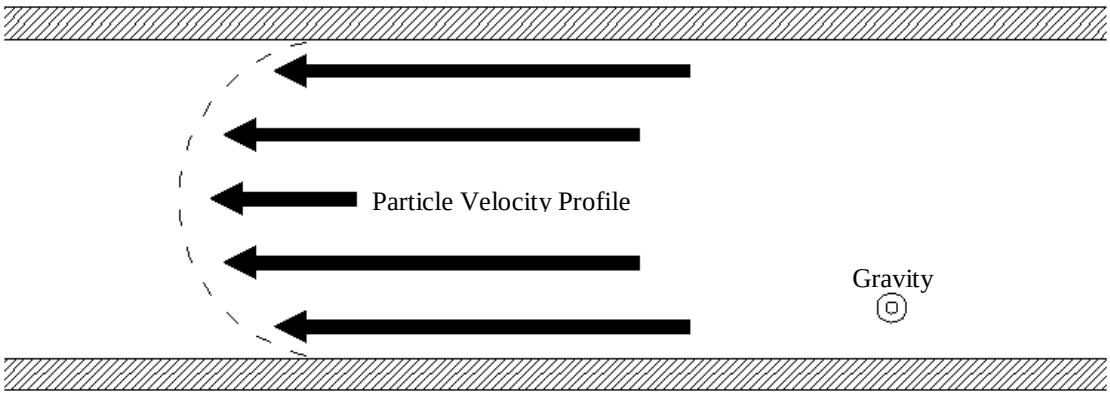

Fig. 1.3 Illustration of the expected particle velocity profile on a developed dilute phase flow on a horizontal pipe (top view)

1.2.7 Particle Concentration

In dilute-phase flow the particle concentration is low (less than 0.1% by volume). This concentration, however, is not constant across the whole pipe cross section. The particle concentration is dependent on several factors such as:

- Gravity – the effect of gravity can be best seen in the developed flow in a horizontal pipe. Since the particles have a mass gravity pulls the particles to the

bottom of the pipe. Fig. 1.4 demonstrates the expected particle concentration profile with the higher particle concentration at the bottom of the pipe.

- Particle Velocity – the velocity of the particles will also affect the particle concentration profile. This is because for lower particle velocities the particles will fall out of suspension and suffer from saltation. This will cause higher particle concentration in the direction of the pull of gravity [3].
- Pipework Design - the design of the pipe network similarly affects the particle concentration profile. Pipe sections such as right-angle bends will cause the particles to be forced along the outer radius of the bend due to centrifugal force causing a phenomenon known as roping which is illustrated in Fig. 1.5 [4].

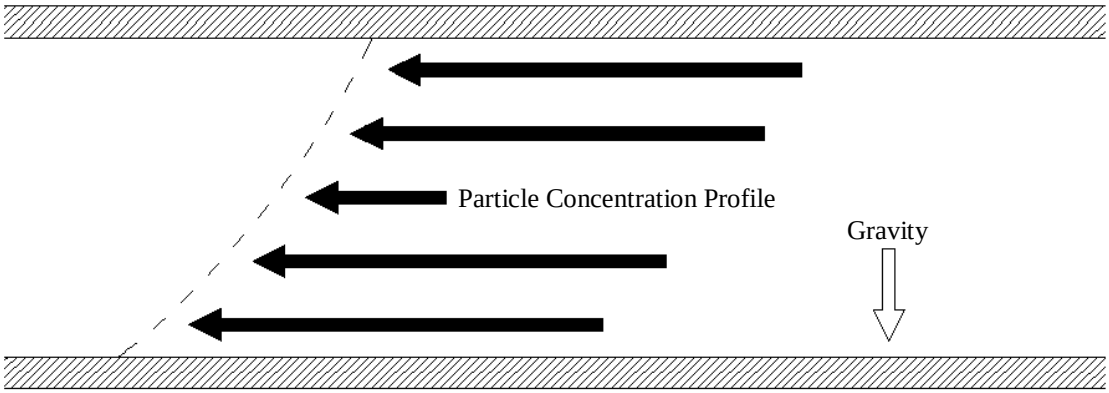

Fig. 1.4 Illustration of the expected particle concentration profile on a developed dilute phase flow on a horizontal pipe

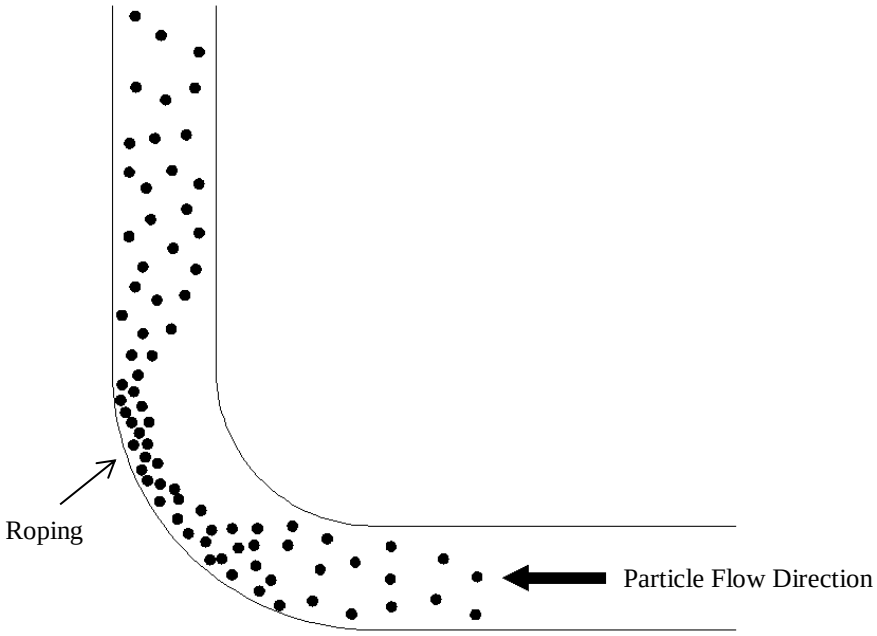

Fig. 1.5 Diagram illustrating the roping flow regime caused by a right angle pipe bend

1.2.8 Particle Size Distribution

Particle size distribution is the physical size of the individual particles that make up the conveyed pulverised material. In Dilute phase particle flow the particle size distribution has an effect on both the particle velocity and the particle concentration profile [1]. The size of the particle has an effect on the particle velocity (in relation to the conveying gas velocity) since larger particles have a larger surface area; consequently they have a higher drag factor [1]. Particle size also has an effect on the particle concentration profile. Since larger particles have a higher volume they would have a larger mass; accordingly they would be affected to a greater extent by forces such as gravity. An example of this would be on particle flow in a horizontal pipe with a low conveying gas velocity; since the conveying gas velocity would not be high enough to fully suspend the higher mass particles they would be forced to travel along the bottom of the pipe due to the force of gravity [1]. This effect is illustrated in Fig. 1.6 which shows the particles increasing in size along the bottom of the pipe in the direction of the gravitational force.

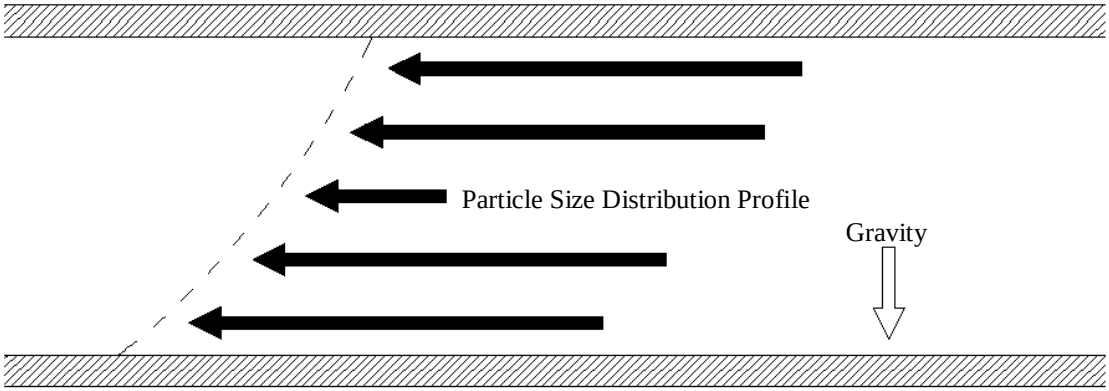

Fig. 1.6 Illustration of the expected particle size distribution profile on a developed dilute phase flow on a horizontal pipe

1.3 Implementation of Pneumatic Bulk Solid Conveying

Pneumatic bulk solid conveying systems are used in a variety of industries such as chemical, pharmaceutical, steel and energy. They allow the efficient transport of pulverised/granular material across a network of pipes. One industrial sector where the use of pneumatic conveying systems is fundamental to its operation is in the power generation industry in coal fired power stations.

1.3.1 Measurement of Pneumatic Conveyed Bulk Solids

The measurement of mass-flow rate and particle size distribution of the pneumatic conveyed bulk solids are important in many industries for quality control and ensuring the correct quantity of material is conveyed. Measurements of the mass flow rate of the pulverised/granular material can be taken as the material enters or leaves the pneumatic conveying system via load cells. The particle size distribution (which is important for quality control) can also be taken using off-line testing of the material before and after the pulverised/granular material has left the pneumatic conveying system.

In some industries, however, it is desirable to monitor the mass flow rate and the particle size distribution of the conveyed material as it is being conveyed inside the pneumatic conveying system (on-line monitoring). Particle size distribution can be

monitored independently but the mass flow rate requires the particle velocity and concentration to be known.

1.3.2 Coal Fired Power Stations

Burning coal as a fuel has been the primary source for electricity generation for over a hundred years. Since the early 1970s coal has been the major source of fuel for electricity generation worldwide as illustrated in Fig. 1.7. Even today in the twenty-first century electricity generated through burning coal as a fuel source makes up around 41% of the world's electricity generation capacity [5]. The reason for coal's continuing popularity is its cheapness; which is not only limited to the cost of the coal fuel itself but also with the price of construction of coal fired power stations. For this reason developing countries, such as China with their rapid industrialisation, have chosen coal to be the fuel that delivers their ever increasing need for more electricity generation capacity.

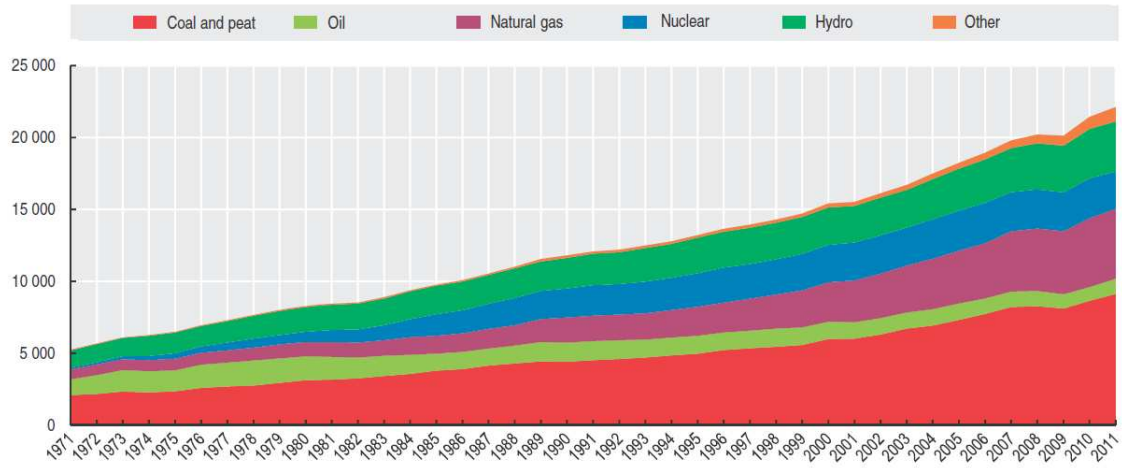

Fig. 1.7 World electricity generation by source of energy in terawatt hours (TWh)

Despite coal having the advantage that it is a low cost source of electricity generation, it does however have a major disadvantage; it is a fossil fuel. Being a fossil fuel, burning it introduces carbon dioxide which has been stored underground for millions of years back into the atmosphere. The burning of coal to generate electricity is responsible for 44% of the global carbon dioxide emissions [6]. The process of burning of coal also

emits large amounts of air pollution into the surrounding environment which has a detrimental effect on human health [7].

In coal fired power stations electricity is generated by using the heat generated from burning coal to produce high pressure steam to turn a turbine illustrated in Fig. 1.8.

- Coal Storage – the coal is delivered to the power plant by train or ship and is stored in its natural form (lumps of coal).
- Pulveriser – in order for the coal to be transported to the furnace and burnt efficiently the coal first needs to be pulverised. The coal is pulverised in a ball or tube mill which converts the lumps of coal into a fine powder.
- Input Metering – the pulverised coal is then metered into the pneumatic conveying system. This is carried out by either a rotary feeder or a screw feeder.
- Pneumatic Conveying System – warm air is then used to convey the pulverised coal to the furnace. The coal is fully suspended in the conveying air (dilute phase flow).
- Furnace – the pulverised coal is then blown into the furnace where the coal is burnt to generate heat. This heat is then used to heat water to generate high pressure steam which turns a turbine that drives a generator.
- Boiler – heat from the furnace heats water to generate steam at high pressure to generate super-heated steam.
- Turbine – the super-heated steam from the boiler is then used to turn the turbine. In order to improve efficiency there are three turbines: high pressure, intermediate pressure and low pressure. Each one of the turbines uses recycled steam from the previous turbine.
- Generator – rotational force from the turbine turns a generator which generates the electricity.

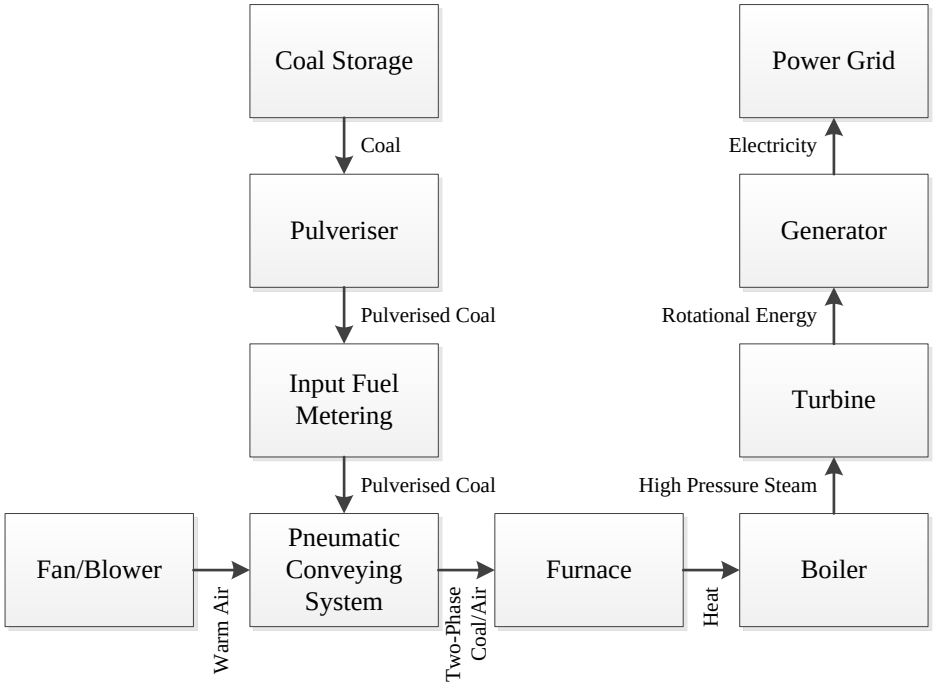

Fig. 1.8 Block diagram of a coal fired power station

1.3.3 Co-Fired/Biomass Fired Power Stations

One way countries around the world are increasing the proportion of renewable fuels used for electricity generation is to convert coal fired power stations to co-fired (biomass/coal fired) or converting coal fired power stations to burn only biomass fuels (such as the Drax Group converting its UK coal fired power stations to biomass fuelled, thus increasing the proportion of renewable electricity being generated in the UK [8]). As of 2015 9.1% of electricity in the UK was generated by burning biomass (this figure however includes energy crops, sewage, animal waste and recycled wood) [9].

The process of generating electricity from burning biomass is similar to burning coal. First the biomass is pulverised and is then conveyed along a pneumatic conveying system to a furnace as shown in Fig. 1.9.

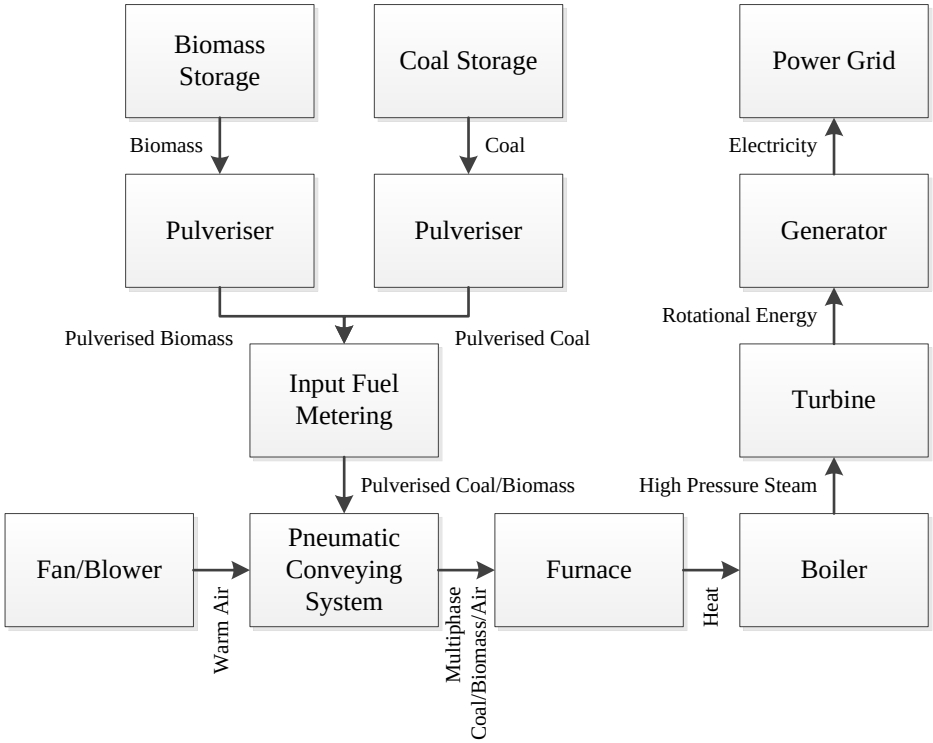

Fig. 1.9 Block diagram of a co-fired power station

1.3.4 Biomass Fuel

Biomass fuel is derived from organic materials that are also combustible. Biomass fuel is carbon neural meaning that the carbon dioxide that is created from burning the biomass fuel is reabsorbed by the plants/trees that will eventually become biomass fuel. Biomass fuel for electricity generation can be derived from:

- Recycled Wood – this is wood that has been reclaimed or is the by-product of wood manufacturing (sawdust and off cuts from timber manufacture) [8].
- Energy Crops – these are specific crops that are grown to be harvested and burnt as fuel such as willow [8].
- Food waste – these are products of food manufacturing which are of no use in the finished product but are combustible (peanut husks) [8].

When converting a coal fired power station to be co-firing or to be fully biomass fired there are challenges involved. Biomass fuels present technical challenges such as increase in slagging and fouling in the furnace. Slagging is where molten ash from the combustion process adheres and builds up on the parts of the boiler where radiative heat transfer occurs. Fouling occurs in the conductive heat transfers region of the boiler and is caused by the deposition of ash [10]. The primary effect of slagging and fouling is a reduced efficiency due to diminished heat transfer rates. The deposits themselves can likewise cause damage to the boiler by restricting gas flows inside the boiler which will have the effect of making the boiler unmanageable. Additionally, the deposits can cause corrosion to parts to the heat transfer system inside the boiler [10].

1.3.5 Online Measurement of Coal/Biomass Multi-Phase Flow

The ability to monitor the mass-flow rate and particle size of the pulverised coal/biomass fuel as it is being transported to the furnace in a pneumatic conveying system is very important. Being able to monitor the mass-flow rate would allow more advanced control systems to be developed which could allow the combustion process to be made more efficient. This would not only reduce the amount of greenhouse gas emissions released but would similarly reduce the amount of fuel being used which would reduce costs. Furthermore, having an online sensor to monitor the particle size of the pulverised coal/biomass would improve burning efficiency; this is because the combustion process requires the particle size to be a specified size since particles larger than the specified size would not burn as efficiently [11]. The ability to monitor the particle size online would be beneficial from a maintenance stand point; since if the particle size went out of the desired size range this would be an indication that the pulveriser would need servicing.

1.3.6 Measurement Challenges of Coal/Biomass Multi-Phase Flow

The online measurement of the mass-flow rate and particle size distribution of multiphase coal/biomass/gas in dilute phase particle flow presents certain challenges:

- Low Particle Concentration – since the particle flow is dilute phase flow the particle concentration is less than 0.1% by volume. This would require any online measurement system to be sensitive enough to detect low particle concentration.
- Non-uniform Particle Size – pulverised coal has a more uniform size distribution when pulverised compared to biomass. The reason for this is that, unlike coal which is a mineral mostly consisting of carbon; biomass is made up of fibres which do not lend themselves to being pulverised [12].
- Irregular Particle Shape – coal particles are generally more uniform in shape. In contrast biomass particles, due to their fibrous structure, are more elongated. This presents challenges in measuring them since particle spin is more apparent on biomass particles compared to coal particles [12].

1.4 Objectives of Research

The primary goal of this research is to develop a novel sensor design that is capable of measuring complex dilute multi-phase flow. To this end, the developed sensor technology will be capable of determining the particle velocity profiles, concentration profiles and the particle size distribution profiles of pneumatically conveyed bulk solids. This sensor technology will be an on-line measurement system capable of measuring the complex particle flow in real time. In order to increase the commercial value of this research all efforts will be done to ensure the developed sensor is robust, inexpensive and designed so that the sensor can be retrofitted to existing systems with minimal modification to the existing equipment. To achieve these goals the primary objectives of this research are:

Review of state-of-the-art of sensor technologies – a literature review will be carried out on the current state of research in the area of developing sensors to measure dilute phase pneumatically conveyed bulk solids. This literary review will focus on sensor paradigms that that are capable of measuring particle velocity, concentration and size distribution of pneumatically conveyed bulk solids. This will be of benefit to the coal/biomass fired power generation industry since this will allow more advanced control systems to be developed to improve the combustion process.

Design and construction of an electrostatic sensor array – current generations of electrostatic sensors have been applied to determine particle velocity, concentration and size distribution using either ring, arc and probe electrodes. These configurations of electrostatic sensor electrodes are only capable of measuring the particle flow parameters such as particle velocity and concentration in a small area inside the pipe. In order to measure the complex multi-phase particle flow in the full areas of the pipe cross section that previous electrostatic sensors have been unable achieve, a novel electrostatic sensor array will be designed, constructed and tested. This electrostatic sensor array will be an invasive sensor design (comes into contact with the particle flow) and will consist of an array of individual electrostatic sensors that span the diameter of the pipe. Using this electrostatic sensor array the particle velocity and concentration profiles will be able to be measured in real time. This will allow the complex dilute multi-phase flow associated with pneumatically conveyed coal/biomass blends to be measured. The electrostatic sensor array will be designed in such a way that will allow existing bulk solid pneumatic conveying systems to be retrofitted with the electrostatic sensor array with minimal modification.

Design and construction of a piezoelectric sensor array – like electrostatic sensors the current series of sensors that detect particle concentration and size distribution

through the measurement of particle impacts are only capable of monitoring a small area of the pipe cross section. To achieve a more complete picture of the complex multi-phase particle flow in the pipe cross section a novel piezoelectric sensor array will be designed, constructed and tested. The piezoelectric sensor array will consist of an array of individual piezoelectric impact sensors that span the diameter of the pipe. The piezoelectric sensor array will be capable of determining particle concentration and particle size distribution profiles across the diameter of the pipe. The piezoelectric sensor array will be an on-line sensor technology. To this end the particle concentration will be determined by counting the number of particle impacts that occur on each of the piezoelectric elements in the array. A system model will be developed to determine the particle size though analysis of the magnitude of the impact signals. The piezoelectric sensor array will be designed in such a way that will allow existing bulk solid pneumatic conveying systems to be retrofitted with the piezoelectric sensor array with minimal modification.

Design and commissioning of on-line and off-line test rigs – research facilities at the University of Kent have a fully functional negative pressure bulk solid pneumatic conveying system suitable for on-line experimentation. The negative pressure test rig is capable of conveying a variety of pulverised/granular materials such as flour, biomass and glass/plastic shot at a range of different particle velocities for both horizontal and vertical pipe orientations. To increase the choice of materials and flow conditions a positive pressure bulk solid pneumatic conveying system will be commissioned. The positive pressure test rig will use positive pressure high speed air to convey pulverised/granular material along both horizontal and vertical pipe sections which will allow on-line experimentation. Due to its design the positive pressure test rig will allow coal and coal/biomass blends to be conveyed at a range of air velocities. Both the negative and positive pressure test rigs will accommodate both the electrostatic and piezoelectric sensor arrays.

To test the performance of the piezoelectric sensor array under controlled conditions, an off-line test rig will be constructed. This test rig will guide ball bearings of different sizes and materials onto individual elements of the piezoelectric sensor array. The off-line test rig will independently measure the particle impact velocity of each particle before it impacts the piezoelectric sensor. The purpose of the off-line test rig is to validate the developed system model for the piezoelectric sensor array.

Experimentation of particle flow characteristics – to test the full capabilities of both the electrostatic and piezoelectric sensor arrays a wide range of experimentation will be carried out. Experimental investigation will be carried out to determine:

- If the electrostatic sensor array can determine the particle velocity and concentration profiles of dilute multi-phase particle flow using a variety of different pulverised/granular materials.
- If the electrostatic sensor array is capable of determining particle flow characteristics such as areas of the pipe that have higher turbulence compared to others.
- If the electrostatic sensor array can detect if different materials or different particle sizes have specific flow characteristics. This area of experimentation will focus on coal/biomass blends.
- If the piezoelectric sensor array is capable of determining particle concentration and size distribution profiles.

1.5 Thesis Outline

Chapter 1: Introduction

This chapter will introduce the challenges in measuring gas/solid multi-phase flow and give an overview of industrial application and why this research is being carried out. Moreover, information will be provided about principles of gas/solid multi-phase flow

as well as information about different flow regimes encountered in gas/solid multi-phase flow.

Chapter 2: Review of Particle Flow Sensor Technologies

This chapter will present an overview of previous research carried out to monitor particle velocity, size and particle concentration in a gas/solid multi-phase flow. The review will present all the sensor technologies including: electrostatic, capacitive, optical, radiometric, impact and ultrasonic, and will illustrate their advantages and disadvantages.

Chapter 3: Concept and Design of the Electrostatic Sensor Array

This chapter will cover an introduction to the electrostatic sensor array concept and present its novelty and advantages. The evolution of the sensor design will be demonstrated showing the reasons for design features to overcome technical difficulties and improve performance. Detailed technical specification will be shown in the form of circuit schematics and mechanical designs.

Chapter 4: Concept and Design of the Piezoelectric Sensor Array

This chapter will cover an introduction to the piezoelectric sensor array and reveal its novelty and advantages. The principle of the sensor concept will be illustrated and reasons for design features, such as the use of the piezoelectric film, will be presented. Detailed information will be provided in the form of technical drawings and circuit schematics as well as specialist information on manufacturing techniques used to fabricate the piezoelectric film transducers.

Chapter 5: Description of Particle Flow Test Rigs and Experimental Procedures

This chapter will introduce the in house laboratory scale on-line test rigs (positive and negative pressure) used to perform experimentation. The off-line test rig used to test the

performance of the piezoelectric sensor array will also feature. Technical details will be provided, such as changeable variables for each rig as well as safety features on the test rigs. Furthermore, advantages and disadvantages will be presented detailing specifications such as the types of material each rig can test.

Chapter 6: Results and Discussion

This chapter will show the results from practical experimentation carried out using the electrostatic sensor array using a variety of different pulverised materials and flow conditions. Results from the piezoelectric sensor array will be presented and compared to theoretical results obtained using the system model developed for the piezoelectric sensor array.

Chapter 7: Conclusion and Recommendations for Future Work

This chapter will present the conclusions made for the electrostatic sensor array and the piezoelectric sensor array experiments. Recommendations for future work will also be discussed in this chapter.

Chapter 2

Review of Particle Flow Sensor Technologies

2.1 Introduction

This chapter will introduce the various sensing technologies that have been researched and implemented to determine characteristics such as particle velocity, concentration and size distribution of pneumatically conveyed bulk solids. This chapter will cover capacitive sensors, digital imaging sensing methods, electrostatic sensors, impact sensors, optical method and ultrasonic sensors. The chapter will illustrate the advantages and disadvantages of each of the sensor paradigms as well as a detailed overview of the principles of each sensing technique.

The chapter will also summarise and identify the deficiency of previous sensor technologies in measuring complex multi-phase particle flow for the whole diameter of the pipe (such as the particle velocity profile inside a pipe). A proposition will be made that the ideal solution for a robust on-line sensor to measure particle velocity, concentration and size distribution for the pipe cross section can be achieved through

the use of a combination of sensing technologies. Particle velocity and concentration will be determined by an electrostatic sensor array constructed across the pipe cross section. Particle concentration and size distribution will be determined via an impact sensor array that also spans the diameter of the pipe

2.2 Capacitive Sensors

Capacitive sensors, in respect to measuring parameters of flow in a pneumatic bulk solid conveyor system, use the principle of the permittivity of the dielectric changes when particles pass between the sensor plates (an active sensor plate and ground plate); this is shown in Fig. 2.1. A signal conditioning circuit, such as an AC deflection bridge, would be used to convert the capacitance into a usable output signal that can be digitised by an analogue to digital converter [13].

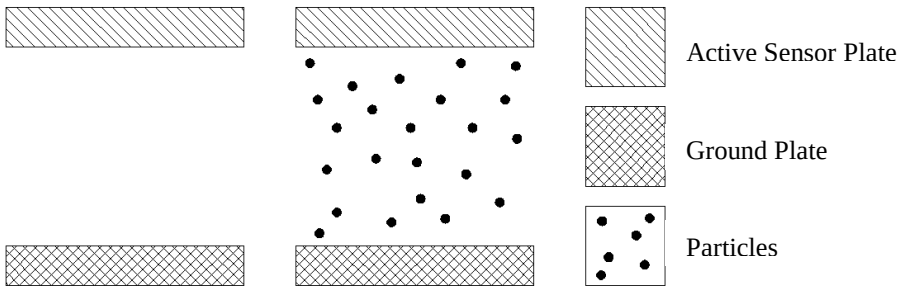

Fig. 2.1 Diagram of capacitive sensor plate configuration, without particles (left) and with particles (right)

Capacitive sensors have been used to measure the particle concentration as well as particle velocity allowing them to determine mass flow rate of pneumatically conveyed bulk solids.

2.2.1 Particle Concentration using Capacitive Sensors

Capacitive sensors have been applied to determine the particle concentration of pneumatically conveyed bulk solids [14] – [17]. The capacitive sensing plates are constructed inside the wall of the pipe as shown in Fig. 2.2. This design of sensor plates

has the advantage that the sensor is non-intrusive since it does not come into contact with the particle flow. However this sensor design is often constructed inside a pipe spool which can cause problems in retrofitting onto existing pneumatic conveying systems due to increased installation costs (especially if the spool is installed at a high level).

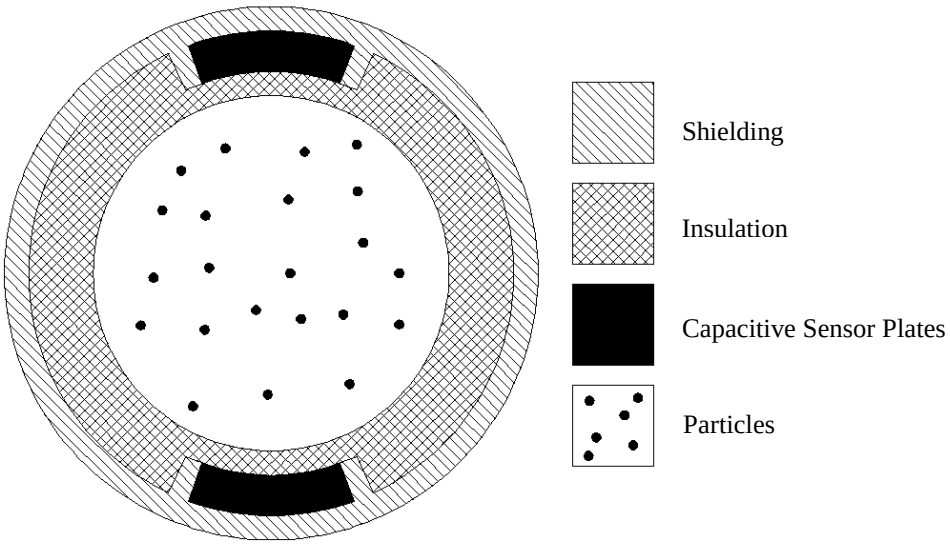

Fig. 2.2 Cross section diagram of capacitive sensors inside a pipe with particles

Likewise, capacitive sensors have a disadvantage since they use the relative permittivity of the dielectric between the sensor plates to detect the capacitance; this makes them susceptible to the moisture content of the pulverised material [16].

2.2.1.1 Electrical Capacitance Tomography

Electrical Capacitive Tomography (ECT) uses an array of capacitive sensor plates around the inner wall of the pipe. By measuring the changes in the capacitance level between difference sensor plates as shown in Fig. 2.3 the particle concentration for the whole pipe cross section can be measured [18] – [25].

The advantage of this sensing method is that it is capable of being able to detect specific flow regimes inside the pipe. However since an array of sensor plates are being used this requires a large amount of digital signal processing (DSP). Cui et al. [21]

implemented an ECT sensor using an FPGA for the DSP which negated this problem. With the improved computational speed provided by the implementation of a FPGA the sensor allowed specific flow regimes such as slug flow to be detected.

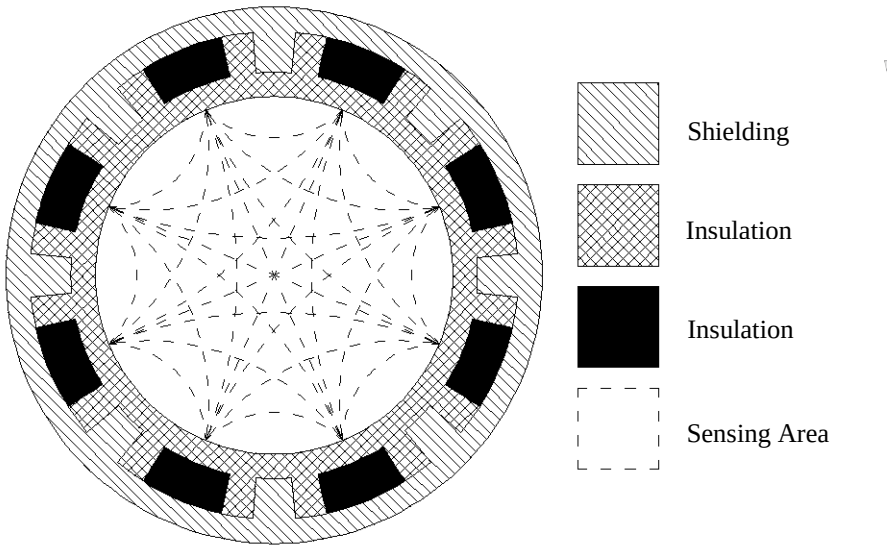

Fig. 2.3 Cross section diagram of ECT sensor configuration inside a pipe with illustrated sensor area

2.2.2 Velocity Measurement using Capacitive Sensors

2.2.2.1 Particle Velocity using Cross Correlation

In order to measure mass flow rate the particle velocity needs to be determined; to this end capacitive sensors have been adapted to measure particle velocity. Various methods have been implemented such as using the cross correlation method [26]. This method uses capacitive sensing plates in an upstream/downstream configuration as shown in Fig. 2.4.

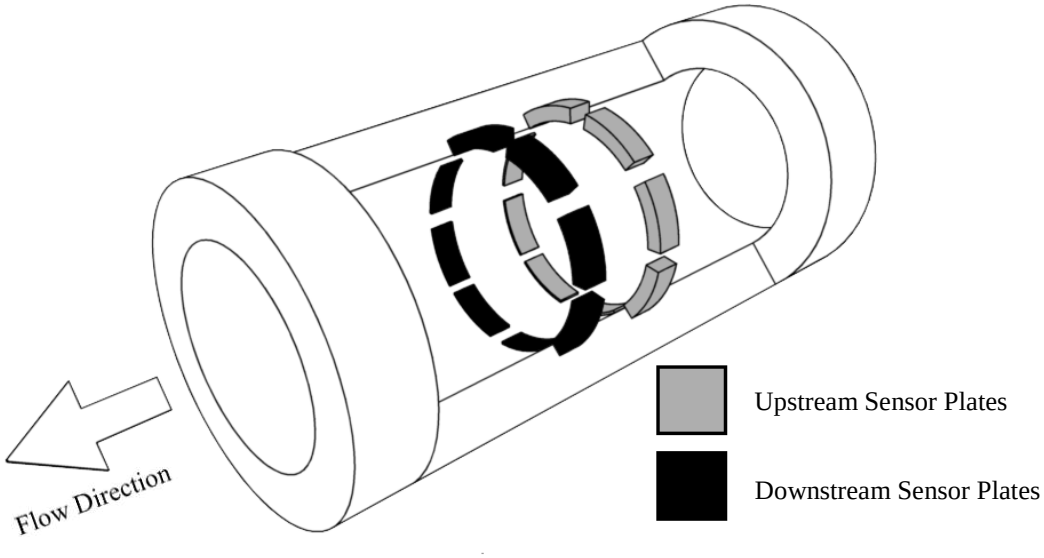

Fig. 2.4 Cutaway view of upstream downstream capacitive sensor plate configuration used to determine particle velocity [26]

As the particles travel between the capacitive sensor plates the upstream/downstream signal output changes. Since the particle flow is traveling in one direction the signal from the upstream sensor plate will be the same as the signal from the downstream sensor plate except there will be delay between the two signals. The distance between the sensor plates is known and the delay can be determined using the cross correlation method thus allowing the particle velocity to be determined.

2.2.2.2 Particle Velocity using Frequency Analysis

Particle velocity has also been determined using capacitive sensors implementing frequency analysis of the sensor output [27]. This system uses the principle that the faster the particles are traveling the less time they are in between the sensing plates; the less time the particles are between the sensor plates the higher the frequency component of the signal spectrum. This method has the advantage that it only requires a single ring of capacitive sensor plates as shown in Fig. 2.5.

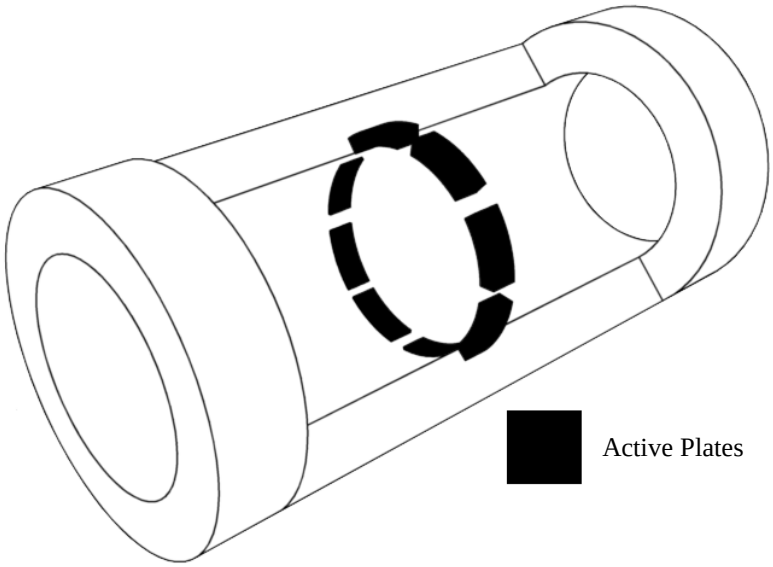

Fig. 2.5 Cutaway view of single layer of capacitive sensor plates used to determine particle velocity through frequency analysis [27]

2.3 Digital Imaging Sensors

Digital imaging sensors are capable of determining particle size distribution [28] – [39], velocity [37] – [41] and concentration [38] – [39]. Digital imaging uses a camera to capture an image of the particles whether the sensor is on-line (as particles are traveling inside the pipe) or off-line (where samples of particles are taken out of the system to be analysed). For on-line measurement of particle parameters the digital imaging sensor consists of two parts: a camera and a method of illuminating the particles (due to the dark environment inside the pipe). The illuminator often chosen is a laser diode that projects a laser screen across the cross section of the pipe as shown in Fig. 2.6 [33]. The thickness of the laser screen is important; if the laser screen is too thick (even in dilute phase flow) too many particles will be illuminated which could create errors because of particle overlap (laser screen thickness set between 0.5 and 1.5 times the maximum particle size) [31]. This configuration of illuminating the particles in the pipe and using

a CCD camera to capture the image is capable of on-line measurement of particle size, velocity and concentration.

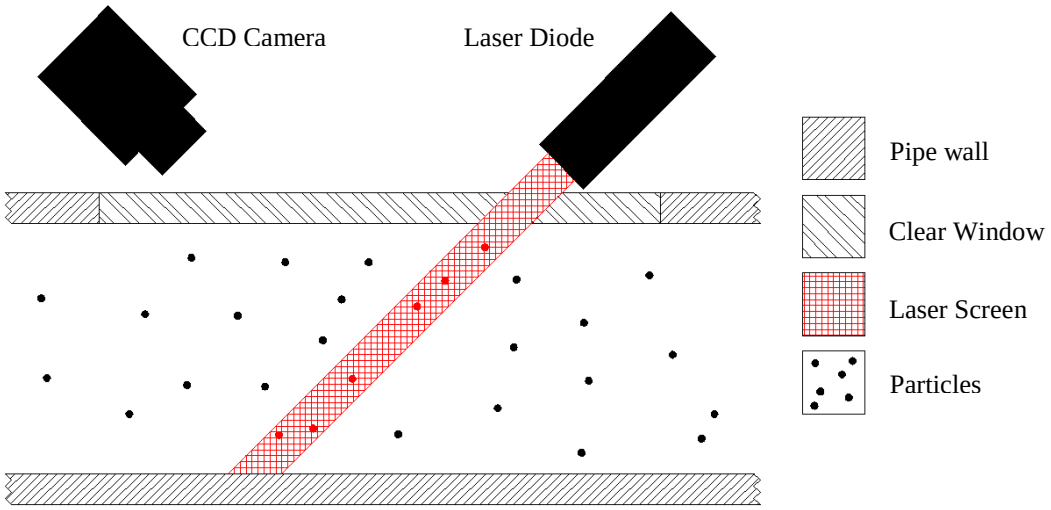

Fig. 2.6 Diagram of an on-line digital imaging sensor on a pneumatically conveying bulk solid pipe [33]

On-line digital imaging sensors have the advantage that they are nonintrusive as they do not obstruct the particle flow. However using this method presents a challenge for use on industrial systems since it requires a transparent window on the pipe and this is susceptible to contamination from the pulverised material. This drawback, however, has been addressed by Gao et al. [28] which implemented an air purging system that prevented contamination of the window with pulverised material.

2.3.1 Particle Size/shape using Digital Imaging Sensors

2.3.1.1 Off-Line

Particle size distribution and shape can be determined using either off-line methods or on-line methods. For off-line methods a sample is taken from the material being conveyed inside a pneumatic conveying system (this can be manually done by an operator or automatically done [42]). A sample of particles is then placed into a lightbox and an image is taken using a CCD camera which is then analysed as shown in Fig. 2.7 [43].

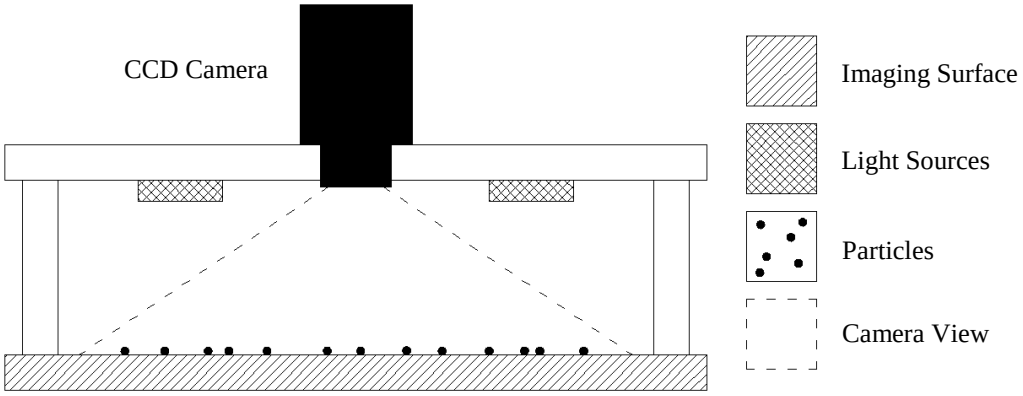

Fig. 2.7 Diagram of off-line particle size imagine sensor system [43]

2.3.1.2 On-line

The use of on-line particle sizing on pneumatic conveying systems requires a transparent window to be placed in the pipe wall. The particles are then illuminated using a laser diode to create a laser screen across the pipe cross section as illustrated in Fig 2.6. The principle of using this method is based on the contrast between the illuminated particles and the black background of the dark pipe [28] and [36]. An image analysis algorithm is then used to determine the boundary of the edge of the particle and this determines the particle size and shape [31]. This sensing method is susceptible to noise caused by the laser reflecting off the pipe wall or contamination to the lens so a threshold value is used to reduce these errors [28].

2.3.2 Particle Velocity using Digital Imaging Sensors

Particle velocity has been determined using on-line digital imaging sensors. Since these sensors have to work on-line they have to be mounted on the pipe line. To accomplish this they use the configuration of an illuminator to light up the particles inside a dark pipe and a CCD camera with a clear window in the pipe as shown in Fig. 2.6.

2.3.2.1 Particle Velocity Using Cross-Correlation of Digital Images

The principle of using the cross-correlation method of determining particle velocity using digital imaging camera and an illuminator is shown in Fig. 2.8 [37]. As the particles travel across the illuminated screen (the illuminating screen pulses at the same

rate as the camera's frame rate) the camera captures images at a set frame rate. In order to determine velocity two frames are required. The movement of the particles in the two frames are then assessed by a two dimensional cross-correlation algorithm with the velocity determined by the position of the peak correlation coefficient [37]. However Carter and Yan [37] point out that this configuration of the laser screen has the disadvantage that particles may enter the laser screen or exit the screen between frames causing particles to be in one frame and not the other.

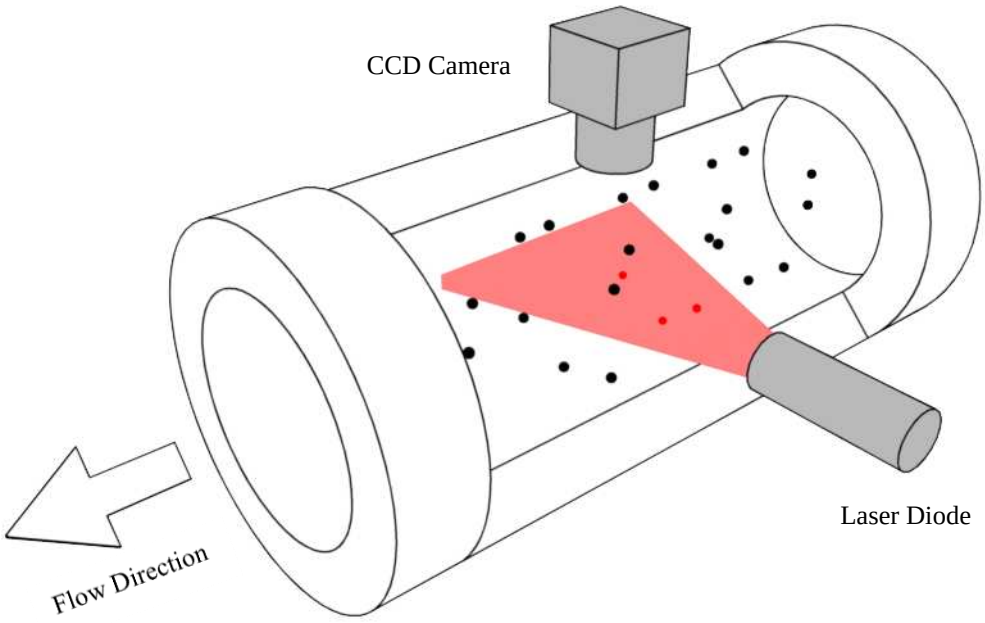

Fig. 2.8 Cutaway diagram of on-line particle velocity measurement using digital imaging and cross correlation as implemented by Carter and Yan [37]

2.3.2.2 Particle Velocity Using Motion Blur of Digital Images

Particle velocity has also been determined using the motion blur caused when a still image is taken of a moving object [40] – [41]. Song et al. used a laser diode to generate a laser screen to illuminate particles in a dark pipe as shown in Fig. 2.9 [40]. Fuchs et al. [41] uses a clear section of pipe with a spotlight to ensure good illumination. For both setups the length of the motion blur is what is used to determine the particle velocity (the longer the blur the higher the particle velocity). For this method the

camera's exposure time is very important since the longer the exposure time the longer the motion blur will be.

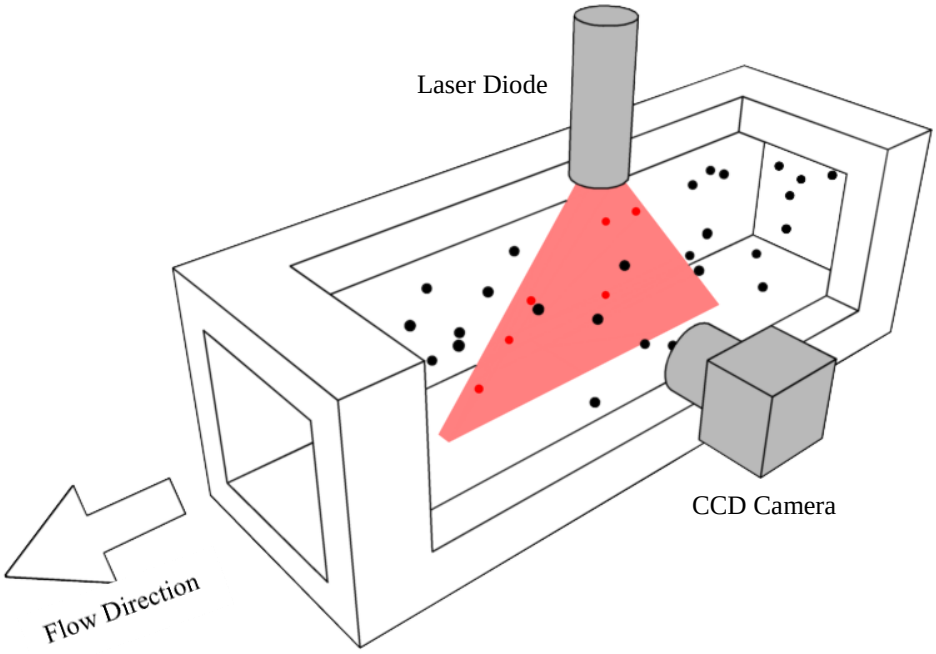

Fig. 2.9 Cutaway diagram of on-line particle velocity measurement using digital imaging and motion blur analysis as implemented by Song et al. [41]

2.3.2.3 Particle Concentration using Digital Imaging Sensors

Digital imaging has been implemented to determine particle concentration in pneumatically conveyed bulk solids [38] – [39]. This method uses a laser diode to produce a laser screen to illuminate the particles in a dark pipe and a CCD camera to capture the image as shown in Fig. 2.6. The principle of using digital imaging to determine particle concentration is similar to the method to determine particle size; except the particle concentration is determined by the number of particles detected in relation to the volume of empty space in the laser screen [38].

2.4 Electrostatic Sensors

Electrostatic sensors have been implemented in determining particle velocity [44] – [56], concentration [53] – [57] and particle size [58] – [60]. The fundamental principle of using electrostatic sensors is that as solid particles are conveyed down the pipe in a pneumatic conveying system they pick up electrostatic charge [1]. The level and distribution of this charge is random due to the nature of how it is generated inside the pipe through interaction and friction between the air and other particles [1]. The electrostatic electrostatic charge carried by the particles can be detected using an electrode as the particles pass in close proximity of the electrode since a small amount of charge is induced on the electrode [61].

2.4.1 Electrostatic Electrode Design

In order to detect this electrostatic charge three main types of electrode have been implemented: ring [44], [45], [48], [50], [53], [54], [56] and [60], arc [46], [47], [52], [54] and [55] and probe [48], [49], [51], [57] and [62] as shown in Fig. 2.10. The electrode is then interfaced with a signal conditioning circuit that consists of a pre-amplifier that can amplify the detected charge to a level that can be digitised in an analogue to digital converted (ADC) since the level of charge detected on the electrodes is in the region of nA.

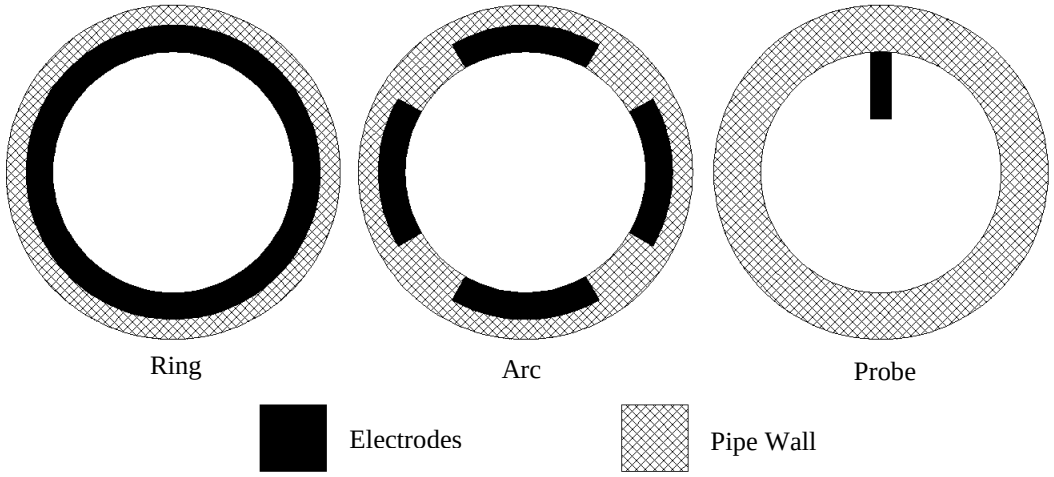

Fig. 2.10 Cross section diagram of electrostatic ring, arc and probe electrode configuration

2.4.1.1 Ring Electrodes

Ring electrodes have the advantage that they are non-invasive since they are constructed inside the pipe wall and thus do not come into contact with the particle flow. Ring electrodes also can be easily adapted for different shaped pipe such as square pipe as shown in Fig 2.11, however for square pipes it was found that the particle flow in the corners of the square pipe was more complex [63]. Ring electrodes do, however, have disadvantages; since they are constructed inside the pipe wall they are often constructed inside a pipe spool and this can increase costs when a system is retrofitted with this type of electrode (especially if the pipe spool is to be mounted at high level). Moreover, since the ring electrode spans the whole circumference of the pipe wall they are not as effective in measuring multi-phase flow due to different areas of the particle flow having different flow characteristics [48]. Ring electrodes have also been implemented into commercial systems for determining particle velocity and concentration [64].

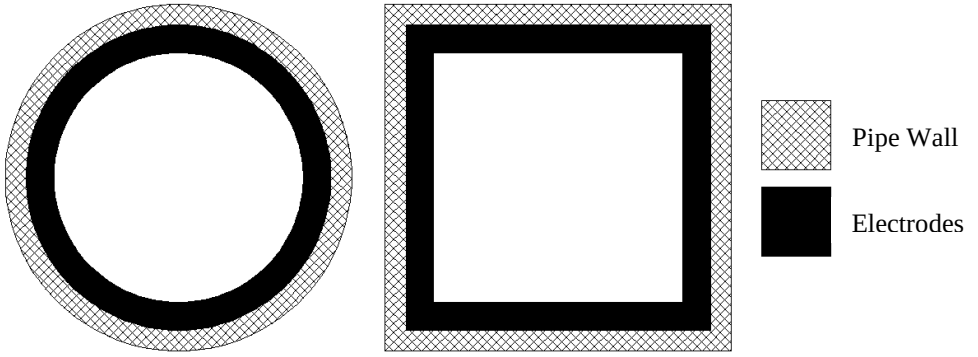

Fig. 2.11 Cross section diagram of ring electrode on a round pipe (left) and square pipe (right)

2.4.1.2 Arc Electrodes

Arc electrodes are a similar design to ring electrodes (since they are constructed inside the pipe wall and as such are non-intrusive) but unlike ring electrodes (that cover the whole circumference of the pipe wall with a single electrode), arc electrodes are separated into individual electrodes that only cover a small proportion of the circumference of the pipe wall as shown in Fig. 2.10. Because of this it increases their ability to measure multi-phase flow [54]. They are, however, like ring electrodes and are constructed inside the pipe wall whereby they are mounted inside a pipe spool and as such can increase installation costs on existing systems.

2.4.1.3 Probe Electrodes

Unlike ring and arc electrodes, probe electrodes are invasive sensors since they come into contact with the particle flow, however this does not cause a significant problem in dilute phase flow due to low particle concentration. For practical reasons it is recommended that the probe electrodes have a round cross section [51]. Since probe electrodes are intrusive they have a much more localised sensing area which improves their ability to measure multi-phase flow [65]. Due to their design, probe electrodes have the advantage that they are relatively simple to retro fit onto existing systems since to install a probe electrode on a system all that is required is a hole to be drilled and tapped in the pipe of a pneumatic conveying system.

2.4.2 Particle Velocity using Electrostatic Sensors

Electrostatic sensors have been applied to determine on-line particle velocity in bulk solid pneumatic conveying pipelines [44] – [56]. To determine particle velocity two methods have been used: spatial filtering [44] – [47] and the cross-correlation method [48] – [52] and [54] – [57].

2.4.2.1 Particle Velocity using Spatial Filtering

Determining particle velocity using the spatial filtering method has been implemented using ring [44], [45] and arc [46], [47] electrodes. The spatial filtering method uses the principle that the signal output from the electrostatic sensor in the frequency domain changes depending on the particle velocity. It does this because the time the particles take to pass in close proximity to the electrostatic sensing electrode is dependent on the particle velocity; the higher particle velocity the higher the dominate frequency of the sensor output. For determining the particle velocity using the spatial filtering method the ring electrodes are placed in a linear array [45] or arc electrodes are placed in a linear matrix [47] configuration as shown in Fig. 2.12. It was determined through experimentation and finite element modelling (FEM) that the optimum number of electrodes should be between 4 and 10. It was also suggested that the ratio between the electrode spacing compared to the electrode width should be between 7 and 10, and the electrode width to pipe radius should be in the range of 0.1-0.2 [44]. The use of the spatial filtering method, however, requires that the sensor be calibrated to the particle size which has to be known beforehand since this factor can significantly affect the frequency output [66].

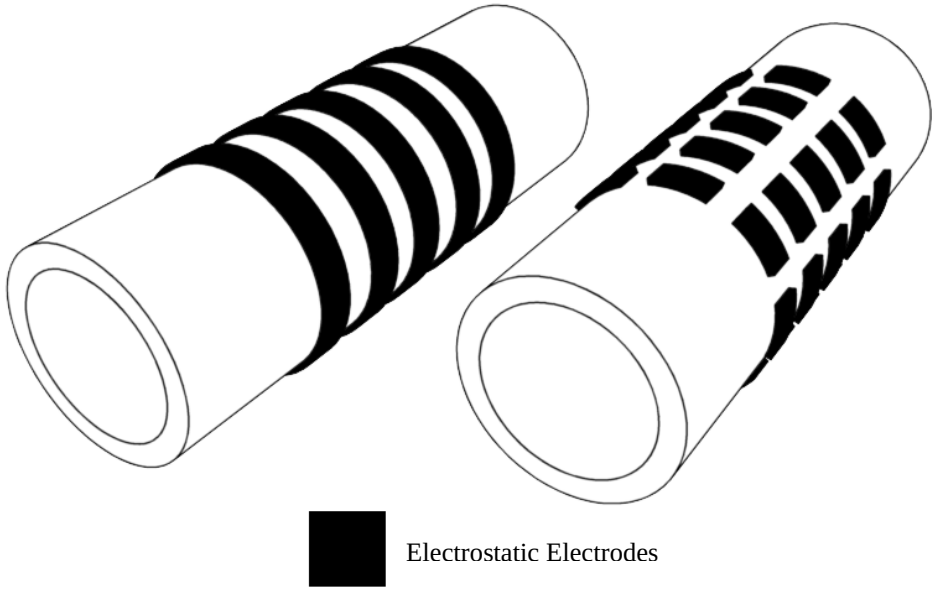

Fig. 2.12 Diagram showing spatial filtering electrode configuration; linear ring electrodes [45] (left) and linear arc electrode matrix [47] (right)

2.4.2.2 Particle Velocity using Cross-Correlation

The cross-correlation method has been implemented with electrostatic sensors using ring [53], arc [55] and probe [51] electrodes. Using the cross correlation method to measure particle velocity of particles traveling inside the pneumatic conveying pipe involves the use of two electrodes arranged in an upstream/downstream configuration as shown in Fig. 2.13 [61].

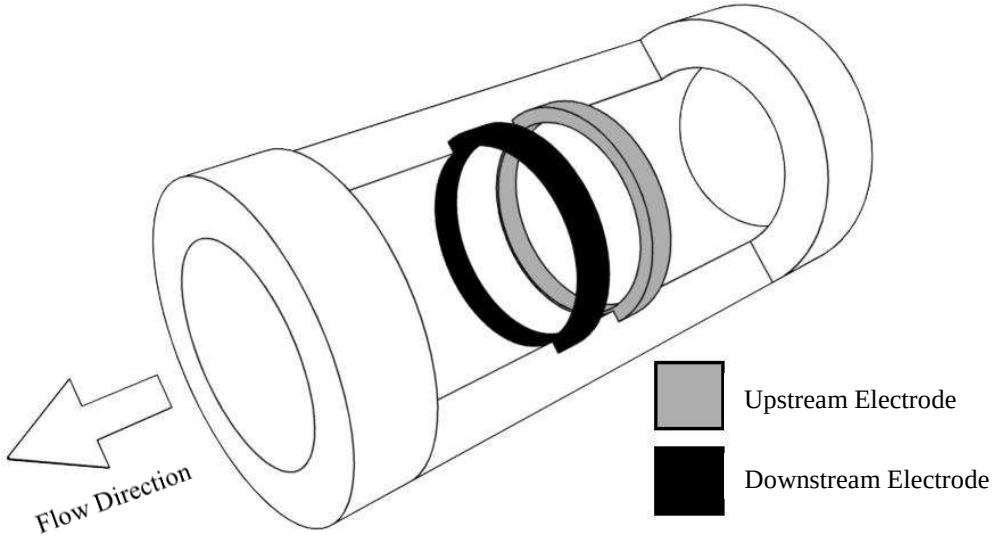

Fig. 2.13 Diagram of the upstream/downstream electrostatic electrode configuration for determining particle velocity using the cross correlation method

As the charged particles travel past the electrodes the charge on the surface of the particle is detected by the sensor electrodes. If both electrodes and the signal conditioning circuits are identical the signal from the upstream electrode will be the same as the signal on the downstream electrode except the downstream signal will be time delayed as shown in Fig. 2.14. Since the distance between the upstream and downstream electrodes is known, particle velocity (V_c) can be calculated from:

$$V_c = \frac{L}{\tau_m} \tag{2.1}$$

Where L is the spacing between the upstream and downstream electrodes and τ_m is the time difference between the upstream and downstream signals. To determine τ_m the cross-correlation method is used. The delay between the two signals is determined from the location of the dominant peak in the cross correlation function [57]. The position of the dominant peak for the resulting correlation function - known as the correlation coefficient - indicates the delay between the upstream and downstream signals, as illustrated in Fig. 2.15.

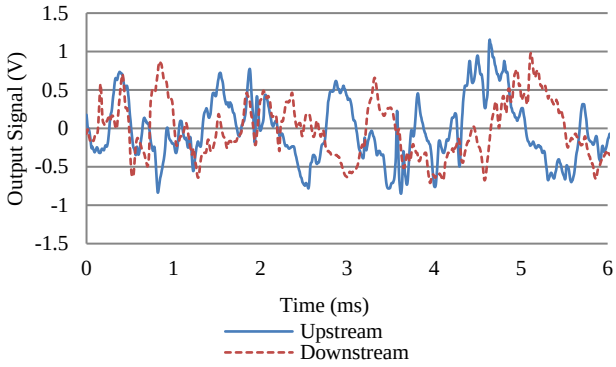

Fig. 2.14 Upstream and downstream signals from electrostatic sensors

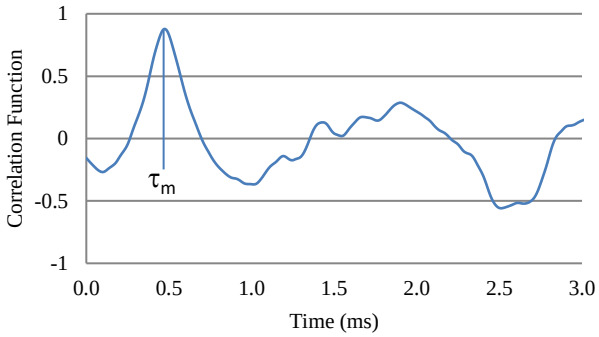

Fig. 2.15 Correlation function between the upstream and downstream sensor signals

When using the cross-correlation method the distance between the upstream and downstream electrodes is a significant factor. Qian and Yan [54] used ring and arc electrodes and found that when the upstream and downstream electrodes were closer together this improved the quality of the correlation coefficient. The reason for this is that the further away the upstream and downstream electrodes are to each other the more changes can happen to the particles. This is most apparent with elongated materials since their orientation can change between the upstream and downstream electrodes due to particle spin. The design of the electrostatic electrodes plays an important part in the measured particle velocity and the quality of the correlation coefficient when using the cross-correlation method. Shao et al. [67] assessed the performance of probe electrodes through a combination of practical on-line experimentation and off-line finite element modelling. It was found that a probe

electrode with an electrode depth of 0.3-0.5 of the pipe diameter would give a reasonable estimate of the true mean velocity for regular velocity profiles. In addition, it was found that the rod electrodes had a higher correlation coefficient compared to the traditional ring electrode design with the rod electrodes obtaining a correlation coefficient of around 0.55-0.75 compared to 0.35-0.50 for the ring electrodes under the conditions tested; this is due to the fact that the sensitivity of the rod electrodes is much more localised [62].

2.4.3 Particle Concentration using Electrostatic Sensors

Electrostatic sensors have been applied to determine particle concentration using ring [54], [56], arc [54] and probe [57] electrodes. Particle concentration is determined using the principle that the higher the particle concentration the higher the electrostatic charge detected by the electrostatic sensors. The design of the electrostatic electrodes will determine the location in the pipe where the concentration is measured. Ring and arc electrodes will only measure the particle concentration along the pipe wall. Whereas probe, since they have a localised sensing area, are able to give specific particle concentration in areas of the pipe. An adaption of the probe electrode was implemented by Jurjevčič et al. [68]; an electrostatic probe electrode was divided up into multiple probe electrodes, thus creating a probe array across a section of pneumatic transportation ducting, which was implemented on a coal fired power station illustrated in Fig. 2.16. Using multiple of these electrostatic probe arrays an electrostatic matrix was created that was able to determine the particle concentration for the cross section of the ducting. Utilising this matrix it was likewise possible to detect roping caused by the centrifugal force from the particle flow exiting a right angle bend when the fans were set on higher speeds [68].

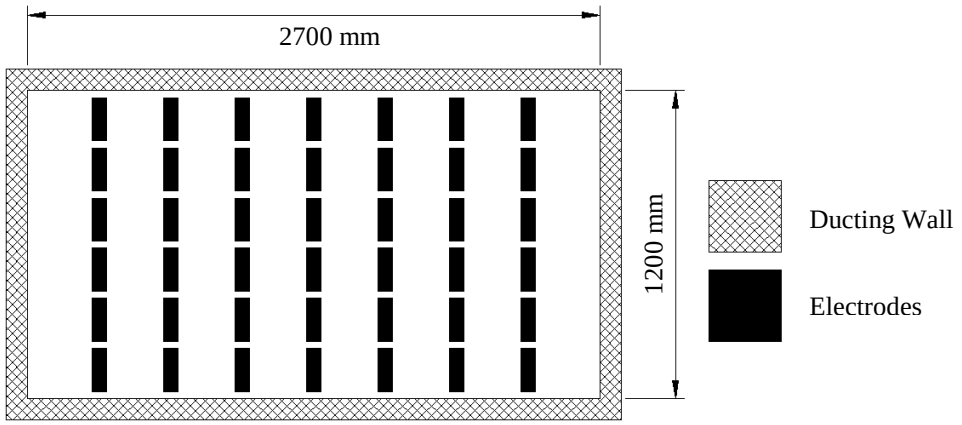

Fig. 2.16 Diagram of electrostatic probe matrix used by Jurjevčič et al. [68] to determine particle concentration for the cross section of a section of pneumatic transportation ducting

2.4.4 Particle Size using Electrostatic Sensors

Particle size of pneumatically conveyed bulk solids has been determined using electrostatic sensors. This has been achieved by using characteristics of the electrostatic sensor signal output in either the time domain [58], [59] or the frequency domain [60].

2.4.4.1 Particle Size using Time Domain

Zhang and Yan [58] proposed a method of using the output signal from an electrostatic sensor in the time domain to determine particle size. The principle of this method is that larger particles have a larger surface area and consequently have a higher electrostatic charge. Therefore, when the larger particles travel passed the electrostatic electrodes the magnitude of the electrostatic sensor signal is higher. The electrode design used by Zhang and Yan [58] is a mesh type as illustrated in Fig. 2.17. The mesh was constructed from 0.5 mm wire to minimise the effect of the mesh on the particle flow. This sensor design and measuring principle has several disadvantages: firstly the design of the sensor is prone to erosion; and secondly the sensing principle is dependent on the mass flow rate being independently measured [58].

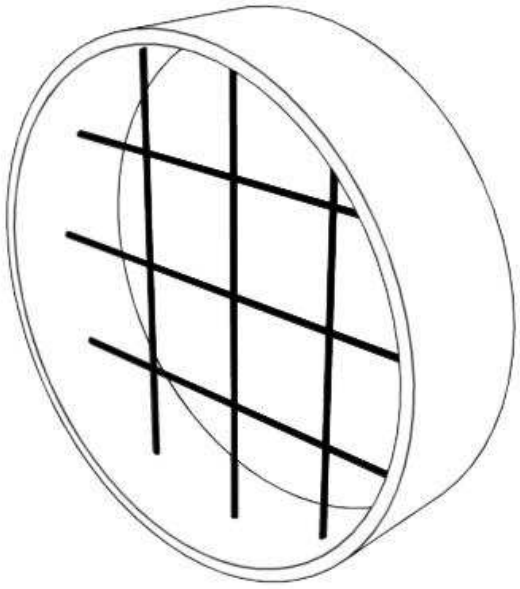

Fig. 2.17 Diagram of electrostatic mesh electrodes used by Zhang and Yan [58] to determine particle size distribution for pneumatically conveyed particles

2.4.4.2 Particle Size using Frequency Domain

Particle size has been established by determining the dominant peak in the frequency domain from an electrostatic sensor. Tajdari et al. [60] employed a ring electrode design and used the principle that as the particles pass the electrostatic electrode the smaller the particle the higher the dominant frequency. This is because larger particles will be detected for longer as they pass the electrostatic electrode compared to smaller particles [60]. However, this sensing method would require the sensor to be calibrated to the particle velocity since this would affect the spectral frequency. This is similar to the drawback of using the spatial filtering method to determine particle velocity which requires that the sensor to be calibrated to the particle size [66].

2.5 Impact Sensors

Impact sensors have been utilised to determine particle size distribution [69] – [77] and particle concentration [77] – [79]. When a moving particle collides with a fixed solid surface the kinetic energy of the moving particle is converted into an impact force. Several sensor technologies have been researched to detect this impact force such as piezoelectric transducers [69] – [73], [78] – [79], acoustic emission sensors [74], [75] and accelerometer [76], [77].

2.5.1 Particle Size using Impact Sensors

The use of impact sensors to determine particle size uses the principle that the larger the particle size the larger the mass of the particle and so the larger the impact force would be. When a moving particle impacts an object its kinetic energy is converted into an impact force. During the impact acoustic waves are induced in the material of the impact target [74]. An offline method was implemented by Müller et al. [75] where they used an acoustic sensor on an impact plate to measure the vibrations caused by a particle impact. It was found that if the particle velocity was known then the particle size could be determined by measuring the magnitude of the impact signal detected by the acoustic sensor. This off-line sensor arrangement would be unsuitable for online particle sizing since the impact plate would have a large surface area and suffer from simultaneous impacts which could cause measurement errors.

An on-line method has been implemented using an impact bar arrangement [69], [72] – [73], [76], and [77]. This method is an invasive measuring technology since it utilises an impact bar that comes into contact with the particle flow. This impact bar acts as a waveguide to the vibration sensor for the vibrations in the waveguide caused by particle impacts. Goa et al. [73] employed this sensor arrangement using piezoelectric film to measure the vibrations caused by particles hitting the impact bar. The piezoelectric film was fixed to the impact bar as shown in Fig. 2.18. The

piezoelectric film for this sensor is operating in ‘bending mode’ since this allows the sensor to be more sensitive to smaller impact forces [73].

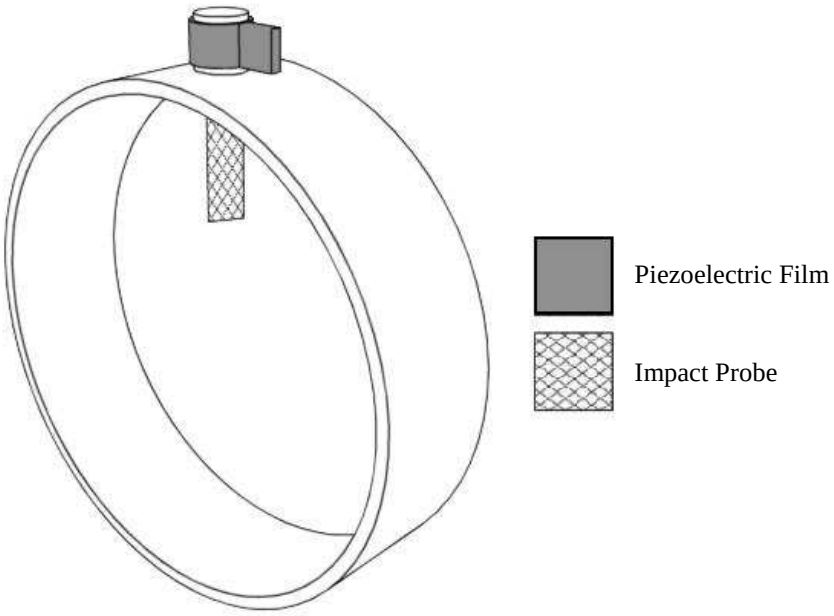

Fig. 2.18 Sensor design implemented by Goa et al. [73]

Hu et al. [74] implemented the impact bar sensor arrangement using an acoustic sensor to detect the vibrations caused by particles impacting the sensor bar, which is illustrated in Fig. 2.19. Using electrostatic sensors to independently measure the particle velocity Hu et al. [74] were able to determine particle size distribution of glass beads.

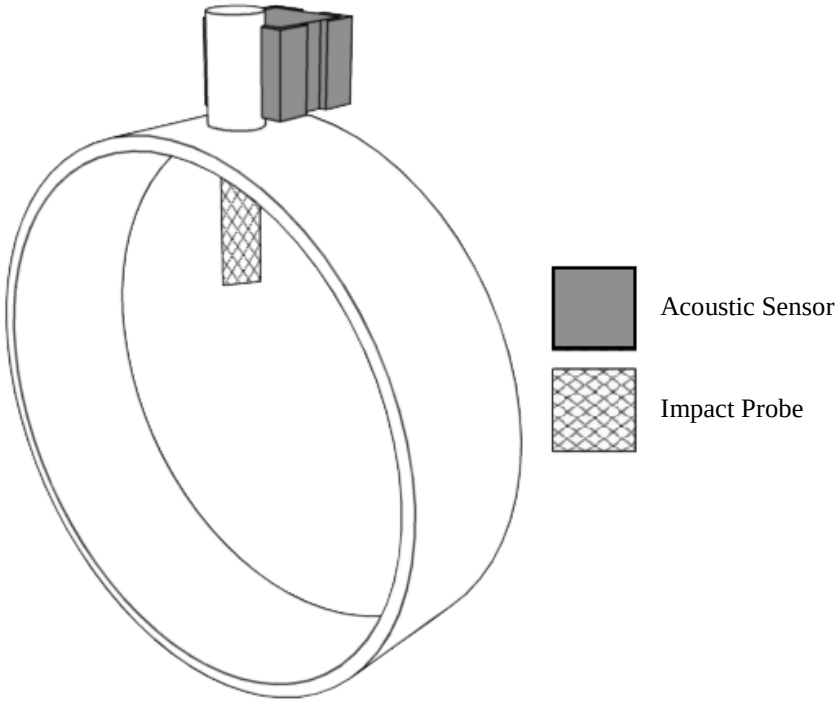

Fig. 2.19 Impact sensor design implimented by Hu et al. [74]

Accelerometers have also been used to measure the impact force of particles impacting an invasive impact bar. Meunier et al. [77] used an impact bar that came into contact with the particle flow with an accelerometer mounted on the opposite end of the impact bar as shown in Fig. 2.20. The advantage of this sensor arrangement is that the components, such as the accelerometer, are inexpensive and simple to construct.

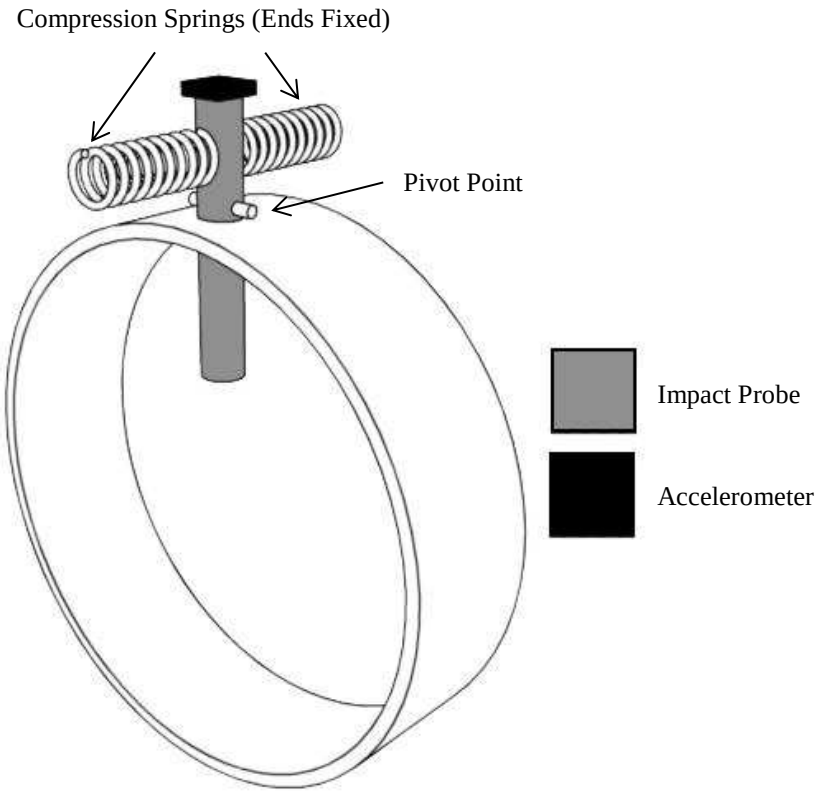

Fig. 2.20 Impact sensor design implemented by Meunier et al. [77]

Despite the impact probe having only a small area it is still relatively large in comparison to the particle size. Consequently, even in dilute phase flow multiple simultaneous impacts may occur that would cause measurement errors.

An adaption of the intrusive impact bar sensor design was implemented by Coghill [71]. For this design only has a small part of the impact bar is active. This was achieved by masking all but the active area on the sensor. The active area on the sensor is a 'hit' plate design as shown in Fig. 2.21. The outside of the plate is coated in ceramic for abrasive resistant with a layer of piezoelectric film inside the plate which detects the vibrations caused particles impacting the plate. The advantage of this sensor design is that it can detect the particle size distribution in a very local area (however the plate

design used by Coghill [71] is 19 mm diameter which would only be suitable for large diameter pipes).

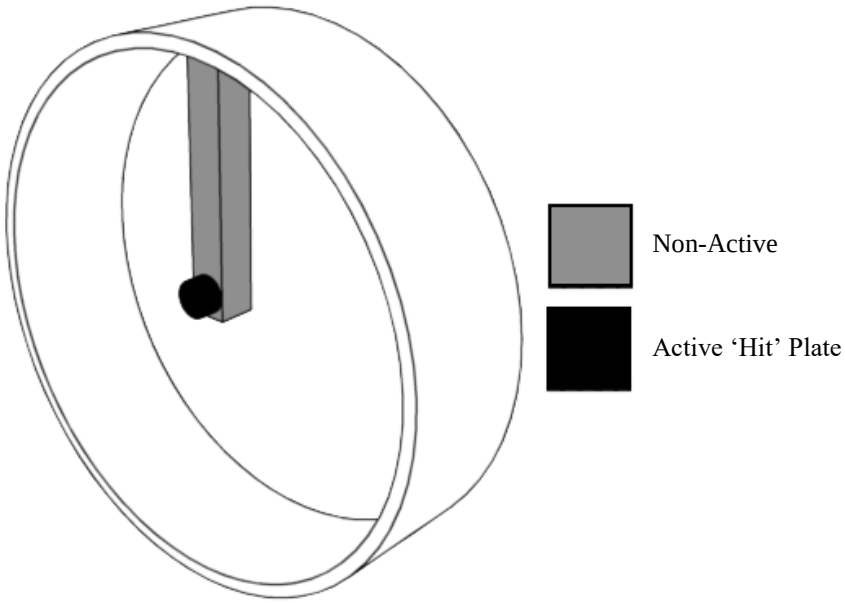

Fig. 2.21 Sensor design implemented by Coghill [71]

2.5.2 Particle Concentration using Impact Sensors

Particle concentration has been determined using impact sensors either by measuring the number of particle impacts [78] or by measuring the spectral frequency [79]. Zhan and Jing [78] used piezoelectric film to measure the impacts of grain as it fell onto the piezoelectric film in order to determine grain loss. By measuring the number of impacts in the time domain the grain loss (particle concentration) was able to be determined. This sensor arrangement would be unsuitable to determine particle concentration in a pneumatic conveying system since having the particle flow directly impacting the piezoelectric film would cause damage to the film due to the particles' erosive effects.

Wang et al. [79] used piezoelectric sensors and the principle of measuring the spectral frequency of the particle impacts. It was found that the higher the frequency component the higher the particle concentration due to more number of particle impacts. The sensor presented by Wang et al. [79] is non-invasive since it is mounted on the

outside of the pipe on a right angle pipe bend. The primary advantage of this is that it would be simple to retrofit onto an existing system.

2.6 Optical Sensors

Optical sensors have been applied to determine particle velocity [80]. Optical sensing techniques differ from digital imaging sensors in that an expensive camera and image analysis equipment is not required.

2.6.1 Particle velocity using Optical Sensors

Particle velocity has been determined using optical sensors. The optical sensor arrangement uses an optical emitter and an optical receiver. Mahmod et al. [80] used an LED of the optical emitter and a photodiode for the receiver in a configuration illustrated in Fig. 2.22.

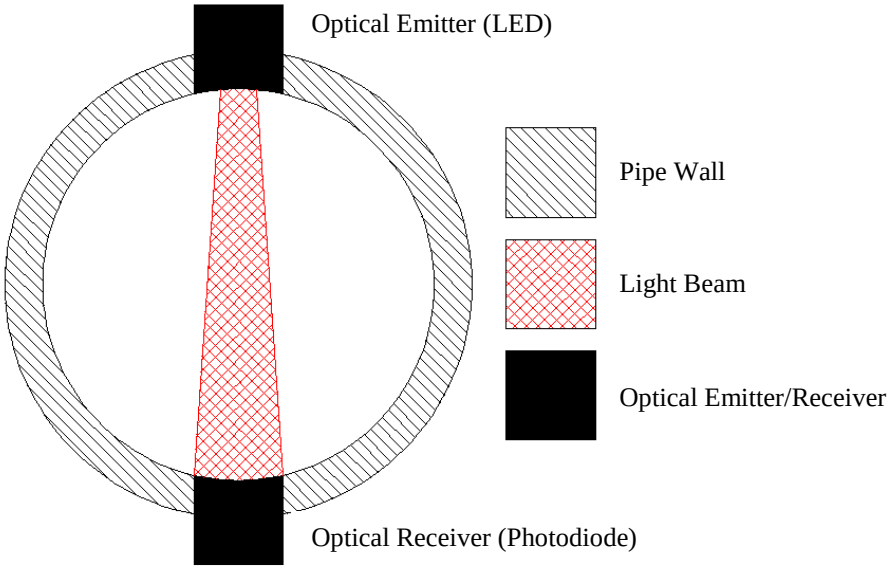

Fig. 2.22 Optical sensor configuration implemented by Mahmod et al. [80]

Particle velocity was determined using two pairs of optical emitters/receivers in an upstream/downstream arrangement. As particles in a dilute phase flow pass between the optical emitters and receivers the light from the emitter that is detected by the receiver is

attenuated randomly. Using the signal outputs from the upstream/downstream sensors and using the cross correlation method the particle velocity can be determined. This sensor design has the advantage that is it a non-invasive sensing technology. This sensor, however, has the same problem as digital imaging sensing techniques as it requires a transparent window in the pipe which can be contaminated by particles.

2.7 Radiometric Sensors

Radiometric sensors are a non-intrusive sensor that work on the principal of a Gamma-ray source (e.g. Americium-241) projecting a radiation beam across the cross section of a pipe which is detected by a detector (photodiode) with an appropriate signal conditioning circuit as shown in Fig. 2.23 [81].

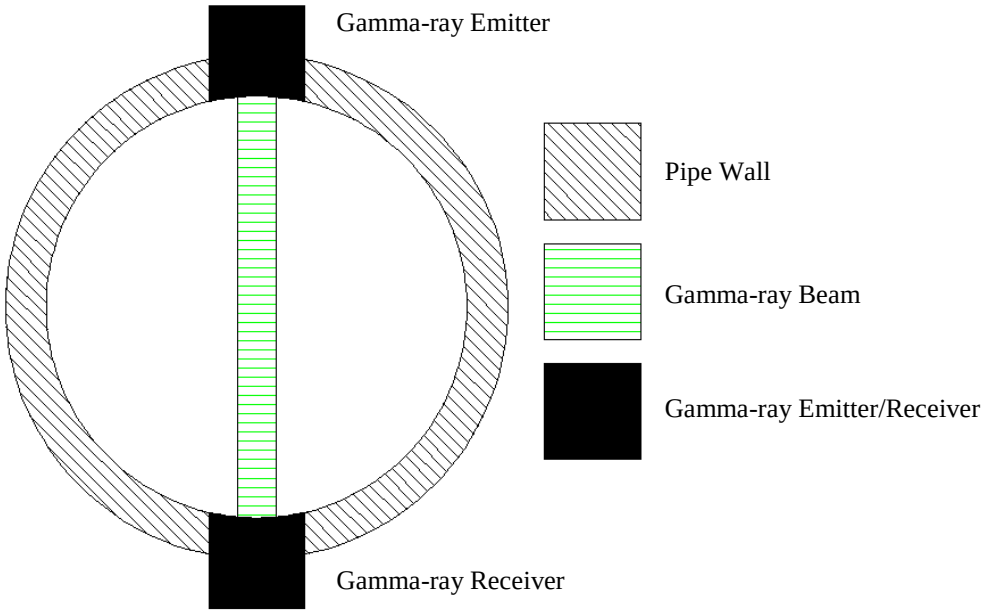

Fig. 2.23 Diagram of the basic components of a radiometric sensor in a pipe.

When the pipe is empty the output signal from the detector remains constant, however the detector output will vary as the particle flow travels through the radiation beam.

2.7.1 Particle Concentration Radiometric Sensors

Barratt et al. [81], instead of using a single narrow radiation beam, used a strip source approach and an array of detectors as shown in Fig. 2.24. Using this method a matrix of gamma-ray was formed in the pipe. Particle concertation is determined by the attenuation of the gamma-ray beam; the higher the particle concentration the higher the attenuation of the gamma-ray beam. This design was able to get data of the particle concentration from the whole cross section of the pipe.

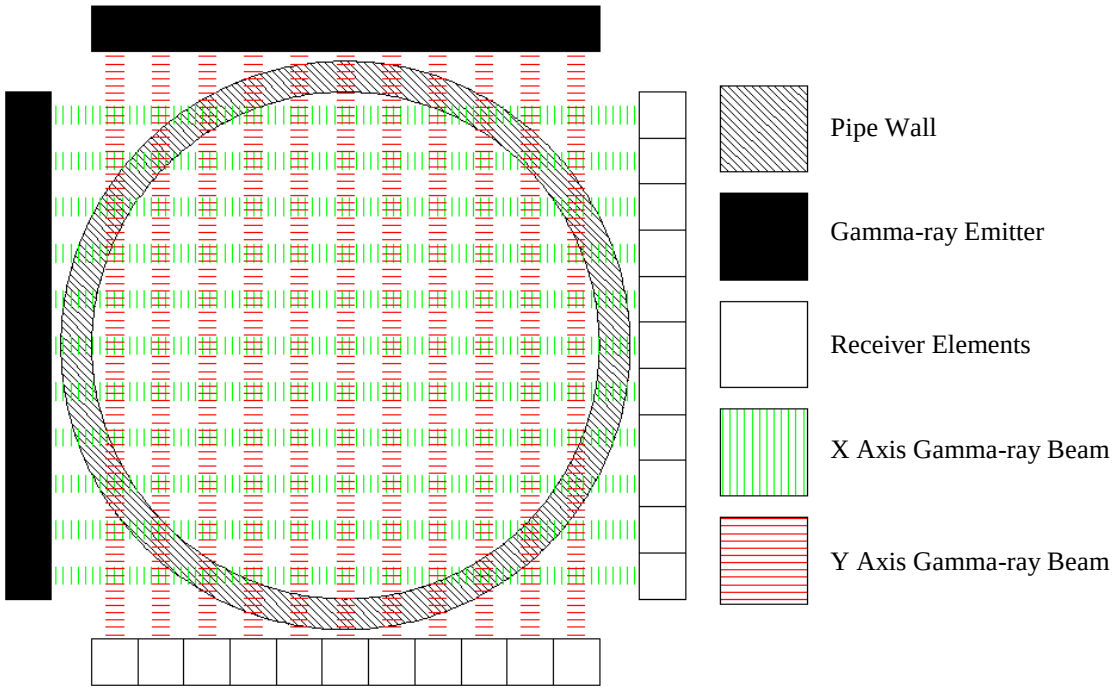

Fig. 2.24 Diagram of Barratt et al. [81] radiometric sensor using a strip gamma-ray source used to detect particle concentration for the whole pipe cross section.

2.7.2 Particle velocity using Radiometric Sensors

Barratt et al. [81] also used the method shown in Fig. 2.24 to determine particle velocity by using two identical sensors in an upstream and downstream arrangement and using a cross-correlation method. Using data fusion of the particle concentration and particle velocity, the mass flow rate was able to be determined. Barratt et al. [81], however, states that this system is not in its current form an on-line system, but an on-line continuous system could be achieved by adding more identical radiation beam elements.

It is important to point out that the radiometric sensors contain a radiation source. Consequently their use would cause administrative problems as well as personal concerns about safety because of the public's concern over radiation.

2.8 Ultrasonic Sensors

Ultrasonic Sensors are on-line sensors that are capable of determining both the particle velocity and particle concentration in a pneumatic bulk solid conveyor system making them capable of determining the mass flow rate. The sensor arrangement consists of two parts: the ultrasonic transmitter and the receiver as shown in Fig. 2.25 [82].

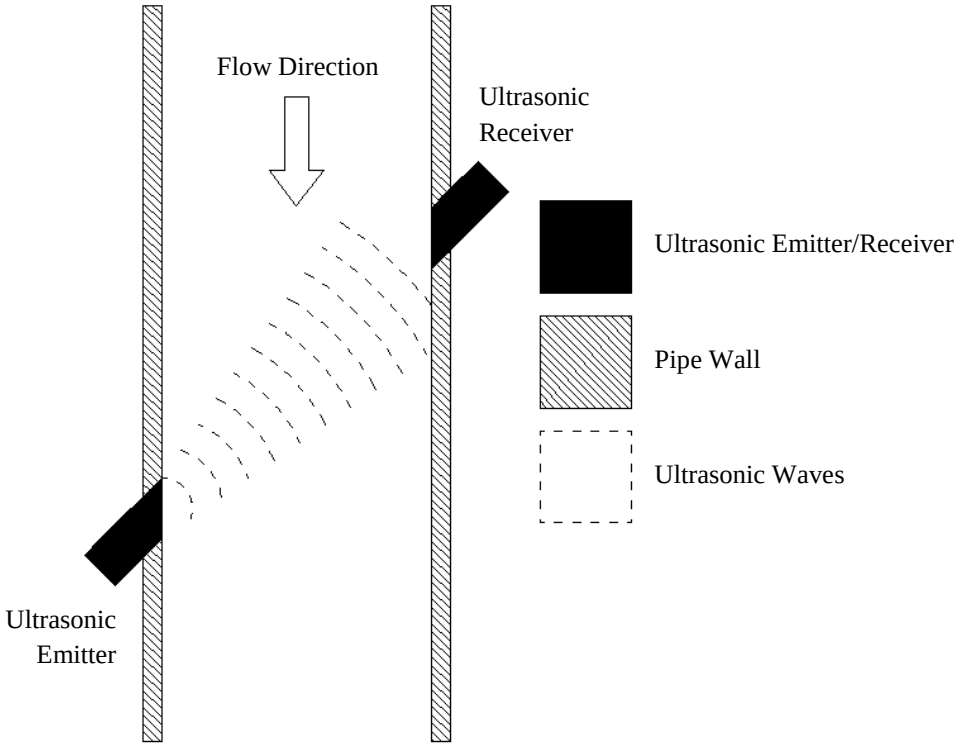

Fig. 2.25 Configuration of an Ultrasonic flow sensor

2.8.1 Particle Concentration using Ultrasonic Sensors

The particle concentration is determined by the attenuation of the pulsed ultrasonic beam as it is transmitted across the pipe since the higher the particle concentration the more attenuation is experienced in the ultrasonic beam [82].

2.8.2 Particle Velocity using Ultrasonic Sensors

The particle velocity is determined by using an ultrasonic contra-propagation method, where the air velocity is determined by the difference in the transit time compared to when there is no air flow in the pipe. The contra-propagation method is used to determine the velocity in a pneumatic system since the speed of sound in air (340m/s) is relatively low compared to the speed of sound in water (1500m/s) making the propagation easier to measure [82].

Abernethy et al. [83] successfully trialled an ultrasonic sensor to determine mass flow rate on a pulverized coal fuel line to a 660MW boiler at Bayswater Power Station in NSW Australia, where it was installed on a 500mm diameter pipe with particle velocities of 25m/s with particle concentrations between 0.8 and 1.2kg/m^3.

2.9 Summary

From this review of sensor technologies of work carried out by previous scholars, it is the opinion of this author that the ideal solution for an online system for monitoring particle velocity, size distribution and concentration would be to use a combination of sensing techniques.

The ideal sensing technique for determining particle velocity is the electrostatic method using cross correlation due to its robustness and low cost. Furthermore, the electrostatic sensor will be able to determine particle concentration. It is also the opinion of this author that the ideal sensing technique for determining true particle concentration and particle size distribution is to use the impact sensing techniques; this is due to its

simplicity of the sensor design and that impact sensors can determine particle concentration and size distribution in a single sensor.

It has been noted in this literary review that work carried out on sensors, such as electrostatic sensors and impact sensors, has revealed that they have a very local sensing area and do not provide a complete picture of what is happening in the whole cross section of the pipe (not considering digital imaging sensors). This will cause problems with multi-phase flow since different parts of the cross section of the pipe will be traveling at different velocities as well as different particle concentrations and size distributions. So in order to overcome this deficiency the electrostatic sensors (for determining particle velocity/concentration) and impact sensors (for determining particle concentration/size distribution) should be constructed in an array across the diameter of the pipe. This will allow the particle velocity/concentration/size distribution profiles to be monitored by an on-line sensor.

Chapter 3

Design and Implementation of the Electrostatic Sensor Array

3.1 Introduction

This chapter will explain the concept and principle of the electrostatic sensor array design and will illustrate the novel features of the sensor array which will be capable of determining the particle velocity and particle concentration profiles for the whole diameter of the pipe. This will allow the electrostatic sensor array to measure the complex multi-phase flow that previous types of electrostatic sensors have been unable to achieve. All aspects of the sensor hardware design will be covered including: the structure and shape of the sensor array; the design and configuration of the sensor electrodes; signal conditioning circuit designs for the electrostatic sensors; digital selecting of each element of the sensor array; the use of an external high-speed analogue to digital converter (ADC) for digitisation of the electrostatic sensor signals; and the use

of an embedded microcontroller to determine particle velocity through cross correlation. Experimental procedure and results will be discussed in later chapters.

3.2 Electrostatic Sensor Principle

As solid particles are conveyed down the pipe in a pneumatic conveying system they pick up electrostatic charge. The level and distribution of this charge is random due to the nature of how it is generated inside the pipe through interaction and friction between the air and other particles [1]. The electrostatic charge carried by the particles can be detected using a sensor electrode. As the particles pass in close proximity of the sensor electrode a small amount of charge is induced on the sensor electrode [61]. Using this detected charge the particle velocity can be determined by either the spectral filtering method or the cross correlation method (depending on the electrode configuration). The relative particle concentration can be determined by measuring magnitude of the r.m.s. of the electrostatic charge (the higher the r.m.s. charge detected the higher the particle concentration).

3.3 Electrostatic Array Concept

This design of electrostatic sensor array is an invasive sensor design like the electrostatic probe electrode sensor in that the sensor electrodes comes into direct contact with the particle flow. Unlike the probe electrode design, however, the electrostatic sensor array is separated into individual electrode pairs spaced equally across the pipe diameter as shown in Fig. 3.1.

The advantage of this sensor design is that the electrostatic sensor array will be capable of determining both the particle velocity and particle concentration profiles for the whole diameter of the pipe. This will allow the complex flow characteristics

associated with multi-phase flow (air/coal and air/coal/biomass) to be monitored as well as specific flow regimes such as roping that occur within the sensors sensing range.

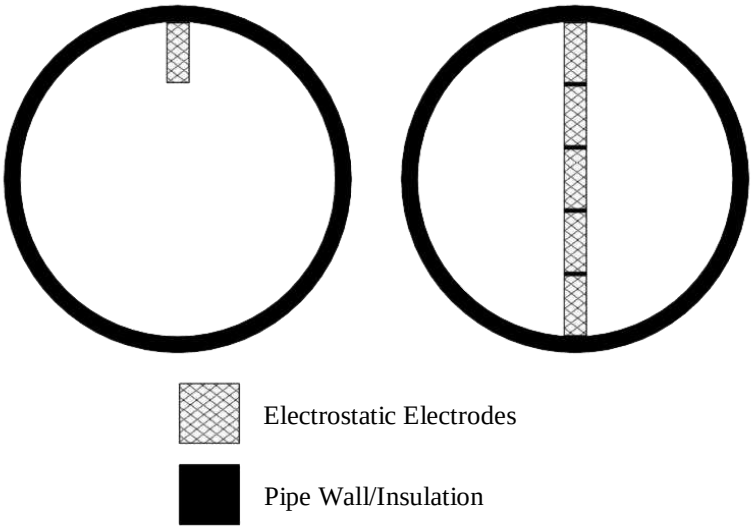

Fig. 3.1 Comparison of the probe electrode (left) and the electrostatic sensor array (right)

3.4 Electrostatic Sensor Array Design

When devising the electrostatic sensor array design there are two possible designs for the main sensor structure. The first was to take the standard design for the electrostatic probe design and divide each probe into to isolated sections as shown in Fig. 3.2. This has the disadvantage of being complex to construct due to the fact each element of the electrodes has to be isolated and then each element connected to an external signal conditioning circuit (pre-amplifier). The extended connection distance between each sensor element to the pre-amplifier circuit would also cause a problem with noise contamination which would overwhelm the small signal from the electrodes.

The second electrostatic sensor array design is the blade design also shown in Fig. 3.2. The blade sensor design has the advantage of being able to construct the pre-amplifier circuit directly inside the sensor blade. The advantage of this would be the

reduced distance between the electrodes and the pre-amplifier circuit reducing unwanted noise from entering the circuit and thus improving signal to noise ratio.

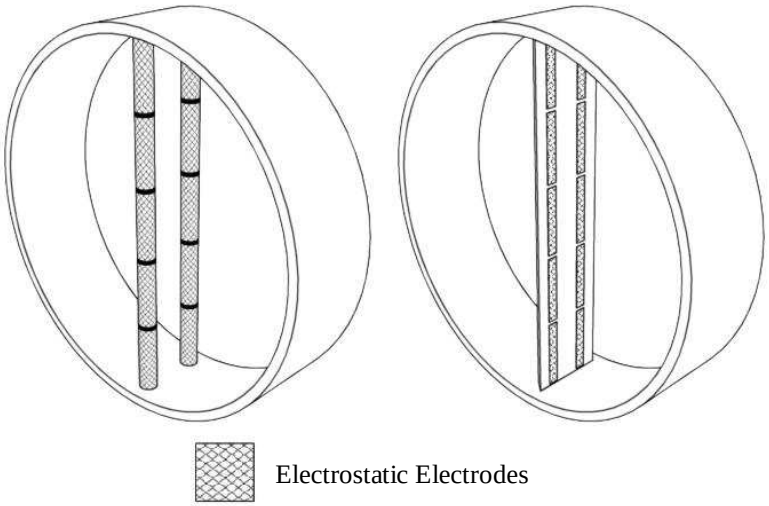

Fig. 3.2 Diagram of electrostatic sensor array formed using probe electrodes (left) and sensor blade (right)

Since the electrostatic sensor array is an invasive sensor its cross sectional area has to be kept as small as possible. Because the sensor array has to cross the whole diameter of the pipe the main factor in reducing the cross sectional area is to keep the sensor as thin as possible to reduce the impact the sensor array has on the particle flow. Even though the current sensor array design has the pre-amplifier circuits constructed inside the blade, the current electrostatic sensor array is 2.5 mm thick meaning that for a 50 mm bore pipe the sensor array's cross sectional area takes up less than 6.4% of the pipe cross section. This, however, could be reduced for commercial versions by using thinner printed circuit board as well as using other manufacturing processes for fabricating the sensor blade.

Another consideration for the design of the blade shape of the sensor array is how it will affect the flow characteristics such as creating turbulence and causing velocity changes. For these reasons the sensing electrodes are only constructed on one side of the sensor blade with a 45 degree knife edge on the leading edge of the senor array. The 45 degree knife edge increase the aerodynamics of the sensor array and also

it deflects most of the turbulence and velocity change caused by the sensor array behind the sensing electrodes. Wind tunnel simulations (using CFD Motion created by Autodesk) were carried out to analyse the effect the sensor has on the conveying air (Fig. 3.3). The wind tunnel simulation confirms that most of the velocity change happens behind the sensor array's electrodes. The simulation was carried out with a developed air flow of 20 m/s with a mesh count of 16,000 elements per plane.

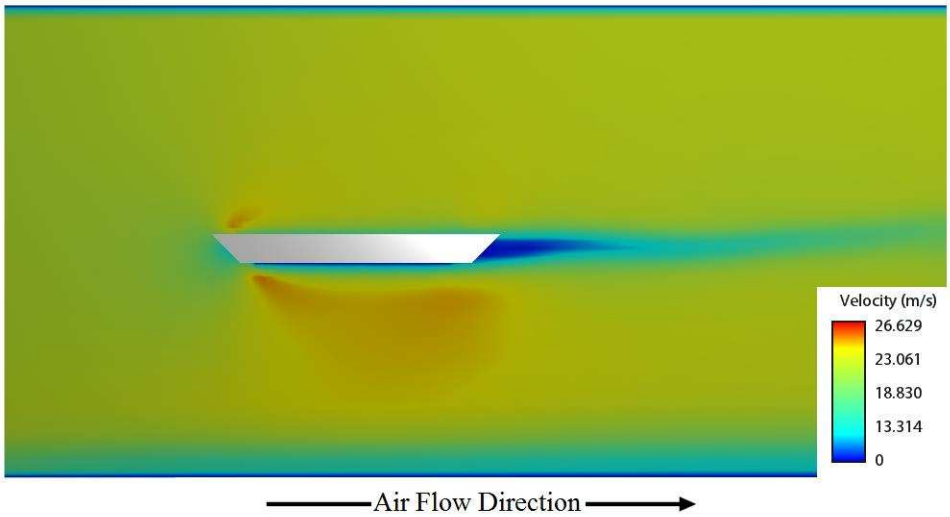

Fig. 3.3 Wind tunnel simulation of the effect of the sensor array's cross section on air velocity

The sensor array blade housing is constructed from grounded metal to shield the pre-amplifiers from external noise. This similarly has the advantage that any particle that impacts the leading edge of the sensor array blade will have its electrostatic charge discharged and hence it would not be detected by the electrostatic sensor arrays. Consequently any particles that have slowed down due to impacting the sensor blade will not be detected.

3.4.1 Sensor Electrode Configuration

There are two methods to determine particle velocity using electrostatic sensors: the spatial filtering method [44] and the cross correlation method [57]. Since the spatial filtering method uses a linear array of electrodes in the direction of the flow it was unsuitable for use with the electrostatic sensor array presented in this study due to space

constraints on the sensor blade. Using the cross correlation method to measure the velocity of particles traveling inside the pneumatic conveying pipe involves the use of two electrodes arranged in a configuration as shown in Fig. 3.4 [61].

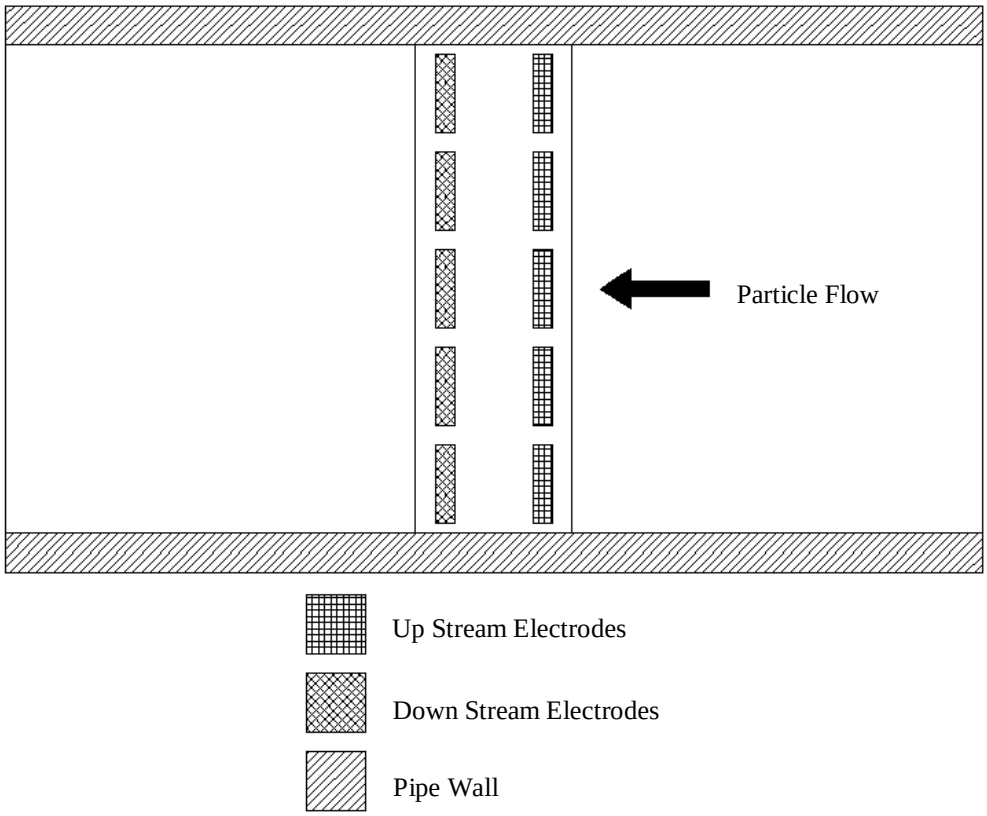

Fig. 3.4 Electrode configuration of the electrostatic sensor array inside a pipe

The electrostatic sensors array consists of five pairs of electrodes across the diameter of the pipe. The physical size of the electronics for the pre-amplifier was the determining factor for the number of electrostatic electrodes able to be constructed across the pipe diameter.

3.4.2 Design of the Sensor Electrode

The electrodes for the electrostatic sensor array are manufactured on a double sided printed circuit board (PCB). The advantage of this is that the signal conditioning circuit can be constructed directly behind the electrodes on the other side of the PCB with the

electrode and signal condition circuit connected using via pins. Another advantage of manufacturing the electrodes on PCB is that different electrode designs can be constructed and tested quickly. However, for commercial use PCB electrodes are not suitable since prolonged exposer to the particle flow will erode the electrodes.

The cross correlation uses the input of a pair of electrodes in an upstream downstream configuration. The upstream and downstream electrodes are set as close as possible (10 mm apart). The physical size of the pre-amplifier was the determining factor in the electrode spacing. This is done to improve the magnitude of the correlation coefficient. The width of the electrode affects the bandwidth of the sensor signal with narrower width electrodes having a wider bandwidth. For this reason the electrodes in the current design were kept as narrow as possible (1 mm) [54]. The length of the electrodes governs the number of points that can be used to determine the particle velocity and concentration profile. The primary factor in determining the length of electrodes is the physical size of the signal conditioning circuits for each pair of electrodes. For a 50 mm bore pipe the maximum number of elements in the sensor array were five pairs of electrostatic sensors with each electrode having a length of 8 mm (with a 2 mm gap between each of the elements).

3.4.3 Design of the Sensor Mounting Spool

A custom sensor mounting spool was constructed to allow the sensor array to be mounted on the laboratory scale test rig. The sensor mounting spool has a pipe bore of 50 mm which is compatible with both the negative and positive pressure test rigs. The sensor mounting spool is capable of rotating the sensor array around the cross sectional axis of the pipe as shown in Fig. 3.5. Several parts of the sensor mounting spool were constructed from Nylon using a laser sintering 3D printer. This was done to ensure a tight seal between the sensor array and the mounting spool.

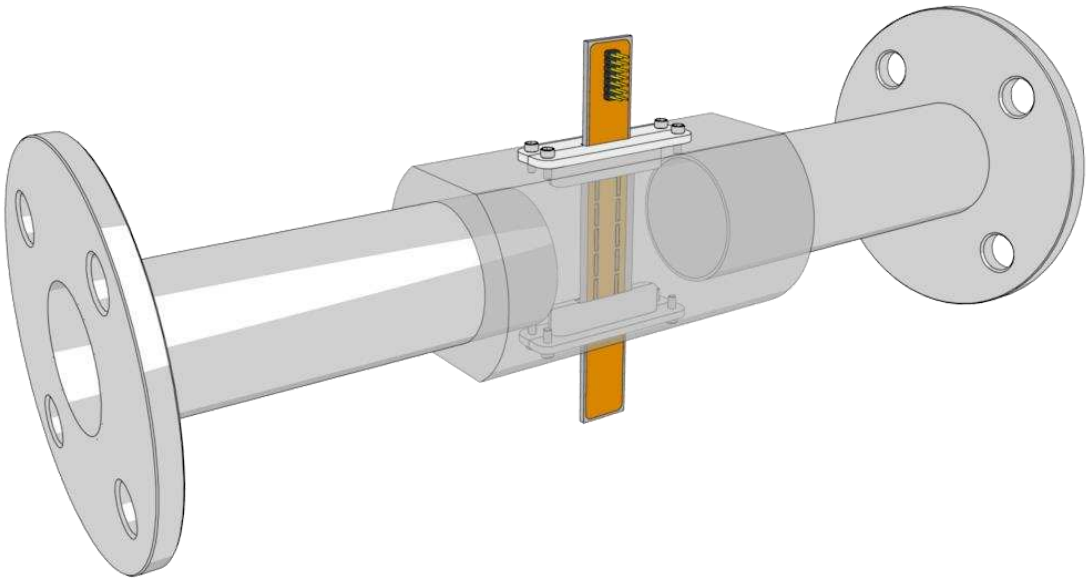

Fig. 3.5 Illustration of the electrostatic sensor array mounted inside the custom pipe spool

3.5 Design of the Electronic Hardware

Since the electrostatic charge inducted on the sensor electrodes is so weak (in the region of nA) a special signal conditioning circuit is required to amplify the signal to a usable level. The signal conditioning circuit consists of a pre-amplifier, a variable secondary amplifier and a low pass filter. Since the electrostatic signal from the electrodes is so weak the pre-amplifier is constructed close to the sensing electrodes in the sensor blade as shown in Fig. 3.6. Two stages of amplification are used for amplifying the signal from the electrodes since a single stage would require a large feedback resistor (100MΩ). Furthermore, another advantage of a two stage amplification process is that the secondary amplifier can be configured to have a variable gain which would improve the sensors adaptability.

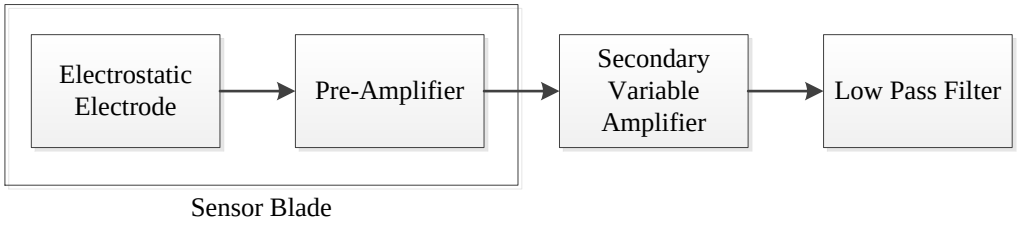

Fig. 3.6 Block diagram of the signal conditioning circuit for the electrostatic sensor

3.5.1 Design of the Pre-Amplifier

In order to convert the electrostatic charge detected on the electrode to a usable voltage signal, a current to voltage converter is used. The current to voltage converter uses the AD8601 operational amplifier (op-amp) configuration (Fig. 3.7). The AD8601 op-amp by ANALOG Devices was chosen because [84]:

- Availability in single (AD8601), dual (AD8602) and quad (AD8604) packages allowing an increase in the component density of the circuits
- Single supply operation (removes the need for dual rail power supply)
- Wide bandwidth (8 MHz)
- Fast slew rate (5V/μs)
- Low offset voltage (500 μV Max)

The relationship between the input current and the output voltage signal is [7]:

$$V_{out} = V_{ref} - I_{in}\, R_f \tag{3.1}$$

The feedback capacitor C_f in parallel with R_f is used to ensure closed-loop stability of the amplifier [7]. Since the ADC used for digitisation can only accept positive input voltages, V_{ref} (VDD/2) is used to bias the pre-amplifier between 0V and VDD (3.3V).

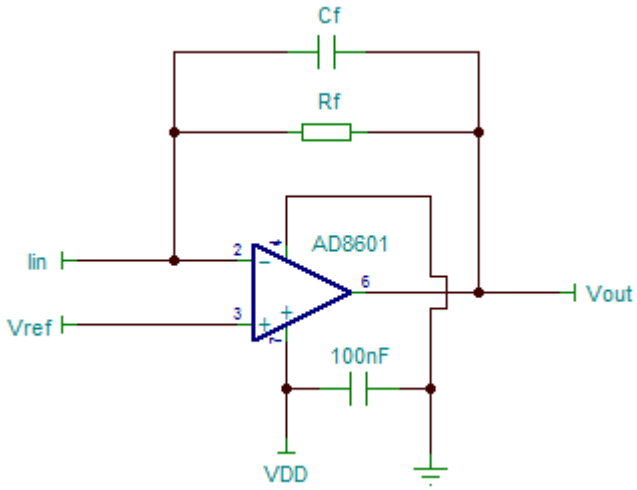

Fig. 3.7 Schematic design of the current to voltage pre-amplifier using an AD8601 operational amplifier

The conventional design for a current to voltage converter using an op-amp configuration, as shown in Fig. 3.7, uses a high resistor value for R_f for small current applications. However, high resistor values for R_f will decrease the accuracy of the output signal due to temperature drift error. Moreover using large resistor values for R_f would affect the stability of the circuit. Nevertheless the sensitivity of the current to voltage converter can be increased without using a high value resistor for R_f by using a resistive "T" network as shown in Fig. 3.8; however using a resistive "T" network may cause an increase in offset and noise gain [85].

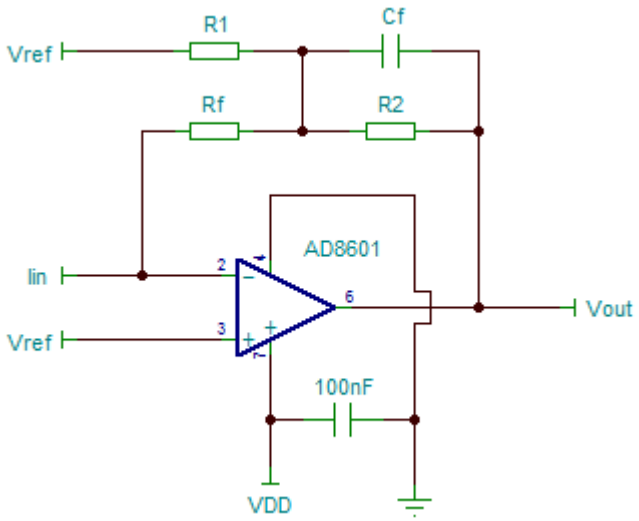

Fig. 3.8 Schematic design of the current to voltage pre-amplifier using a resistive "T" network using an AD8601 operational amplifier

The relationship between the input current and output voltage for the resistive "T" network is express as [85]:

$$V_{out} = V_{ref} - I_{in}\left(R_2 + R_f + \frac{R_2 R_f}{R_1}\right) \tag{3.2}$$

Due to the low particle concentrations in a dilute phase flow and the small surface area of the electrodes, the pre-amplifier requires a high scaling factor to make the pre-amplifier sensitive enough to detect the particle flow. Using resistor values of 2 kΩ for R_1 and 200kΩ R_2 and R_f creates a scaling factor equivalent of approximately 20MΩ. However the addition of two extra resistors in the pre-amplifier will require smaller surface mount (SMD) components to be used in the construction of the pre-amplifier due to space constraints.

3.5.2 Design of the Variable Secondary Amplifier

The output signal from the pre-amplifier will still be in the region of millivolts so the output signal will not make full use of the whole range of the ADC. For this reason, a secondary amplifier is required to amplify the signal to a sufficient magnitude. Since the magnitude of the electrostatic signal is dependent on factors such as: what sort of

pulverised material is under test; the time particles have had to charge; and particle size, the secondary amplifier has an adjustable gain to increase its durability over different experimental conditions. The secondary amplifier is an op-amp in a non-inverting configuration as shown in Fig. 3.9 using an AD8601 op-amp [85].

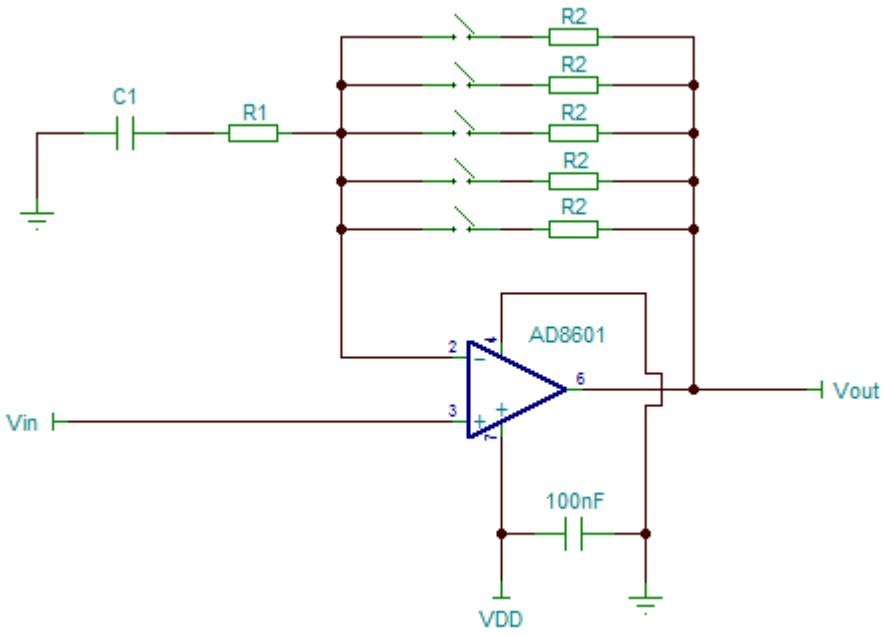

Fig. 3.9 Schematic design of the variable AC coupled non-inverting amplifier using an AD8601 operational amplifier

Since the output of the pre-amplifier has a DC component (V_{ref}) the secondary amplifier is AC coupled to prevent the DC component being amplified and causing saturation. The output voltage of the secondary amplifier is calculated using the equation [85]:

$$V_{out} = V_{ref} + V_{in}\left(1 + \frac{R_2}{R_1}\right) \tag{3.3}$$

The secondary amplifier gain is controlled via jumper pins that select different values of R_2. R_2 was selected as the variable resistor rather than R_1 since the value of R_1 is used to determine the closed-loop upper cut off frequency (f_c) of the amplifier which is calculated using [86]:

$$f_c = \frac{1}{2\,\pi\,R_1\,C_1} \tag{3.4}$$

Additionally, changing the value of R_1 would change the cut off frequency of the amplifier as well as the gain. In order to ensure the maximum frequency response for the secondary amplifier the value of f_c was set as close to DC as possible with C_1 being set to 22 μf and R_1 being set to 15 kΩ the value of f_c achieved was approximately 0.5 Hz.

3.5.3 Design of the Anti-Aliasing Low-Pass Filter

Since the cross-correlation method is being used to determine the particle velocity it is essential that the signals from the electrostatic sensors contain as little noise as possible. For this reason, a second order Sallen-Key low pass filter was used to remove high frequency noise from the sensor output signals. The use of the Sallen-Key low-pass filter also provides anti-aliasing for the output signal. Fig. 3.10 shows the schematic diagram of the Sallen-Key low-pass filter.

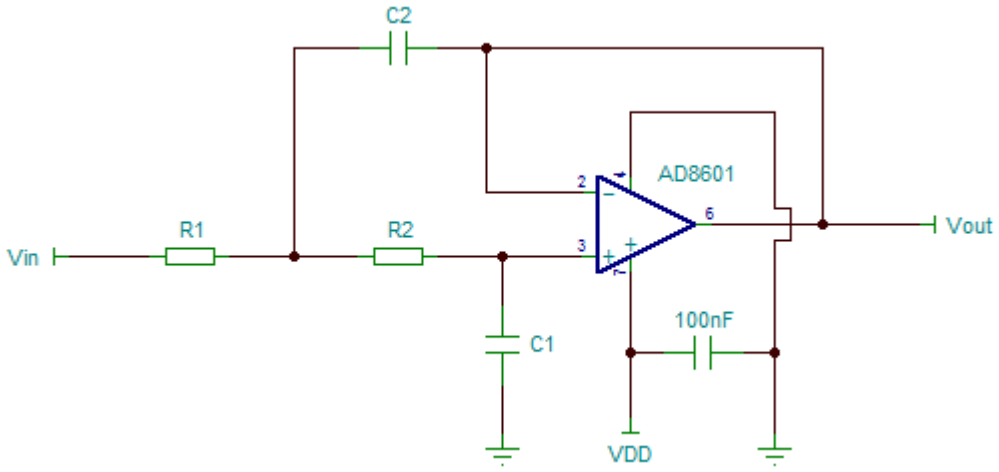

Fig. 3.10 Schematic design of the second order Sallen-Key low pass filter using an AD8601 operational amplifier

The cut-off frequency (f_c) for the Sallen-Key filter is determined by [87]:

$$f_c = \frac{1}{2\,\pi\,R\,C\,\sqrt{mn}} \tag{3.5}$$

Where mn is assumed to be set to 1 for unity gain. Previous work carried out using electrostatic sensors used a cut-off frequency of 15 kHz [88]. The values for R_1 and R_2 are set at 47 kΩ and the values for C_1 and C_2 are set at 220 pF giving a cut-off frequency of approximately 15 kHz.

3.5.4 Electrostatic Protection

As in previous work [88] a BZA408B quadruple bidirectional ESD transient voltage suppressor is used to protect the circuit from any voltage surges caused by electrostatic discharges from the particles [89]. Each of the upstream/downstream electrostatic electrodes is connected to the input pins on a BZA408B.

3.5.5 Design of the V_{ref} Input Circuit

In order to bias the pre-amp to VDD/2 a reference voltage (V_{ref}) needs to be generated. The reference voltage is generated using a simple resistive voltage divider network tapped off VDD with the output determined by:

$$V_{ref} = \frac{R_2}{R_1 + R_2} VDD \tag{3.6}$$

The resistors used in the voltage divider are high tolerance resistors (+-0.5%) and are matched during circuit construction. The schematic diagram for the V_{ref} circuit is shown in Fig. 3.11. The V_{ref} output has to be as noise free as possible to ensure that it does not create additional noise in the sensor system. Capacitors C_1 and C_2 are used to eliminate power supply (VDD) pick-up noise. An op-amp (AD8601) is connected in a voltage follower configuration on the output of the voltage divider network. This is used to ensure a stable output voltage and remove any cross-coupling. The use of an op-amp also allows higher values of resistors to be used in the voltage divider network to reduce power consumption.

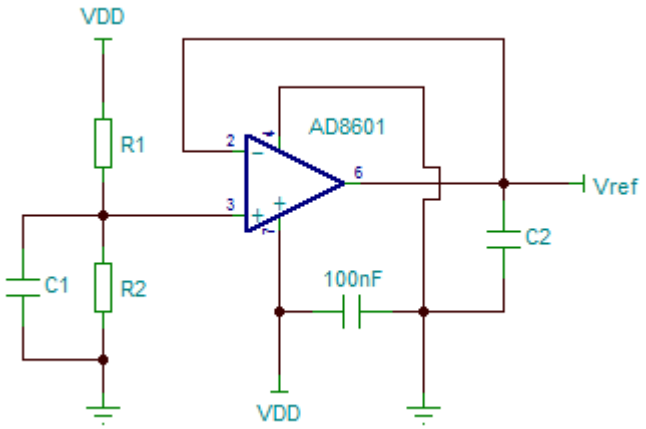

Fig. 3.11 Schematic design of the voltage divider circuit used to generate V_{ref} with an AD8601 operational amplifier in a voltage follower configuration

3.5.6 Design of the Power Supply Circuit

The power supply for all parts of the signal conditioning circuit runs on a common 3.3V supply which was chosen since the op-amp's (AD8601) supply voltage is 2.7-5.5V. The input voltage is 12V DC since this is the supply used to power the microcontroller. However the voltage between 12V and 3.3V requires a two stage voltage regulator configuration as shown in Fig. 3.12. The two stage power supply also allows both 3.3V and 5V components to be powered.

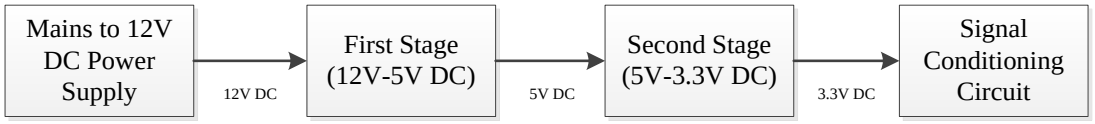

Fig. 3.12 Block diagram of the multi stage power supply unit

The voltage regulator used for the first stage (12V-5V) is the SPX3819 voltage regulator by EXAR. This voltage regulator was chosen because [90]:

- Low output noise (40µV)
- High Accuracy (less than 1%)
- Available in fixed output values

To ensure low noise operation for the output voltage a 10 pF capacitor is connected between the bypass pin (pin 4) and ground as shown in schematic in Fig. 3.13.

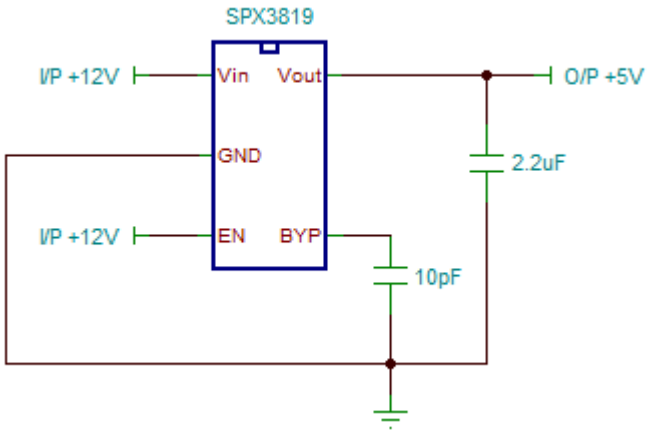

Fig. 3.13 Schematic design of the 12V-5V DC power supply using the SPX3819 voltage regulator

The second stage voltage regulator (5V-3.3V) uses the SP6205 voltage regulator from EXAR. This voltage regulator was chosen because [91]:

- Low output noise (12μV)
- Stable output voltage
- Available in fixed output values

To ensure low noise operation for the output voltage a 10 pF capacitor is connected between the bypass pin (pin 4) and ground as shown in schematic in Fig. 3.14.

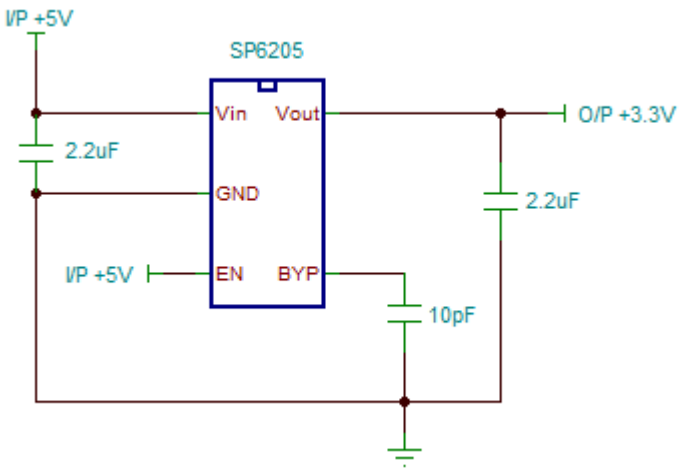

Fig. 3.14 Schematic design of the 12V-5V DC power supply using the SP6205 voltage regulator

3.5.7 Design of the Analogue Multiplexer

In order to maximise hardware resources an analogue multiplexer (MUX) controlled by the microcontroller is required. This allows the microcontroller to select each element (pair of upstream and downstream electrodes) of the electrostatic sensor array. The chosen analogue MUX was the ADG707 by ANALOG DEVICES. This analogue MUX was selected since [92]:

- 1.8V-5.5V supply voltage
- Low internal resistance (2.5Ω initial 0.5Ω constant)
- Fast switching time (40nS)

The ADG707 is also a dual analogue MUX meaning that for each address the microcontroller selects a pair of inputs as shown in Fig. 3.15; this improves resource management for the microcontroller.

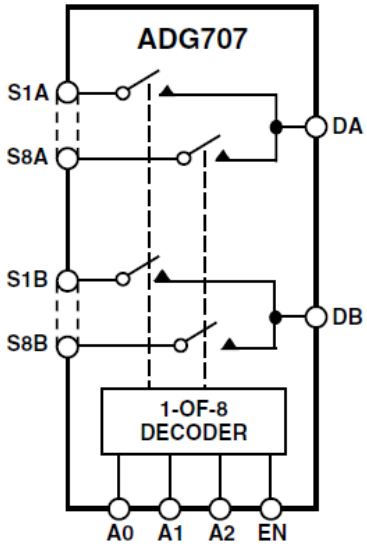

Fig. 3.15 Diagram of the ADG707 duel analogue multiplexer [92]

Table 3.1 shows the truth table for each switch pair on the ADG707 analogue MUX. The software for controlling the analogue MUX is embedded into the microcontroller (pin 21 = EN, pin 22 = A0, pin 23 = A1 and pin 24 = A2 on the MBED microcontroller). However, for the current design only pairs 1-5 are used since the

electrostatic sensor array only has five elements for a 50 mm bore pipe (this can be increased for larger bore pipes).

Table 3.1

ADG707 Truth Table

A2	A1	A0	EN	ON Switch Pair
X	X	X	0	NONE
0	0	0	1	1
0	0	1	1	2
0	1	0	1	3
0	1	1	1	4
1	0	0	1	5
1	0	1	1	6
1	1	0	1	7
1	1	1	1	8

X = Don't Care

3.5.8 ADC Implementation

In order to digitise the analogue signal from the electrostatic sensors to perform the cross correlation, an ADC is required. The two main factors in the selection of an ADC are the resolution and the sampling rate. The resolution has to be suitably high enough so that minute changes in the output signal from the electrostatic sensor can be detected, and the sampling rate has to be sufficient so as not to cause aliasing on the digitised signal (at least twice the highest frequency 30 kHz).

The original design used the inbuilt ADC on the MBED microcontroller which has a 12-bit resolution [93]. However initial trials showed that the internal ADC only had a sampling rate of approximately 27 kHz which would be below the requirement of twice the highest frequency. Using modified software code to call the analogue conversion function [94], the sampling rate was able to be increased to approximately 70 kHz per channel; however the digitised signal suffers from voltage spikes. Fig. 3.16 illustrates the voltage spikes on ADC with a constant reference voltage of 1.65V as an input.

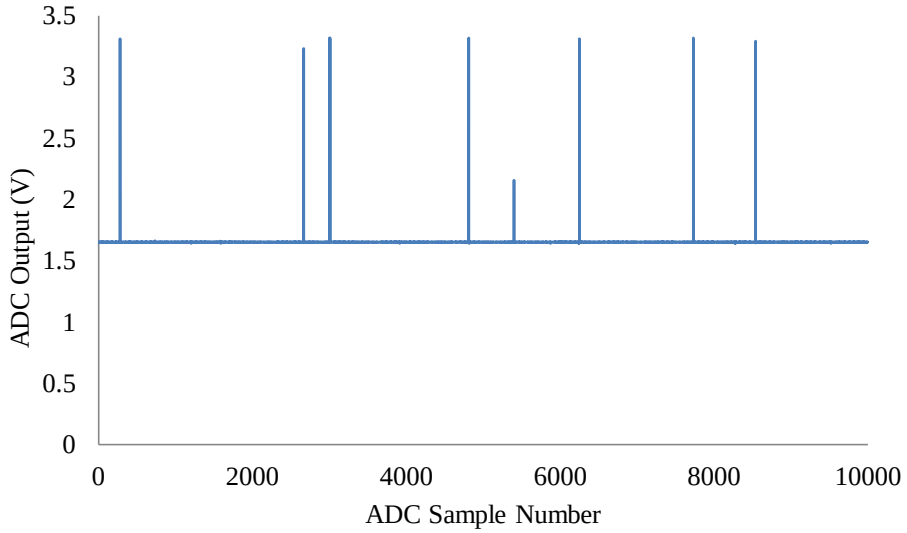

Fig. 3.16 Internal MBED ADC readings showing voltage spikes (with only V_{ref})

Since the cross correlation method is used to determine particle velocity the presence of such voltage spikes would affect the quality and similarity of the signals. The presence of the voltage spikes has been documented on the MBED support website which gave advice regarding reducing voltage spikes by grounding unused analogue input pins [95]. This method did reduce the number of voltage spikes but they still occurred. Consequently the internal ADC on the MBED microcontroller was unsuitable for digitisation of the sensor array output signals.

The solution was to use an external ADC chip interfaced with the MBED microcontroller. The selected external ADC was the AD7490 by ANALOG DEVICES. This external ADC chip was selected because [96]:

- 12-bit resolution
- Up to 1 MHz sampling rate (at 5V supply)
- Sampling rate is controlled by the clock on the SPI interface enabling sampling rate to be controlled through software

Using a modified open source library [97] for the MBED microcontroller a sampling rate of 150 kHz (10 times the highest frequency) per channel was achieved. Unlike the

internal MBED ADC, the digitised signal from the AD7490 did not suffer from voltage spikes. Only 2 of the 16 channels of the AD7490 are used for the digitisation of the upstream and downstream signals from the electrostatic sensors with all unused inputs grounded to reduce noise. The AD7490 is interfaced with the MBED microcontroller through the SPI port on pins 11, 12 and 13.

However the AD7490 has the disadvantage that its analogue signal input range is from 0-2.5V and the analogue signal from the electrostatic sensor signal conditioning circuits is 0-3.3V. The solution to this was to use a voltage divider resistor network to scale down the signal from the electrostatic sensor conditioning circuit as shown in the schematic in Fig. 3.17. An op-amp in a voltage follower configuration is placed between the voltage divider and the ADC to prevent the resistance in the divider network affecting the ADC.

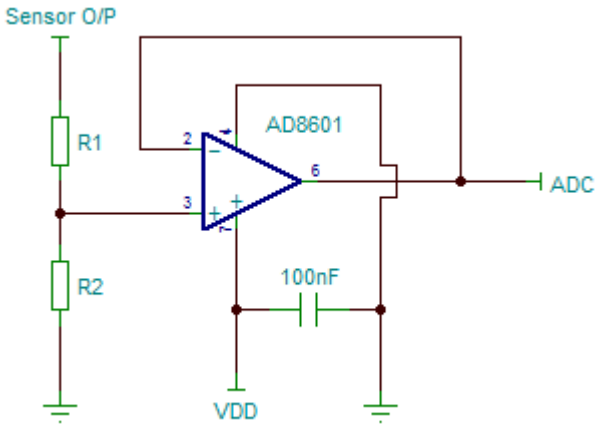

Fig. 3.17 Schematic diagram of the ADC input scaling circuit

3.5.9 Design of the Complete Signal Conditioning Circuit

The original design for the signal conditioning circuit on the electrostatic sensor array was to have the analogue MUX placed directly after the five pairs of pre-amplifiers as shown in Fig. 3.18. This was done since having the analogue MUX after the pre-amplifiers would reduce the amount of electronics needed to construct the complete signal conditioning circuit.

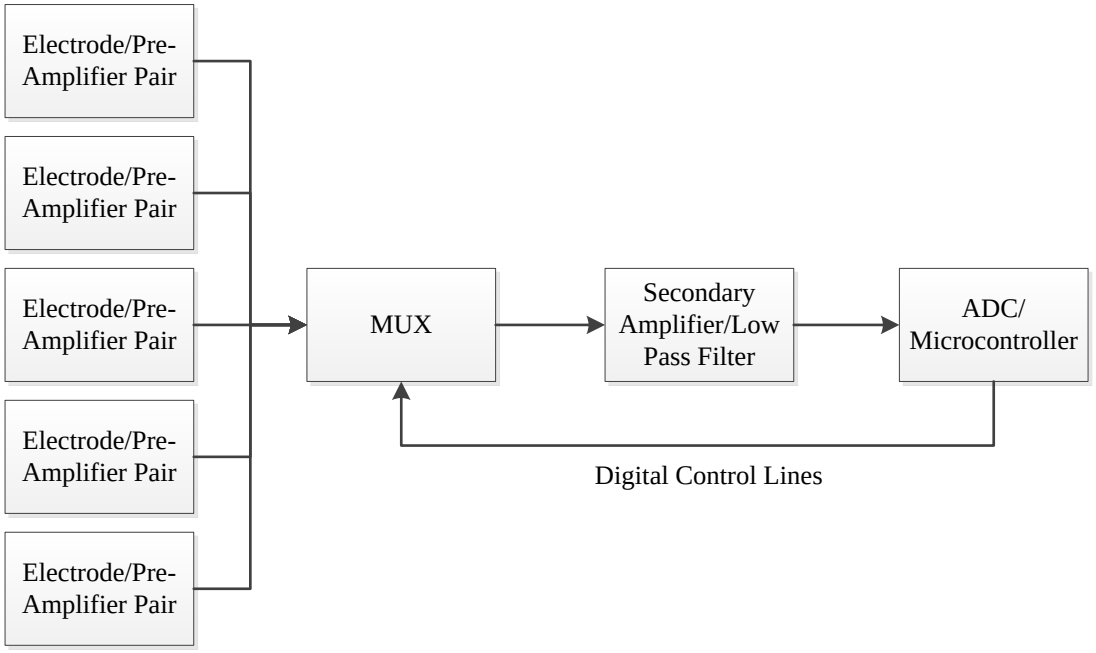

Fig. 3.18 Block diagram of the complete electrostatic with signal duel secondary amplifiers

Trials were carried out using the design of having the analogue MUX directly after the pre-amplifiers and it was found that output signal from the signal conditioning circuit would saturate for several seconds when switching of the analogue MUX occurred before stabilising to V_{ref}. The cause of this was due to the AC coupling capacitors in the variable secondary amplifiers. Since the capacitor charging time (t) is governed by [13]:

$$t = -R\ C\ Ln\left(1 - \frac{V_{ref}}{V_{in}}\right) \tag{3.7}$$

Where V_{in} is the input signal voltage to the secondary amplifier. Consequently until the AC coupling capacitor was charged to the level of V_{ref} the variable secondary amplifier would behave like a DC coupled non-inverting amplifier and amplify the DC reference voltage causing saturation on the output. A solution to this problem was first implemented in the software on the microcontroller where a delay was placed between switching the MUX and performing the ADC function. However, since the AC coupling capacitors on the variable secondary amplifiers are set at 22 μF, a delay of approximately 2.5 seconds had to implement in the software. The consequences of this

meant that to perform a single velocity profile reading across the diameter would take 12.5 seconds (not including time to perform the cross correlation operation for each velocity measurement). This was deemed unacceptable.

The solution was to place the analogue MUX after the low-pass filter stage as shown in the block diagram in Fig. 3.19. This solution has the disadvantage of requiring more signal conditioning circuitry. Nevertheless the main advantage of using this configuration is that the only limitation on the time taken to perform the velocity reading for the whole diameter of the pipe is the time for the microcontroller to perform the correlation coefficient operation.

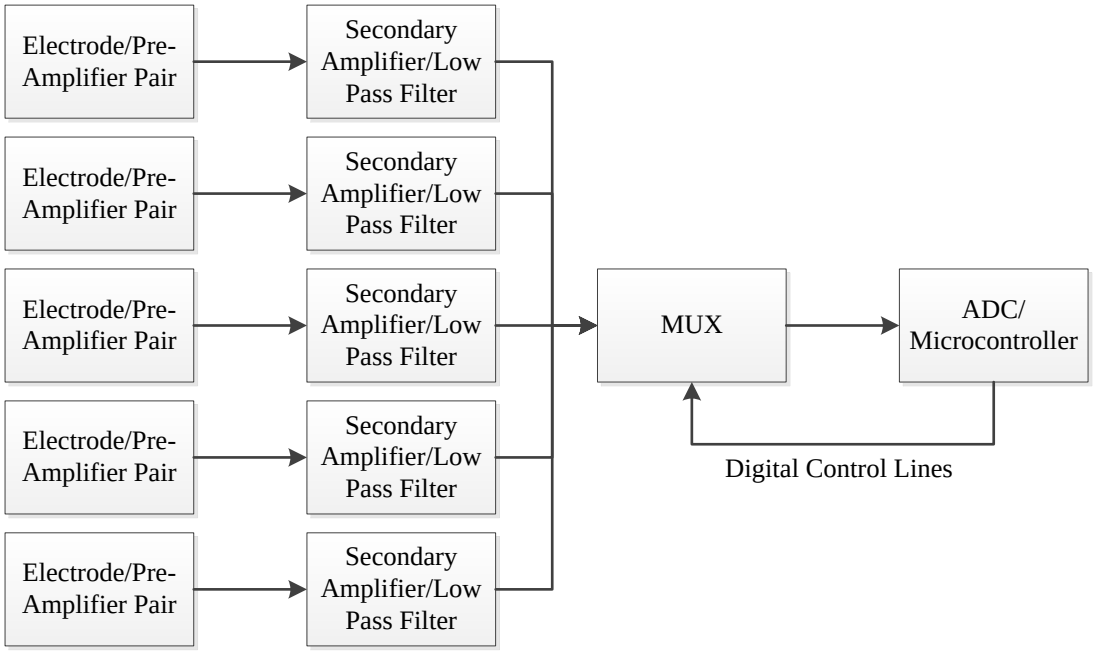

Fig. 3.19 Block diagram of the final design of the electrostatic sensor array system

3.5.10 Microcontroller Selection

The purpose of the microcontroller is to perform the cross-correlation to determine the particle velocity and the r.m.s. calculation to determine particle concentration. The MBED NXP LPC1768 microcontroller using the 32-bit ARM Cortex-M3 chip was selected because [98]:

- The 32-bit ARM Cortex-M3 chip runs at 96 MHz allowing it to perform the cross-correlation calculation.
- 32 KB of RAM which is sufficient to perform the cross-correlation calculation using 1024 samples on both upstream and downstream electrodes.

The MBED microcontroller was also selected because of its number of different interfaces which will allow the MBED to interface with external devices such as ADCs using the SPI line and analogue MUXs as shown in Fig. 3.20.

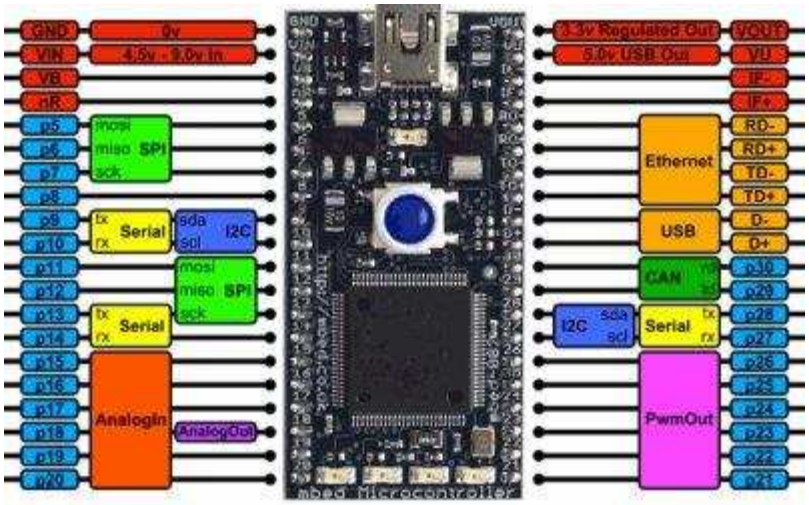

Fig. 3.20 Interface diagram of the MBED NXP LPC1768 microcontroller [98]

The MBED microcontroller outputs the data to either a PC via a USB serial line or data can be stored on an SD card.

3.6 Embedded Software

All data processing software (calculating velocity via the cross-correlation method and calculating the r.m.s charge level) is embedded into the MBED microcontroller and outputs the relevant data (Particle velocity, r.m.s charge level and correlation coefficient) for each element in the array via a USB serial line. Using the current MBED microcontroller, the particle velocity for each element of the array can be carried out in

approximately 100ms (so the sensor has a refresh rate of 500ms for all five elements of the array). Full data logging can be carried out (recording of the upstream/downstream electrode sensor output and the correlation coefficient values) with the data being stored on an SD card; however this significantly reduces the sensor refresh rate due to the time taken to record the data to the SD card.

3.6.1 Embedded Software Operation

Fig. 3.21 illustrates the operation of the embedded software used for data sampling of the upstream/downstream sensor outputs and the data processing software. Once the microcontroller is activated it:

- Selects the element of the array via the address on the MUX control lines (pin 21 = EN, pin 22 = A0, pin 23 = A1 and pin 24 = A2).
- The external ADC is then configured (selects analogue input pins on the external ADC).
- Once the ADC is configured the upstream and downstream sensor outputs are sampled with 1024 samples taken from both upstream and downstream sensor outputs. During the sampling process the time period between each sample is recorded using the internal timer on the MBED as a reference.
- Once the sampling process is complete the particle velocity is calculated using the cross-correlation method and particle concentration by calculating the r.m.s of the sampled data.
- The data is then output via the USB serial communications line or, for full data collection, saved to a SD card.
- The next element in the array is selected by the MUX.
- The system will continue looping until a sufficient number of velocity/concentration measurements have been taken.

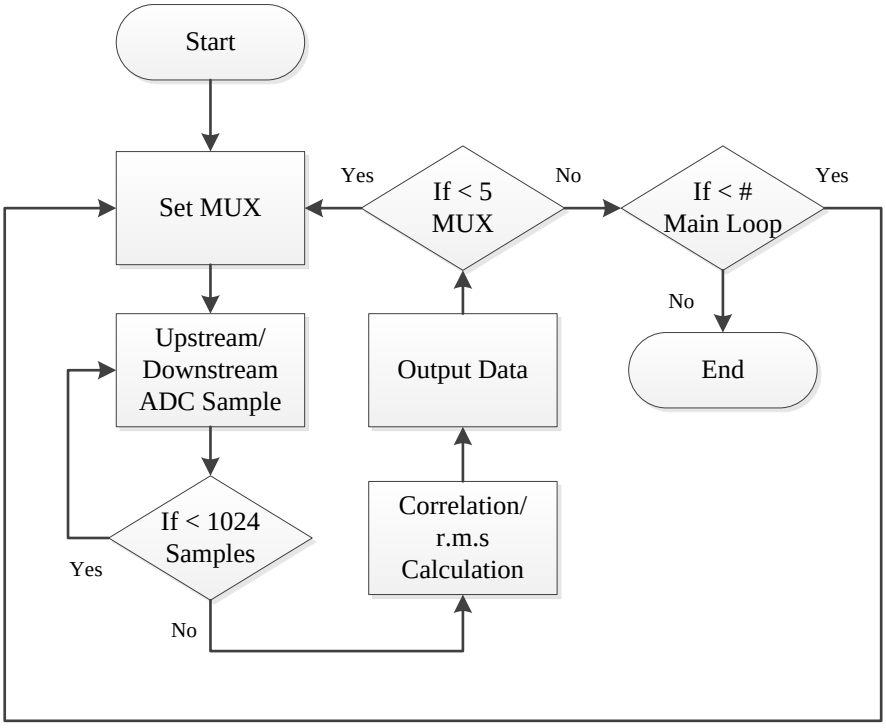

Fig. 3.21 Software flow chart for determining particle velocity and concentration using the electrostatic sensor array

3.6.2 Cross-Correlation Algorithm

To determine the particle velocity the cross-correlation method is used to determine the delay time between the upstream and downstream signals. Since the distance between the upstream and downstream electrodes is known the particle velocity V_c can be calculated by:

$$V_c = \frac{L}{\tau_m} \tag{3.8}$$

Where L is the spacing between the upstream and downstream electrodes and τ_m is the time difference between the upstream and downstream signals. The delay τ_m between the two signals is determined from the location of the dominant peak in the cross correlation function [57]. The normalised correlation function is determined by [99]:

$$Rxy[m] = \frac{\sum_{n=1}^{N} x[n]y[n+m]}{\sqrt{\sum_{n=1}^{N/2} x[n]^2 \ \sum_{n=1}^{N/2} y[n]^2}} \tag{3.9}$$

Where x[n] and y[n] are the digitised signals from the upstream and downstream electrodes respectively. The cross correlation function is determined by using 1024 samples taken on both the upstream and downstream electrodes (this number of samples was the maximum able to be utilised using the MBED's internal memory). The correlation coefficient (the dominant peak of the correlation function) is determined by a software algorithm illustrated in Fig. 3.22. From the location of the dominant peak the delay in the time domain is determined by the ADC sampling period (which was determined using the MBED's internal timer function).

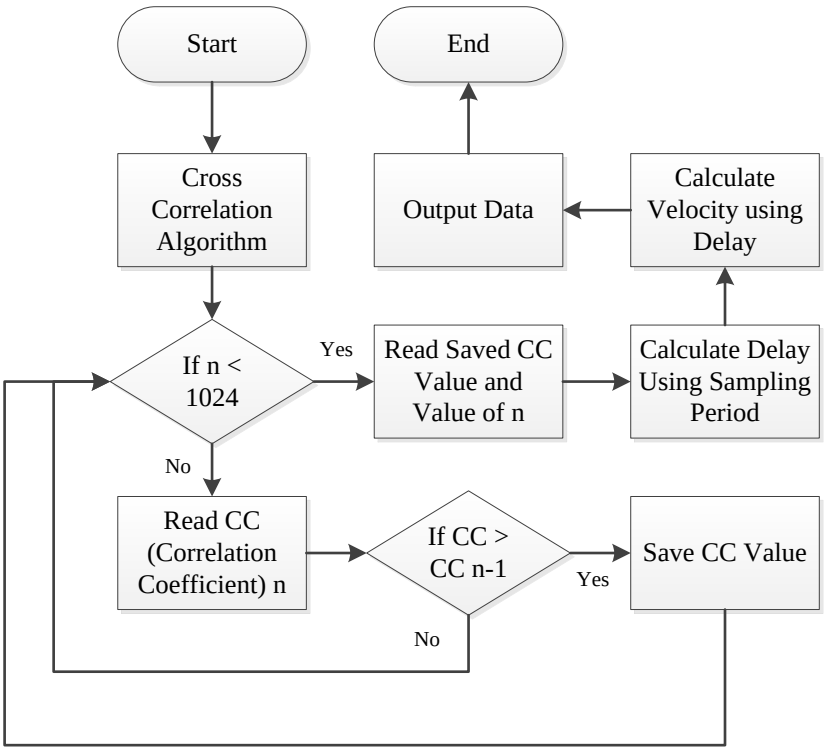

Fig. 3.22 Flow chart of the embedded software used to determine particle velocity using the position of the correlation coefficient

3.6.3 Algorithm for R.M.S Particle Concentration

Since the charged particles is random and can have either a positive or negative charge [56] the particle concentration is determined and represented by the magnitude of the r.m.s. charge level of the electrostatic signal detected by the electrostatic sensor.

$$V_{rms} = \sqrt{\frac{\sum_{n=1}^{N} x[n]^2}{N}} \tag{3.10}$$

Where x is the signal from the electrostatic sensor electrode, n is the sample number and N is the total number of samples.

3.7 Summary

All aspect of the design of the electrostatic sensor array designed to measure the particle velocity and concentration profiles of pneumatically conveyed bulk solids have been presented in this chapter. This includes: the development of the structure of the electrostatic sensor array, the design of the electrostatic sensing electrodes, design of the custom pipe spool to allow the electrostatic sensor array to be mounted on a laboratory scale test rig, all designs of the signal conditioning circuits, the implementation of a high speed external ADC and the embedded digital signal processing used to determine the particle velocity (cross correlation software) and particle concentration (by measuring the magnitude of the r.m.s charge).

Chapter 4

Design and Implementation of the Piezoelectric Sensor Array

4.1 Introduction

This chapter will explain the concept and principle of the piezoelectric impact sensor array design. This chapter will also illustrate how the sensor array will have the novel feature allowing it to be capable of determining the particle concentration and particle size distribution profiles for the whole diameter of the pipe in a complex multi-phase flow. All aspects of the sensor hardware design will be covered including: the structure and shape of the sensor array; the design and configuration of the impact sensor; justification of the use of piezoelectric film transducers, design of anti-vibration shielding for non-active areas of the sensor array (which will allow the sensor array to have a very local sensing area as well as reduce the chances of measurement errors caused by simultaneous particle impacts); signal conditioning circuit designs for the

piezoelectric transducers; digital selecting of each element of the sensor array; the use of an external high-speed analogue to digital converter (ADC) for digitisation of the impact sensor signals; the use of an embedded microcontroller for data logging of the impact data; and theoretical system modelling of the piezoelectric impact sensor. This chapter will also illustrate the need of another sensor technology such as an electrostatic sensor to independently measure the particle velocity in order to determine particle size through impact analysis. Both on-line and off-line experimental data using the piezoelectric sensor array will be presented in following chapters.

4.2 Piezoelectric Impact Sensor Principle

While particles are traveling in a pneumatic conveying system they have kinetic energy. The level of kinetic energy is determined by the particle velocity and the particle mass. When the moving particle collides with a fixed surface the kinetic energy is transferred to the fixed surface in the form of an impact force. Piezoelectric impact sensors work on the principle of using a piezoelectric transducer to measure the impact force. Piezoelectric materials are materials that output an electrical charge when mechanical stress is applied. The particle size distribution is determined by measuring the magnitude of the impact signal from the piezoelectric transduces. Using this method to determine the particle size, the particle velocity has to be independently measured and the particle's mechanical properties likewise have to be known, so conversely the only unknown variable is the particle's mass which can be determined using the impact signal magnitude. Particle concentration is determined by measuring the number of particle impact events. This would have the advantage that it would provide a true particle concentration measurement.

4.3 Concept of the Piezoelectric Impact Sensor Array

Much like previous work the piezoelectric impact sensor array is an invasive sensor design which is similar to previous work carried out using impact sensors to determine particle size and particle concentration in pneumatically conveyed solids [73]. Unlike previous impact sensor designs, however, the piezoelectric impact sensor array is separated into individual impact sensors spaced equally across the pipe diameter as shown in Fig. 4.1.

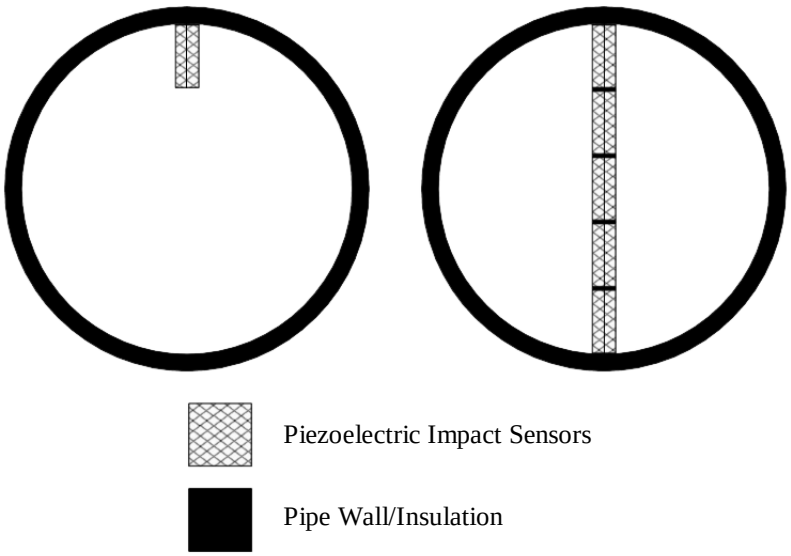

Fig. 4.1 Comparison of previous impact sensor design (left) and the piezoelectric impact sensor array concept (right)

The advantage of this sensor design is that piezoelectric impact sensor array will be capable of determining both the particle concentration and particle size distribution profiles for the whole diameter of the pipe. This will allow the complex flow characteristics associated with multi-phase flow (air/coal and air/coal/biomass) to be monitored as well as specific flow regimes such as roping.

4.4 Design of the Piezoelectric Impact Sensor Array

Since the piezoelectric impact sensor array is an invasive sensor design (it comes into contact with the particle flow), the effect of erosion caused by the particle flow needs to be taken into consideration. For this reason a mechanical interface (waveguide) would be placed between the particle flow and the piezoelectric transducer. Consequently the vibrations caused by a particle impact would be transferred through the waveguide into the piezoelectric transducer.

The first design of the piezoelectric impact sensor array was a blade design which would have five (to have conformity with the electrostatic sensor array) equally sized knife edge impact plate shaped waveguides placed across the diameter of the pipe. This design would have the piezoelectric transducer placed between the impact plate waveguide and a ridged back plate as shown in Fig. 4.2.

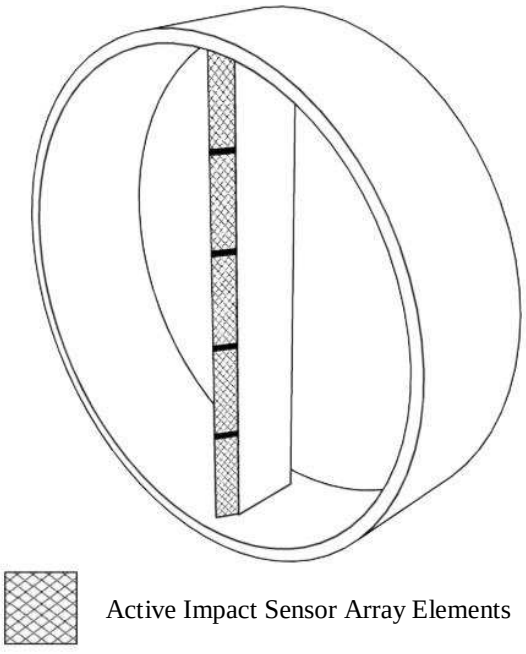

Fig. 4.2 First design of the particle piezoelectric impact sensor array

However, each element of the impact sensor array would have had a large active sensing area (6 x 8 mm) meaning that even in a dilute phase flow the chances of simultaneous impacts occurring and causing measurement errors would be high.

The solution to reducing the chances of simultaneous impacts was to reduce the active sensing area on each element of the piezoelectric impact sensor array. The final design for the piezoelectric impact sensor array was to have a 45° knife edge blade design with the vast majority of the sensor blades' cross sectional area non-active with narrow active waveguides protruding from the sensor blades' leading edge to create impact sensors, as shown in Fig. 4.3.

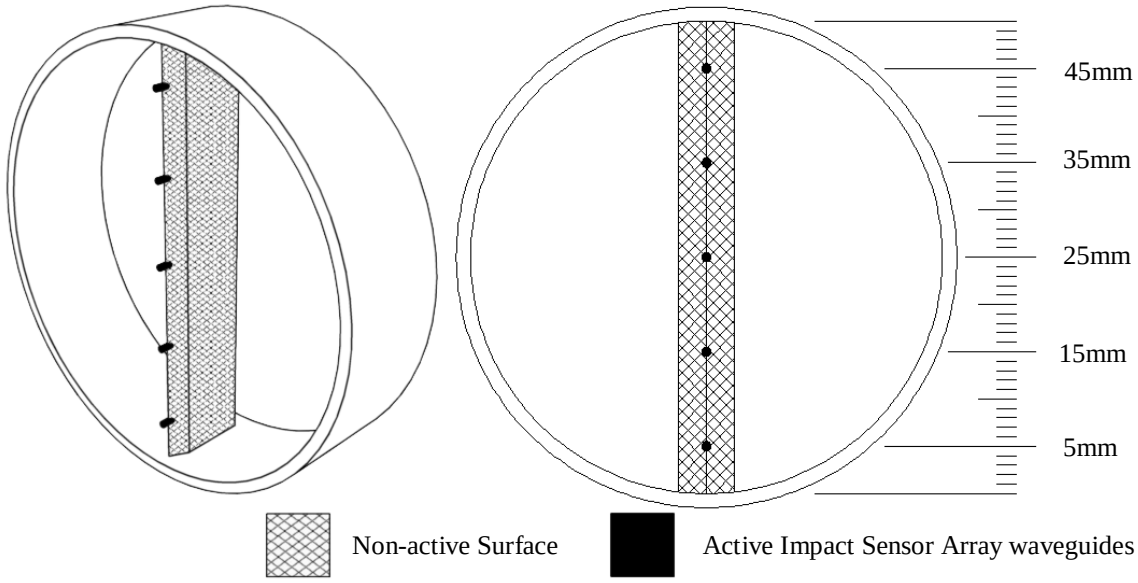

Fig. 4.3 Final design of the piezoelectric impact sensor array

For a 50 mm bore pipe five independent impact sensors are arranged across the diameter of the pipe. Each impact sensor is set 10 mm apart as illustrated in Fig. 4.3. This design of array was chosen since it conforms to the design of the electrostatic array. Each of the impact sensors has an active diameter of 1 mm (0.04% of the cross sectional area of a 50 mm bore pipe). The sensor array blade has a width of 6 mm which takes up approximately 15% of the cross sectional area of a 50 mm bore pipe. The diameter of

the waveguides was set to 1 m diameter to reduce the chances of simultaneous impacts as well as it reduced the thickness of the sensor blade.

4.4.1 PVDF Film

The piezoelectric material chosen for the piezoelectric transducer was polyvinylidene fluoride (PVDF) film. PVDF film was chosen for the piezoelectric transducer since it has the advantage of [100]:

- Wide frequency range 0.001 Hz to 10^9 Hz.
- High voltage output (10 times greater than piezo ceramics for the same force input).
- Highly flexible allowing it to be fabricated into unusual designs.

The PVDF transducer is fabricated by having a layer of PVDF film sandwiched between two metal surfaces. The metal surfaces are applied to the PVDF surface by evaporatively deposited metals such as copper, nickel, silver or gold with the metal layer being between 500 – 1000 Å thick [100]. The active area on the PVDF transducer is determined by where the metal surfaces overlap to form an electrode as shown in Fig. 4.4. These electrode shapes can be fabricated using chemical etching techniques [100].

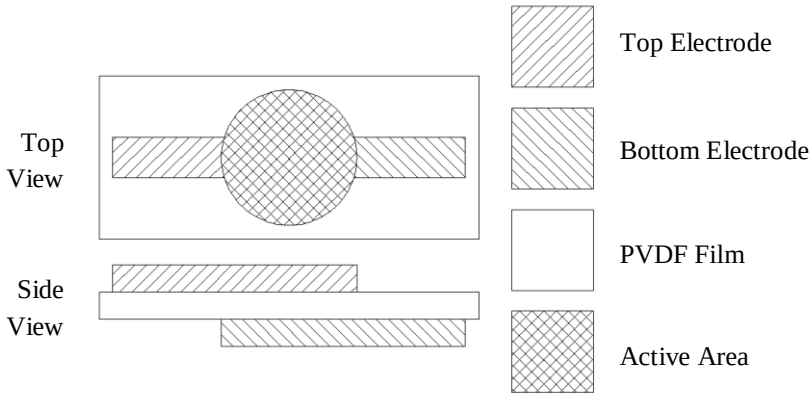

Fig. 4.4 Diagram of how a piezoelectric film transducer is formed

When stress is applied to the active area on the PVDF transducer the deformation changes the charge density of the material, this change causes a charge or voltage to be

generated between the two electrodes. The output charge or voltage is directly proportional to the magnitude and frequency of the applied stress [100].

PVDF film is anisotropic which means the charge or voltage output is dependent upon which axis the mechanical stress is applied as shown in Fig. 4.5. These piezo coefficients are most commonly used in either charge or voltage modes (d_{3n} or g_{3n} respectively).

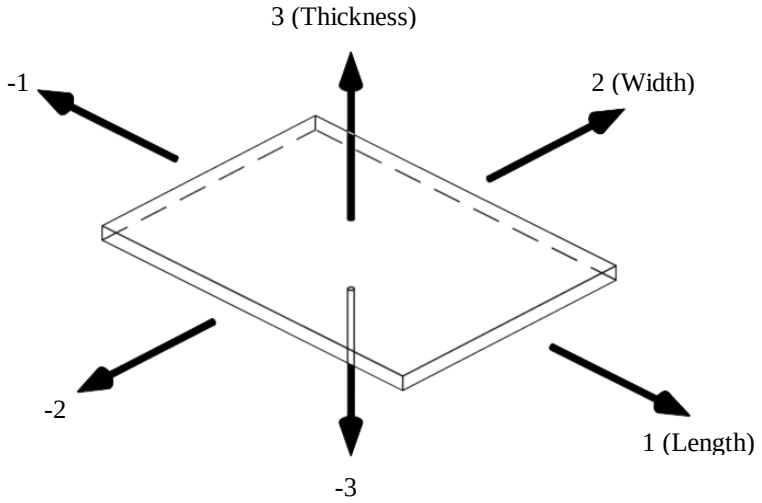

Fig. 4.5 Diagram of the numerical stress axes for PVDF film

The output of the PVDF film can be either charge or voltage. The output charge in charge mode is represented by [100]:

$$D = \frac{Q}{A} = d_{3n} F_n \tag{4.1}$$

Where D is the charge density developed, Q is the charge developed A is the conductive area of the electrodes, d_{3n} is the axis of the applied stress or strain and F_n is the applied stress in the specified direction. When configured in voltage mode the output voltage is represented by [100]:

$$V_o = g_{3n} X_n \ t_f \tag{4.2}$$

Where V_o is the output voltage of the PVDF film transducer, g_{3n} is the axis of the applied stress or strain, X_n is the applied stress in the specified direction and t_f is the thickness of the PVDF film.

4.4.2 Design of the Piezoelectric Transducer

The piezoelectric transducer used in the piezoelectric sensor array is a custom design that was constructed using 110 μm thick PVDF film with evaporatively deposited nickel copper alloy plating. The 110 μm thickness of PVDF film was chosen because the piezoelectric transducer will operate in one axis of stress (compressive stress on the thickness axis as expressed in Fig. 4.5). The nickel copper alloy plating was chosen since the alloy can be fabricated into electrodes via a chemical etching process using ferric chloride in the same way as a printed circuit board [100] (since the evaporatively deposited metal layer is only between 500 – 1000 Å thick the etching process only takes seconds to completely etch the electrodes). The active area of the piezoelectric transducer is 2.5 mm diameter as shown in Fig 4.6 with electrode leads etched on the top and bottom nickel copper alloy plating acting as tracts to the active area. The piezo transducer is insulated with a layer of silicone to prevent short circuiting between the electrode and waveguide. The silicone insulation also protects the delicate electrodes. The ends of the electrodes however are not insulated, thus enabling an interface for the piezoelectric transducer and the signal conditioning circuit to be created which is illustrated in Fig. 4.6.

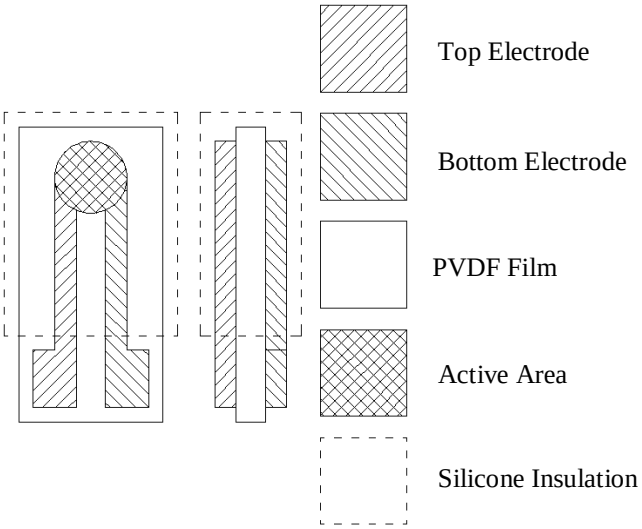

Fig. 4.6 Design of the custom piezoelectric film transducer used for the piezoelectric impact sensor array (not to scale)

4.4.3 Anti-vibration Shielding

In order to allow only selective parts of the piezoelectric impact sensor array to be active the majority of the leading edge of the sensor blade has to be shielded against vibrations caused by particle impacts. To do this, a variety of materials were used in a layered structure as shown in Fig. 4.7:

- The first layer (working from the front of the leading edge of the sensor blade) is the front impact plate, this plate is a 45° knife edge (to improve the aerodynamics of the sensor blade) constructed out of brass for ease of manufacture (for commercial designs this impact plate would be made of ceramic or ceramic coated steel for abrasion resistance).
- The second layer is a layer of rubber to attenuate the vibrations caused by particles impacting the front impact plate.
- The third layer is another brass plate, this plate has screw mountings that allow the first two layers to be fixed to the fifth nylon layer (the screw mountings are recessed inside the pipe spool housing so do not come into contact with the particle flow.

- The fourth layer is another layer of rubber for vibration attenuation.
- The fifth layer is used to mount layers 1 – 4 to the main aluminium sensor housing, the fifth layer is constructed from 3D printed nylon using the laser sintering method.

The waveguide passes through all layers of anti-vibration shielding and is isolated from the layers by an air gap of approximately 0.1 mm. The sides of the sensor array blade do not have as much anti-vibration shielding as the leading edge of the sensor blade since they are constructed out of printed circuit board. This does not cause a problem since particles will not be impacting the side of the sensor blade since they will be traveling in parallel to it.

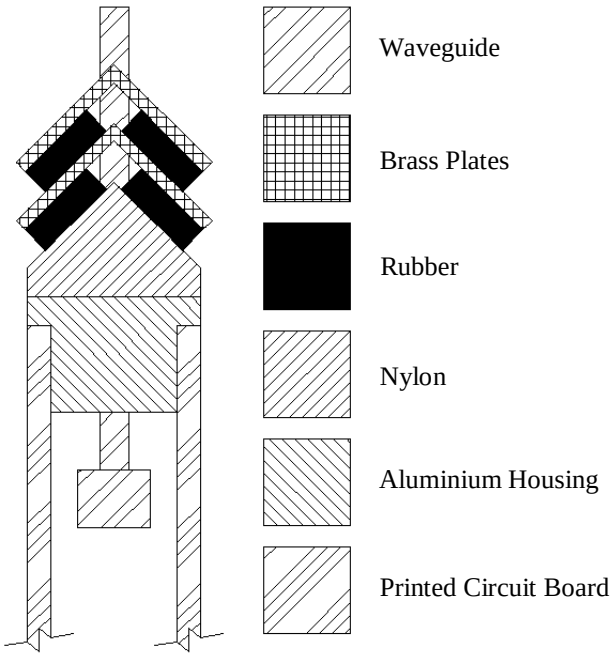

Fig. 4.7 Cutaway view of the piezoelectric impact sensor array showing the layers of anti-vibration shielding

4.4.4 Waveguide Design

The waveguides protrude from the leading edge of the sensor blade so particles impact the waveguide head on. The impact face of the waveguide is a flat surface to reduce the

complexity of the impact mechanics. The waveguides are machined from brass for convenience and ease of machining (for commercial designs the waveguides would be fabricated from hardened steel). The impact face of the waveguide is 1 mm diameter (if mounted inside a 50 mm bore pipe each impact face has the equivalent area of 0.04% of the pipe bore).

When the particles impact the waveguide the vibrations caused by the particle impacts travel along the waveguide into the piezoelectric transducer. The waveguide and piezoelectric transducer are fixed together using specialist adhesive for gluing silicone based rubbers.

The waveguides are assembled into the aluminium housing of the sensor blade using tight fitting rubber washers as shown in Fig. 4.8. These rubber washers restrict the axial movement of the waveguide restricting them to one dimension of vibration. The reason for this is to ensure that mechanical stress is only applied to the piezoelectric transducer in one axis (compressive stress on the thickness axis as expressed in Fig. 4.5. Each of the waveguides is 17 mm in length (from tip to the base where it is fixed to the piezoelectric film transducer) allowing it to pass through the leading edge anti vibration shielding. The waveguides protrude from the leading edge by 2 mm to form the active sensor area of each element.

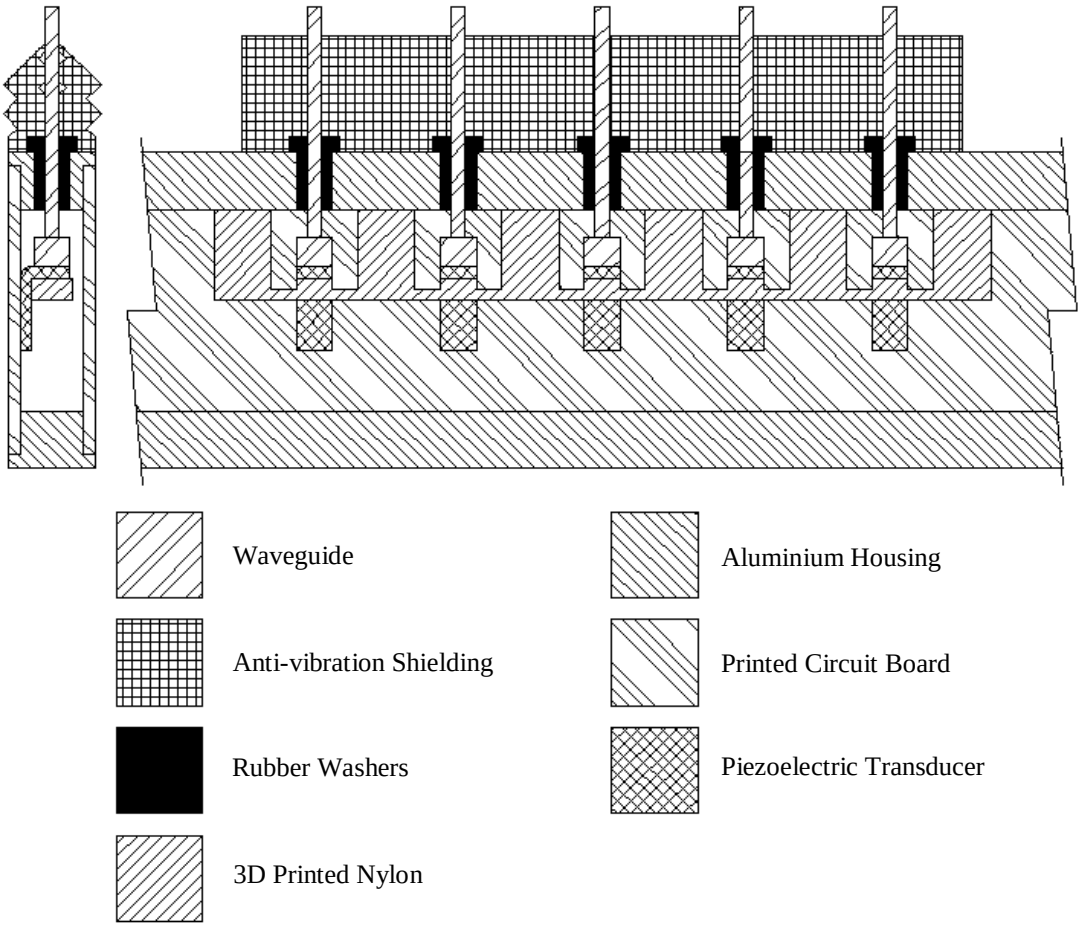

Fig. 4.8 Cutaway view of the piezoelectric impact sensor array showing the structure of the piezoelectric impact sensor array

4.4.5 Design of the Sensor Mounting Spool

A custom sensor mounting spool was constructed to allow the piezoelectric sensor array to be mounted on the laboratory scale test rig. The sensor mounting spool has a pipe bore of 50 mm which is compatible with both the negative and positive pressure test rigs. The sensor mounting spool is capable of rotating the sensor array around the cross sectional axis of the pipe as shown in Fig. 4.9. Several parts of the sensor mounting spool were constructed from Nylon using a laser sintering 3D printer. This was done to ensure a tight seal between the sensor array and the mounting spool.

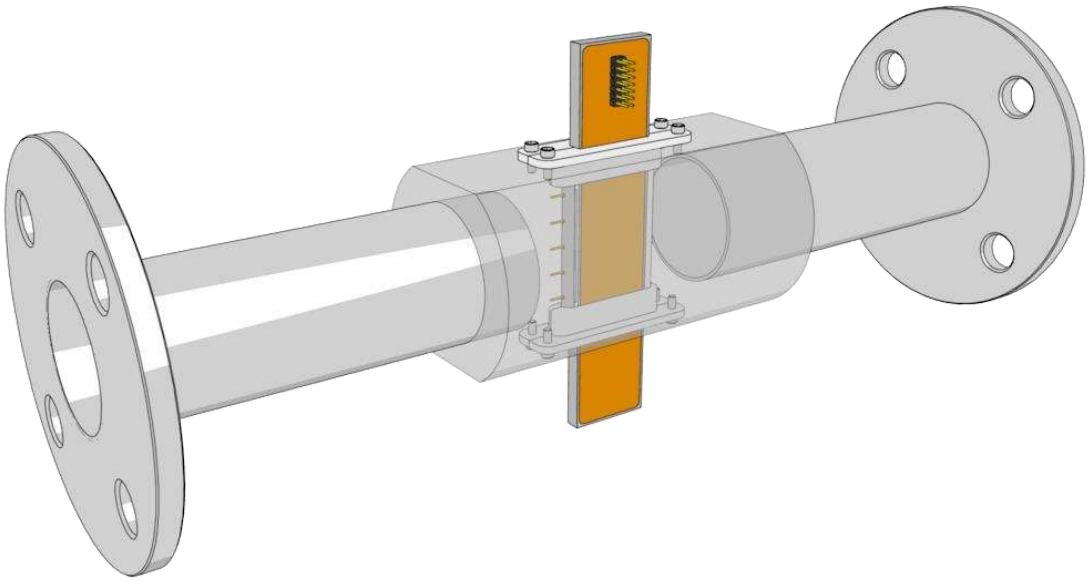

Fig. 4.9 Illustration of the piezoelectric impact sensor array mounted inside the custom pipe spool

4.4.6 Piezoelectric Transducer Interface

One of the main challenges in using custom fabricated piezoelectric film transducers is the method to mechanically/electronically interface them to the signal conditioning circuit (pre-amplifier). Some of the standard methods include [100]:

- **Rivets/eyelets**. This method uses a rivet or eyelet that is pressed through the piezoelectric film and in doing so makes a conductive contact with the evaporatively deposited metal layer and the rivet or eyelet is then attached to a wire. However; this method was not used because of space constraints inside the sensor blade housing.
- **Crimp connectors**. This uses a specialist crimp that is pressed through the piezoelectric film and makes a conductive contact with the evaporatively deposited metal layer. The crimps have solder tags for easy soldering to wires. This method was not used since the crimps would require a crimping tool that was financially uneconomical for the low number of piezoelectric transducers that would be fabricated.

- **Direct soldering**. This requires wires to be directly soldered to the evaporatively deposited metal layer. This is the simplest method; however the low melting temperature of the piezoelectric film makes this unadvisable.
- **Conductive transfer tape**. For this method conductive tape is affixed to the evaporatively deposited metal layer and a wire soldered to the conductive tape. The use of conductive tape is ideal for short term experimentation with piezoelectric film; however long term the adhesive on the tape degrades which made it unsuitable for use in the piezoelectric sensor array.
- **Conductive epoxy resin**. This process uses conductive epoxy resin to form the connection with the evaporatively deposited metal layer and a cable connector. This method was not used since the restricted space in the sensor array blade would make it difficult to control the placement of the epoxy resin.

The chosen method was to use a clamping system illustrated in Fig. 4.10. This method has the advantage of both creating a good electrical connection as well as a strong mechanical fixing to ensure the piezoelectric film transducer did not lose connectivity over time. The clamp surfaces are fabricated from printed circuit board using the copper layer as a conductive contact face to the evaporatively deposited metal layer. The clamp faces are compressed against the piezoelectric film using two M1.2 screws and nuts. The bottom printed circuit board (PCB) clamp is formed from one of the sensor blade's outer PCB walls (the advantage of this is that the pre-amplifier can be constructed very close to the piezoelectric transducer thus improving the signal to noise ratio). The compression screws are insulated from the conductive surfaces on the clamp to ensure they do not cause a short circuit and are countersunk into the PCB to reduce the width of the sensor blade.

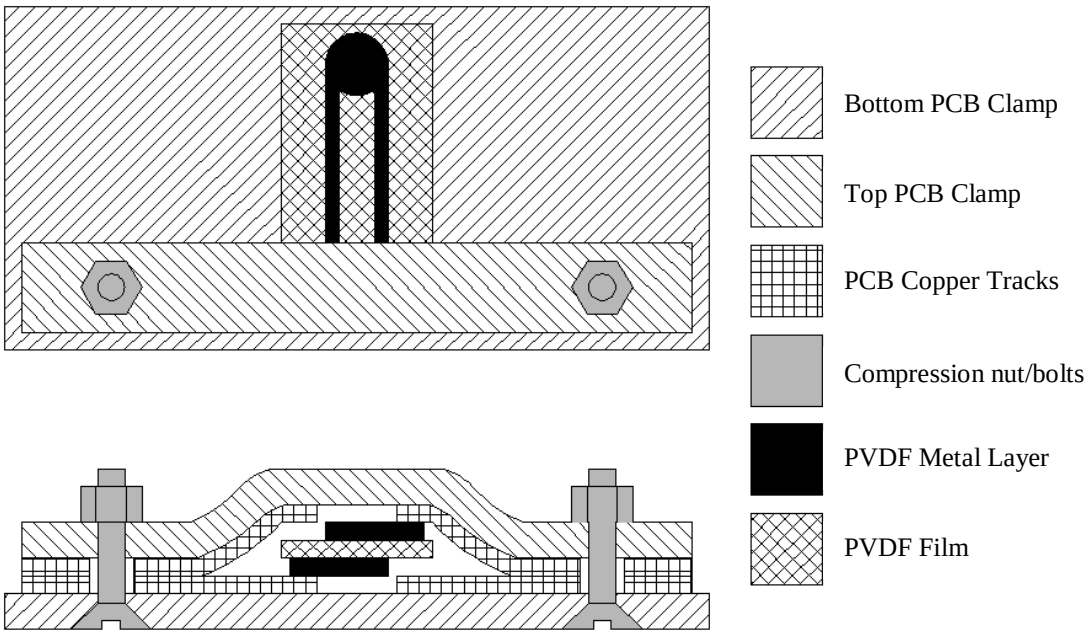

Fig. 4.10 Diagram of the clamping system used to interface the piezoelectric film transducer to the signal conditioning circuit

4.5 Design of the Signal Conditioning Unit

The signal output from the piezoelectric transducer can either be in charge or voltage mode. The mode in which the piezoelectric transducer operates is determined by the configuration of the pre-amplifier. In order to increase the flexibility of the piezoelectric sensor array (increase the range of particle sizes it can be used to measure) a variable secondary amplifier is placed on the output of the pre-amplifier. Since the impact signal from a particle impact may consist of different frequencies that relate to different particle impact parameters (such as particle impact velocity and particle size) an adjustable band-pass filter is placed on the output of the variable secondary amplifier as shown in Fig. 4.11. This bandpass filter can also be bypassed for experiments to allow the full frequency spectrum to be analysed.

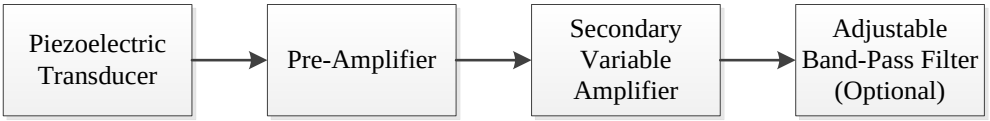

Fig. 4.11 Block diagram of the piezoelectric impact sensor array signal conditioning circuit

4.5.1 Design of the Pre-Amplifier

The piezoelectric transducer can be configured in either charge or voltage mode. The piezoelectric transducer is modelled in charge mode as a charge source with a shunt capacitor and resistor or in voltage mode with a series capacitor and resistor as shown in Fig. 4.12 [101].

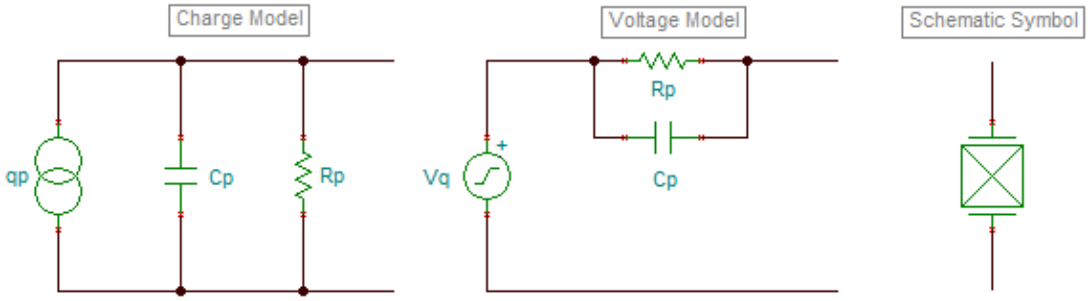

Fig. 4.12 Schematics of the charge model and the voltage model of the piezoelectric film transducer

The configuration of the pre-amplifier is what determines the mode in which the piezoelectric transducer operates in. Fig. 4.13 shows the schematic of a charge amplifier which sets the pre-amplifier in charge mode.

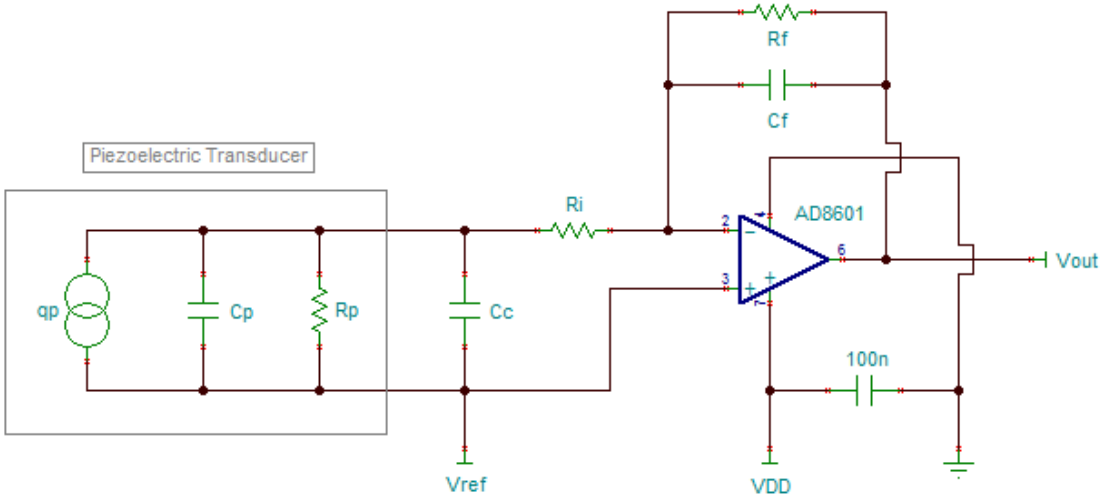

Fig. 4.13 Circuit schematic – charge mode

The advantage of using a piezoelectric transducer in charge mode is that long cables can be used to connect the piezoelectric transducer [100]. The gain of the piezoelectric transducer using the pre-amplifier in charge mode is determined by [100]:

$$A_o = -\frac{Q}{C_f} \tag{4.3}$$

Where A_o is the gain, Q is the charge developed and C_f is the feedback capacitor. The pre-amplifier in charge mode likewise affects the operating frequency of the piezoelectric transducer with the lower cut-off frequency f_L determined by [101]:

$$f_L = \frac{1}{2\,\pi\,R_f\,C_f} \tag{4.4}$$

With C_f being the feedback capacitor and R_f being the feedback resistor (Fig. 4.13). The upper cut-off frequency f_H is determined by [101]:

$$f_H = \frac{1}{2\,\pi\,R_i(C_p\,C_c)} \tag{4.5}$$

Where R_i and C_c are the resistance and capacitance respectively of the input cable linking the piezoelectric transducer to the pre-amplifier and C_p is the capacitance of the piezoelectric transducer.

The schematic shown in Fig. 4.14 shows the circuit topography of the pre-amplifier for the piezoelectric transducer in voltage mode. The advantage of using piezoelectric transducer in voltage mode is that changes in temperature have little effect on the voltage sensitivity [100]. However, using the piezoelectric transducer in voltage has the disadvantage that the pre-amplifier has to be constructed close to the piezoelectric transducer.

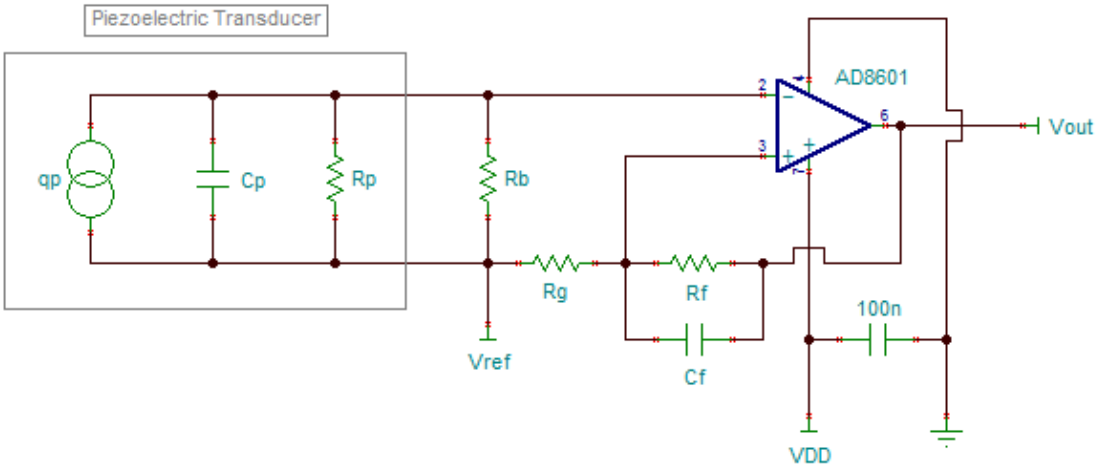

Fig. 4.14 Circuit schematic – voltage mode

The pre-amplifier in voltage mode is a non-inverting amplifier and the voltage gain is determined by:

$$A_o = 1 + \frac{R_f}{R_g} \tag{4.6}$$

Consequently the output voltage of the pre-amplifier in voltage mode using a piezoelectric PVDF film transducer is determined by:

$$V_o = (V_{in}\, A_o) + V_{ref} \tag{4.7}$$

Where V_o is the output voltage from the voltage mode pre-amplifier, V_{in} is the voltage output from the PVDF film transducer when mechanical stress is applied which is calculated using (4.2), A_o is the voltage gain of the voltage mode pre-amplifier calculated using (4.6) and V_{ref} is the bias voltage. The pre-amplifier in voltage mode

also affects the operating frequency of the piezoelectric transducer with the lower cut-off frequency f_L determined by [101]:

$$f_L = \frac{1}{2\,\pi(R_p \parallel R_b)(C_p \parallel C_c)} \tag{4.8}$$

Where R_p is the resistance of the PVDF film, R_b is a high value resistor that provides a DC bias path for the amplifier input stage (Fig. 4.14), C_p is the capacitance of the PVDF film and C_c is the capacitance of the input cables (Fig. 4.14.). The upper cut-off frequency f_H is determined by [101]:

$$f_H = \frac{1}{2\,\pi\,R_f\,C_f} \tag{4.9}$$

With C_f being the feedback capacitor and R_f being the feedback resistor.

For the pre-amplifier presented in this study the non-inverting amplifier (voltage mode) was used. The primary reason for this decision was that changes in temperature have little effect on the voltage sensitivity [100]. However this would require the pre-amplifier to be constructed inside the sensor blade close to the piezoelectric transducer. The voltage mode pre-amplifier uses the AD8601 op-amp. The AD8601 op-amp by ANALOG Devices was chosen because [84]:

- Available in single (AD8601), dual (AD8602) and quad (AD8604) packages to increase component density in circuits
- Single supply operation (removes the need for dual rail power supply)
- Wide bandwidth (8 MHz)
- Fast slew rate (5V/us)

The value for R_g and R_f was 10 kΩ and 1 kΩ respectively giving the pre-amplifier a gain of 1.1; this was done so the amplifier's gain would be as close to 1 as practically possible. The value of R_b was set to 10 MΩ [101]. The feedback capacitor C_f was set to 15 nF giving an upper cut-off frequency of approximately 10 kHz. Since the ADC used for digitisation can only accept positive input voltages V_{ref} (VDD/2) is used to bias the pre-amplifier between 0V and VDD (3.3V).

4.5.2 Design of the Secondary Variable Circuit

The purpose of the secondary amplifiers is to increase the signal output from the pre-amplifier to a level that utilises the full range of the ADC. The variable secondary amplifier also:

- Improves the robustness of the sensor to allow it to detect a wide range of particle sizes at different impact velocities.
- Allows each of the secondary variable amplifiers to calibrate each of the piezoelectric impact sensors in the array. The reason for this is that the piezoelectric impact sensor is an electromechanical sensor and variations in the mechanical manufacture will require each sensor in the array to be calibrated.

The design of the secondary variable amplifier is an AC coupled non-inverting amplifier; the circuit topography is the same design as the secondary variable amplifier used on the electrostatic sensor array described in chapter 3.

4.5.3 Design of the Adjustable Bandpass Filter

When the piezoelectric impact sensor is struck by a particle; the vibrations caused by the impact travel along the impact waveguide to the piezoelectric film transducer which will induce a signal proportional to the frequency of this vibration. In order to increase the adaptability of the impact sensor, an adjustable bandpass is placed on the output of the variable secondary amplifier. This is to filter out frequencies that are not related to a direct particle impact on the active part of the sensor array.

The bandpass filter is formed by a second order low-pass Sallen-Key filter and a second order high-pass Sallen-Key filter. The schematics of the low-pass Sallen-Key filter and a second order high-pass Sallen-Key filter are illustrated in Fig. 4.15 and Fig. 4.16 respectively. The cut-off frequencies are set by jumpers that select different value resistors and capacitors

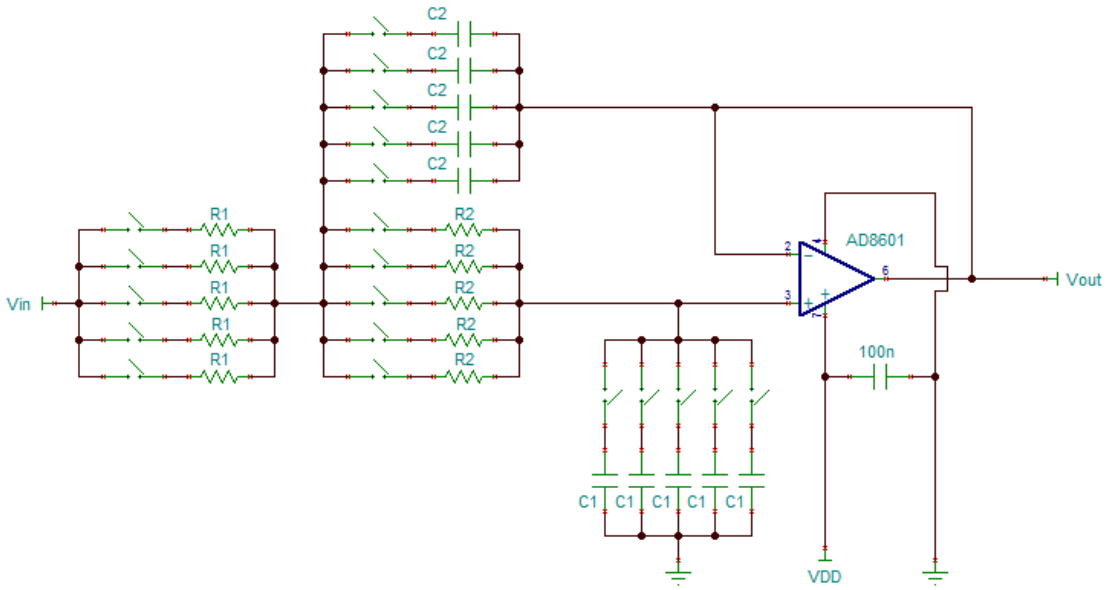

Fig. 4.15 Circuit schematic of the Sallen-Key low-pass filter

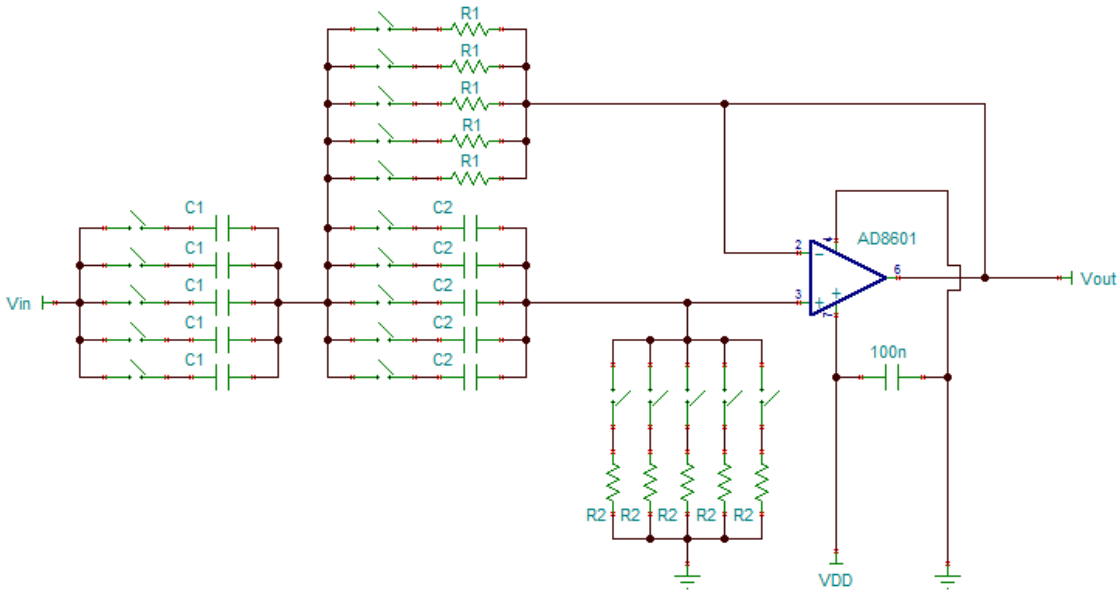

Fig. 4.16 Circuit schematic of the Sallen-Key high-pass filter

The cut-off frequency (f_L) for the low-pass Sallen-Key filter is determined by [87]:

$$f_L = \frac{1}{2\,\pi\,R\,C\,\sqrt{mn}} \tag{4.10}$$

Where mn is assumed to be set to 1 for unity gain. The cut-off frequency (f_H) for the high-pass Sallen-Key filter is determined by [87]:

$$f_H = \frac{1}{\sqrt{R_1 R_2 C_1 C_2}} \tag{4.11}$$

The bandpass filter is optional and can be bypassed in the sensor hardware. The reason for this is to allow full data collection of all frequency components of the signal. A bandpass filter can also be applied off-line using digital signal processing (DSP).

4.5.4 Design of the V_{ref} Input Circuit

In order to bias the pre-amp to VDD/2 a reference voltage (V_{ref}) needs to be generated. The reference voltage is generated using a simple resistive voltage divider network tapped off of VDD with a voltage follower. This circuit design is explained in detail in chapter 3.

4.5.5 Design of the Power Supply Circuit

In order to reduce noise in the signal conditioning circuit the power supply design used for the piezoelectric impact sensor array is the same design used on the electrostatic sensor array described in chapter 3.

4.5.6 Design of the Analogue Multiplexer Circuit

In order to maximise hardware resources an analogue multiplexer (MUX) controlled by the microcontroller is required. This allows the microcontroller to select each element (piezoelectric impact sensor) of the electrostatic sensor array. The chosen analogue MUX is the ADG706 by ANALOG DEVICES. This analogue MUX was selected in view of the following features [92]:

- 1.8V-5.5V supply voltage
- Low internal resistance (2.5Ω initial 0.5Ω constant)
- Fast switching time (40nS)

The ADG707 is also a single end analogue MUX meaning that for each address the microcontroller selects one of the inputs as shown in Fig. 4.17

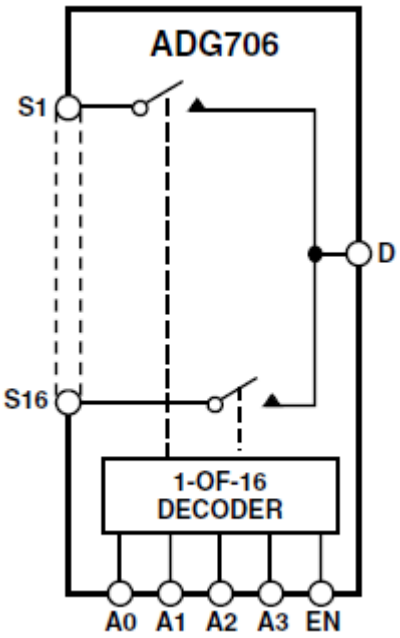

Fig. 4.17 Diagram of the ADG706 single ended analogue multiplexer [92]

Table 4.1 shows the truth table for each switch on the ADG706 analogue MUX. The software for controlling the analogue MUX is embedded into the microcontroller (pin 25 = EN, pin 24 = A0, pin 23 = A1, pin 22 = A2 and pin 21 = A3 on the MBED microcontroller). For the current design, however, only 1-5 are used since the piezoelectric sensor array only has five elements for a 50 mm bore pipe (this can be increased for larger bore pipes).

Table 4.1

ADG706 Truth Table

A3	A2	A1	A0	EN	ON Switch
X	X	X	X	0	NONE
0	0	0	0	1	1
0	0	0	1	1	2
0	0	1	0	1	3
0	0	1	1	1	4
0	1	0	0	1	5
0	1	0	1	1	6
0	1	1	0	1	7
0	1	1	1	1	8
1	0	0	0	1	9
1	0	0	1	1	10
1	0	1	0	1	11
1	0	1	1	1	12
1	1	0	0	1	13
1	1	0	1	1	14
1	1	1	0	1	15
1	1	1	1	1	16

X = Don't Care

4.5.7 Implementation of the ADC Data Logger

The analogue to digital converter used to digitise the signal output from the piezoelectric sensor array uses the same external ADC (AD7490) described in chapter 3. The embedded algorithm in the MBED microcontroller used to control the sampling rate in the external ADC is different. Unlike the sampling process for the cross correlation algorithm used on the electrostatic sensor array described in chapter 3, the sampling period for the piezoelectric sensor array has to be exactly consistent. The reason for this is that a spectral analysis will be carried out on the impact signal to determine the frequency components of the impact signal. To ensure a constant sampling rate an algorithm was developed and embedded into the MBED microcontroller that linked the sampling operation of the external ADC to the internal

timer on the MBED microcontroller. The sampling frequency was set to 200 kHz (twice the highest frequency expected from a piezoelectric transducer in one dimension of mechanical stress [100]) in the embedded software.

To ensure the accuracy of this algorithm the ADC was bench tested using a signal generator to generate a sine wave and have the ADC sample the output. Three sine waves were inputted into the ADC from the signal generator: 10 kHz, 30 kHz and 50 kHz. A power spectral analysis was then applied to the captured data as shown in Fig. 4.18 which shows dominant peaks at 10 kHz, 30 kHz and 50 kHz. This verifies that the sampling period of the ADC is constant and suitable for spectral analysis of the impact signal from the piezoelectric impact sensor.

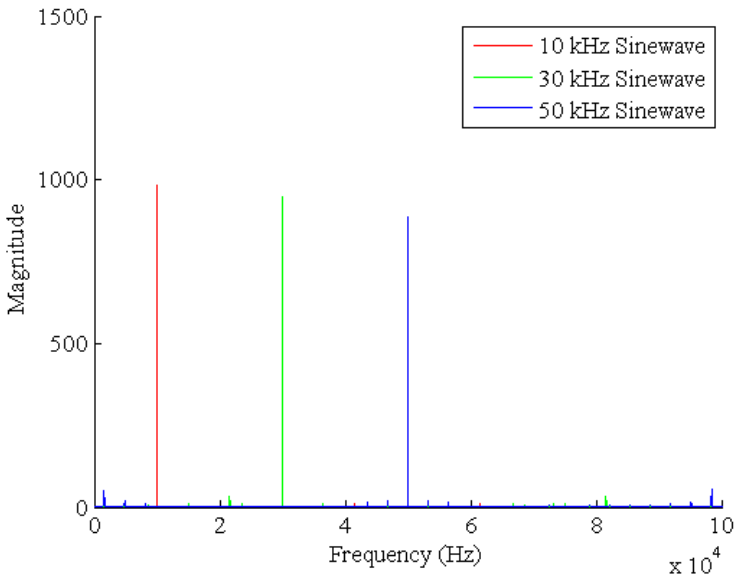

Fig. 4.18 Power spectral analysis of 10 kHz, 30 kHz and 50 kHz sine wave generated by a signal generator

4.5.8 Microcontroller Selection

It was decided that all data logging and digital control of the piezoelectric sensor array would be carried out by a dedicated microcontroller. The reason for this was that a microcontroller would allow the piezoelectric impact sensor array to be easily adapted and configured for individual experimentation (such as being able to interface with

sensors on a test rig). The selected microcontroller was the MBED NXP LPC1768 microcontroller using the 32-bit ARM Cortex-M3 chip. The reason for this selection can be seen in chapter 3.

4.5.9 Design of the Complete Signal Conditioning Circuit

Since both the secondary amplifier and the optional bandpass filter are both adjustable these components of the signal conditioning circuit for the piezoelectric sensor array have to be replicated for each of the five elements of the sensor array illustrated in Fig. 4.19.

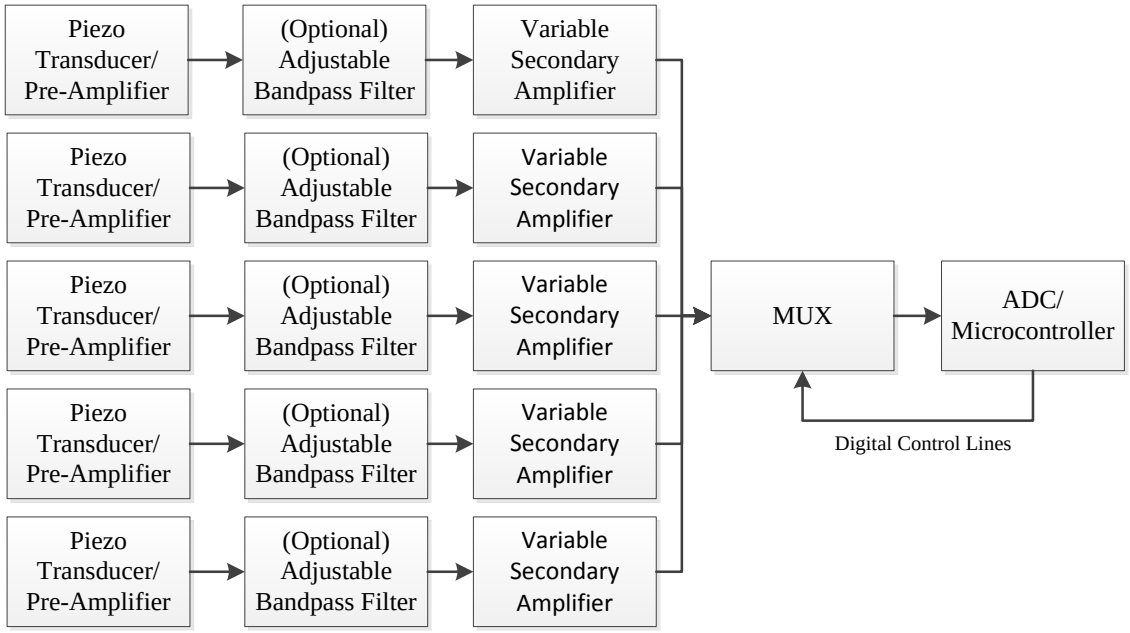

Fig. 4.19 Block diagram of the complete piezoelectric impact sensor array signal conditioning circuit

4.5.10 SD Card Interface Design

Due to the large amount of data that will be collected during experimentation with the piezoelectric sensor array, a SD card is interfaced with the MBED microcontroller. The SD card is interfaced with the MBED microcontroller (pin 5 = DI, pin 6 = DO, pin 7 = CLK, pin 8 = CS and pin 40 = VDD). The software for interfacing is an open source library [102] and is embedded into the MBED microcontroller. The data from the piezoelectric sensor array is saved as a .txt file in the SD card.

4.6 Modelling of the Piezoelectric Impact Sensor

When a moving particle collides with a fixed solid surface the kinetic energy of the moving particle is converted into an impact force. Hertz was the first to pioneer this work [103]. In order to determine the impact force the particle is assumed to be a dry sphere. This is because many particles in industry such as coal particles in the energy industry or shot in manufacturing are close to being spherical in shape. In order to calculate the impact force the mechanical properties of the impact surface and particle have to be taken into account. To determine the particle size the particle velocity will have to be independently measured using another sensing technology such as the electrostatic sensor. The effective elastic modulus E* can be determined by [104]:

$$E^* = 2\left(\frac{1-\nu_1^2}{E_1}+\frac{1-\nu_2^2}{E_2}\right)^{-1} \tag{4.12}$$

Where ν_1 and ν_2 is the Poisson's ratio of the particle and surface respectively and E_1 and E_2 are the Young's modulus of the particle and surface respectively. The size (radius) of the particle also has to be taken into account. The median radius R* of the contact surfaces is defined as [104]:

$$R^* = \left(\frac{1}{R_1}+\frac{1}{R_2}\right)^{-1} \approx R_1 \tag{4.13}$$

Where R_1 and R_2 are the radius of the particle and surface respectively.

The effective mass m* of both the contact parameters is defined as [104]:

$$m^* = \left(\frac{1}{m_1}+\frac{1}{m_2}\right)^{-1} \tag{4.14}$$

Where m_1 and m_2 are the masses of the impacting particle and target respectively. From the moment that a collision occurs until the moment the particle velocity reduces to zero, elastic deformations occur. The time t (duration of impact) is determined by [104]:

$$t = 3.78\left(\frac{m^{*2}}{V\ R^*\ E^{*2}}\right)^{1/5} \tag{4.15}$$

Where m* is the effective mass of the particle and V is the velocity of the particle. The maximum impact force is defined by [104]:

$$F_{max} = \left(\frac{125\, m^{*3}\ E^{*2}\, R^{*}\ V^{6}}{144}\right)^{1/5} \tag{4.16}$$

To measure the impact force of the colliding particle a piezoelectric transducer is used to measure the vibrations caused by the particle's impact. Piezoelectric materials convert mechanical stress and strain into charge or voltage expressed in (4.1) and (4.2) respectively [105].

The piezoelectric transducers used in the piezoelectric sensor array are configured in voltage mode which is expressed in (4.2). X_n is the applied stress in the specified direction and t is the thickness of the PVDF film. The mechanical stress X_n is calculated by:

$$X_n = \frac{F_{max}}{A} \tag{4.17}$$

The particles do not directly impact the piezoelectric transducer since this would damage the piezoelectric film. The particles impact the waveguide which has the primary function to act as a conduit for the vibrations caused by the particle impacts. The waveguide is secured using tightly fitting rubber washers which limits the directional axis of movement to one direction (one dimension of movement). By doing this the rubber washer also applies friction to this dimension of movement and this would reduce the amount of stress applied to the piezo transducer during impact. For this the output voltage is calculated by:

$$V_o = \frac{g_{3n}\, X_n\, t}{f_f} \tag{4.18}$$

Where f_f is the friction acting against the waveguide from the rubber washer during the particle impact. However it is difficult to quantify the value of the friction acting between the rubber washer due to the complexity of the surface texture of the waveguide, rubber washer and the force between the washer and waveguide [106]. For this reason the value f_f is an estimate. This estimate will be determined using an off-line testing method under controlled conditions applying known variables which will be explained in detail in Chapter 5.

4.7 Summary

All aspect of the design of the piezoelectric sensor array designed to measure the particle size distribution and concentration profiles of pneumatically conveyed bulk solids have been presented in this chapter. This includes: the development of the structure of the piezoelectric sensor array, the design of the vibration shielding that allows a very small area to be active reducing the risk of simultaneous particle impacts, design of the custom pipe spool to allow the piezoelectric sensor array to be mounted on a laboratory scale test rig, all designs of the signal conditioning circuits and the implementation of a high speed external ADC. This chapter also presents the theoretical system model for the piezoelectric impact sensors. This model allows the particle size (particle diameter) to be determined assuming the particle velocity can be independently measured using another sensing technology (such as an electrostatic sensor) and the mechanical properties of the particles is known.

Chapter 5

Particle Flow Test Rigs and Experimental Procedures

5.1 Introduction

For validation of the performance of both the electrostatic and piezoelectric sensor arrays, laboratory experimentation has to be carried out. For this purpose, on-line laboratory scale pneumatic bulk solid conveying test rigs were designed and constructed as well as a specific off-line test rig for testing and calibrating the piezoelectric sensor array. This chapter covers the specific design features of both the on-line pneumatic conveying systems (negative and positive pressure rigs) and the off-line test rig for the piezoelectric sensor array.

Testing procedures such as: modes of testing for each test rig; specific analysis tools used (such as the off-line digital imaging system for measuring particle size and shape); and preparation procedures for each type of experiment. Health and safety considerations when carrying out experimentation will be expressed in this chapter. All experimental results will be presented in Chapter 6.

5.2 Pulverised Materials and Handling

A variety of pulverised materials were used in on-line pneumatic conveying test rigs. These pulverised materials include flour, coal, plastic shot and a variety of pulverised biomass materials. Before the pulverised materials can be used for experimentation they have to be prepared (separated into specific particle sizes) and their size and shape analysed.

5.2.1 Particle Size and Shape Analysis

In order to characterise the particle size and shape in 2D an off-line digital imaging system was used. The particle size and shape digital imaging system consists of a USB imaging scanner and the BioMscan software developed by Robert Carter at the University of Kent [43]. When using the particle imaging scanner the procedure is:

- Open the scanner lid and clean the glass of the scanning table of any unwanted particles.
- Lightly sprinkle the test particles on the glass scanner table ensuring that only a small concentration of particles is present and close the scanner lid.
- Run the BioMscan software (shown in Fig. 5.1). If particle concentration is above 3% clean the glass scanning table and reapply particles (since higher particle concentrations will cause measurement errors).
- Particle size and shape can be displayed on the user interface or exported as a .csv file.

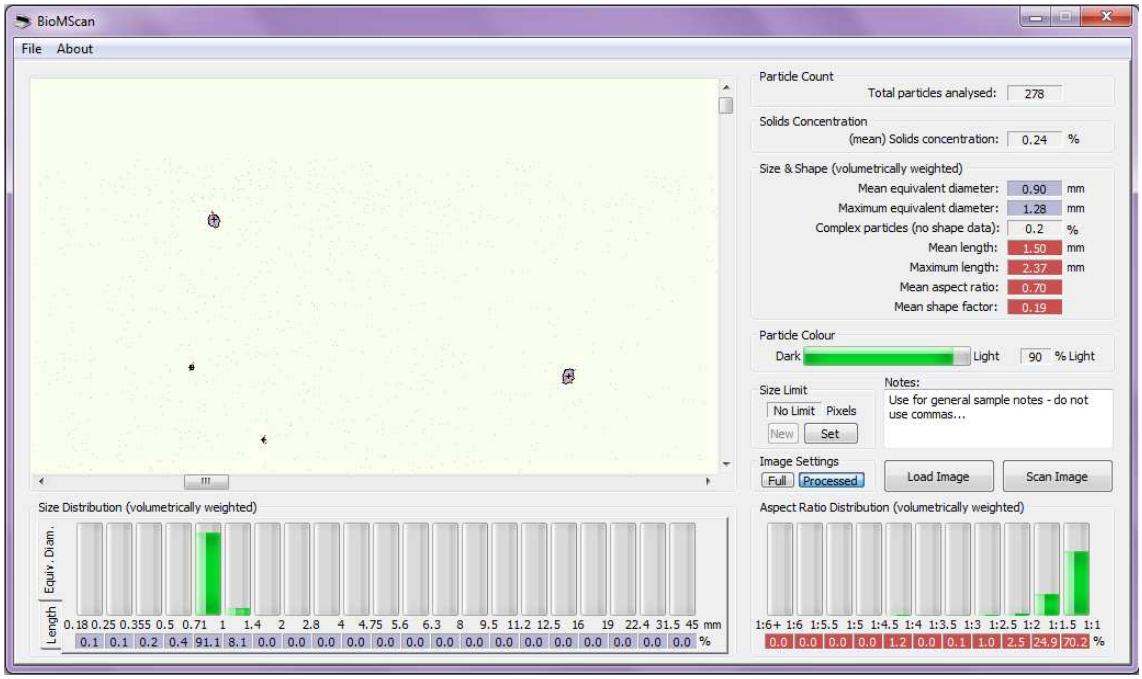

Fig. 5.1 Screenshot of the user interface of the BioMscan software

5.2.2 Particle Size Separation Using Sieving

In some experiments the effect of particle size on particle flow characteristics is to be examined. In order to achieve this, pulverised materials have to be separated by particle size. This is carried out by sieving the pulverised through the desired mesh size. Once enough pulverised material has been sieved, the material is analysed to ensure the particle size corresponds to the mesh size of sieve.

5.2.3 Handling of Pulverised Material

Before handling the pulverised materials a full risk assessment is carried out on the type of material being used to ensure correct handling and storage procedure is being followed. When handling the pulverised materials specific personal protective equipment is used:

- **Overalls** – these are used to protect the user's clothes from fine pulverised materials such as coal.

- **Protective Glasses** - these are used to protect the user's eyes in the event the pulverised material becomes airborne (such as in the event of containment loss in the storage tank on the positive pressure test rig).
- **Dust Mask** - these are used to protect the user from breathing in the fine particles used during experimentation (P3 specification filters were used [107]).

5.2.4 Blending Procedure of Pulverised Material

For experimentation on the characteristics of multi-phase particle flow different materials are required to be blended together. The separate pulverised materials are first analysed using the digital particle size imager; the separate pulverised materials were first weighed out using digital scales (blend ratios are determined by weight); they were then mixed together by hand. The mixing process was carried out by hand to reduce the chance that the mixing process would affect the particle size of the pulverised materials during the mixing process compared to using a machine to blend the material which could grind the material to smaller particle sizes.

5.2.5 Storage Procedure of Pulverised Material

All pulverised materials are stored in labelled containers that can be resealed. All combustible materials are stored in designated storage areas (workshop fire store).

5.3 Negative Pressure Bulk Solid Conveying Test Rig

In order to examine the performance of the electrostatic and piezoelectric sensor arrays, laboratory scale bulk solid conveying systems were designed and constructed. The negative pressure test rig was designed and constructed by a team of researchers at the University of Kent. The negative pressure test rig uses negative pressure to convey the pulverised material at high velocity along both horizontal and vertical pipes (50 mm pipe bore) illustrated in Fig. 5.2 and consists of:

- **Vacuum Plant** – this is used to generate a vacuum that sucks the pulverised material along the system's pipes. The vacuum plant also collects the pulverised material once it outputs from the pipe system. The particle velocity is controlled by changing the fan speed on the vacuum plant which is controlled by a manual variable transformer.
- **Vibration Feeder** – the vibration feeder controls the particle feed rate into the input pipe. The feed rate of the vibration feeder is controlled by adjusting the magnitude of the vibrations in the unit. This is achieved manually by a controller.
- **Sensor Mounting on Horizontal Pipe** – the horizontal pipe sensor mounting allows a 400 mm long pipe spool to be mounted. This pipe spool can be fitted with the electrostatic or the piezoelectric sensor arrays as well as a hot wire anemometer for independent conveying air velocity measurement. The sensor mounting pipe spool can be orientated to allow the sensor array to mount on different axis which is displayed in Fig. 5.3. The horizontal pipe sensor mounting is placed 2600 mm (52 pipe diameters) from the particle input, consequently allowing developed particle flow to be analysed.
- **Sensor Mounting on Vertical Pipe** – the vertical pipe sensor mounting allows a 400 mm long pipe spool to be mounted. This pipe spool can be fitted with either the electrostatic or the piezoelectric sensor arrays. The sensor mounting pipe spool can be orientated to allow the sensor array to mount on different axis which is displayed in Fig. 5.3. The horizontal pipe sensor mounting is placed 400 mm (8 pipe diameters) from a right angle pipe bend. Consequently the particle flow measurements obtained from this location will be undeveloped.

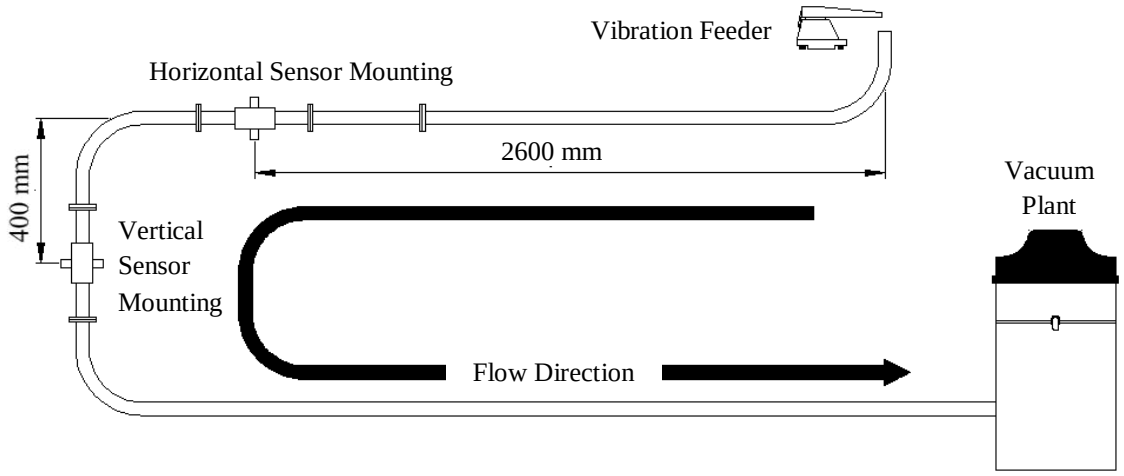

Fig. 5.2 Layout of the negative-pressure pneumatic conveying test rig

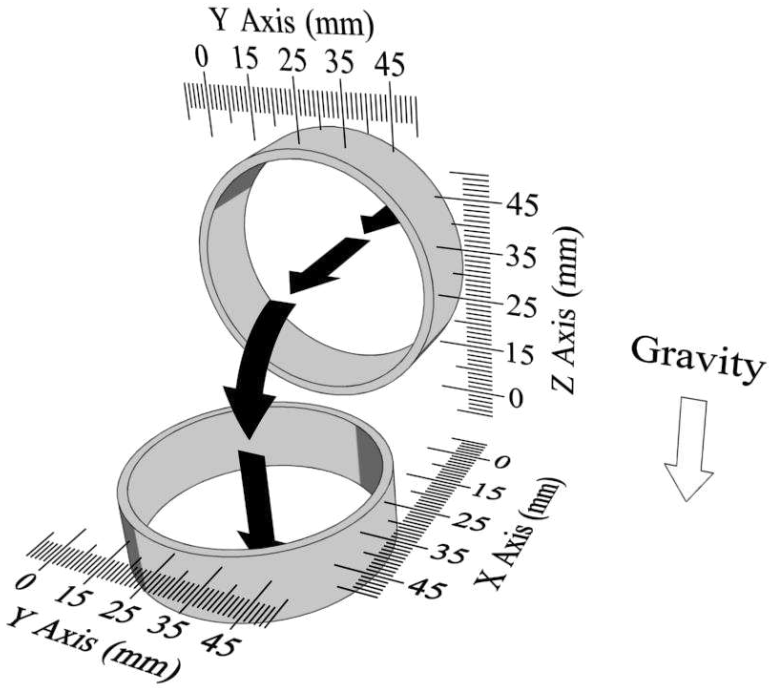

Fig. 5.3 Diagram of the sensor axis orientations for both horizontal and vertical pipe mountings for the negative pressure test rig (including particle direction through right angle pipe bend)

5.3.1 Operating Procedure of the Negative-Pressure Test Rig

To ensure consistent parameters between experiments a testing procedure was developed and implemented.

1. **Cleaning System** – if a new type of pulverised material is to be used with the negative pressure test rig the system is fully cleaned out including pipes and the catcher tank on the vacuum plant.
2. **Cleaning Filters** – before each experiment the filters on the vacuum plant are cleaned out. This is carried out to ensure repeatability of the conveying air velocity for a specific fan speed on the vacuum plant.
3. **Temperature and Humidity Levels** – during each experiment the average temperature and humidity is monitored and recorded to allow consistent testing conditions.
4. **Powering up the Vacuum Plant** – to start up the vacuum plant the manual transformer is first turned on at 100% power for a few seconds to overcome the torque on the fan blades. Once the fans are running at full speed the manual transformer is set to the desired power level.
5. **Starting the Particle Feeder** – once the conveying air velocity is stable the vibration feeder is turned on at the desired feed rate.
6. **Begin Data Logging** – when there are particles traveling along the pipe the data logging of the sensor output on either the electrostatic/piezoelectric sensor arrays can begin. On both the electrostatic and piezoelectric sensor arrays this is an automatic process that starts as soon as the ‘start button’ is pressed on the MBED microcontroller.
7. **Data Logging Complete** – once data collection is complete first turn off the vibration feeder then after a few seconds turn off the vacuum plant. This is done to ensure that there are no particles remaining in the pipe when the vacuum plant is turned off.

5.3.2 Advantages and Disadvantages of the Negative Pressure Test Rig

The negative pressure test rig has advantages and disadvantages that dictate the type of experiments that can be conducted utilising it:

Advantages:

- **Simple to Operate** – the manual controls for the vacuum plant and vibration make the negative pressure test rig simple to operate and change parameters such as conveying air velocity.
- **Wide Range of Conveying Air Velocities** – the negative pressure test rig is capable of a range of conveying air velocities from low air velocities (< 10 m/s) up to high conveying air velocities (40 m/s).

Disadvantages:

- **Can't Convey Pulverised Coal** – the negative pressure test rig is unable to convey pulverised coal. The reason for this is that the fine coal particles clog the filter on the vacuum plant in a matter of minutes. Consequently the conveying air velocity decreases.
- **Long Setup Time** – the negative pressure has a long set up time for each individual experiment since the filters have to be cleaned after each test.
- **Short Experimental Duration** – long experiments (> 30 minutes) cannot be performed using the negative pressure rig since the motor on the vacuum plant overheats. Additionally the filters get clogged causing the conveying air velocity to decrease.
- **No Monitoring of Mass Flow Rate** – the monitoring of the mass flow rate of individual experiments cannot be performed on the negative pressure test rig. The reason for this is that the design of the catcher tank on the vacuum plant does not allow the full collection of the used pulverised material after the experiment has concluded (since material embeds itself in difficult to reach places in the tank). Additionally material is lost when the filters are cleaned out for this reason the input particle mass flow rate is estimated in a separate

experiment by measuring how much material is metered out by the vibration feeder in a period of time.

5.3.3 Safety Features of the Negative Pressure Test Rig

In order to prevent fire/explosion triggered by arcs generated by electrostatic discharges inside the pipes or the catcher tank on the negative pressure test rig, all sections of the test rig are earthed. Additionally only a small amount of pulverised material is used for each test (< 0.3 kg) and the material is emptied from the catcher tank after each experiment.

5.4 Positive Pressure Bulk Solid Conveying Test Rig

The laboratory scale positive pressure test rig at the University of Kent was originally designed by previous researchers at the University of Kent. However, substantial changes have been made from the original design. The positive pressure test rig uses positive pressure to convey the pulverised material at high velocity along both horizontal and vertical pipes (50 mm pipe bore) illustrated in Fig. 5.4 and consists of:

- **Centrifugal Fan** – the original design for the positive pressure test rig used high velocity air generated by compressors. This system was unable to sustain a stable conveying air velocity due to flow restrictions caused by an extended compressed air supply pipe from the compressor. The solution to this problem was to use a centrifugal fan instead of compressed air generated by compressors. The centrifugal fan is driven by an inverter controlled 3-phase 5.5 kW motor which allows the conveying air velocity to be changed by changing the speed of the driving motor on the fan. The centrifugal fan supplied by FANS & BLOWERS LTD is capable of delivering an air flow rate of 400 m^3/h with 100 mBar back pressure [108].
- **Particle Input Feeder** - the original design for the positive pressure test rig used a rotary feeder to input the particles into the system. It was found that when the

rotary feeder was used the particles were "pulsed" into the system causing uneven particle flow. The solution was to use a vibration feeder with a custom designed venturi eductor. The venturi eductor creates a negative pressure (suction) on the particle input allowing the particles to be inputted into a positive pressure. The feed rate of the vibration feeder is controlled by adjusting the magnitude of the vibrations in the unit. This is achieved manually by a controller.

- **Sensor Mounting on Horizontal Pipe** – the horizontal pipe sensor mounting allows a 400 mm long pipe spool to be mounted. This pipe spool can be fitted with the electrostatic or the piezoelectric sensor arrays as well as a hot wire anemometer for independent conveying air velocity measurement. The sensor mounting pipe spool can be orientated to allow the sensor array to mount on different axis which is displayed in Fig. 5.5. The horizontal pipe sensor mounting is placed 6400 mm (128 pipe diameters) from the particle input consequently allowing developed particle flow to be analysed.
- **Sensor Mounting on Vertical Pipe** – the vertical pipe sensor mounting allows a 400 mm long pipe spool to be mounted. This pipe spool can be fitted with either the electrostatic or the piezoelectric sensor arrays. The sensor mounting pipe spool can be orientated to allow the sensor array to mount on different axis which is displayed in Fig. 5.5. The horizontal pipe sensor mounting is placed 1350 mm (27 pipe diameters) from a right angle pipe bend.
- **Catcher Tank** – after the pulverised material has left the pipe it is first decelerated in a cyclone deceleration chamber which is above the catcher tank. The pulverised material then falls into the catcher tank by gravity. The pulverised material is then emptied out of the catcher tank by opening the butterfly valve under the catcher tank.

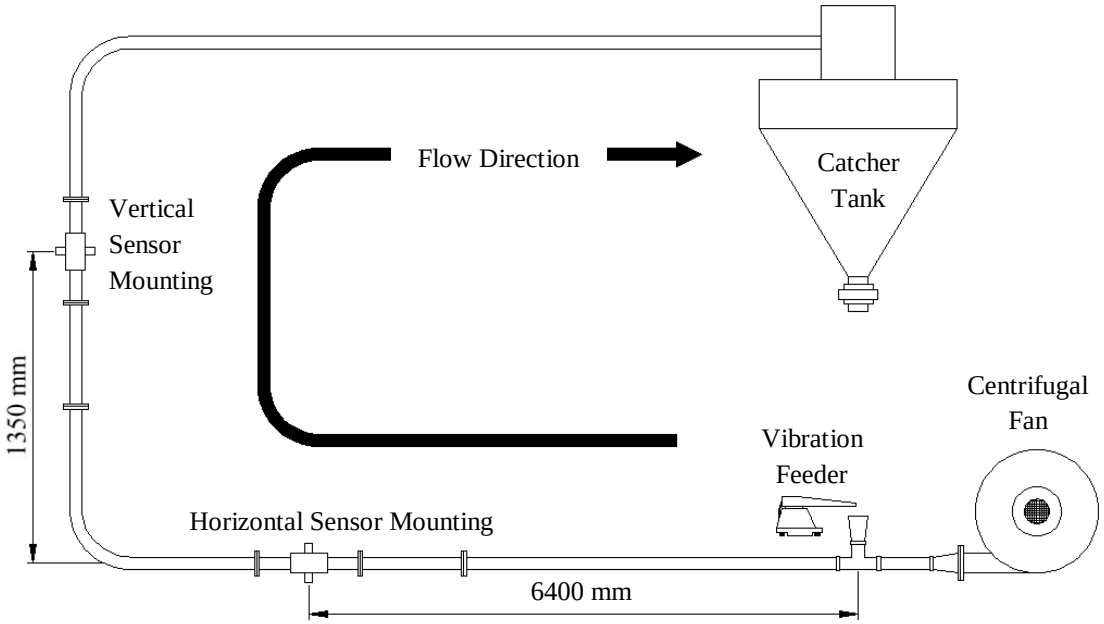

Fig. 5.4 Layout of the positive-pressure pneumatic conveying test rig

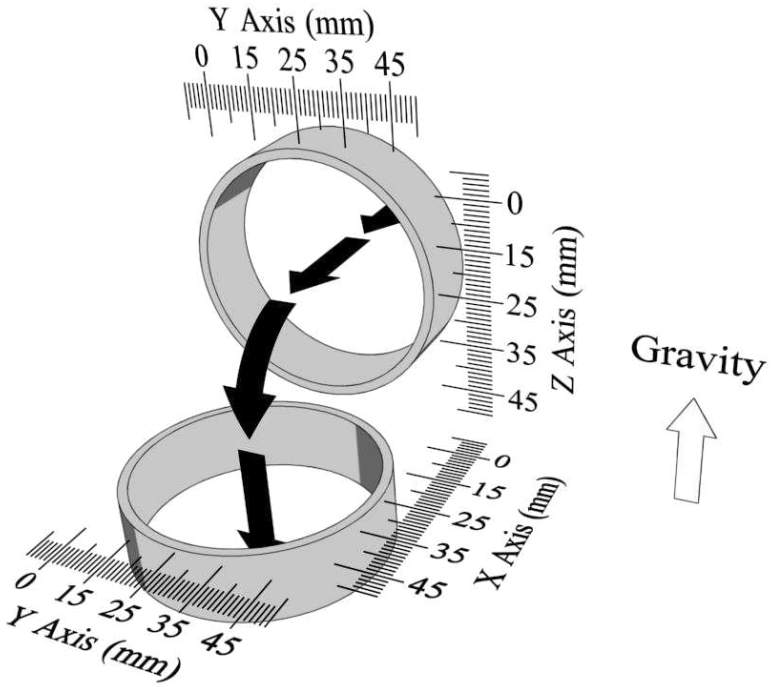

Fig. 5.5 Diagram of the sensor axis orientations for both horizontal and vertical pipe mountings for the positive pressure test rig (including particle direction through right angle pipe bend)

5.4.1 Operating Procedure of the Positive Pressure Test Rig

To ensure consistent parameters between experiments a testing procedure was developed and implemented for the positive pressure test rig.

1. **Cleaning System** – if a new type of pulverised material is to be used with the negative pressure test rig the system is fully cleaned out including pipes and the catcher tank on the vacuum plant.
2. **Temperature and Humidity Levels** – during each experiment the average temperature and humidity is monitored and recorded to allow consistent testing conditions.
3. **Powering up the Centrifugal Fan** – to start up the centrifugal fan the desired fan speed is selected manually on the inverter control panel using the "up/down" controls. Once the desired speed is selected the fan is started with the green "Start" button.
4. **Starting the Particle Feeder** – once the conveying air velocity is stable the vibration feeder is turned on at the desired feed rate. At this moment a timer is also started to measure the experiment duration which is used to estimate the average particle feed rate.
5. **Begin Data Logging** – when there are particles traveling along the pipe the data logging of the sensor output on either the electrostatic/piezoelectric sensor arrays can begin. On both the electrostatic and piezoelectric sensor arrays this is an automatic process that starts as soon as the 'start button' is pressed on the MBED microcontroller.
6. **Data Logging Complete** – once data collection is complete first turn off the vibration feeder (also recording the experiment duration), then after a few seconds turn off the vacuum plant. This is done to ensure that there are no particles remaining in the pipe when the vacuum plant is turned off.
7. **Weighing the Pulverised Material** – the material used for the duration of the experiment is then emptied from the catcher tank by opening the butterfly valve

and weighed to calculate the estimated flow rate of the pulverised material during the experiment.

5.4.2 Advantages and Disadvantages of the Positive Pressure Test Rig

The positive pressure test rig has advantages and disadvantages that dictate the type of experiments that can be conducted utilising it:

Advantages:

- **Simple to Operate** – the manual controls for the inverter controlled centrifugal fan and vibration make the positive pressure test rig simple to operate and change parameters such as conveying air velocity.
- **Wide Range of Conveyable Materials –** the positive pressure test rig is able to convey a wide range of pulverised materials including pulverised coal
- **Short Setup Time** – since the pulverised material can be easily removed from the catcher tank and the positive pressure does not have any filters so the setup time is reduced
- **Capable of Prolonged Experiments** – with the large internal volume on the catcher tank and the design of the inverter controlled centrifugal fan (self-cooling of the motor) individual experiments can be carried out over a long time period
- **Capable of Monitoring Mass Flow Rate** – the design of the catcher tank allows all the pulverised material used during the experiment to be collected and weighed thus allowing the mass flow rate of the pulverised material to be estimated

Disadvantages:

- **Lower Conveying Air Velocity** – unlike the negative pressure test rig the positive pressure test rig has a reduced range of conveying air velocities (10 m/s – 19 m/s) on a horizontal pipe
- **Only Able to Convey Small Particles** – due to the reduced conveying air velocity coupled with the upward direction the particles has to travel in the

vertical pipe section particle with a higher mass (large biomass particles) cannot be conveyed

5.4.3 Safety Features of the Positive Pressure Test Rig

In order to prevent fire/explosion triggered by arcs generated by electrostatic discharges inside the pipes or the catcher tank on the positive pressure test rig, all sections of the test rig are earthed. Additionally only a small amount of pulverised material is used for each test (< 0.3 kg) and the material is emptied from the catcher tank after each experiment.

5.5 Off-line Impact Test Rig

In order to conduct experiments on the piezoelectric impact sensor array under controlled conditions, an off-line impact test rig was designed and constructed. The off-line impact test rig is used to investigate individual particle impacts on the piezoelectric impact sensors using spherical particles (ball bearings).

The impact sensor is rigidly mounted in a vice to prevent movement. A vertical guiding tube is centred above the impact sensor to guide the ball bearing onto the impact sensor. The guiding tube can be adjusted to different lengths (500 mm, 750 mm, 1000 mm and 1250 mm), allowing the ball bearing under test to be dropped from different heights for different impact velocities. The guiding tube bore is 4 mm diameter consequently the maximum diameter ball bearings that can be tested with the off-line test rig are 3.5 mm in diameter.

To independently measure the impact velocity of the ball bearing before impact at the end of the guiding tube (just before the impact sensor), a pair of optical sensors set 25 mm apart were used, as shown in Fig. 5.6 and Fig. 5.7. The optical sensors consist of an IR (infra-red) emitter that creates an IR beam across the inside of the tube. This IR beam is detected by an IR receiver (IR photodiode). The optical sensors are connected to the digital inputs on the MBED microcontroller (p19 upstream and p20

downstream). When the ball bearing breaks the upstream IR beam the microcontroller triggers the timer. When the falling ball bearing breaks the downstream IR beam the microcontroller reads the time taken for the ball bearing to travel from the upstream to the downstream sensor. The average velocity of the ball bearing is calculated from the spacing between the sensors and the measured time. Since the velocity measurement requires the ball bearings to break the IR beam the smallest ball bearings that can be used on the off-line test rig are 2.5 mm (smaller ball bearings sometimes miss the IR beam consequently not triggering the IR sensor).

As soon as the downstream IR sensor was triggered the microcontroller begins data logging from the ADC since an impact was imminent. All data from the impact sensor output was saved onto a SD memory card and an algorithm in the microcontroller determined the peak amplitude of the impact signal.

5.5.1 Operating Procedure of the Off-Line impact Test Rig

To ensure consistent parameters between experiments a testing procedure was developed and implemented for the off-line impact test rig.

1. **Align the Active Impact Sensor to Guiding tube -** to ensure that a direct impact occurs and not a glancing impact the centre of the guiding tube bore is aligned to the impact sensor.
2. **Powering Up the Test Rig** – all electronics on the off-line test rig are powered from the MBED microcontroller and will power up as soon as the MBED is connected via USB to the PC (a status LED will indicate when the test rig is ready).
3. **Performing Impact Test** – to carry out a particle impact test drop a single ball bearing down the guiding tube. The impact velocity and impact event (20 ms) will be automatically saved to a .txt file on a SD card interfaced with the MBED microcontroller. The peak impact magnitude and particle impact velocity is also transmitted via the USB to the PC. The status LED on the MBED will indicate when the system is ready for another impact test.

4. **Changing Impact Velocity** – to change the particle impact velocity the guiding tube is extended by screwing extra tube sections to the guiding tube. The guiding tube can be set to 500 mm, 750 mm, 1000 mm and 1250 mm in length.
5. **Powering Down the Test Rig** – once the impact experiments are complete the test rig is powered down by disconnecting the USB cable from the PC. Once the test rig is powered down the SD card can be removed and the collected data analysed.

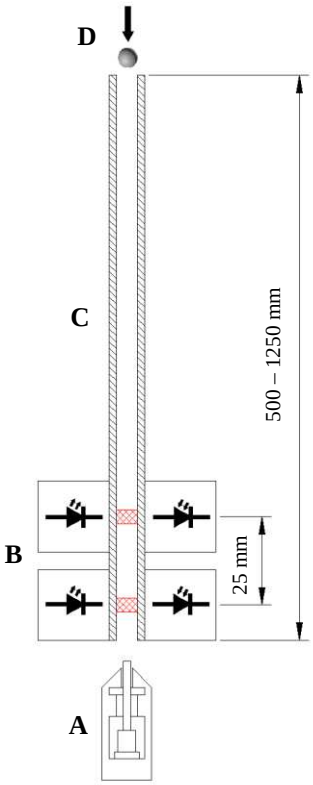

Fig. 5.6 Off-line experimental setup (A) impact sensor, (B) upstream/downstream optical sensors, (C) guiding tube, (D) ball bearing entering the guiding tube

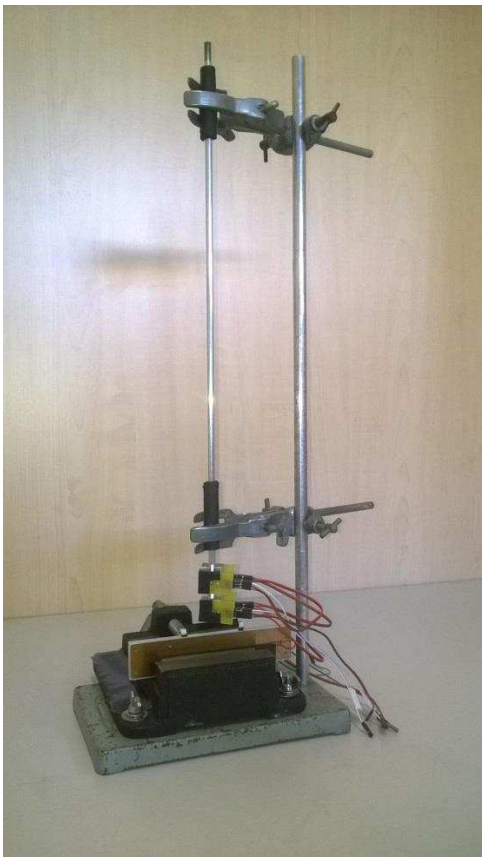

Fig. 5.7 Photo of the off-line impact test rig

5.6 Summary

The technical aspects of the positive and negative pressure bulk solid conveying test rigs as well as the off –line impact test rig have been described in this chapter. Operating procedures of all the test rigs as well as safe working practices for the operation and handling of pulverised material have been covered. The advantages and disadvantages of both the positive and negative pressure test rigs have been described. The sensor orientation classification used for indicating the orientation of both the electrostatic and the piezoelectric sensor arrays on the positive and negative pressure test rigs on both the horizontal and vertical pipe sections have likewise been described.

Chapter 6

Experimental Results and Discussion

6.1 Introduction

In order to validate the measurement potential of both the electrostatic sensor array (to measure the particle velocity and concentration profiles) and the piezoelectric sensor array (to determine the particle concentration profile and size distribution) a comprehensive series of tests have to be carried out. These tests have consisted of both on-line and off-line experimentation which will be carried out on laboratory scale test rigs.

On-line experimentation for the electrostatic sensor array will be carried out using: a range of pulverised materials and particle sizes, a range of different air velocities, positive and negative pressure pneumatic conveying systems; and different pipe and sensor orientations (horizontal and vertical pipe sections). Validation of the on-line electrostatic sensor array tests will be carried out using; commercial measurement equipment (hot wire anemometer to independently measure the air velocity profile with

a comparison to the measured particle velocity profile). Particle size and shape of each conveyed material will be measured using an in-house digital imaging system.

Evaluation of the piezoelectric sensor array will be carried out using both on-line and off-line testing methods. The off-line testing will be used to compare the theoretical system model to the test results as well as being used to calibrate each element of the sensor array. On-line experiments will likewise be carried out on the piezoelectric sensor array using: material with a specific particle size; known mechanical properties and using a variety of particle velocities.

6.2 The Electrostatic Sensor Array

The electrostatic sensor array is designed to determine the particle velocity and the particle concentration across the diameter of the pipe in order to determine the particle velocity and concentration profiles of dilute multi-phase particle flow. The electrostatic sensor array achieves this by using an array or electrostatic electrode pairs across the diameter of the pipe. To this end a wide range of particle flow conditions will be investigated.

6.2.1 Initial Experimentation Using Flour

Initial trials of the electrostatic sensor array were carried out using the negative pressure rig with flour as a pulverised material due to the fine particle size of flour which makes it have good flow characteristics in the pipe. The initial testing was designed to determine if the electrostatic sensor array was capable of determining the particle velocity and concentration profiles. Furthermore comparisons were carried out between the measured particle velocity and the conveying air velocity to determine the difference between the two. The initial tests with flour were implemented with the sensor mounted on a horizontal pipe section.

6.2.1.1 Experimental Conditions

To ensure sensor readings were taken on a developed dilute phase flow the sensor was mounted after a 2600 mm straight horizontal pipe section. During the experiments, temperature (25.3°C average) and relative humidity (47.5% average) were monitored to ensure environmental test conditions were the same for each test. Particle feed rate of the flour was approximately 1.8 kg/hour for all experiments. Particle size and shape analysis of the pulverised flour was taken using an off-line digital particle size imager. The measured particle size distribution and shape distribution (aspect ratio) of the flour particles are shown in Fig. 6.1 and Fig 6.2 respectively.

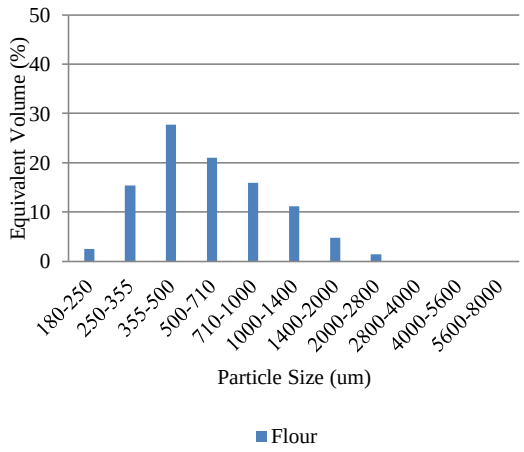

Fig. 6.1 Particle size distribution of flour particles

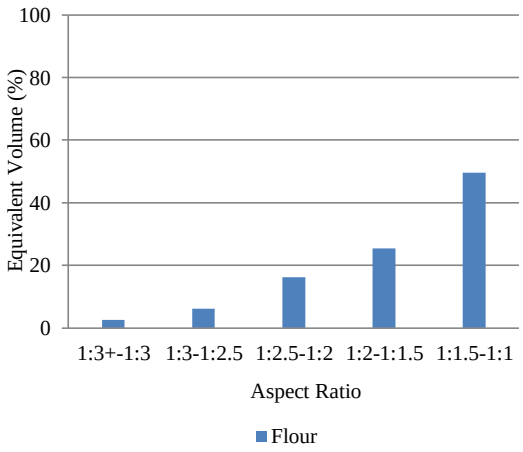

Fig. 6.2 Particle aspect ratio of flour particles

For each of the electrostatic sensor array axis orientations, experiments were carried out on the electrostatic array with five different conveying air velocities. These ranges of particle velocity were achieved by varying the power of the vacuum plant on the negative pressure test rig. The complete test matrix is shown in Table 6.1.

Table 6.1

Flour Test condition matrix

Pulverised Material	Sensor Axis	Pipe Orientation	Vacuum Relative Power (%)
Flour	Z	Horizontal	50, 55, 60, 65, 70
Flour	Y	Horizontal	50, 55, 60, 65, 70

The conveying air velocity profiles were obtained as a reference using a commercial hot wire anemometer. Readings were taken using the hot wire anemometer at the same locations across the pipe diameter as the locations of each of the elements on the electrostatic sensor array. The air velocity profiles for the Z and Y sensor axis is shown in Fig. 6.3 and Fig. 6.4 respectively.

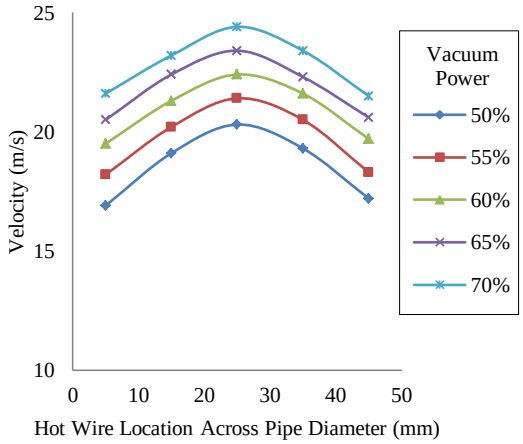

Fig. 6.3 Air velocity profiles measured using a commercial hot wire anemometer on the Z axis at the same locations as the electrostatic sensors

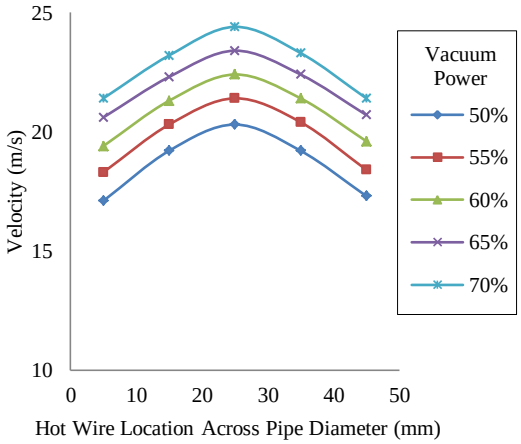

Fig. 6.4 Air velocity profiles measured using a commercial hot wire anemometer on the Y axis at the same locations as the electrostatic sensors

6.2.1.2 Upstream/Downstream Electrostatic Sensor Output

The electrostatic sensor array has two data logging functions: full data logging and basic data logging. Full data logging records the signal output from both the upstream and downstream electrodes on each of the elements on the electrostatic sensor array as well as the correlation function for each cross correlation operation. The basic data logging function only records the measured particle velocity, correlation coefficient, and r.m.s charge level (particle concentration) for each element of the array. For efficient data collection, most experimental data is collected using the basic data logging function. For initial testing, however, full data logging was used on a small number of test runs to observe the upstream and downstream electrostatic signal outputs. Fig. 6.5 shows the upstream/downstream signal outputs for one element of the electrostatic array. The delay between the upstream/downstream signals can be observed. The correlation

function of the upstream/downstream signals can be observed in Fig. 6.6. The position of the dominant peak τ_m (the correlation coefficient) along the time axis denotes the delay between the upstream and the downstream signals.

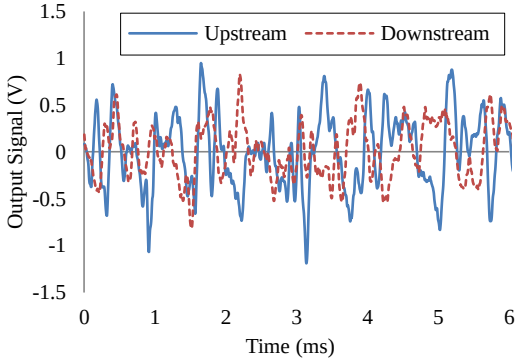

Fig. 6.5 Upstream and downstream signals from a single element in the electrostatic sensor array

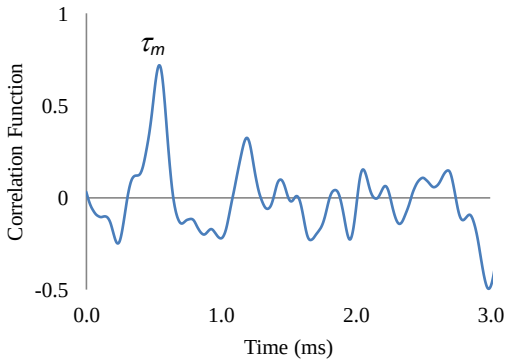

Fig. 6.6 Correlation function between the upstream and downstream sensor signals

6.2.1.3 Measured Particle Velocity Profiles

The electrostatic sensor array is capable of determining the velocity profile of a developed dilute flour/air flow. Fig. 6.7 and Fig. 6.8 show the mean particle velocity profile for a range of air velocities. The profiles clearly show that particles traveling at the centre of the pipe are moving at a higher velocity then those moving along the pipe wall due to the frictional force acting on the conveying air and particles caused by interaction with the pipe wall.

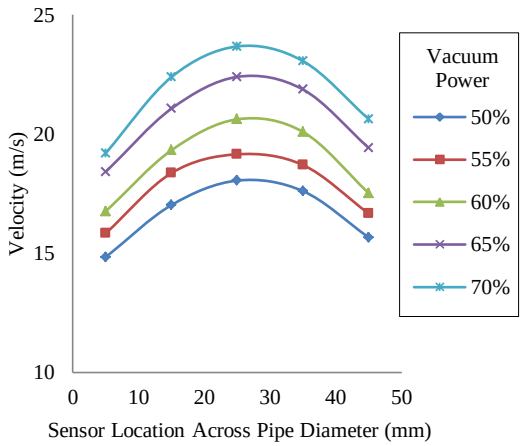

Fig. 6.7 Mean velocity profiles measured by the electrostatic sensor array on the Z axis (data points indicate centre of the electrode)

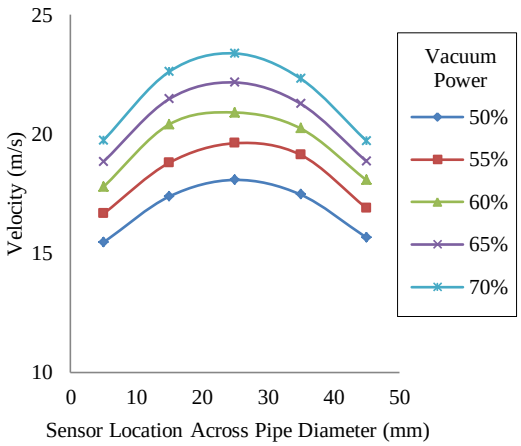

Fig. 6.8 Mean velocity profiles measured by the electrostatic sensor array on the Y axis

The Z axis velocity profile in Fig. 6.7 shows that the velocity at the bottom of the pipe (5 mm) is lower than the velocity at the top of the pipe (45 mm); this is due to gravity's effect on the particles forcing them to come into contact with the pipe wall at the bottom of the pipe. Whereas Fig. 6.8 shows the velocity profile for the Y axis which is more symmetrical compared to the Z axis since gravity is having a uniform effect over the whole pipe diameter.

A comparison of the particle velocity and air velocity profiles shown in Fig. 6.9 and Fig. 6.10 illustrates that the difference between the particle and air velocities decreases for higher air velocities indicating that higher air velocities are better at keeping the particles in suspension.

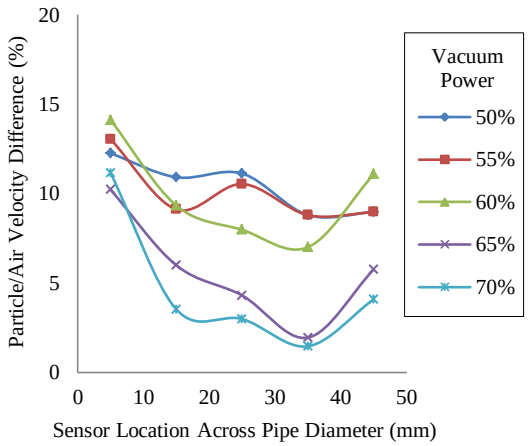

Fig. 6.9 Percentage difference between the air and particle velocity profiles on the Z axis

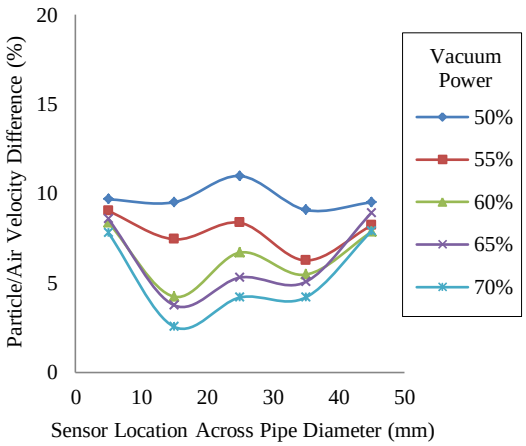

Fig. 6.10 Percentage difference between the air and particle velocity profiles on the Y axis

The reason for the difference between the velocity of the conveying air and particle velocity is because the process of conveying and suspending the particle is one of drag force and hence the particle velocity will be lower than the conveying air [1]. Typically in a horizontal pipe the particle velocity is 80% of the conveying air velocity. However this value can vary depending on parameters such as particle size, shape and density [1]. Conversely, the effect of friction between the pipe wall and particle flow can be seen in Fig. 6.9 and Fig. 6.10 where the difference between the particle and air velocity is higher at 5 mm and 45 mm (however this observation only holds true at higher air velocities, at lower air velocities 50% and 55% power has a more uniform profile since the particles may not be fully suspended). The effect of gravity can be seen in Fig. 6.9 where the difference between the conveying air velocity and the particle velocity is higher the closer to the bottom of the pipe.

The normalised velocity standard deviation profile shown in Fig. 6.11 and Fig. 6.12 shows that the particle velocities measured in the centre of the pipe have a lower deviation compared to those along the pipe wall indicating a more stable particle flow in the centre of the pipe.

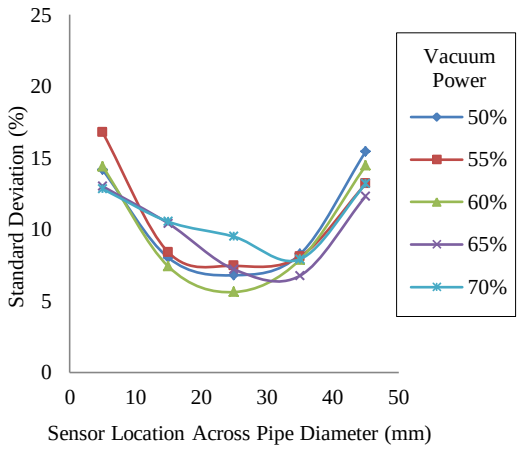

Fig. 6.11 Normalised standard deviation profiles of the velocities on the Z axis

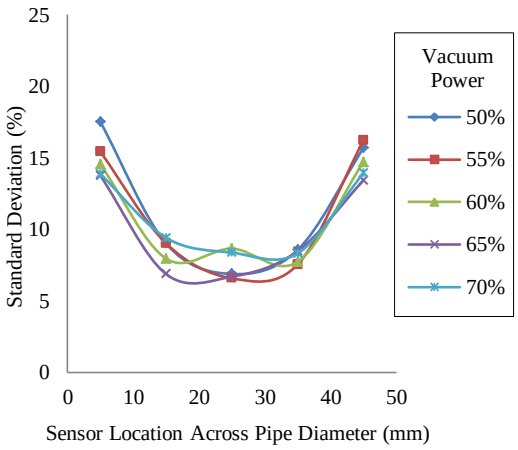

Fig. 6.12 Normalised standard deviation profiles of the velocities on the Y axis

6.2.1.4 Measured Particle Concentration Profiles

The electrostatic sensor array is capable of determining the particle concentration profiles. Fig. 6.13 shows the concentration profile measured by the electrostatic sensor array on the Z axis. The particle concentration increases the closer to the bottom of the pipe due to the effect of gravity. However at the very bottom of the pipe (5 mm) the particle concentration is less compared to the concentration measured on the sensor element above (15 mm). A possible reason for this is that the particle size of the flour used in this experiment is very small; consequently the flour particles would have a lower mass and would therefore be affected more by the turbulence caused by the proximity of the sensor blade and the pipe wall. This turbulence would mean the smaller particles would be unable to enter the smaller volume of space at the bottom of the pipe between the sensor blade and pipe wall thus causing less particles to be detected by the sensor. However, for larger pipe bores this effect would be less dramatic since the pipe radius would be increased. This flow characteristic could conceivably be due to the small flour particles spinning as they are traveling down the pipe causing the Magnus effect [109] where this particle spin pulls the particles away from the pipe wall. The phenomenon of reduced particle concentration along the pipe wall can be seen on the Y

axis particle concentration profile (Fig. 6.14), which shows that the concentration in the centre of the pipe is higher than along the pipe wall. Another possibility is that smaller particles are affected more by the discharging effect of coming into contact with the pipe wall due to the steel pipe being earthed for safety reasons. In addition, Fig. 6.14 shows that for the higher air velocities (60-70% power) the r.m.s charge is increasing in the centre of the pipe (with exception to the r.m.s. measured at the centre of the pipe for 70% power). This is most likely due to a disruption of the particle input on the vibration feeder since it does not appear in other particle velocities). This is feasibly due to the fact that at higher air velocities more particles are being suspended; consequently more particles are able to be detected by the sensor array on the Y axis.

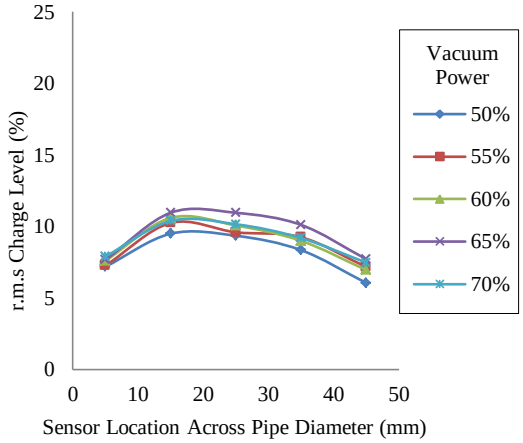

Fig. 6.13 Mean particle concentration profiles on the Z axis

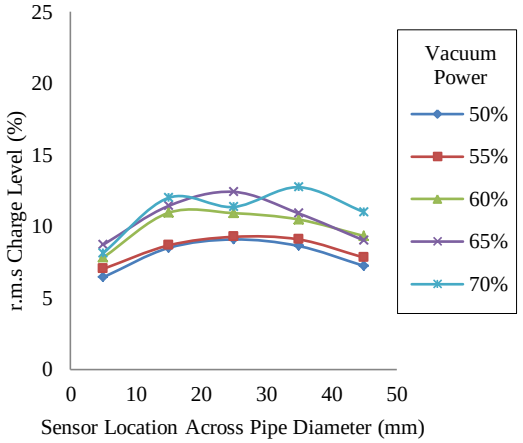

Fig. 6.14 Mean particle concentration profiles on the Y axis

6.2.1.5 Correlation Coefficient Profiles

The magnitude of the correlation coefficient is an indication of the stability of the particle flow [54] (the closer to 1 the correlation coefficient is, the more stable the flow). Fig. 6.15 and Fig. 6.16 show the correlation coefficient profiles (for the Z and Y axis respectively). Across the pipe diameter, it is clear that the correlation coefficient is higher in the centre of the pipe compared to that along the pipe wall, demonstrating that the particle flow is more stable in the centre of the pipe which is consistent over all five particle velocities for both sensor orientations.

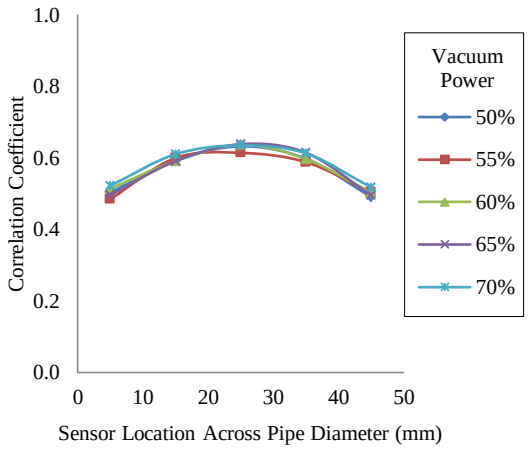

Fig. 6.15 Mean correlation coefficient profiles for the pipe cross section on the Z axis

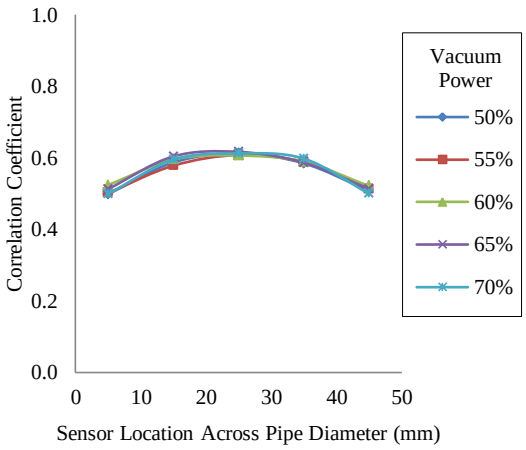

Fig. 6.16 Mean correlation coefficient profiles for the pipe cross section on the Y axis

The normalised standard deviation of the correlation coefficient with the sensor array on the Z axis shown in Fig. 6.17 agrees well with the standard deviation of the velocity in the same orientation (Fig. 6.11), with the correlation coefficient deviating less in the centre of the pipe compared to along the pipe wall. However, the normalised standard deviation of the correlation coefficient with the sensor array on the Y axis (Fig. 6.18) does not agree with the standard deviation of the velocity in the on the Y axis (Fig. 6.12). The normalised standard deviation shows that the correlation coefficient deviated more evenly over the pipe diameter with only a small reduction of the deviation in the centre of the pipe. This effect is not fully understood. This is possibly an indication that a combination of turbulence (caused by the sensor array interacting with the particle flow), a smaller particle size/mass and gravity (since gravity is having a uniform effect) has a significant effect on the standard deviation of the correlation coefficient on a horizontal pipe on the Y axis.

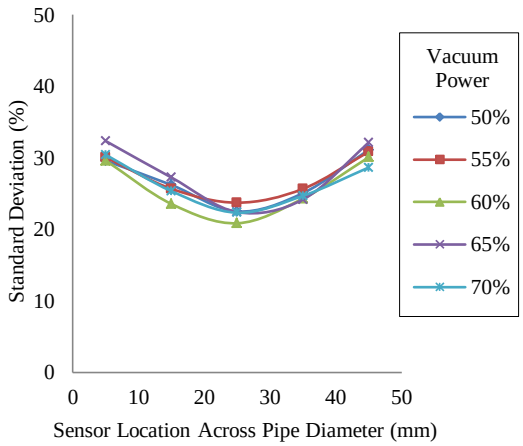

Fig. 6.17 Normalised standard deviation profiles of the correlation coefficient on the Z axis

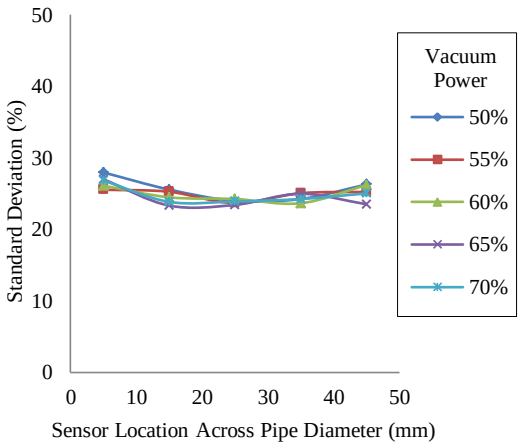

Fig. 6.18 Normalised standard deviation profiles of the correlation coefficient on the Y axis

6.2.1.6 Discussion on the Initial Experimentation Using Flour

The electrostatic sensor array is capable of on-line monitoring of the particle velocity and concentration profiles across the diameter of a pneumatic conveying pipe. Through analysis of the velocity profiles as well as the correlation coefficient profiles the performance of the electrostatic sensor array is in line with particle flow dynamics inside a pipe; this shows the particle flow in the centre of the pipe is more stable than the particle flow along the pipe wall. Comparison of the air velocity profile (measured using a commercial hot wire anemometer) and the particle velocity profile (measured using the electrostatic sensor array) has shown that interaction with the pipe causes velocity loss in the conveyed particles due to friction. The effect of gravity has also been documented on a horizontal pipe since particle velocity at the bottom of the pipe has a higher difference between the conveying air velocity and particle velocity compared to the top of the pipe.

6.2.2 Flow Characteristics of Pneumatically Conveyed Biomass

Biomass fuel is becoming a popular alternative to burning coal to generate electricity since biomass is a renewable fuel. Pneumatically conveyed biomass however presents measurement challenges due to its wider size and shape distribution compared to pulverised coal. For this reason experimental work was carried out to determine the effect that particle size has on the flow characteristics of pneumatically conveyed biomass. Tests were carried out on two different size ranges of pulverised willow biomass (coarse and fine particles), using a range of conveying air velocities, on different pipe orientations (horizontal and vertical pipe sections) and sensor orientations. Pulverised willow was chosen as a pulverised material due to its use as a biofuel. Experimentation was carried out using the negative pressure test rig.

6.2.2.1 Experimental Conditions

Testing was carried out using the negative pressure test rig with the sensor mounted on both horizontal and vertical pipe sections. The sensor mounting on the horizontal pipe section was mounted after a 2600 mm straight horizontal pipe section ensuring measurement of a developed flow. The sensor mounting for the vertical pipe section was placed 400 mm from a right angle bend with the particle flow going in the direction of gravity. During the experiments, temperature (25.3°C average) and relative humidity (47.5% average) were monitored to ensure environmental test conditions were the same for each test. Particle size and shape analysis of the pulverised willow biomass was taken using an off-line digital particle size imager. The measured particle size distribution and shape distribution (aspect ratio) for both the coarse and fine willow biomass particles are shown in Fig. 6.19 and Fig 6.20 respectively.

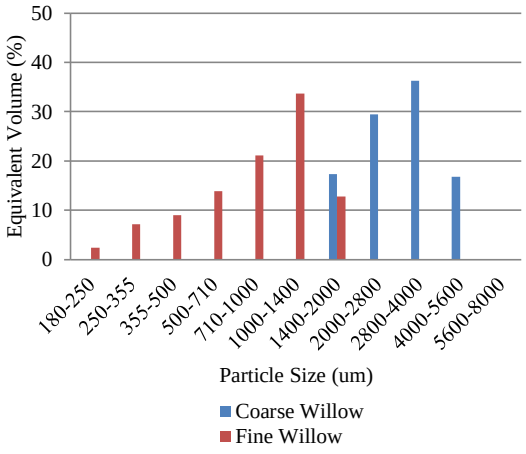

Fig. 6.19 Particle size distribution of coarse and fine willow particles

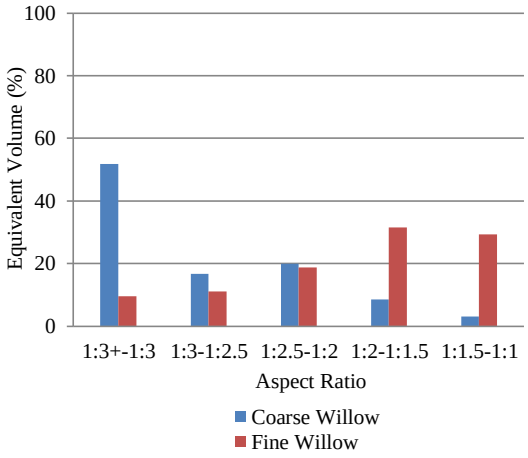

Fig. 6.20 Particle aspect ratio of coarse and fine willow particles

For each of the electrostatic sensor array axis orientations the electrostatic array was placed in, five different conveying air velocities were used. These ranges of particle velocity were achieved by varying the power of the vacuum plant on the negative pressure test rig. The particle feed rate for each type of material was approximately 2.08 kg/hour and 1.48 kg/hour for coarse and fine willow respectively. The complete test matrix is shown in Table 6.2.

Table 6.2

Biomass test condition matrix

Pulverised Material	Sensor Axis	Pipe Orientation	Vacuum Relative Power (%)
Coarse Willow	Z	Horizontal	50, 55, 60, 65, 70
Fine Willow	Z	Horizontal	50, 55, 60, 65, 70
Coarse Willow	Y	Horizontal	50, 55, 60, 65, 70
Fine Willow	Y	Horizontal	50, 55, 60, 65, 70
Coarse Willow	X	Vertical	50, 55, 60, 65, 70
Fine Willow	X	Vertical	50, 55, 60, 65, 70
Coarse Willow	Y	Vertical	50, 55, 60, 65, 70
Fine Willow	Y	Vertical	50, 55, 60, 65, 70

6.2.2.2 Measured Particle Velocity Profiles

Horizontal Particle Flow

The electrostatic sensor array was able to measure the velocity profile for the whole diameter of the pipe. Fig. 6.21 - Fig. 6.24 show the velocity profiles for the sensor array mounted on the Z and Y axis on the horizontal pipe.

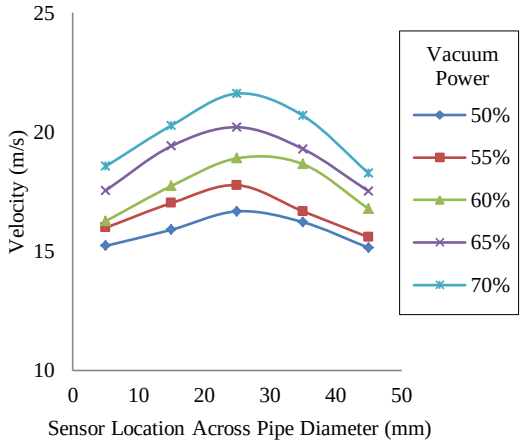

Fig. 6.21 Mean velocity profiles of the coarse willow on the Z axis on a horizontal pipe

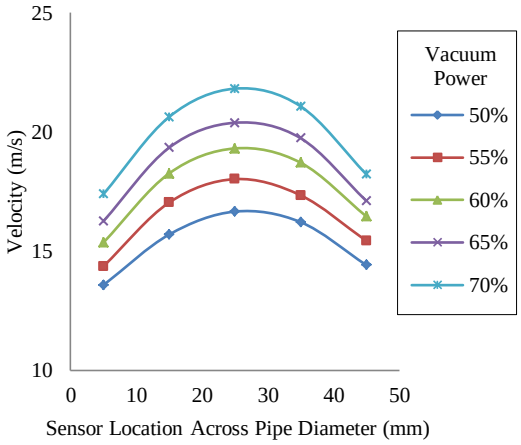

Fig. 6.22 Mean velocity profiles of the fine willow on the Z axis on a horizontal pipe

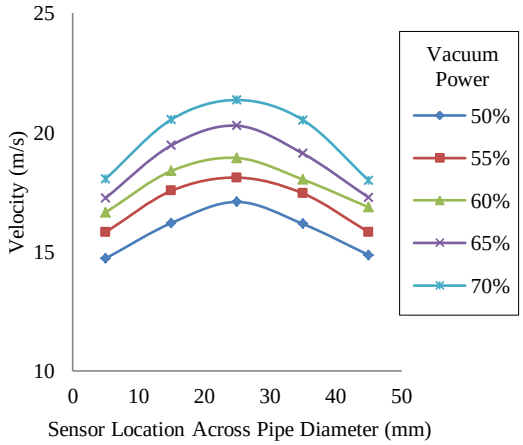

Fig. 6.23 Mean velocity profiles of the coarse willow on the Y axis on a horizontal pipe

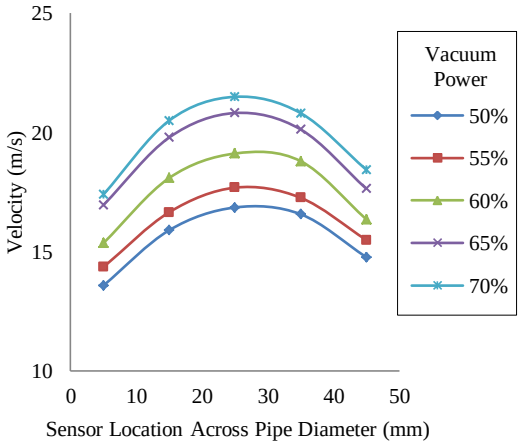

Fig. 6.24 Mean velocity profiles of the fine willow biomass on the Y axis on a horizontal pipe

The particle velocity profiles indicate that the coarse and fine willow particles at the centre of the pipe are travelling at a higher velocity than the particles near the pipe wall

due to the particles colliding with the wall and slowing down due to friction. The shape of the velocity profiles for the fine willow (Fig. 6.22 and Fig. 6.24) are much more homogeneous than the coarse willow profiles (Fig. 6.21 and Fig. 6.23) indicating that smaller particles have more stable flow characteristics.

The normalised standard deviation of the velocity profiles is an indication of flow stability. The coarse willow on the Z and Y axis shown in Fig. 6.25 and Fig. 6.27 illustrates that the velocity standard deviation is uniform across the whole diameter of the pipe. Whereas the velocity standard deviation profiles for the fine willow material (Fig. 6.26 and Fig. 6.28) indicate that the particle velocity in the centre of the pipe deviates less than the particle flow along the pipe wall; this is an indication that the fine willow biomass produces a more stable flow compared to the coarse willow. Moreover, the fine willow produces a standard deviation profile that is in line with flow dynamics; the flow along the pipe wall is more unstable then the flow at the centre of the pipe.

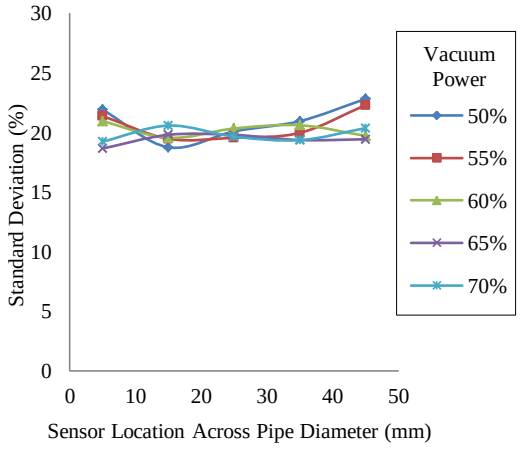

Fig. 6.25 Normalised standard deviation profiles of the velocities for coarse willow on the Z axis on a horizontal pipe

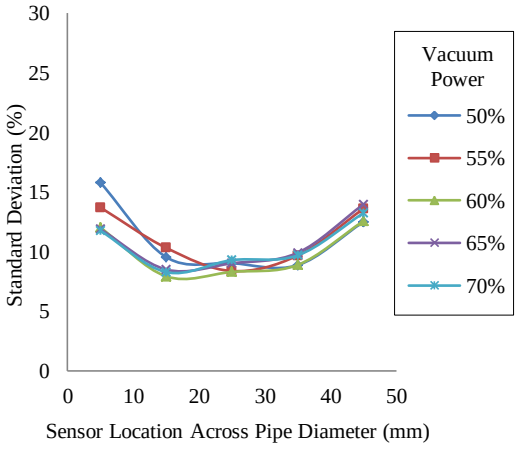

Fig. 6.26 Normalised standard deviation profiles of the velocities for fine willow on the Z axis on a horizontal pipe

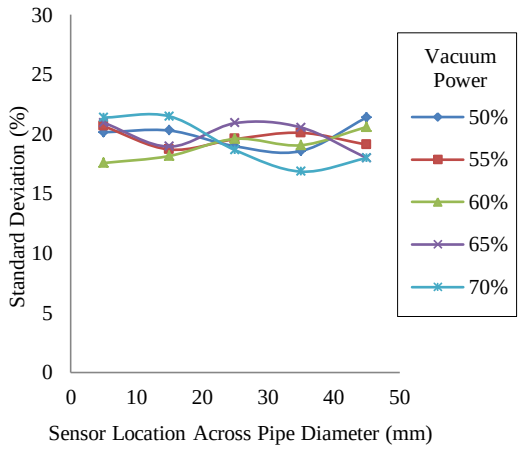

Fig. 6.27 Normalised standard deviation profiles of the velocities for coarse willow on the Y axis on a horizontal pipe

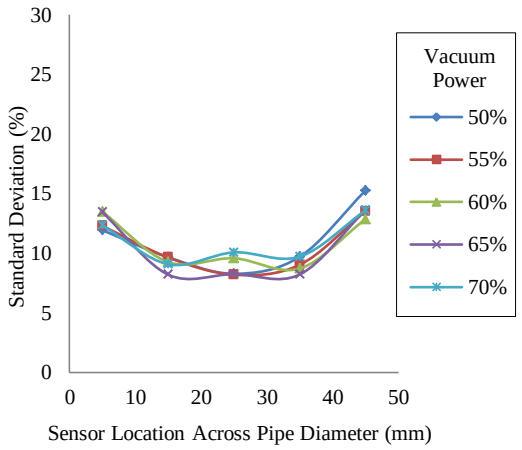

Fig. 6.28 Normalised standard deviation profiles of the velocities for fine willow on the Y axis on a horizontal pipe

Vertical Particle Flow

The velocity profile measured using the electrostatic sensor array mounted on the X and Y axis on the vertical pipe is not a typical velocity profile (Fig. 6.29 – Fig. 6.32). This is because the velocity profile has not yet developed since it has just left the right angle bend.

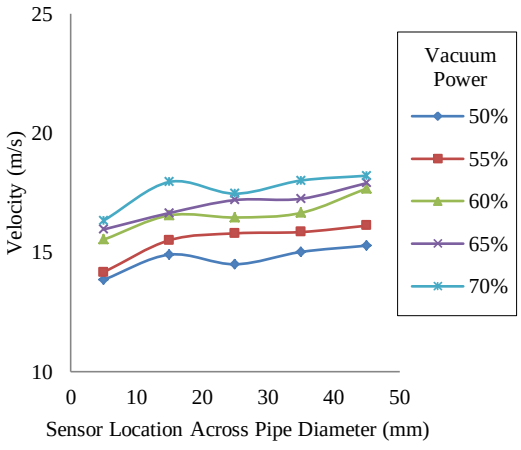

Fig. 6.29 Mean velocity profiles of the coarse willow on the X axis on a Vertical pipe

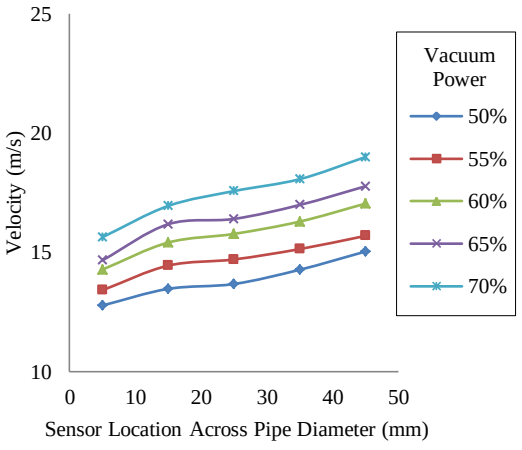

Fig. 6.30 Mean velocity profiles of the fine willow on the X axis on a Vertical pipe

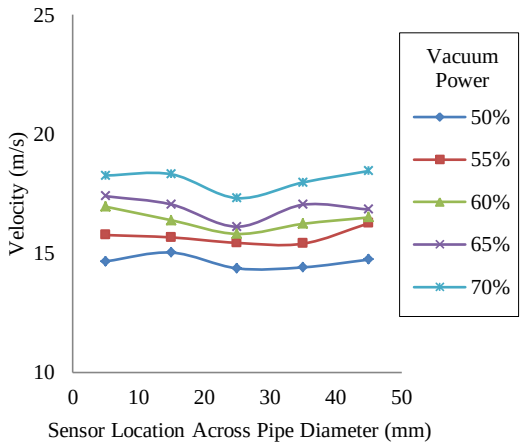

Fig. 6.31 Mean velocity profiles of the coarse willow on the Y axis on a Vertical pipe

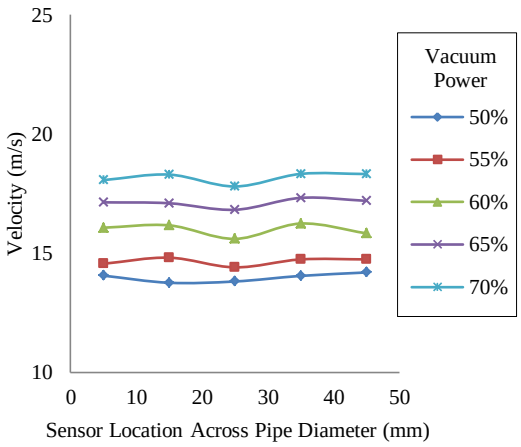

Fig. 6.32 Mean velocity profiles of the fine willow on the Y axis on a Vertical pipe

The shape of the velocity profiles (Fig. 6.29 and Fig. 6.30) indicates that the particle flow along the outer radius (45 mm) is travelling at a higher velocity than particles flowing along the inner radius of the right angle pipe bend. The normalised standard deviation velocity profiles in Fig. 6.33 - Fig. 6.36 show that the fine willow biomass (Fig. 6.34 and Fig. 6.36) deviates less than the coarse willow (Fig. 6.33 and Fig. 6.35).

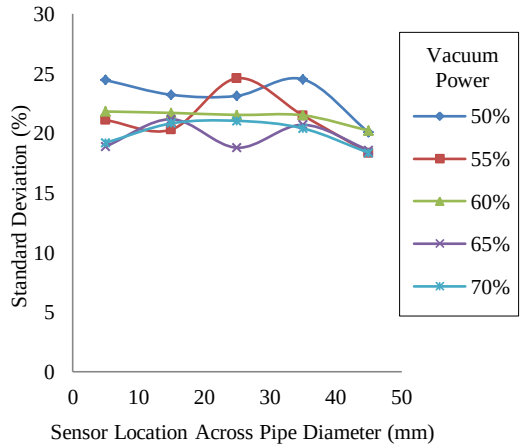

Fig. 6.33 Normalised standard deviation profiles of the velocities for coarse willow biomass measured by the electrostatic array sensor on the X axis on a Vertical pipe

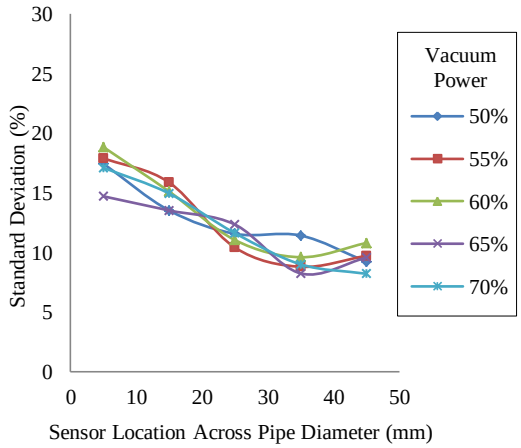

Fig. 6.34 Normalised standard deviation profiles of the velocities for fine willow biomass measured by the electrostatic array sensor on the X axis on a Vertical pipe

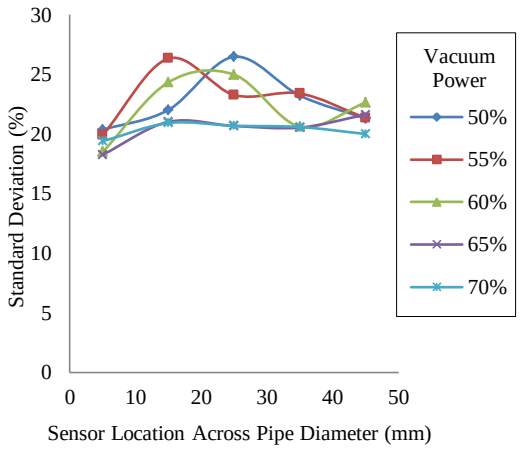

Fig. 6.35 Normalised standard deviation profiles of the velocities for coarse willow on the Y axis on a Vertical pipe

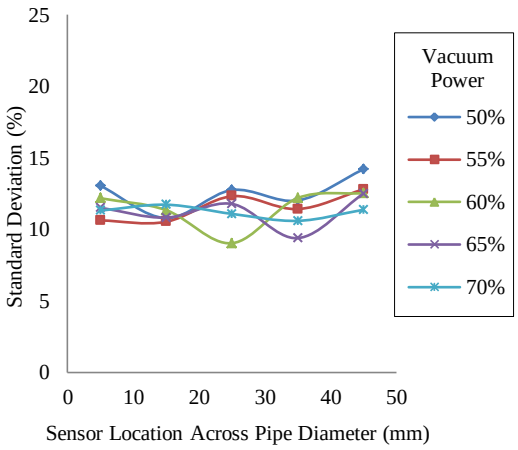

Fig. 6.36 Normalised standard deviation profiles of the velocities for fine willow on the Y axis on a Vertical pipe

This difference in the standard deviation profiles suggest that the fine willow has a more stable flow compared to the coarse willow biomass in an undeveloped flow when traveling in a vertical pipe section.

6.2.2.3 Measured Particle Concentration Profiles

Horizontal Particle Flow

The use of the normalised r.m.s magnitude to determine particle concentration can be seen in Fig. 6.37 - Fig. 6.40. From the analysis of the r.m.s profiles it can be seen that the fine willow biomass (Fig. 6.38 and Fig. 6.40) has a higher r.m.s charge magnitude compared to the coarse willow biomass (Fig. 6.37 and Fig. 6.39). This is an indication that high volume of smaller particles carries a higher electrostatic charge compared to smaller concentrations of larger particles (even though the coarse willow has a higher mass flow rate then the fine willow biomass). This is possibly due to the larger surface area produced by many smaller particles when compared to the surface area created by fewer large particles. The effect of gravity can be seen in the r.m.s profile for the fine willow particles (Fig. 6.38) where the r.m.s charge magnitude is higher on the bottom of the pipe (5 mm) compared to the top of the pipe (45 mm). The increased concentration

shown on Fig. 6.40 on the 5 mm side of the pipe could possibly be down to the vibration feeder unevenly distributing particles into the system.

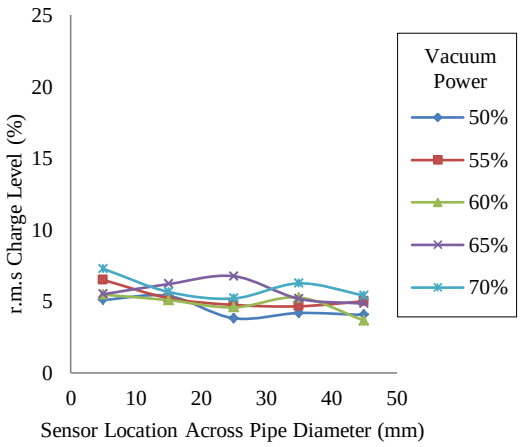

Fig. 6.37 Mean particle concentration profiles of coarse willow on the Z axis on a horizontal pipe

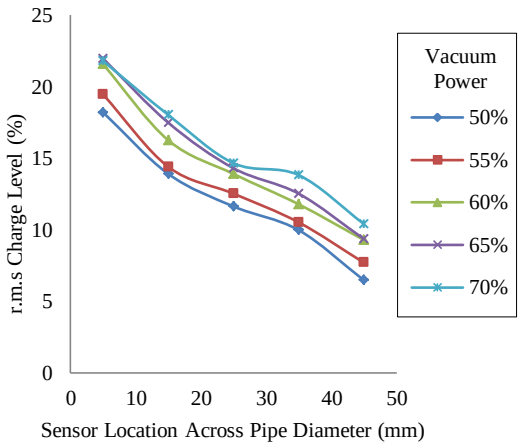

Fig. 6.38 Mean particle concentration profiles of fine willow on the Z axis on a horizontal pipe

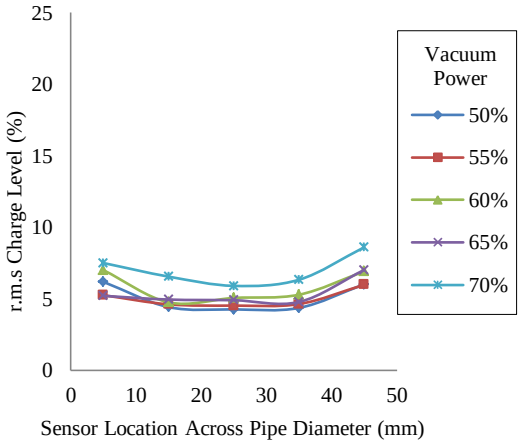

Fig. 6.39 Mean particle concentration profiles of coarse willow on the Y axis on a horizontal pipe

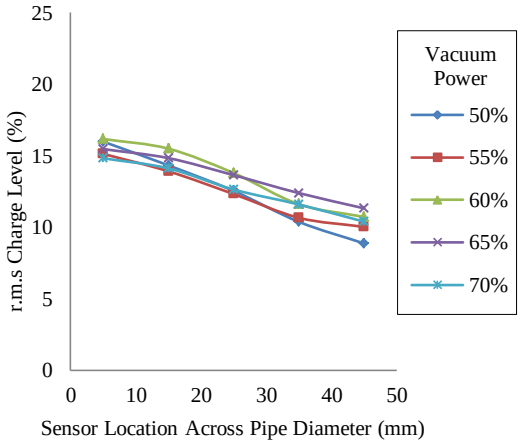

Fig. 6.40 Mean particle concentration profiles of fine willow on the Y axis on a horizontal pipe

Vertical Particle Flow

The normalised r.m.s profiles measured by the sensor array mounted on the vertical pipe section indicates that the smaller particles of the fine willow (Fig. 6.42 and Fig. 6.44)

carry more electrostatic charge compared to the coarse willow biomass (Fig. 6.41 and Fig. 6.43).

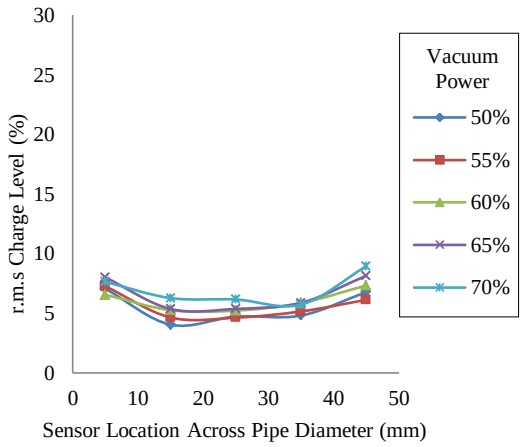

Fig. 6.41 Mean particle concentration profiles of coarse willow on the X axis on a vertical pipe

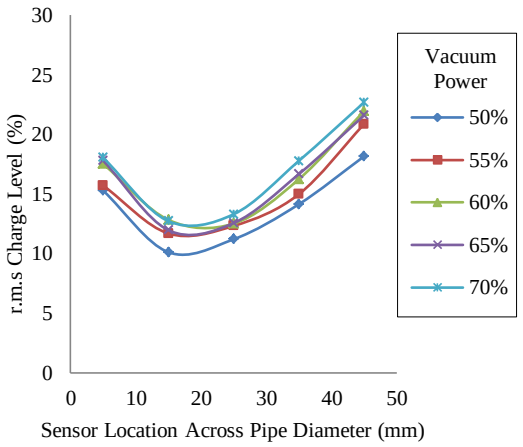

Fig. 6.42 Mean particle concentration profiles of fine willow on the X axis on a vertical pipe

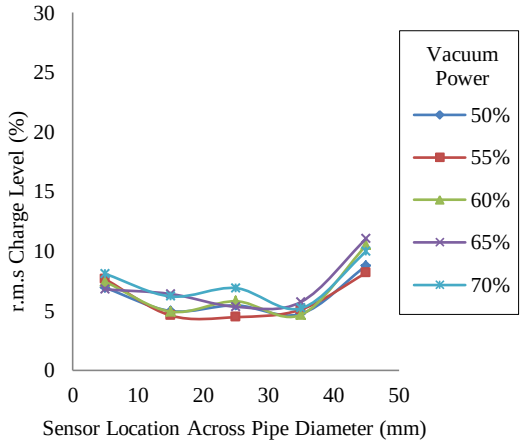

Fig. 6.43 Mean particle concentration profiles of coarse willow on the Y axis on a vertical pipe

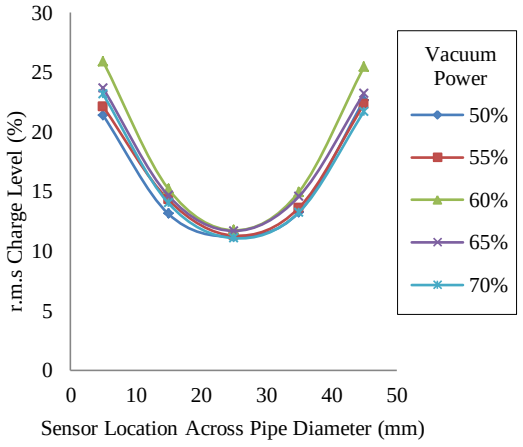

Fig. 6.44 Mean particle concentration profiles of fine willow on the Y axis on a vertical pipe

The shape of the profiles also indicates that the highest particle concentration is along the pipe wall. This illustrates that the particles have been forced along the outer wall due to the centrifugal forces caused by the particles travelling inside the right angle bend. Moreover, this demonstrates that the sensor array is capable of detecting roping inside a pneumatic conveying system.

6.2.2.4 Correlation Coefficient Profiles

Horizontal Particle Flow

The value of the correlation coefficient is additionally an indication of flow stability [54] (the closer to 1 the correlation coefficient, the more stable the flow). The fine willow biomass shown in Fig. 6.46 and Fig. 6.48 has a higher correlation coefficient compared to the coarse willow biomass shown in Fig. 6.45 and Fig. 6.47 indicating that the fine willow biomass has a more stable flow compared to the coarse willow biomass; this is consistent with the velocity standard deviation results.

The correlation coefficient profiles for the fine willow biomass in Fig. 6.46 and Fig. 6.48 also show that the correlation coefficient is higher in the centre of the pipe compared to along the pipe wall, indicating that the particle flow along the pipe wall is more unstable compared to the particle flow in the centre of the pipe.

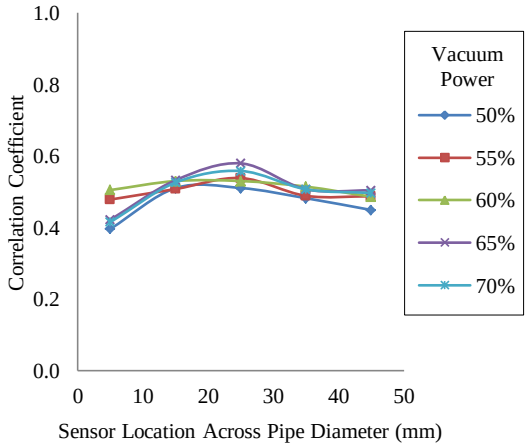

Fig. 6.45 Mean correlation coefficient profiles of coarse willow on a horizontal pipe

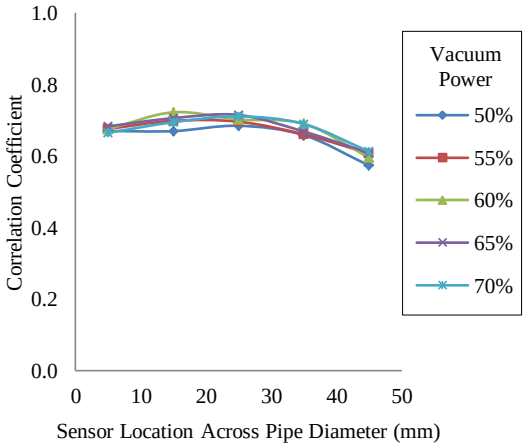

Fig. 6.46 Mean correlation coefficient profiles of fine willow on the Z axis on a horizontal pipe

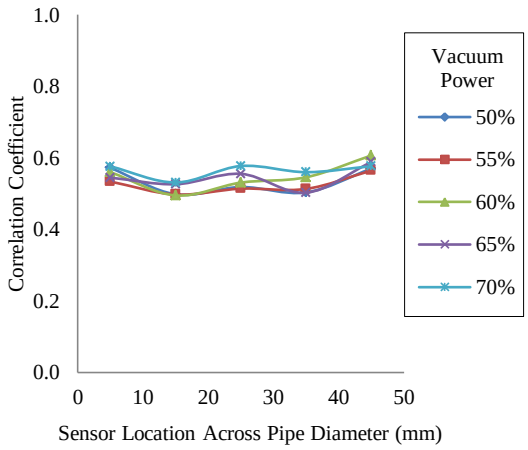

Fig. 6.47 Mean correlation coefficient profiles of coarse willow on the Y axis on a horizontal pipe

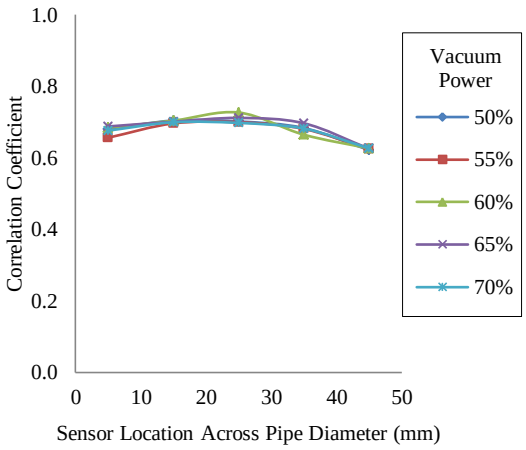

Fig. 6.48 Mean correlation coefficient profiles of fine willow on the Y axis on a horizontal pipe

Analysis of the standard deviation of the correlation coefficient demonstrates that the fine willow biomass (Fig. 6.50 and Fig. 6.52) deviates less than the coarse willow biomass (Fig. 6.49 and Fig. 6.51).

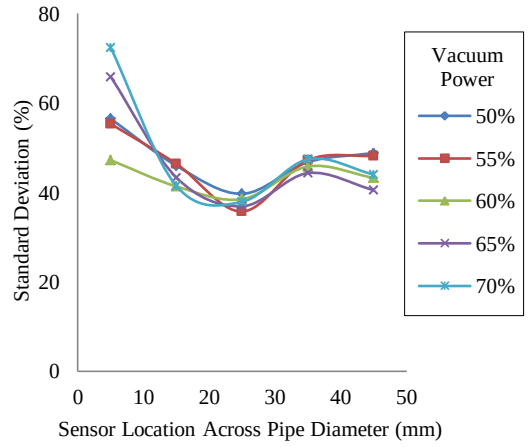

Fig. 6.49 Normalised standard deviation profiles of the correlation coefficient of coarse willow on the Z axis on a horizontal pipe

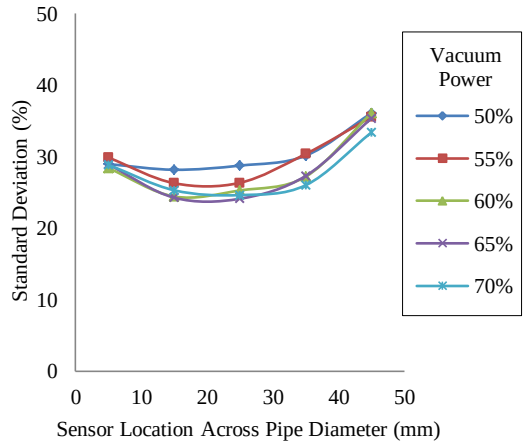

Fig. 6.50 Normalised standard deviation profiles of the correlation coefficient of fine willow on the Z axis on a horizontal pipe

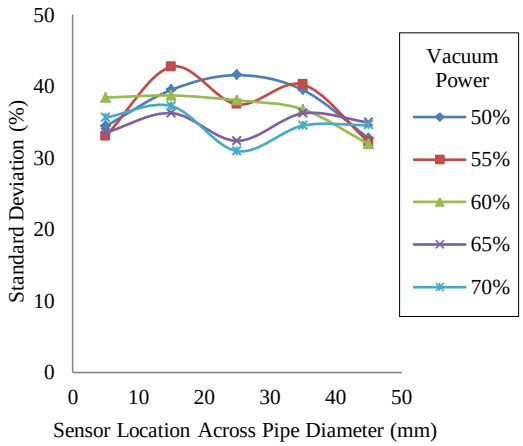

Fig. 6.51 Normalised standard deviation profiles of the correlation coefficient of coarse willow on the Y axis on a horizontal pipe

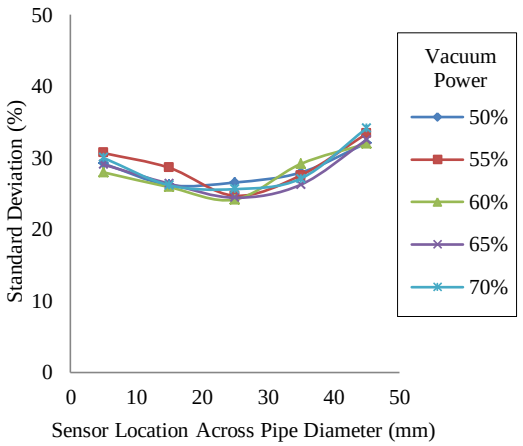

Fig. 6.52 Normalised standard deviation profiles of the correlation coefficient of fine willow on the Y axis on a horizontal pipe

The shape of the profiles for the fine willow biomass (Fig. 6.50 and Fig. 6.52) likewise denotes that the correlation coefficient deviates less in the centre of the pipe compared to along the pipe wall indicating that the flow along the pipe wall is more unstable compared to the flow at the centre of the pipe.

Vertical Particle Flow

The correlation coefficient profiles for the coarse willow biomass flowing along a vertical pipe displayed in Fig. 6.53 and Fig. 6.55 is consistent across the whole pipe diameter. However, the correlation coefficient profile for the fine willow biomass shown in Fig. 6.54 and Fig. 6.56 increases towards the centre of the pipe. This can especially be seen in Fig. 6.56 where the correlation coefficient is around 0.6 along the pipe wall and 0.7 at the centre of the pipe, revealing that the flow in the centre of the pipe is more stable than along the pipe wall. The fine willow biomass shown in Fig. 6.54 and Fig. 6.56 has a higher correlation coefficient compared to the coarse willow biomass shown in Fig. 6.53 and Fig. 6.55 demonstrating that the fine willow biomass has a more stable flow compared to the coarse willow biomass when being conveyed along a vertical pipe.

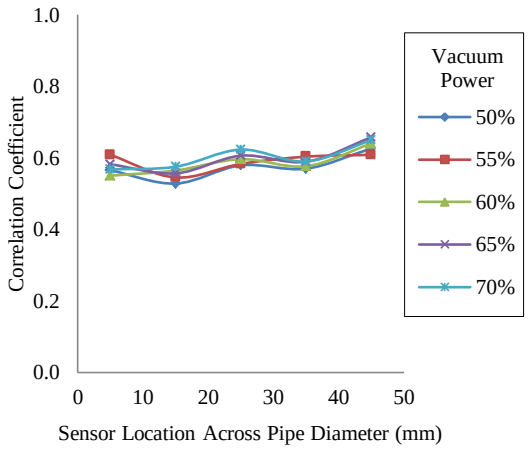

Fig. 6.53 Mean correlation coefficient profiles of coarse willow on the X axis on a vertical pipe

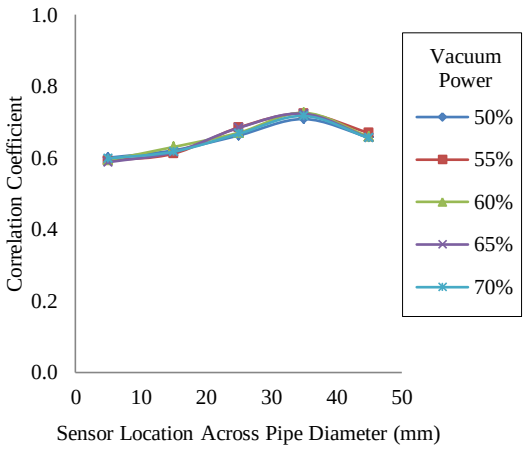

Fig. 6.54 Mean correlation coefficient profiles of fine willow on the X axis on a vertical pipe

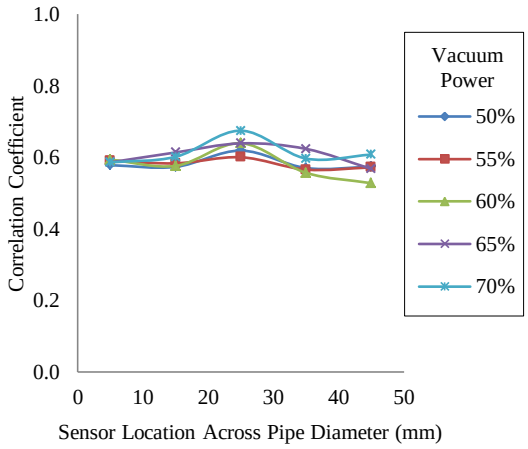

Fig. 6.55 Mean correlation coefficient profiles of coarse willow on the Y axis on a vertical pipe

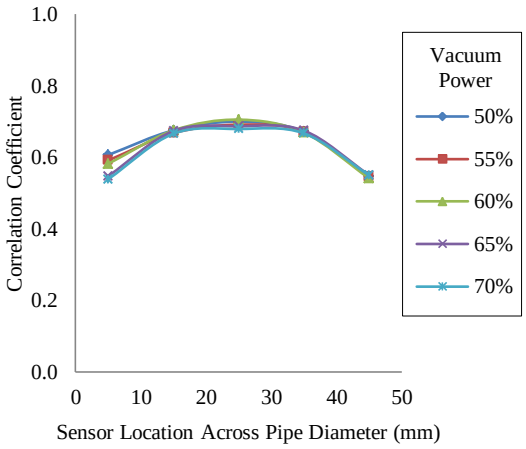

Fig. 6.56 Mean correlation coefficient profiles of fine willow on the Y axis on a vertical pipe

The normalised standard deviation profiles of the correlation coefficient data obtained by the electrostatic sensor array on a vertical pipe for coarse and fine willow biomass are shown in Fig. 6.57 – Fig. 6.60. These profiles indicate that the fine willow (Fig. 6.58 and Fig. 6.60) deviate less than the coarse willow (Fig. 6.57 and Fig. 6.59) suggesting that finer particles of willow biomass have more stable flow characteristics.

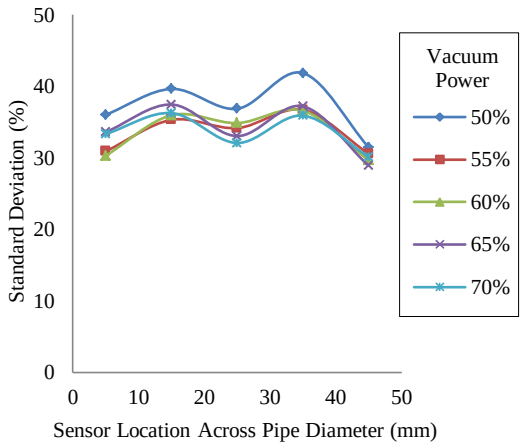

Fig. 6.57 Normalised standard deviation profiles of the correlation coefficient of coarse willow on the X axis on a vertical pipe

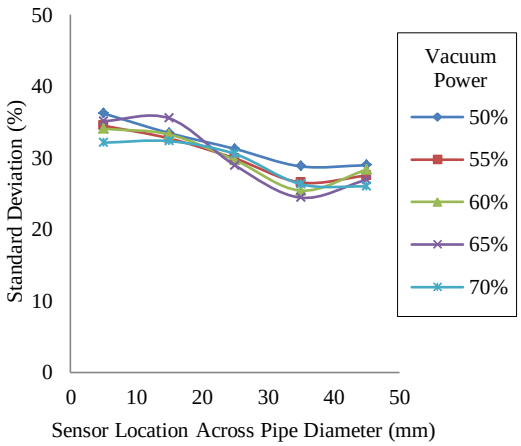

Fig. 6.58 Normalised standard deviation profiles of the correlation coefficient of fine willow on the X axis on a horizontal pipe

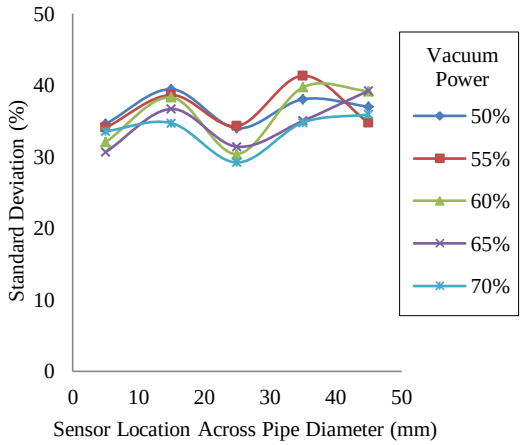

Fig. 6.59 Normalised standard deviation profiles of the correlation coefficient of coarse willow on the Y axis on a vertical pipe

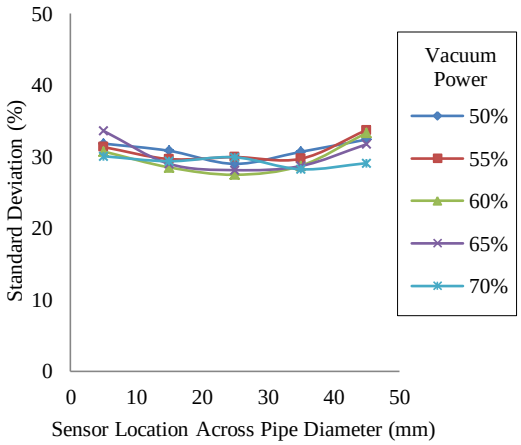

Fig. 6.60 Normalised standard deviation profiles of the correlation coefficient of fine willow on the Y axis on a vertical pipe

6.2.2.5 Discussion on the Flow Characteristics of Pneumatically Conveyed Biomass

An electrostatic sensor array has been successfully used to measure the velocity and concentration profiles of pneumatically conveyed biomass particles. The velocity profiles have clearly demonstrated that the particles along the pipe wall travel at a lower velocity than those in the centre of the pipe. In addition the electrostatic sensor array has also been able to measure the particle concentration profiles. This has been well

documented on the vertical pipe sections since the centrifugal force caused by the particle flow traveling through a right angle bend forces the particles against the pipe wall, which also demonstrates that the electrostatic sensor array is capable of detecting roping flow regimes in a pipeline.

Through analysis of the normalised standard deviation of the velocity profiles, as well as the correlation coefficient profiles, it can be seen that the flow at the centre of the pipe is more stable than that along the pipe wall on developed flow. The comparison between the fine and coarse willow particles has shown that the fine willow produces characteristics of more stable flow compared to the coarse willow on both horizontal and vertical pipe sections. Moreover, the r.m.s profiles have demonstrated that the fine willow generates a sensor signal of a higher magnitude than that of the coarse willow, despite the lower feed rate of the fine willow. The reason for this is the electrostatic charge is stored on the particle surface and higher numbers of smaller particles have a larger combined surface area compared to smaller numbers of large particles.

6.2.3 Flow Characteristics of Pneumatically Conveyed Coal/Biomass Blends

With many coal fired power stations around the world being converted to be co-fired to increase the amount of renewable fuels used in power generation, the particle flow dynamics of the coal/biomass blend has increased. For this reason experimentation has been carried out using the electrostatic sensor array to measure the flow characteristics of pneumatically conveyed coal/biomass blends.

6.2.3.1 Experimental Conditions

Testing was carried out using the positive pressure test rig with the sensor mounted on both horizontal and vertical pipe sections. The sensor mounting on the horizontal pipe section was mounted after a 6400 mm straight horizontal pipe section ensuring measurement of a developed flow. The sensor mounting for the vertical pipe section was placed 1350 mm upstream from a right angle bend with the particle flow going in the up direction against gravity. During the experiments, temperature (20°C average) and relative humidity (45.5% average) were monitored to ensure environmental test

conditions were the same for each test. The biomass used for this experiment was obtained by pulverising biomass fuel pellets (the biomass pellets were formed from waste spruce or pine obtained from saw mill waste [110]). Particle size and shape analysis of the pulverised biomass was obtained using an off-line digital particle size imager. The measured particle size distribution and shape distribution (aspect ratio) for both the pulverised coal and biomass particles are shown in Fig. 6.61 and Fig 6.62 respectively.

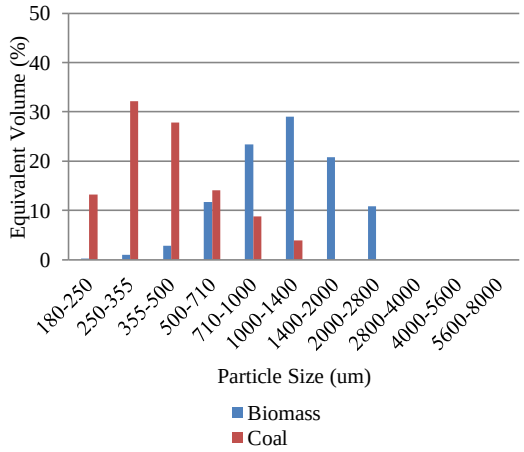

Fig. 6.61 Particle size distribution of pulverised coal and biomass particles

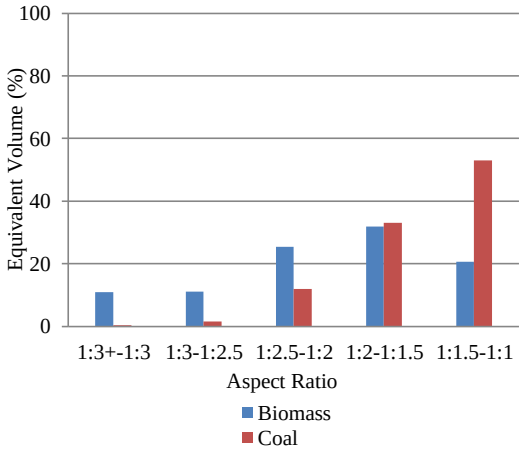

Fig. 6.62 Particle aspect ratio of pulverised coal and biomass particles

Tests were run with pure coal and biomass as well as different coal/biomass ratios by weight (95% coal - 5% biomass, 90% coal - 10% biomass, 85% coal - 15% biomass and 80% coal – 20% biomass). For each of the electrostatic sensor array axis orientations the pulverised material was conveyed using five different air velocities. These ranges of particle velocity were achieved by varying the fan speed of the centrifugal blower on the positive pressure test rig. The time taken for each experiment was recorded as well as the weight of the material collected in the output hopper (to determine the exact particle feed rate). The complete test matrix is described in Table 6.3.

Table 6.3

Coal/Biomass blend test condition matrix

Pulverised Material	Sensor Axis	Pipe Orientation	Fan Speed (RPM)
Coal	Z	Horizontal	750, 800 ,850 , 900 ,950
Coal	Y	Horizontal	750, 800 ,850 , 900 ,950
Coal	X	Vertical	750, 800 ,850 , 900 ,950
Coal	Y	Vertical	750, 800 ,850 , 900 ,950
95% Coal 5% Biomass	Z	Horizontal	750, 800 ,850 , 900 ,950
95% Coal 5% Biomass	Y	Horizontal	750, 800 ,850 , 900 ,950
95% Coal 5% Biomass	X	Vertical	750, 800 ,850 , 900 ,950
95% Coal 5% Biomass	Y	Vertical	750, 800 ,850 , 900 ,950
90% Coal 10% Biomass	Z	Horizontal	750, 800 ,850 , 900 ,950
90% Coal 10% Biomass	Y	Horizontal	750, 800 ,850 , 900 ,950
90% Coal 10% Biomass	X	Vertical	750, 800 ,850 , 900 ,950
90% Coal 10% Biomass	Y	Vertical	750, 800 ,850 , 900 ,950
85% Coal 15% Biomass	Z	Horizontal	750, 800 ,850 , 900 ,950
85% Coal 15% Biomass	Y	Horizontal	750, 800 ,850 , 900 ,950
85% Coal 15% Biomass	X	Vertical	750, 800 ,850 , 900 ,950
85% Coal 15% Biomass	Y	Vertical	750, 800 ,850 , 900 ,950
80% Coal 20% Biomass	Z	Horizontal	750, 800 ,850 , 900 ,950
80% Coal 20% Biomass	Y	Horizontal	750, 800 ,850 , 900 ,950
80% Coal 20% Biomass	X	Vertical	750, 800 ,850 , 900 ,950
80% Coal 20% Biomass	Y	Vertical	750, 800 ,850 , 900 ,950
Biomass	Z	Horizontal	750, 800 ,850 , 900 ,950
Biomass	Y	Horizontal	750, 800 ,850 , 900 ,950
Biomass	X	Vertical	750, 800 ,850 , 900 ,950
Biomass	Y	Vertical	750, 800 ,850 , 900 ,950

6.2.3.2 Measured Particle Velocity Profiles

Horizontal Particle Flow

The electrostatic sensor array was able to measure the velocity profile for the whole diameter of the pipe. Fig. 6.63 - Fig. 6.74 show the developed velocity profiles for the sensor array mounted on the Z and Y axis on the horizontal pipe for coal, biomass and coal/biomass blends. The effect of gravity can be seen for the velocity profiles with the sensor array on the Z axis (Fig. 6.63, Fig. 6.65, Fig. 6.67, Fig. 6.69, Fig. 6.71 and Fig.

6.73) with the particles at the bottom of the pipe (5 mm) traveling at a lower velocity compared to the particles along the top of the pipe (45 mm).

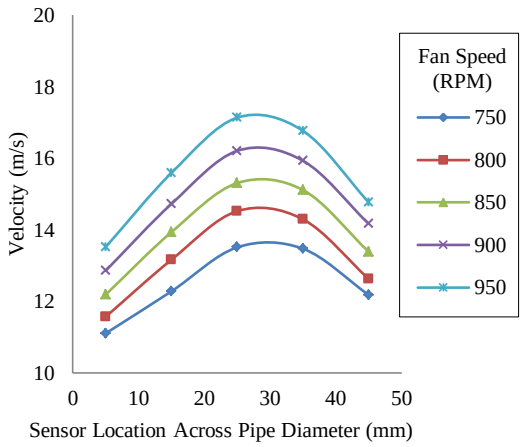

Fig. 6.63 Mean velocity profiles of pulverised coal on the Z axis on a horizontal pipe

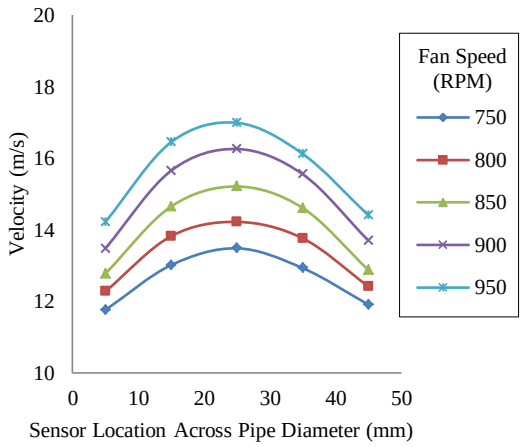

Fig. 6.64 Mean velocity profiles of pulverised coal on the Y axis on a horizontal pipe

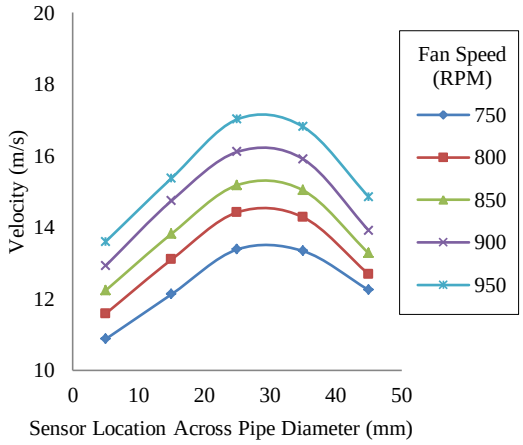

Fig. 6.65 Mean velocity profiles of pulverised coal/biomass (95%/5% blend) on the Z axis on a horizontal pipe

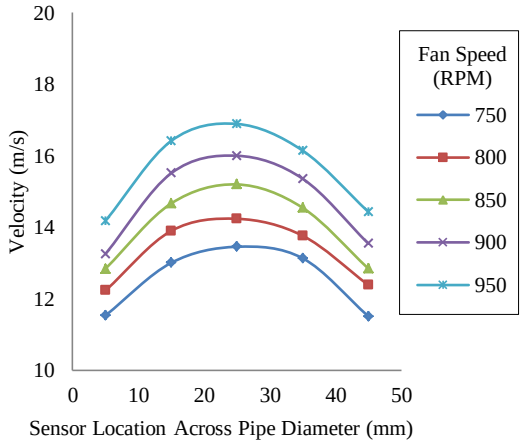

Fig. 6.66 Mean velocity profiles of pulverised coal/biomass (95%/5% blend) on the Y axis on a horizontal pipe

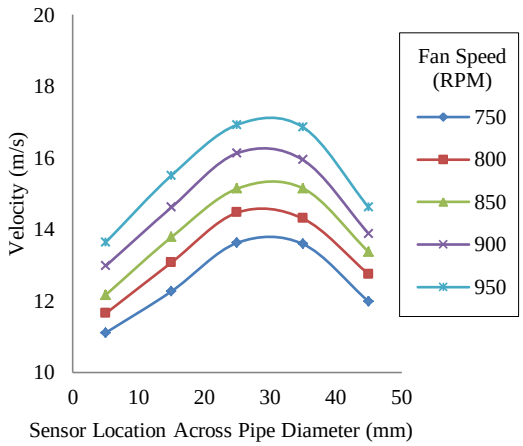

Fig. 6.67 Mean velocity profiles of pulverised coal/biomass (90%/10% blend) on the Z axis on a horizontal pipe

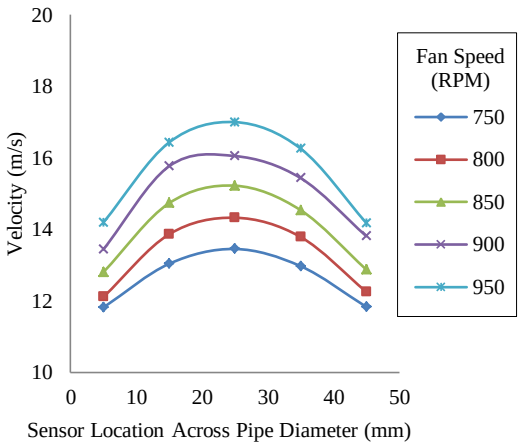

Fig. 6.68 Mean velocity profiles of pulverised coal/biomass (90%/10% blend on the Y axis on a horizontal pipe

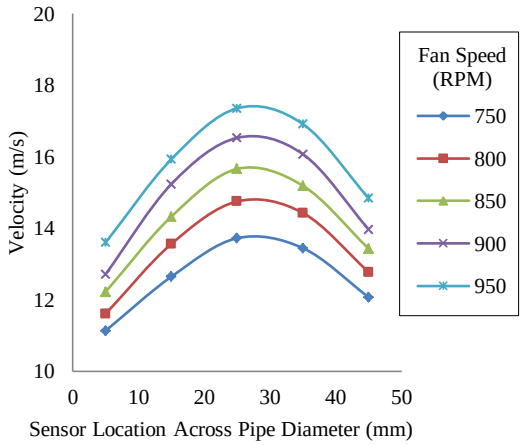

Fig. 6.69 Mean velocity profiles of pulverised coal/biomass (85%/15% blend) on the Z axis on a horizontal pipe

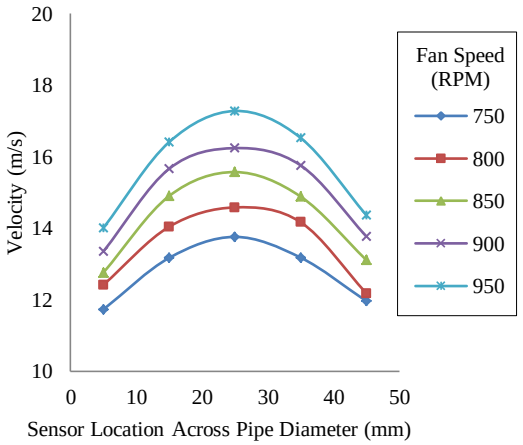

Fig. 6.70 Mean velocity profiles of pulverised coal/biomass (85%/15% blend) on the Y axis on a horizontal pipe

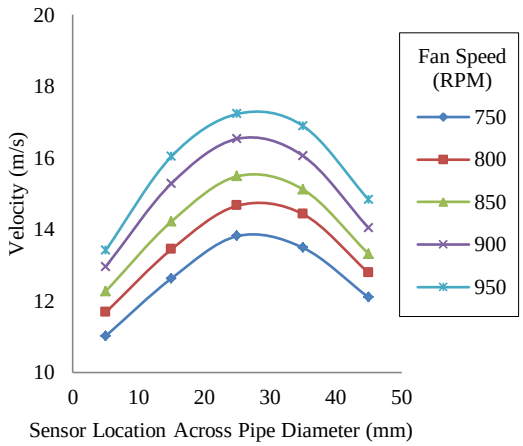

Fig. 6.71 Mean velocity profiles of pulverised coal/biomass (80%/20% blend) on the Z axis on a horizontal pipe

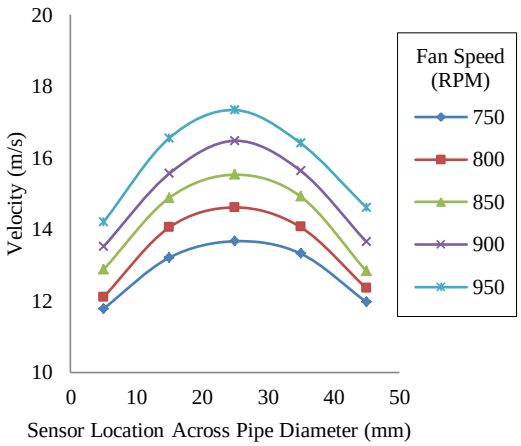

Fig 6.72 Mean velocity profiles of pulverised coal/biomass (80%/20% blend) on the Y axis on a horizontal pipe

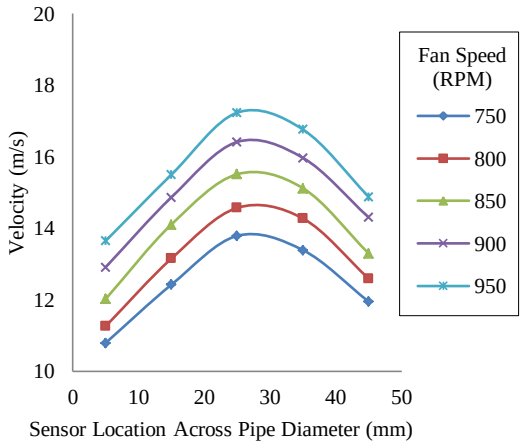

Fig. 6.73 Mean velocity profiles of pulverised biomass on the Z axis on a horizontal pipe

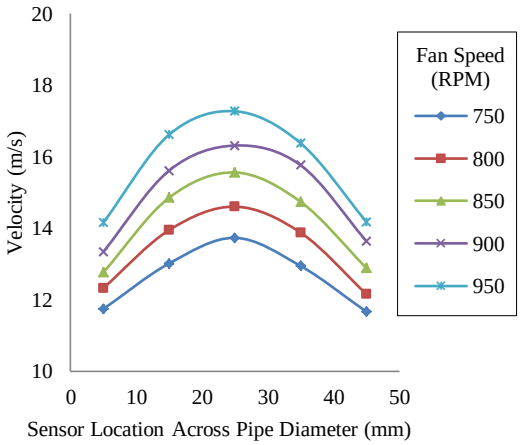

Fig. 6.74 Mean velocity profiles of pulverised biomass on the Y axis on a horizontal pipe

The normalised standard deviation of the velocity profiles of the coal, biomass and coal/biomass blends (Fig. 6.75 – Fig. 6.86) show that the particle velocity deviates less in the centre of the pipe compared to along the pipe wall. This indicates that particle flow is more stable in the centre of the pipe compared to along the pipe wall.

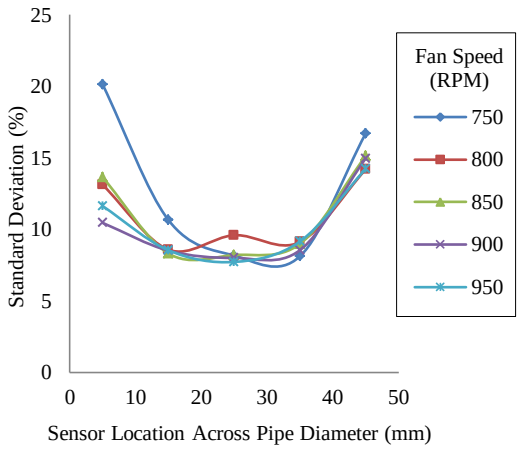

Fig. 6.75 Normalised standard deviation profiles of the velocities for pulverised coal on the Z axis on a horizontal pipe

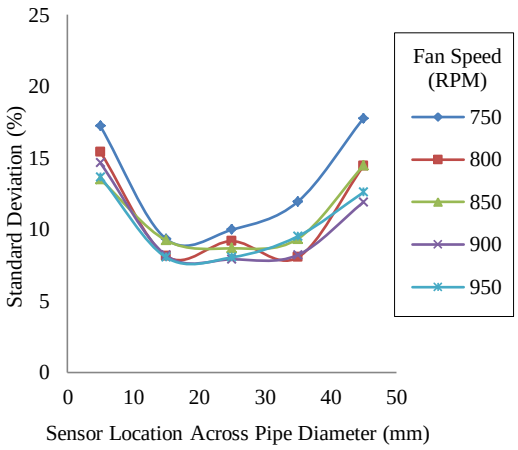

Fig. 6.76 Normalised standard deviation profiles of the velocities for pulverised coal on the Y axis on a horizontal pipe

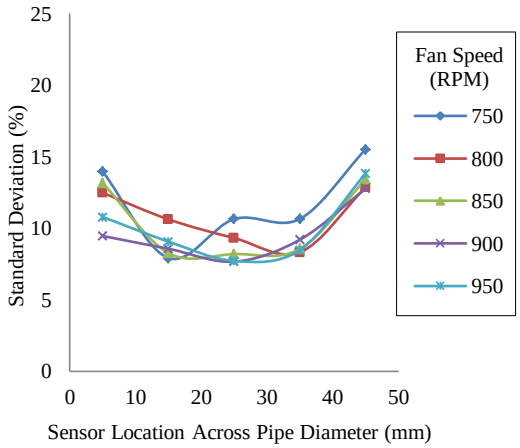

Fig. 6.77 Normalised standard deviation profiles of the velocities for pulverised coal/biomass (95%/5% blend) on the Z axis on a horizontal pipe

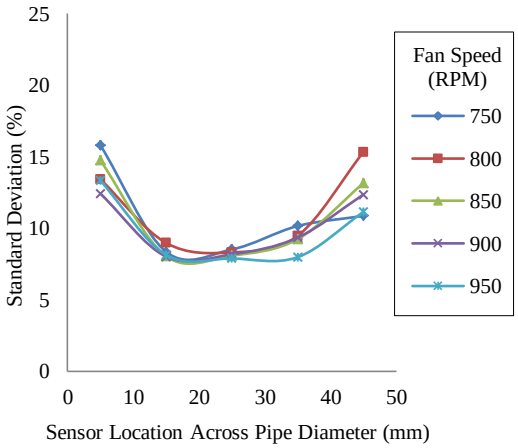

Fig. 6.78 Normalised standard deviation profiles of the velocities for pulverised coal/biomass (95%/5% blend) on the Y axis on a horizontal pipe

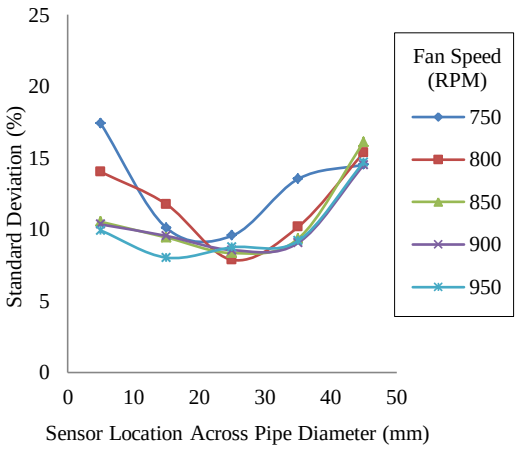

Fig. 6.79 Normalised standard deviation profiles of the velocities for pulverised coal/biomass (90%/10% blend) on the Z axis on a horizontal pipe

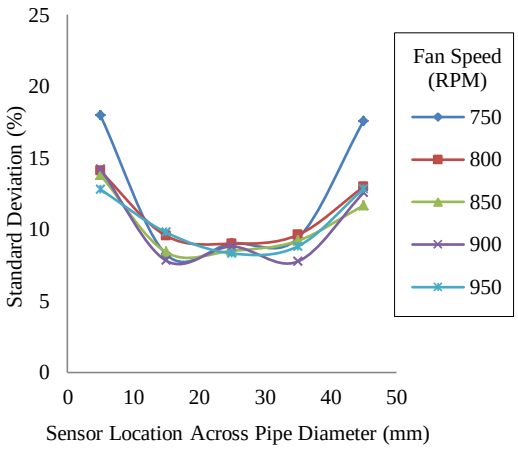

Fig. 6.80 Normalised standard deviation profiles of the velocities for pulverised coal/biomass (90%/10% blend) on the Y axis on a horizontal pipe

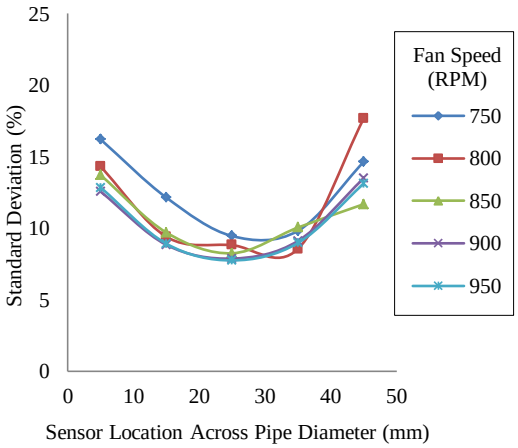

Fig. 6.81 Normalised standard deviation profiles of the velocities for pulverised coal/biomass (85%/15% blend) on the Z axis on a horizontal pipe

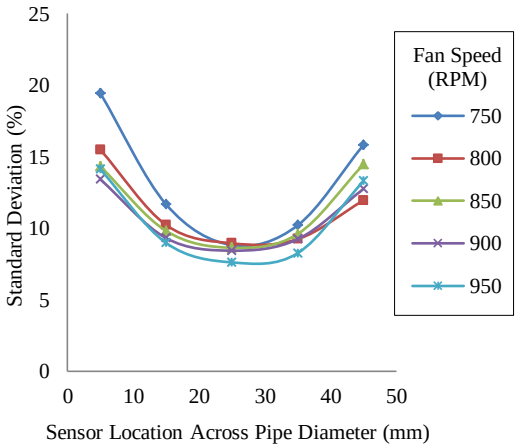

Fig. 6.82 Normalised standard deviation profiles of the velocities for pulverised coal/biomass (85%/15% blend) on the Y axis on a horizontal pipe

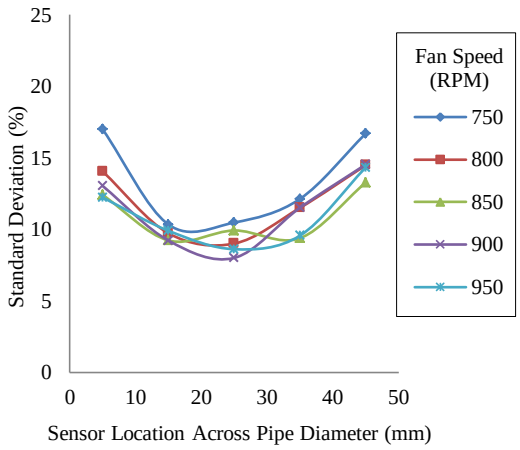

Fig. 6.83 Normalised standard deviation profiles of the velocities for pulverised coal/biomass (80%/20% blend) on the Z axis on a horizontal pipe

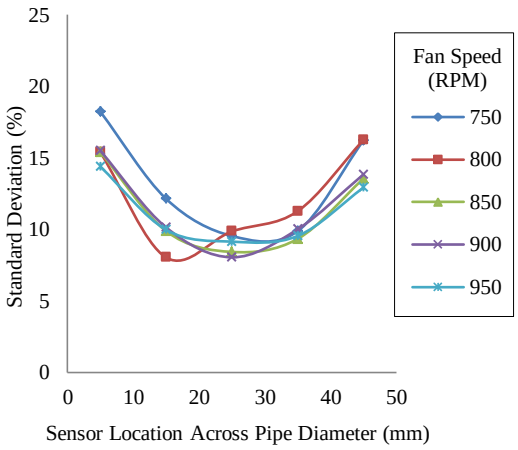

Fig. 6.84 Normalised standard deviation profiles of the velocities for pulverised coal/biomass (80%/20% blend) on the Y axis on a horizontal pipe

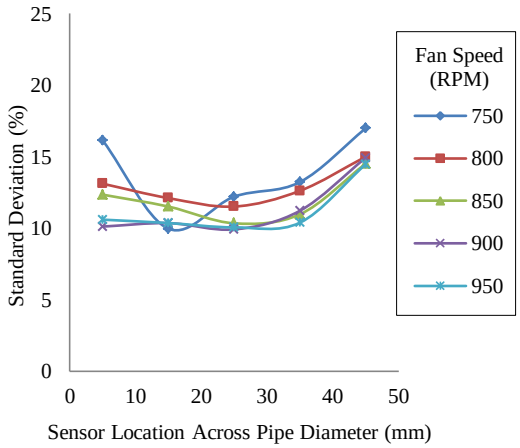

Fig. 6.85 Normalised standard deviation profiles of the velocities for pulverised biomass on the Z axis on a horizontal pipe

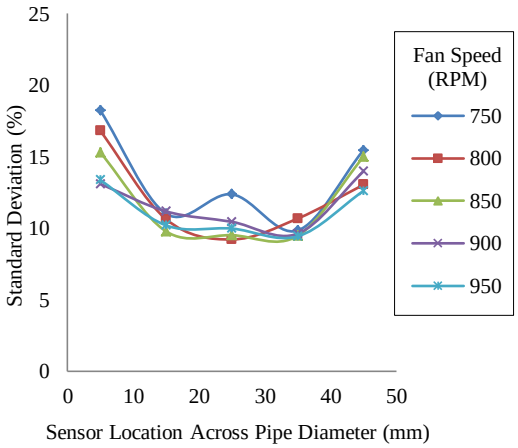

Fig. 6.86 Normalised standard deviation profiles of the velocities for pulverised biomass on the Y axis on a horizontal pipe

Vertical Particle Flow

The electrostatic sensor array has been shown to be capable of determining the velocity of pneumatically conveyed coal, biomass and coal/biomass blends on a vertical pipe section with the particle flow going against gravity. The measured particle velocity profiles for the vertical particle flow illustrated in Fig. 6.87 – Fig. 6.98 appear to be less

developed compared to the velocity profiles measured on the horizontal pipe (Fig. 6.63 - Fig. 6.74). This is conceivably due to the placement of the electrostatic sensor array being only 1350 mm from the right angle bend consequently the flow has not yet developed. Furthermore the measured particle velocity at the centre for the vertical pipe is also lower than the particle velocity in centre of the pipe for the horizontal velocity measurements for the same fan speed. This is conceivably due to gravity slowing down the particle flow in the vertical pipe; because the particles are still in the process of accelerating from exiting the right angle bend or perhaps a combination of the two. The velocity profiles show that the particle velocity along the pipe wall is traveling slower compared to the centre of the pipe. The shape of the velocity profiles show that the measured velocity profiles on the Y axis are more symmetrical compared to the velocity profiles measured on the X axis. (Fig. 6.88, Fig. 6.90, Fig. 6.92, Fig. 6.94, Fig. 6.96 and Fig. 6.98). The shape of the velocity profiles on the X axis displays that the particle velocity is higher on the side of the pipe that corresponds to the outer radius of the right angle-bend (5 mm). This is possibly due to particles maintaining some of their momentum that they built up when they were traveling along the horizontal pipe as they travel along the outer radius of the bend.

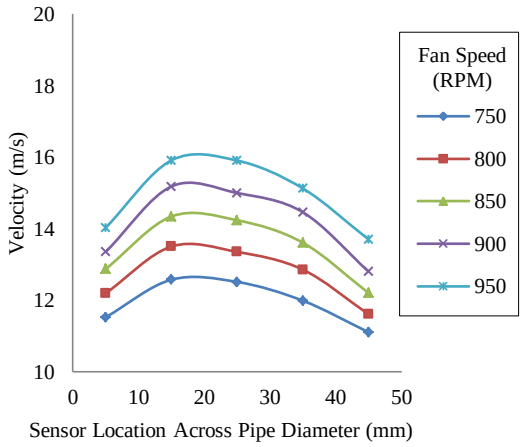

Fig. 6.87 Mean velocity profiles of pulverised coal on the X axis on a vertical pipe

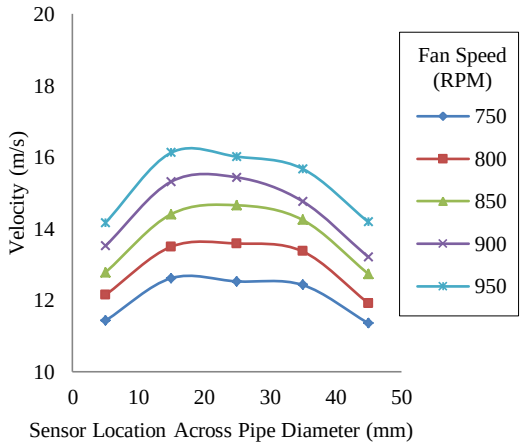

Fig. 6.88 Mean velocity profiles of pulverised coal on the Y axis on a vertical pipe

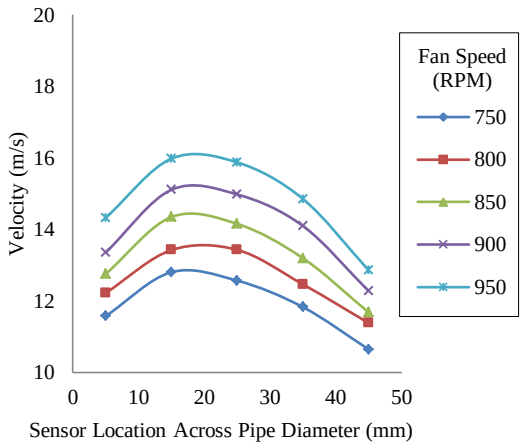

Fig. 6.89 Mean velocity profiles of pulverised coal/biomass (95%/5% blend) on the X axis on a vertical pipe

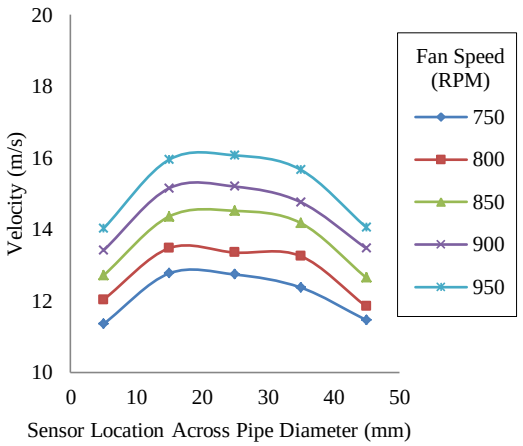

Fig. 6.90 Mean velocity profiles of pulverised coal/biomass (95%/5% blend) on the Y axis on a vertical pipe

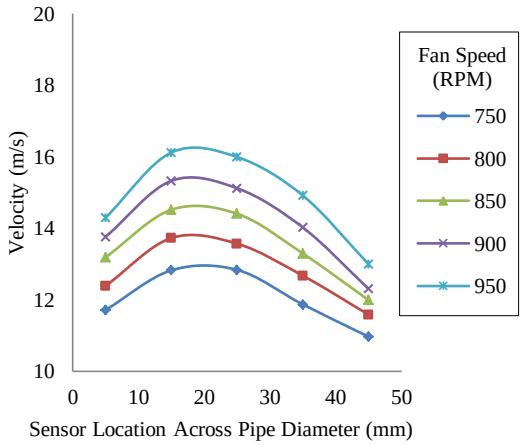

Fig. 6.91 Mean velocity profiles of pulverised coal/biomass (90%/10% blend) on the X axis on a vertical pipe

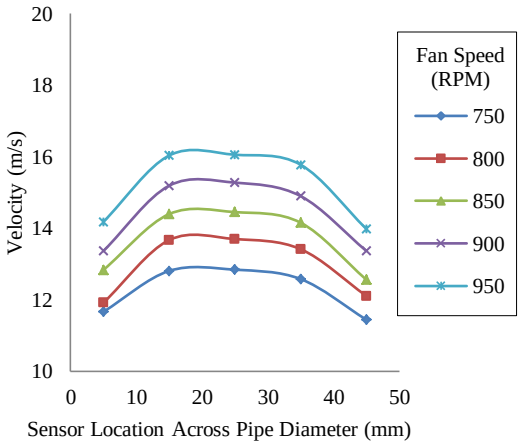

Fig. 6.92 Mean velocity profiles of pulverised coal/biomass (90%/10% blend) on the Y axis on a vertical pipe

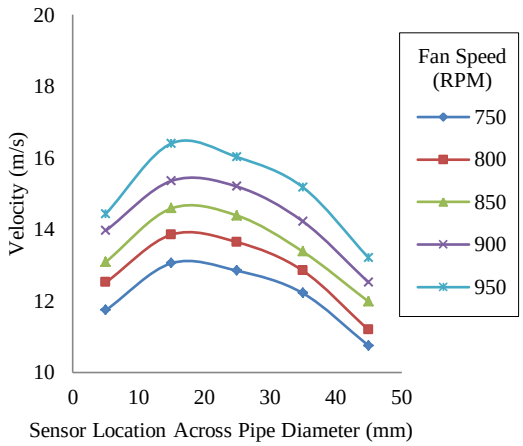

Fig. 6.93 Mean velocity profiles of pulverised coal/biomass (85%/15% blend) on the X axis on a vertical pipe

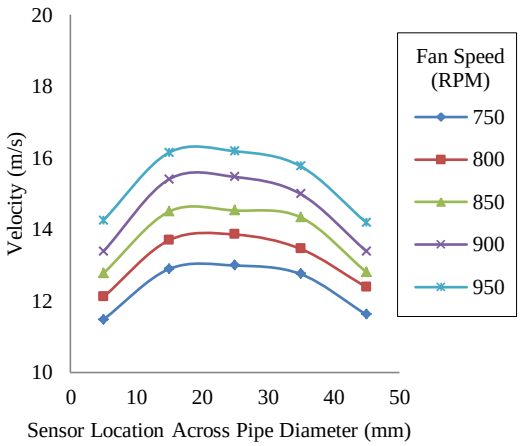

Fig. 6.94 Mean velocity profiles of pulverised coal/biomass (85%/15% blend) on the Y axis on a vertical pipe

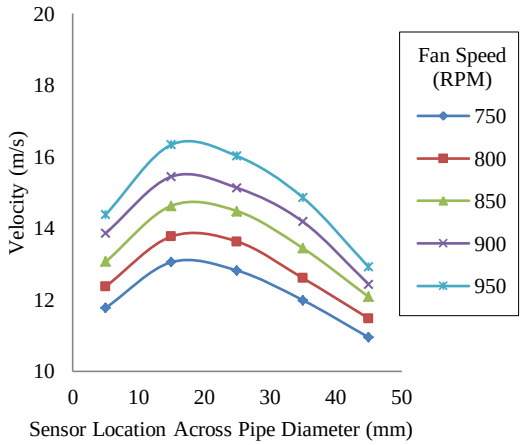

Fig. 6.95 Mean velocity profiles of pulverised coal/biomass (80%/20% blend) on the X axis on a vertical pipe

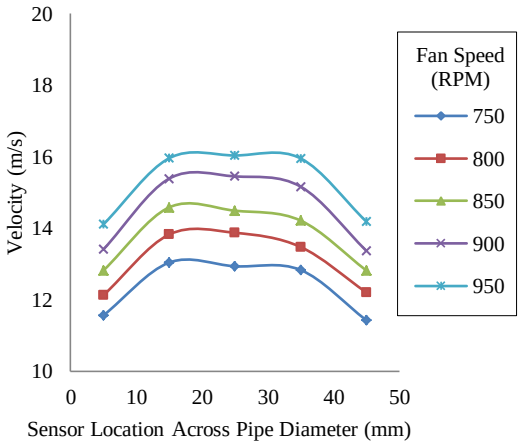

Fig. 6.96 Mean velocity profiles of pulverised coal/biomass (80%/20% blend) on the Y axis on a vertical pipe

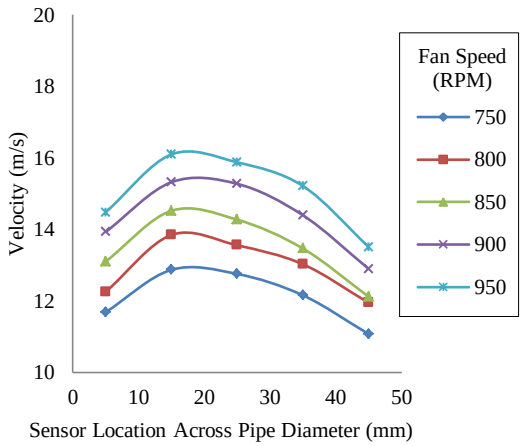

Fig. 6.97 Mean velocity profiles of pulverised biomass on the X axis on a vertical pipe

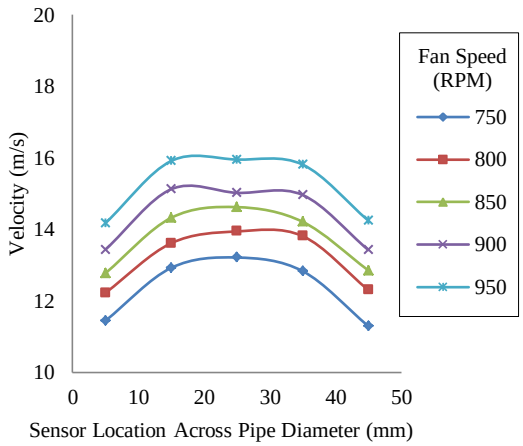

Fig. 6.98 Mean velocity profiles of pulverised biomass on the Y axis on a vertical pipe

The standard deviation profiles of the measured particle velocity profiles shown in Fig. 6.99 – Fig. 6.110 suggests that the particles deviate less in the centre of the pipe compared to along the pipe wall illustrating that the flow along the pipe wall is more unstable compared to the centre of the pipe. The magnitude of this difference between the normalised standard deviation value of the particle flow along the pipe wall and the centre of the pipe decreases for higher ratios of biomass – coal (15% biomass and higher Fig. 6.105 – Fig. 6.110). Hence the normalised standard deviation profiles for the higher ratios of biomass (15% and higher) transitions to resemble the pure biomass standard deviation profiles (more flat across the pipe diameter). A similar change in the shape of the normalised standard deviation profile occurred between the coarse biomass and the fine biomass illustrated in Fig. 6.25 and Fig. 6.26. This is conceivably an indication that higher ratios of biomass – coal have a more unstable particle flow compared to pure coal or lower ratios of biomass.

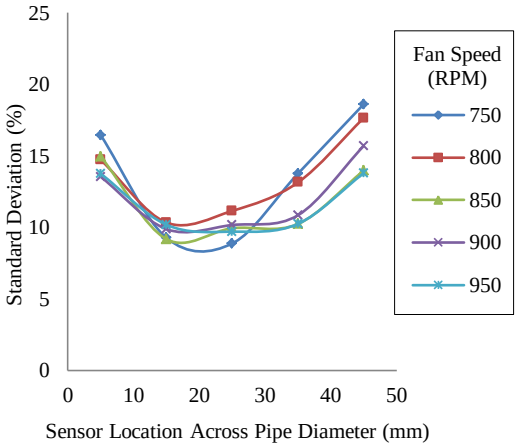

Fig. 6.99 Normalised standard deviation profiles of the velocities for pulverised coal on the X axis on a vertical pipe

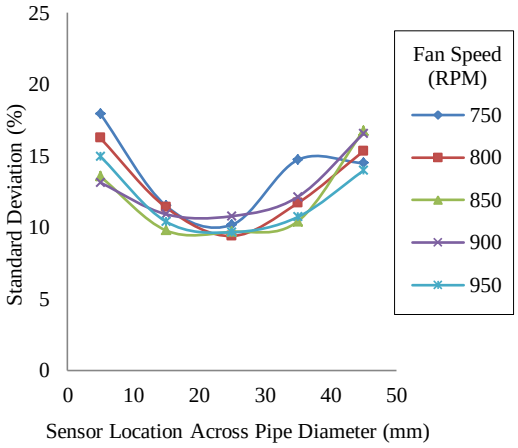

Fig. 6.100 Normalised standard deviation profiles of the velocities for pulverised on the Y axis on a vertical pipe

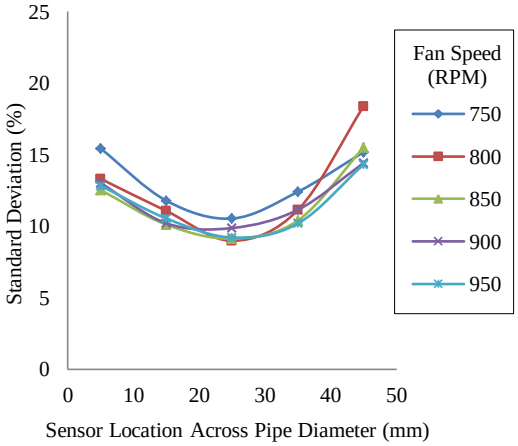

Fig. 6.101 Normalised standard deviation profiles of the velocities for pulverised coal/biomass (95%/5% blend) on the X axis on a vertical pipe

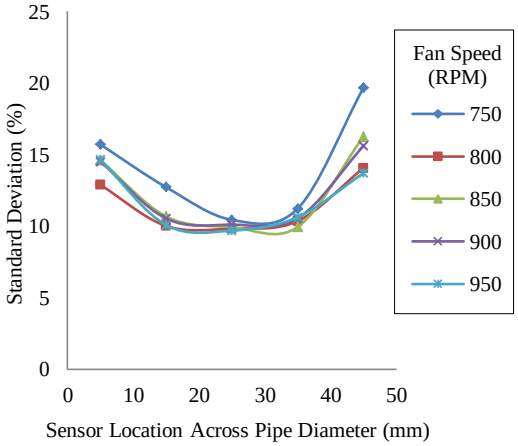

Fig. 6.102 Normalised standard deviation profiles of the velocities for pulverised coal/biomass (95%/5% blend) on the Y axis on a vertical pipe

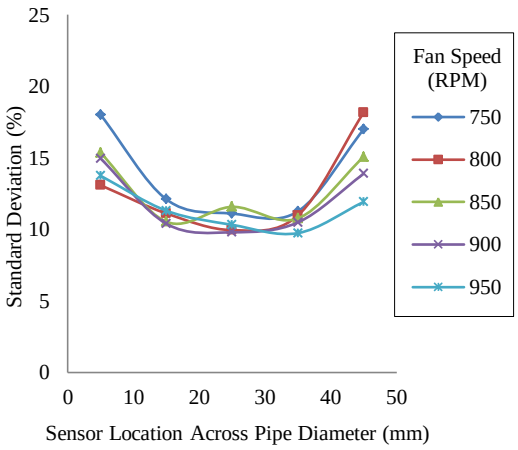

Fig. 6.103 Normalised standard deviation profiles of the velocities for pulverised coal/biomass (90%/10% blend) on the X axis on a vertical pipe

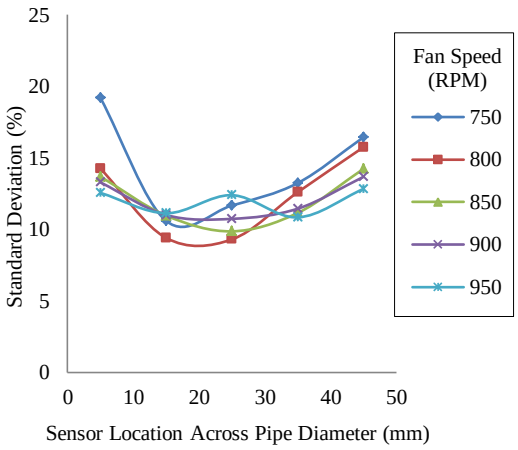

Fig. 6.104 Normalised standard deviation profiles of the velocities for pulverised coal/biomass (90%/10% blend) on the Y axis on a vertical pipe

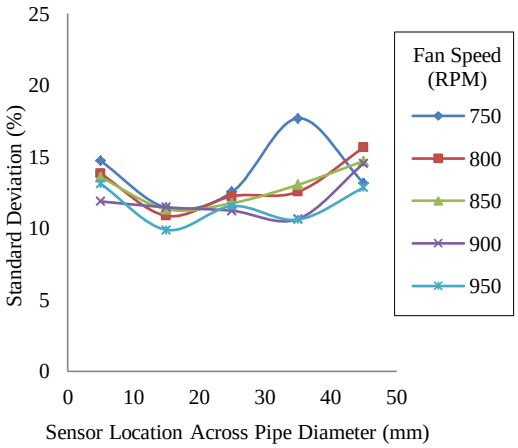

Fig. 6.105 Normalised standard deviation profiles of the velocities for pulverised coal/biomass (85%/15% blend) on the X axis on a vertical pipe

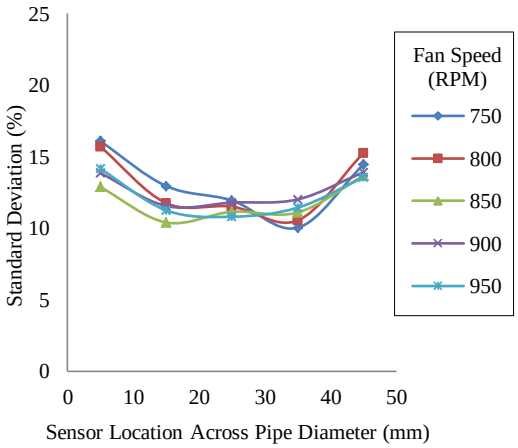

Fig. 6.106 Normalised standard deviation profiles of the velocities for pulverised coal/biomass (85%/15% blend) on the Y axis on a vertical pipe

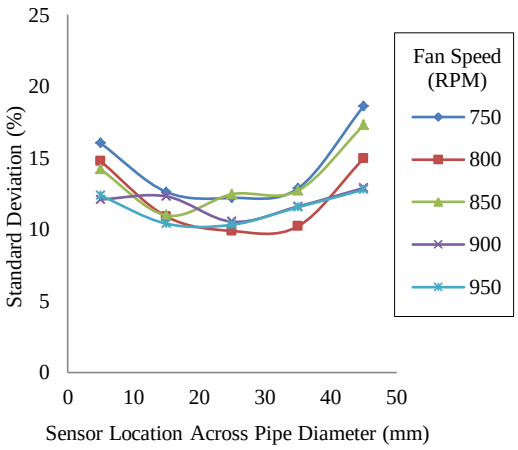

Fig. 6.107 Normalised standard deviation profiles of the velocities for pulverised coal/biomass (80%/20% blend) on the X axis on a vertical pipe

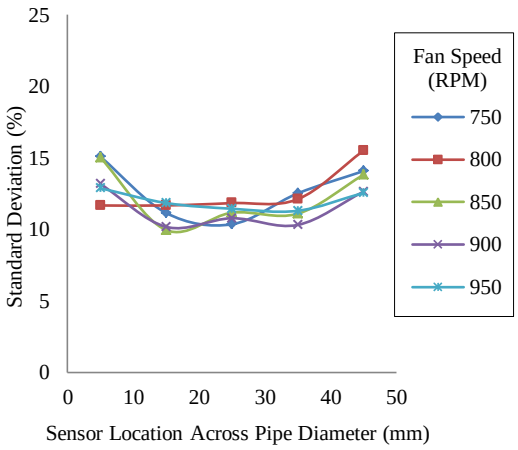

Fig. 6.108 Normalised standard deviation profiles of the velocities for pulverised coal/biomass (80%/20% blend) on the Y axis on a vertical pipe

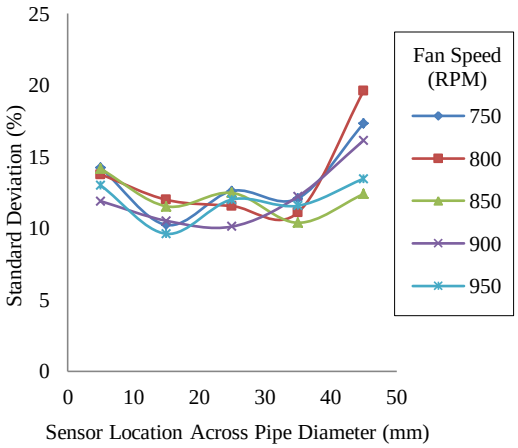

Fig. 6.109 Normalised standard deviation profiles of the velocities for pulverised biomass on the X axis on a vertical pipe

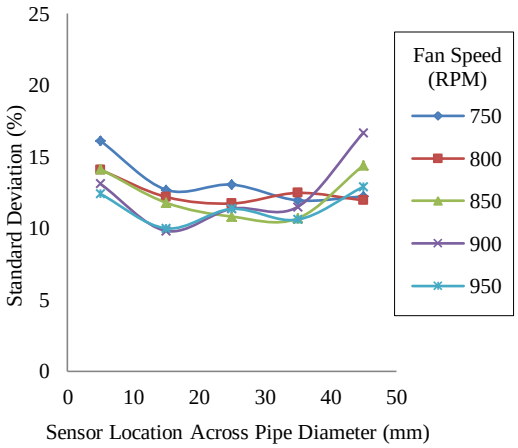

Fig. 6.110 Normalised standard deviation profiles of the velocities for pulverised biomass on the Y axis on a vertical pipe

6.2.3.3 Measured Particle Concentration Profiles

Horizontal Particle Flow

The use of the normalised r.m.s magnitude to determine particle concentration can be seen in Fig. 6.11 - Fig. 6.122. The shape of the concentration profiles measured using the electrostatic sensor array in the Z axis on a horizontal pipe (Fig. 6.11, Fig. 6.13, Fig. 6.15, Fig. 6.17, Fig. 6.19 and Fig. 6.21) illustrates the effect of gravity with the measured particle concentration increasing in the direction of gravity. However, the concentration measurements taken at the very bottom of the pipe for pure coal and low ratios of biomass (< 15% biomass Fig. 6.11, Fig. 6.13 and Fig. 6.15) show that the measured particle concentration at the bottom of the pipe (5 mm) is roughly the same as the measurement taken by the sensor above (15 mm). This phenomenon was also observed on experimentation carried out using flour as a pulverised material on the negative pressure test rig. For pure biomass, however, this reduced concentration at the bottom of the pipe does not occur (Fig. 6.121). The r.m.s concentration profiles indicate that once the ratio of biomass-coal is 15% or higher (by weight) the particle concentration profile flow characteristics transition from coal flow characteristics to biomass flow characteristics. This transition can likewise be observed in the particle concentration profiles measured with the electrostatic sensor array on the horizontal pipe on the Y axis (Fig. 6.112, Fig. 6.114, Fig. 6.116, Fig. 6.118, Fig. 6.120 and Fig. 6.122).

Observation of all the concentration profiles measured on the horizontal pipe (both Z and Y axis sensor orientation) show that the level of r.m.s charge increases for higher particle velocities. Fig. 6.123 and Fig. 6.124 show the feed rates of each of the experiments. This indicates that higher particle velocity has the effect of generating higher electrostatic charge on the particles.

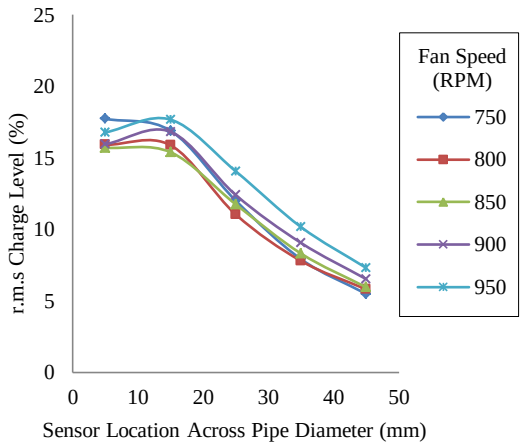

Fig. 6.111 Mean particle concentration profiles of pulverised coal on the Z axis on a horizontal pipe

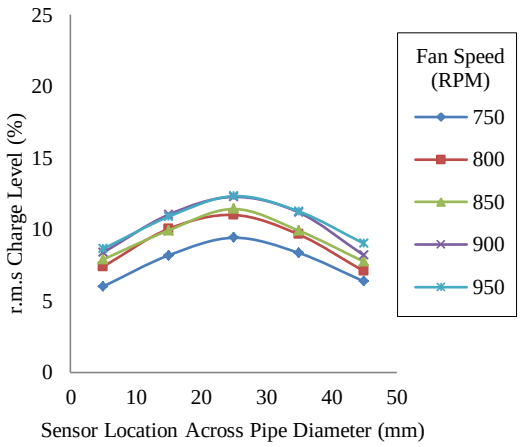

Fig. 6.112 Mean particle concentration profiles of pulverised coal on the Y axis on a horizontal pipe

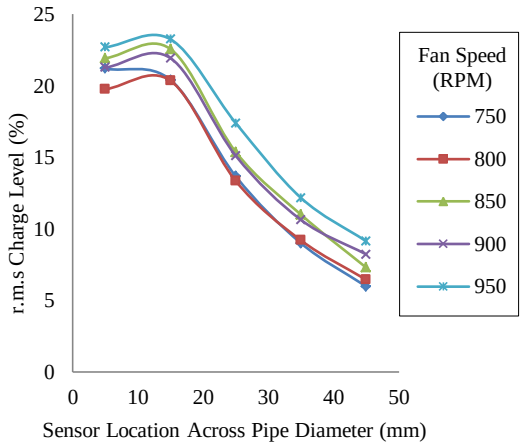

Fig. 6.113 Mean particle concentration profiles of pulverised coal/biomass (95%/5% blend) on the Z axis on a horizontal pipe

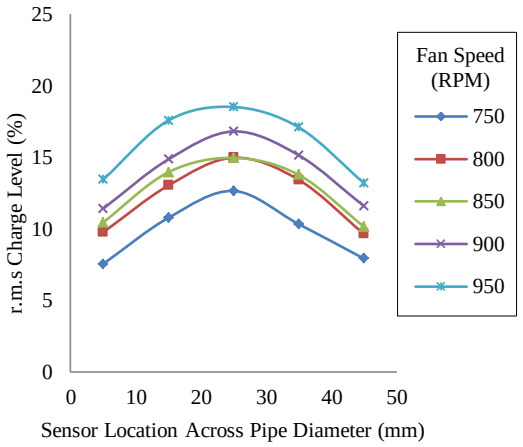

Fig. 6.114 Mean particle concentration profiles of pulverised coal/biomass (95%/5% blend) on the Y axis on a horizontal pipe

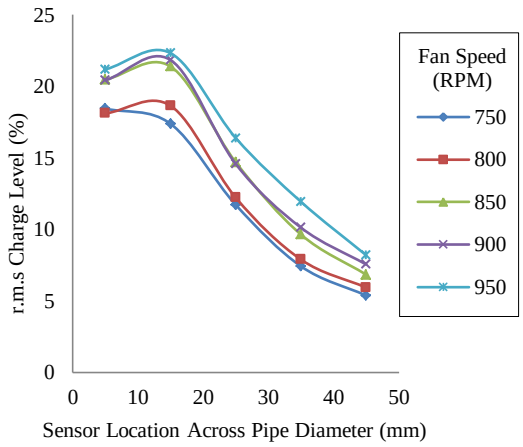

Fig. 6.115 Mean particle concentration profiles of pulverised coal/biomass (90%/10% blend) on the Z axis on a horizontal pipe

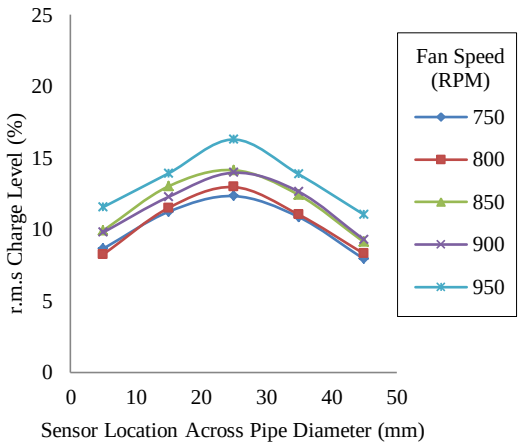

Fig. 6.116 Mean particle concentration profiles of pulverised coal/biomass (90%/10% blend) on the Y axis on a horizontal pipe

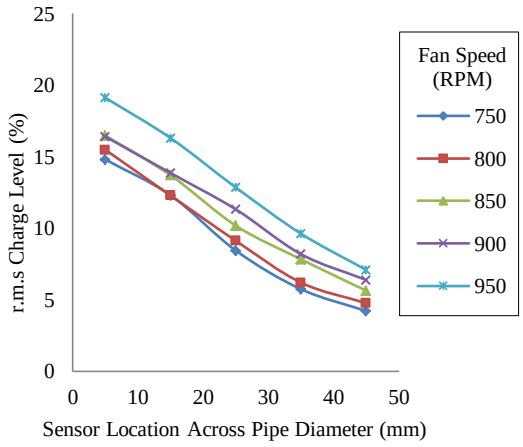

Fig. 6.117 Mean particle concentration profiles of pulverised coal/biomass (85%/15% blend) on the Z axis on a horizontal pipe

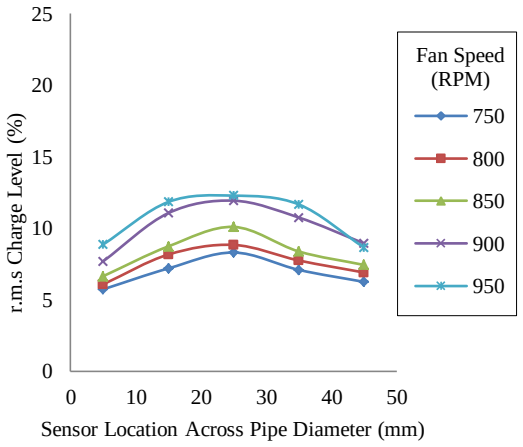

Fig. 6.118 Mean particle concentration profiles of pulverised coal/biomass (85%/15% blend) on the Y axis on a horizontal pipe

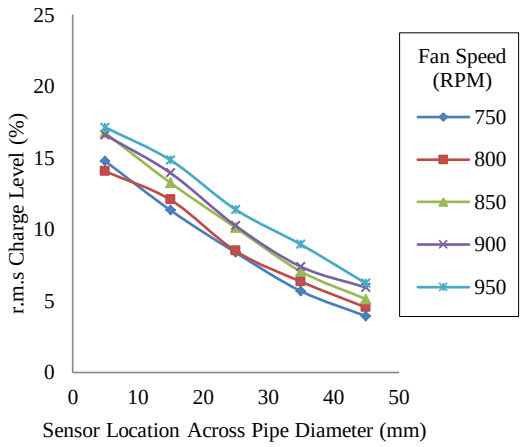

Fig. 6.119 Mean particle concentration profiles of pulverised coal/biomass (80%/20% blend) on the Z axis on a horizontal pipe

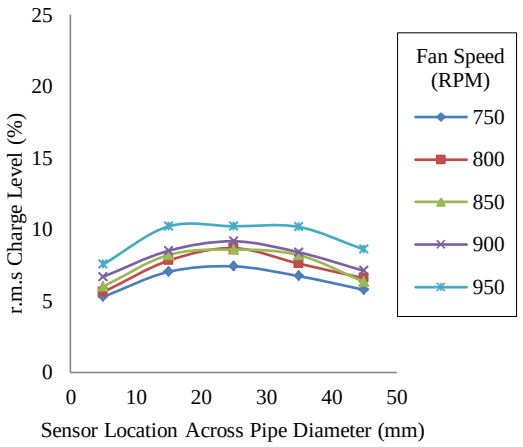

Fig. 6.120 Mean particle concentration profiles of pulverised coal/biomass (80%/20% blend) on the Y axis on a horizontal pipe

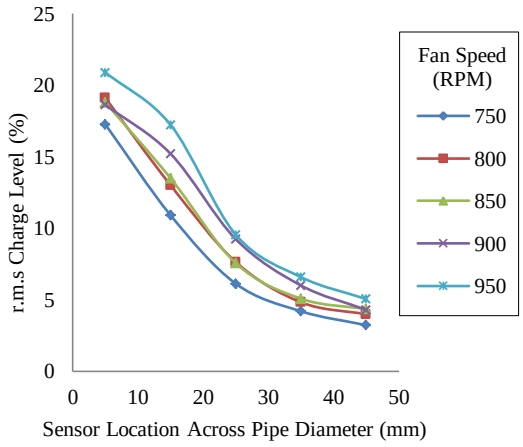

Fig. 6.121 Mean particle concentration profiles of pulverised biomass on the Z axis on a horizontal pipe

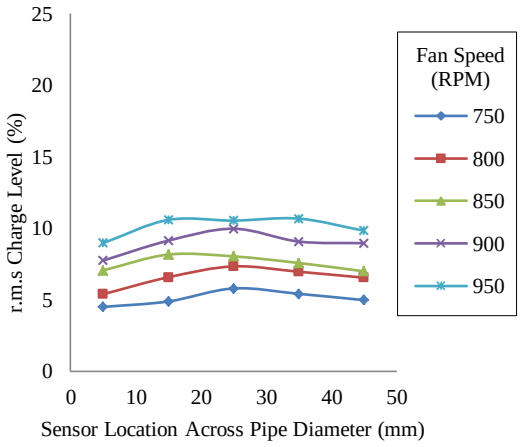

Fig. 6.122 Mean particle concentration profiles of pulverised biomass on the Y axis on a horizontal pipe

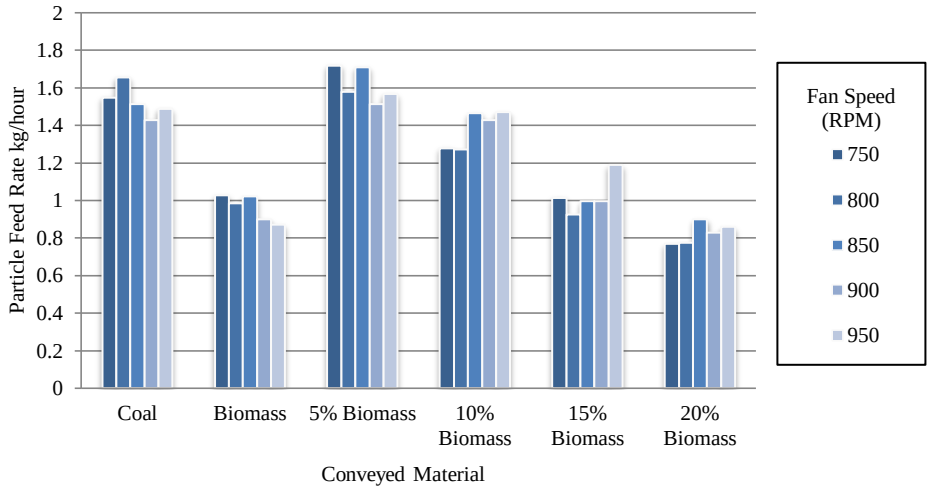

Fig. 6.123 Measured material feed rates carried out on a horizontal pipe on the Z sensor axis

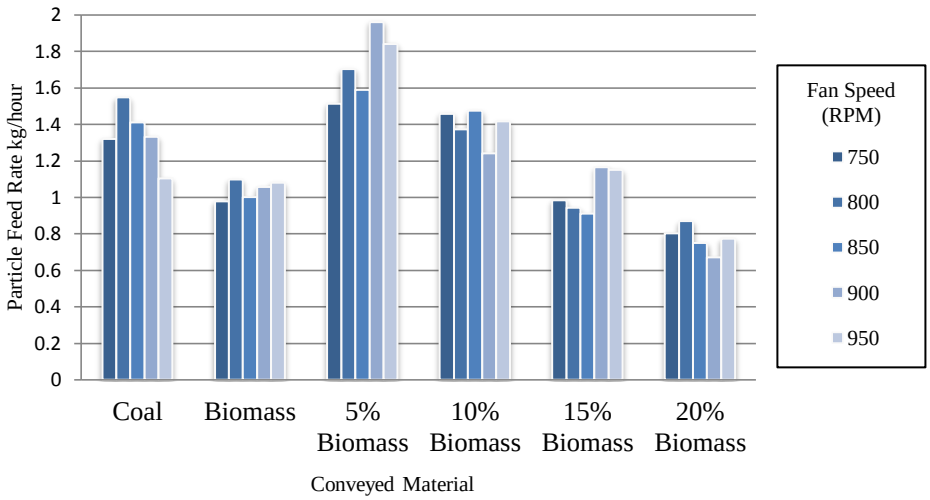

Fig. 6.124 Measured material feed rates carried out on a horizontal pipe on the Y sensor axis

Vertical Particle Flow

The electrostatic sensor array is capable of measuring the particle concentration of coal, biomass and coal/biomass blends in a horizontal pipe (Fig. 6.125 – Fig. 6.136). The phenomenon of lower measured particle concentrations for pure coal and lower ratios of blended biomass along the pipe wall are not observed for the concentration profiles

measured on the vertical pipe. This is conceivably due to the effect of roping caused by the right-angle bend forcing the particles along the pipe wall due to centrifugal forces.

A similar effect of higher particle velocity causing higher r.m.s values can also be observed in the concentration profiles (with the exception of the pure coal 750 RPM profile shown in Fig. 6.125) A possible reason for this could be due to an increase in the particle feed rate for that experiment illustrated in Fig. 6.137. Conversely the effect of increased r.m.s charge caused by increased particle velocity is not as pronounced on the vertical particle flow as it was on the horizontal particle flow. A possible reason for this is the vertical particle flow is not as developed compared to the measurements taken on the horizontal particle flow due to the sensor location in relation to the right-angle pipe bend.

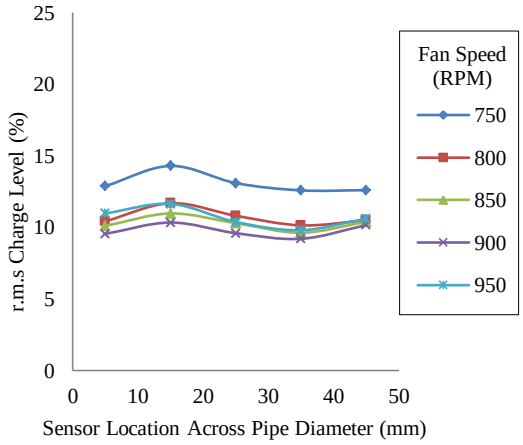

Fig. 6.125 Mean particle concentration profiles of pulverised coal on the X axis on a vertical pipe

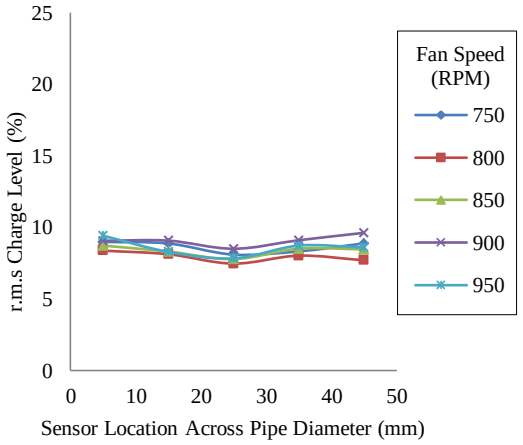

Fig. 6.126 Mean particle concentration profiles of pulverised coal on the Y axis on a vertical pipe

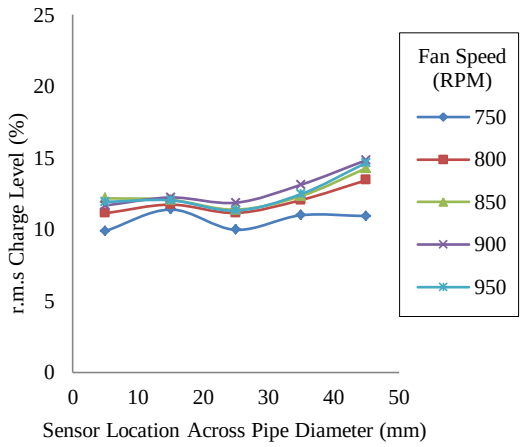

Fig. 6.127 Mean particle concentration profiles of pulverised coal/biomass (95%/5% blend) on the X axis on a vertical pipe

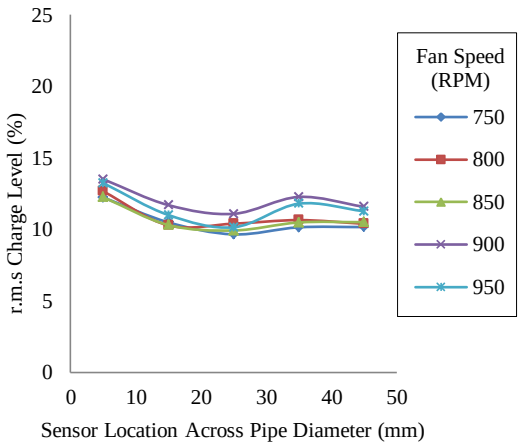

Fig. 6.128 Mean particle concentration profiles of pulverised coal/biomass (95%/5% blend) on the Y axis on a vertical pipe

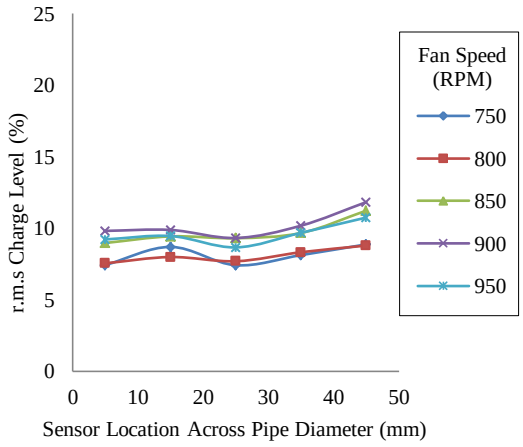

Fig. 6.129 Mean particle concentration profiles of pulverised coal/biomass (90%/10% blend) on the X axis on a vertical pipe

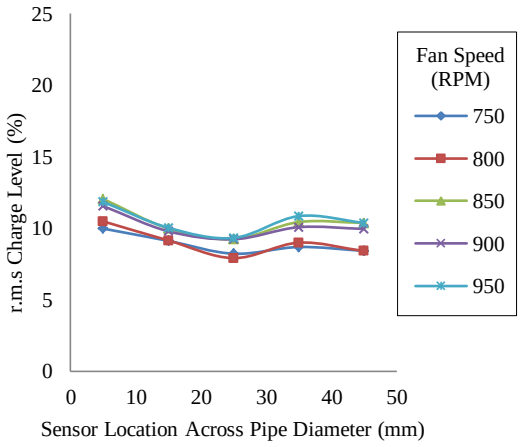

Fig. 6.130 Mean particle concentration profiles of pulverised coal/biomass (90%/10% blend) on the Y axis on a vertical pipe

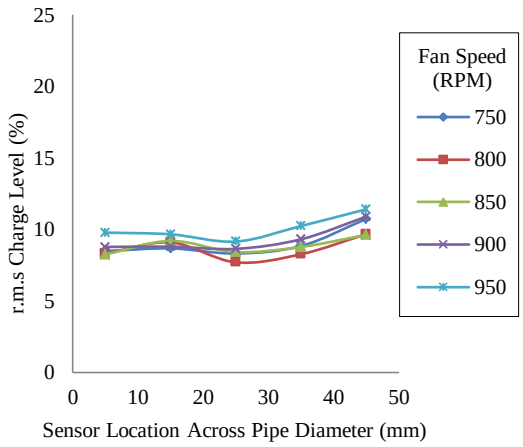

Fig. 6.131 Mean particle concentration profiles of pulverised coal/biomass (85%/15% blend) on the X axis on a vertical pipe

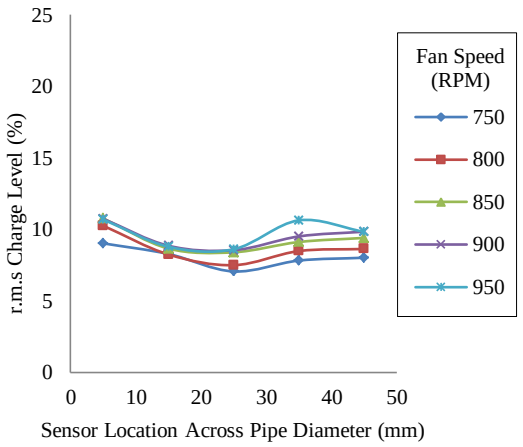

Fig. 6.132 Mean particle concentration profiles of pulverised coal/biomass (85%/15% blend) on the Y axis on a vertical pipe

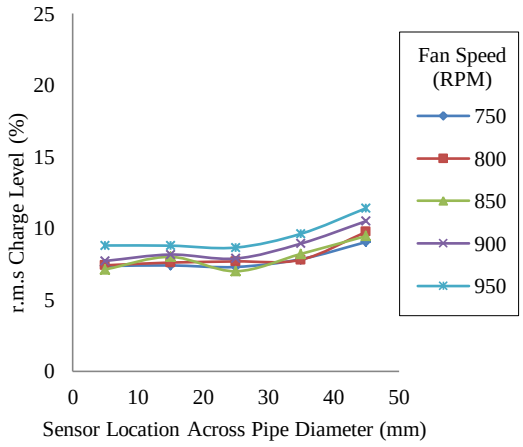

Fig. 6.133 Mean particle concentration profiles of pulverised coal/biomass (80%/20% blend) on the X axis on a vertical pipe

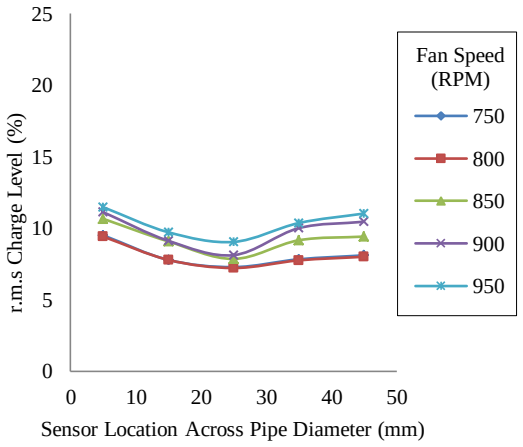

Fig. 6.134 Mean particle concentration profiles of pulverised coal/biomass (80%/20% blend) on the Y axis on a vertical pipe

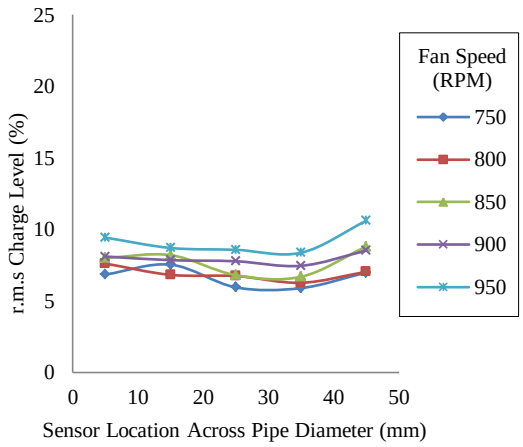

Fig. 6.135 Mean particle concentration profiles of pulverised biomass on the X axis on a vertical pipe

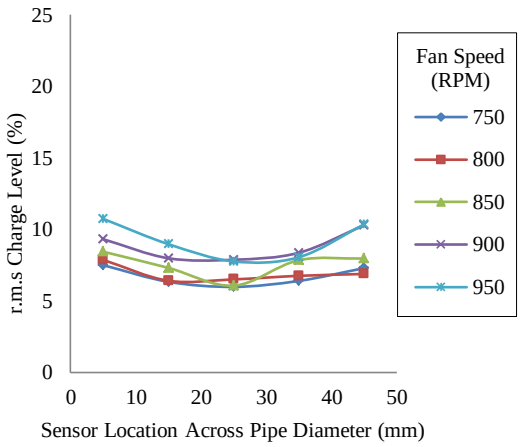

Fig. 6.136 Mean particle concentration profiles of pulverised biomass on the Y axis on a vertical pipe

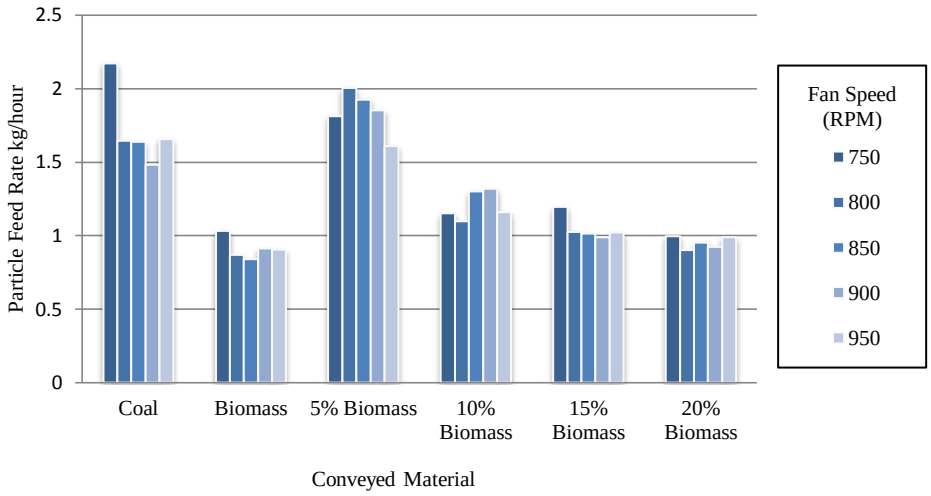

Fig. 6.137 Measured material feed rates carried out on a vertical pipe on the X sensor axis

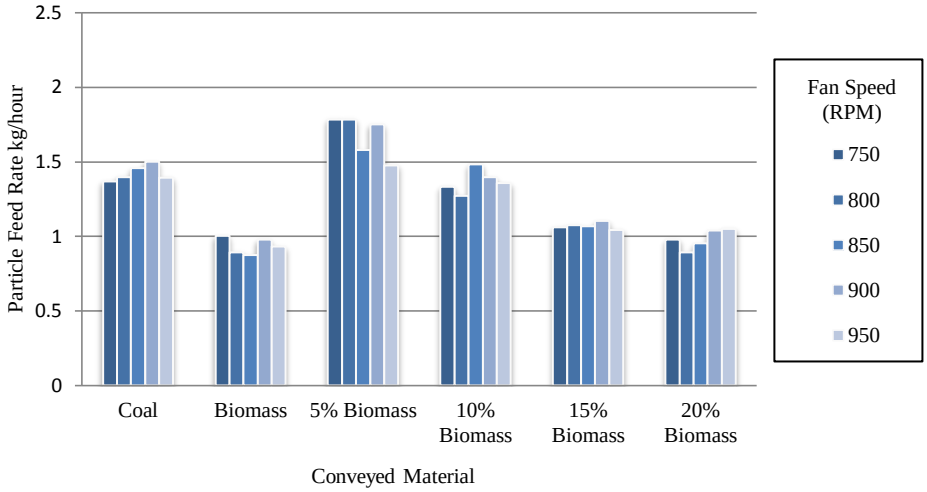

Fig. 6.138 Measured material feed rates carried out on a vertical pipe on the Y sensor axis

6.2.3.4 Correlation Coefficient Profiles

Horizontal Particle Flow

The value of the correlation coefficient is also an indication of flow stability [54] (the closer to 1 the correlation coefficient, the more stable the flow). The correlation coefficient profiles for coal, biomass and coal/biomass blends shown in Fig. 6.139 – Fig. 6.150 have a higher value of correlation coefficient in the centre of the pipe compared to along the pipe wall indicating more stable flow. The correlation coefficient profiles on the Z sensor axis (Fig. 6.139, Fig. 6.141, Fig. 6.143, Fig. 6.145, Fig. 6.147 and Fig. 6.149) are not as symmetrical as the profiles from the sensor on the Y axis (Fig. 6.140, Fig. 6.142, Fig. 6.144, Fig. 6.146, Fig. 6.148 and Fig. 6.150). The shape of the correlation coefficient profiles (Z and Y sensor orientation) bare a similarity to the r.m.s profiles illustrated in Fig. 6.111 – Fig. 6.122 indicating that the quality of the correlation coefficient is also related to the particle concentration. Indicating that higher particle concentrations give rise to higher correlation coefficients. The correlation coefficient profiles for coal and all the coal/biomass blends (Fig. 6.139 - Fig. 6.148) appear to be consistent with each other over their respective particle velocities except for the pure biomass correlation coefficient profiles (Fig. 6.149 and Fig. 6.150). The

pure biomass correlation coefficient profiles seem to increase with particle velocity. This conceivably could be due to the larger particles of biomass having a more stable particle flow at higher particle velocities. It also appears that at higher particle velocities the pure biomass has a higher correlation coefficient compared to the pure coal and coal/biomass blends.

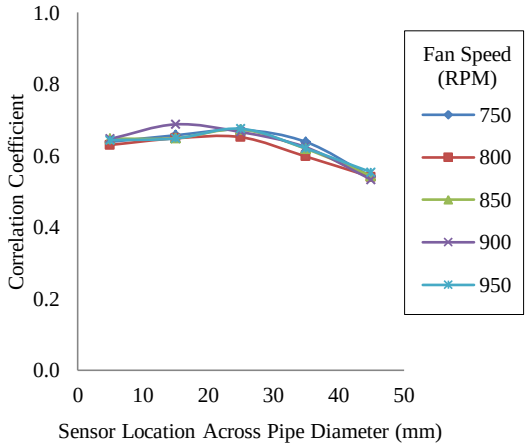

Fig. 6.139 Mean correlation coefficient profiles of pulverised coal on the Z axis on a horizontal pipe

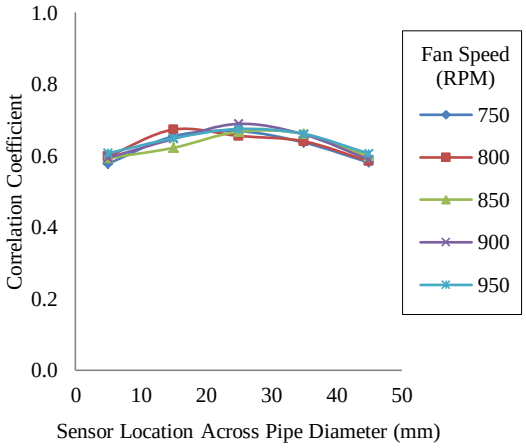

Fig. 6.140 Mean correlation coefficient profiles of pulverised coal on the Y axis on a horizontal pipe

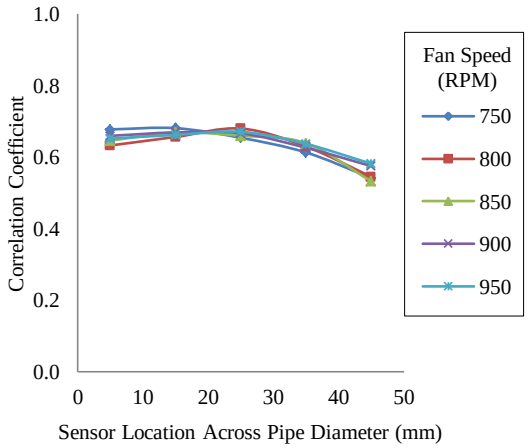

Fig. 6.141 Mean correlation coefficient profiles of pulverised coal/biomass (95%/5% blend) on the Z axis on a horizontal pipe

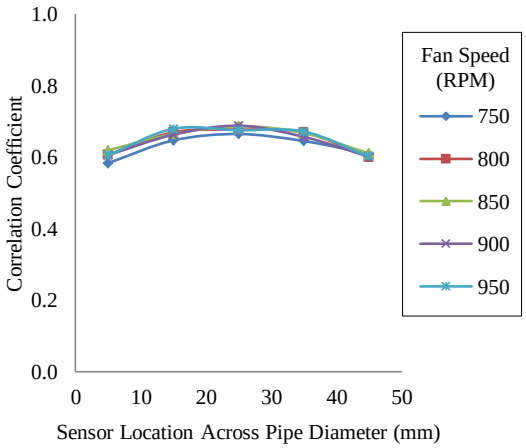

Fig. 6.142 Mean correlation coefficient profiles of pulverised coal/biomass (95%/5% blend) on the Y axis on a horizontal pipe

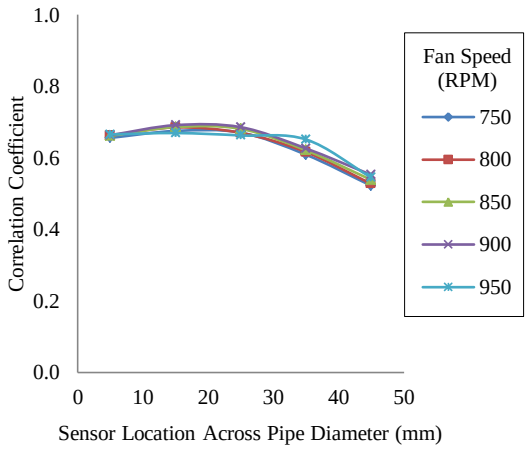

Fig. 6.143 Mean correlation coefficient profiles of pulverised coal/biomass (90%/10% blend) on the Z axis on a horizontal pipe

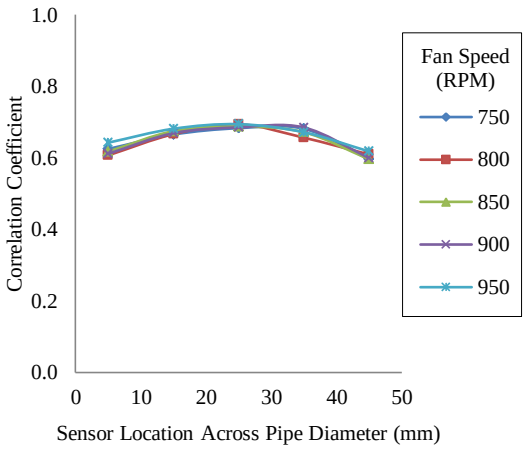

Fig. 6.144 Mean correlation coefficient profiles of pulverised coal/biomass (90%/10% blend) on the Y axis on a horizontal pipe

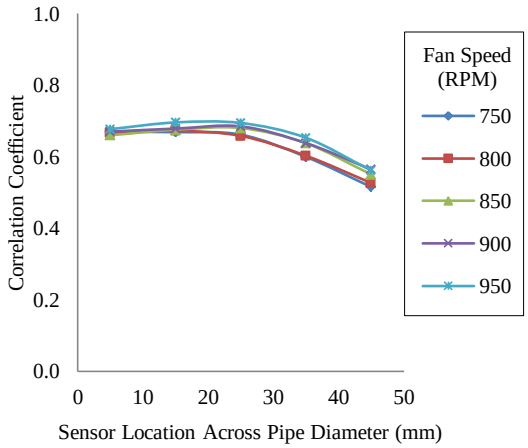

Fig. 6.145 Mean correlation coefficient profiles of pulverised coal/biomass (85%/15% blend) on the Z axis on a horizontal pipe

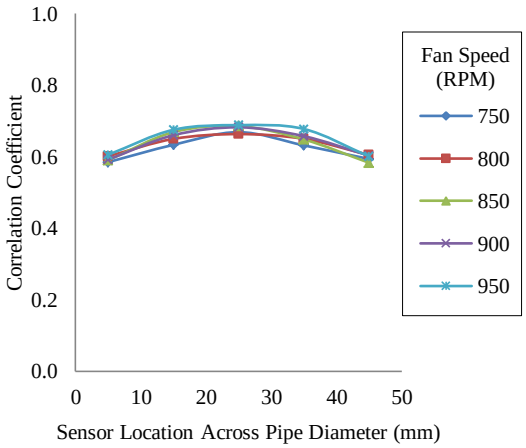

Fig. 6.146 Mean correlation coefficient profiles of pulverised coal/biomass (85%/15% blend) on the Y axis on a horizontal pipe

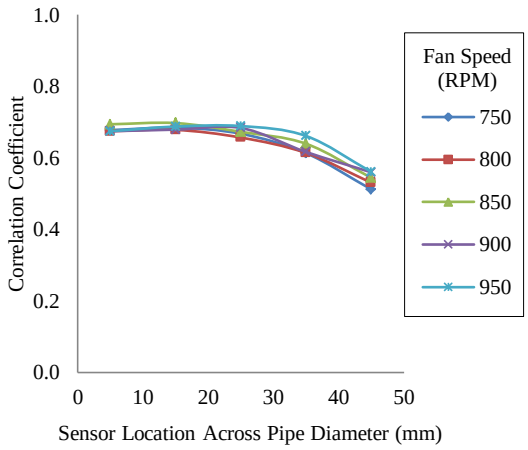

Fig. 6.147 Mean correlation coefficient profiles of pulverised coal/biomass (80%/20% blend) on the Z axis on a horizontal pipe

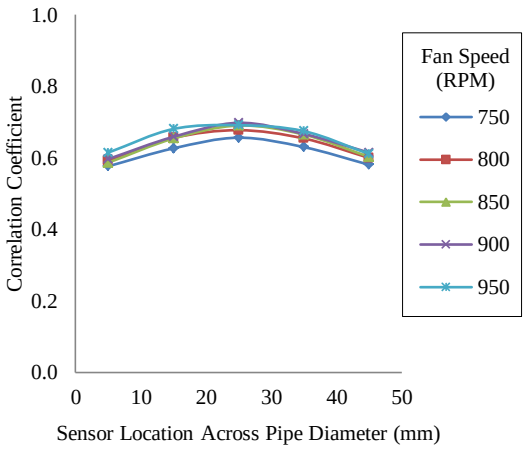

Fig. 6.148 Mean correlation coefficient profiles of pulverised coal/biomass (80%/20% blend) on the Y axis on a horizontal pipe

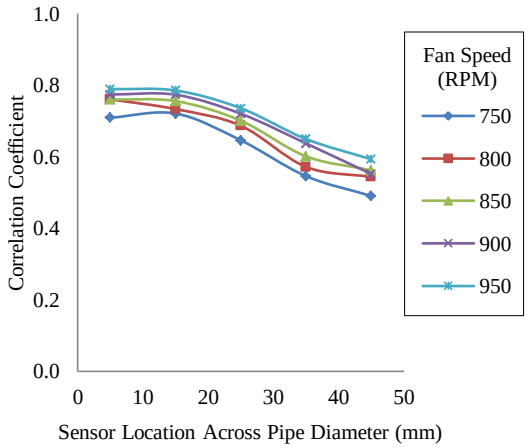

Fig. 6.149 Mean correlation coefficient profiles of pulverised biomass on the Z axis on a horizontal pipe

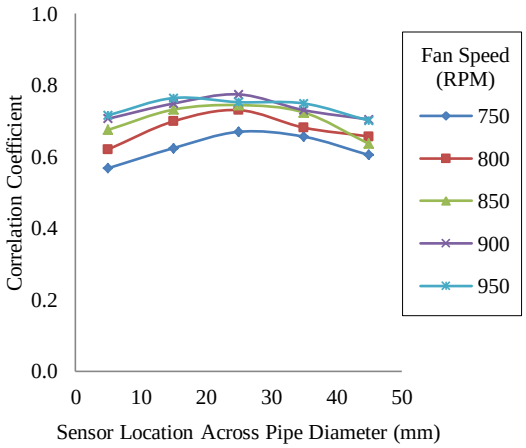

Fig. 6.150 Mean correlation coefficient profiles of pulverised biomass on the Y axis on a horizontal pipe

Analysis of the standard deviation of the correlation coefficient profiles (Fig. 6.151 – Fig. 6.161) on the particle flow along a horizontal pipe shows that the shapes of the profiles are an inverse shape to the correlation coefficient profiles (Fig. 6.139 – Fig. 6.150). This indicates that the particle flow in the centre of the pipe is more stable compared to the particle flow along the pipe wall. The normalised standard deviation of the correlation coefficient profiles for the particle flow of the pure coal remains similar

over the five particle velocities. As the ratio of biomass - coal increases (to pure biomass) the normalised standard deviation correlation coefficient profiles start to deviate from each other. This can best be seen on the Z sensor axis (Fig. 6.151, Fig. 6.153, Fig. 6.155, Fig. 6.157, Fig. 6.159 and Fig. 6161). The standard deviation improves as the particle velocity increases. This indicates that the increase in biomass reduces the flow stability and that higher particle velocity improve the flow stability for biomass.

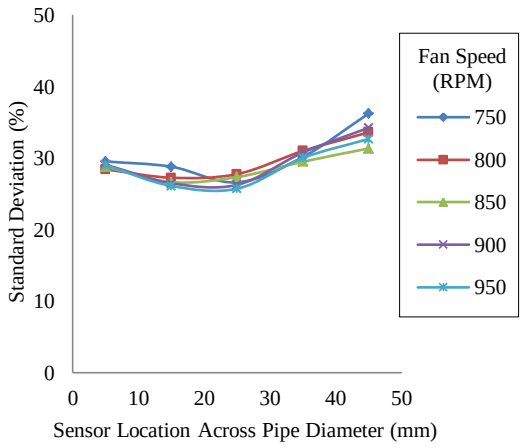

Fig. 6.151 Normalised standard deviation profiles of the correlation coefficient of pulverised coal on the Z axis on a horizontal pipe

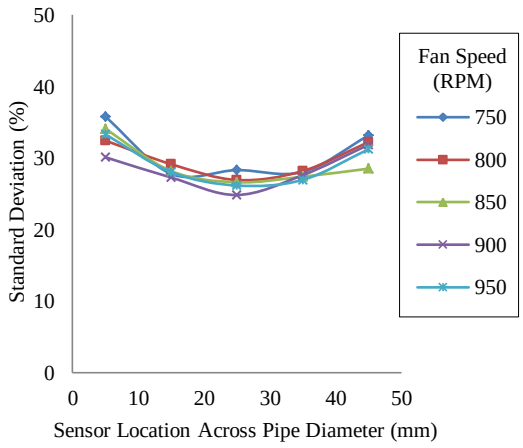

Fig. 6.152 Normalised standard deviation profiles of the correlation coefficient of pulverised coal on the Y axis on a horizontal pipe

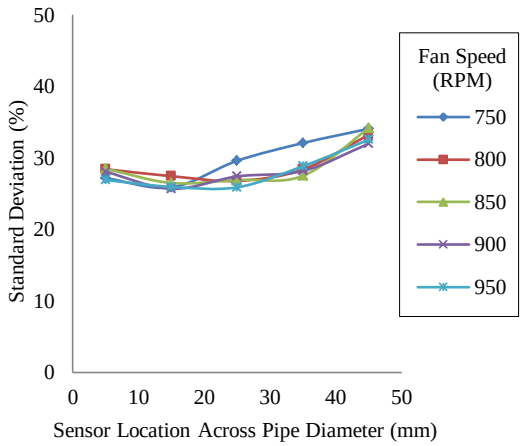

Fig. 6.153 Normalised standard deviation profiles of the correlation coefficient of pulverised coal/biomass (95%/5% blend) on the Z axis on a horizontal pipe

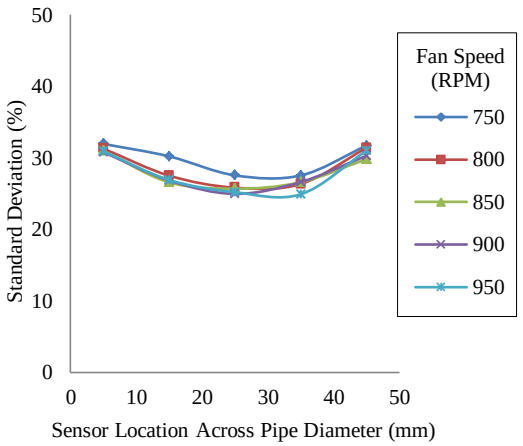

Fig. 6.154 Normalised standard deviation profiles of the correlation coefficient of pulverised coal/biomass (95%/5% blend) on the Y axis on a horizontal pipe

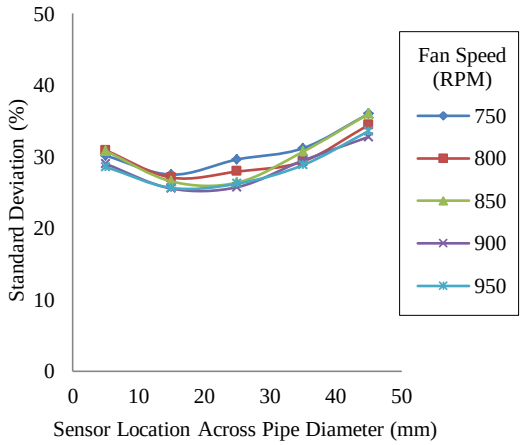

Fig. 6.155 Normalised standard deviation profiles of the correlation coefficient of pulverised coal/biomass (90%/10% blend) on the Z axis on a horizontal pipe

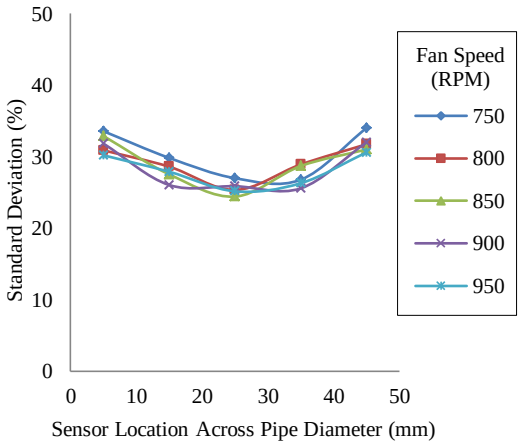

Fig. 6.156 Normalised standard deviation profiles of the correlation coefficient of pulverised coal/biomass (90%/10% blend) on the Y axis on a horizontal pipe

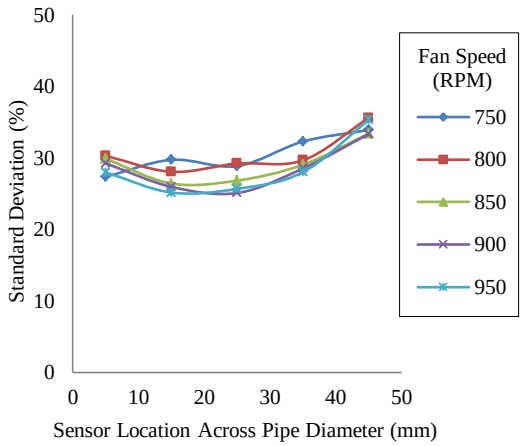

Fig. 6.157 Normalised standard deviation profiles of the correlation coefficient of pulverised coal/biomass (85%/15% blend) on the Z axis on a horizontal pipe

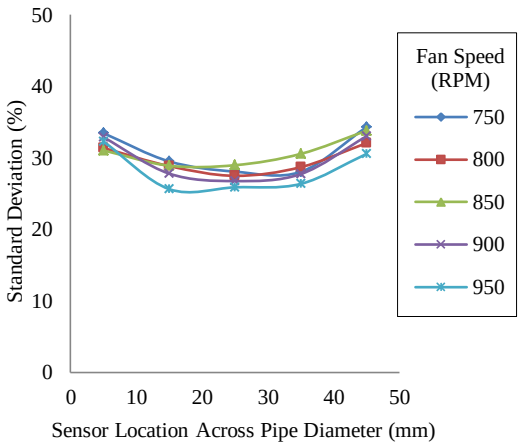

Fig. 6.158 Normalised standard deviation profiles of the correlation coefficient of pulverised coal/biomass (85%/15% blend) on the Y axis on a horizontal pipe

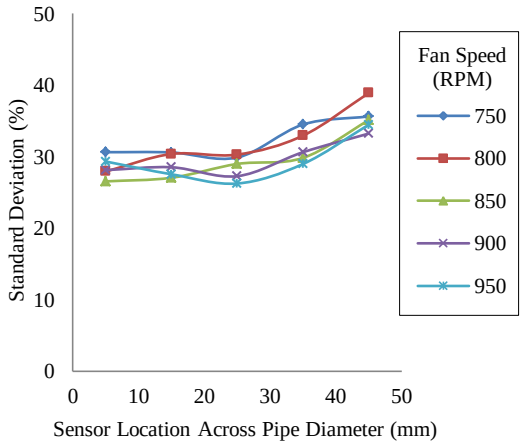

Fig. 6.159 Normalised standard deviation profiles of the correlation coefficient of pulverised coal/biomass (80%/20% blend) on the Z axis on a horizontal pipe

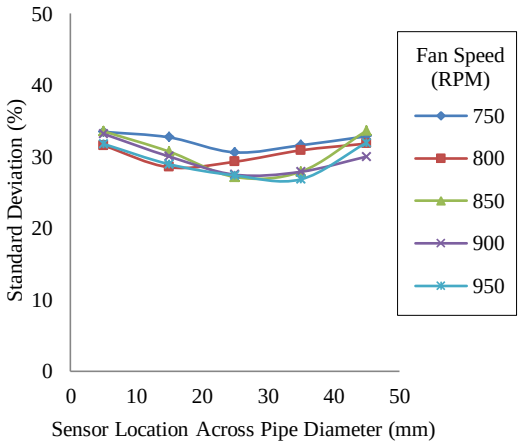

Fig. 6.160 Normalised standard deviation profiles of the correlation coefficient of pulverised coal/biomass (80%/20% blend) on the Y axis on a horizontal pipe

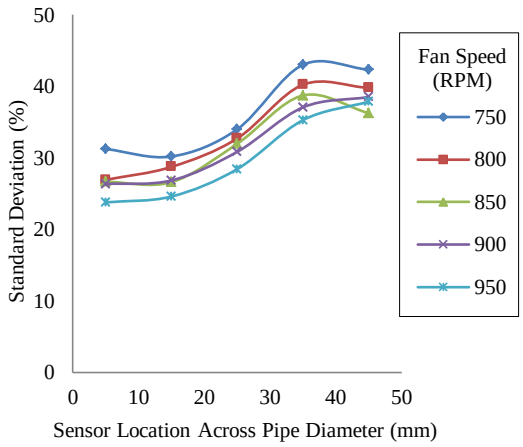

Fig. 6.161 Normalised standard deviation profiles of the correlation coefficient of pulverised biomass on the Z axis on a horizontal pipe

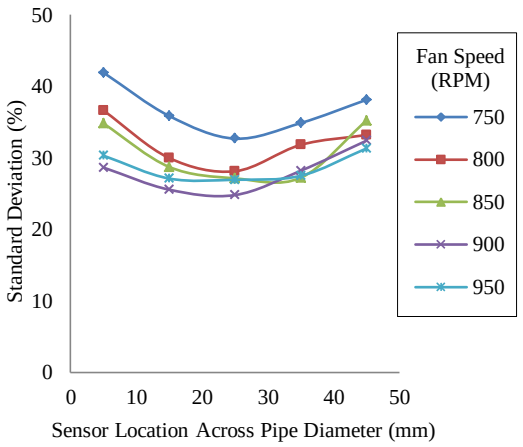

Fig. 6.162 Normalised standard deviation profiles of the correlation coefficient of pulverised biomass on the Y axis on a horizontal pipe

Vertical Particle Flow

The correlation coefficient profiles for the vertical particle flow (Fig. 6.163 – Fig. 6.174) are consistent over the whole diameter of the pipe on both the X and Y sensor axis. This is conceivably due to the flow being undeveloped due to the sensor location in relation to the right-angle bend.

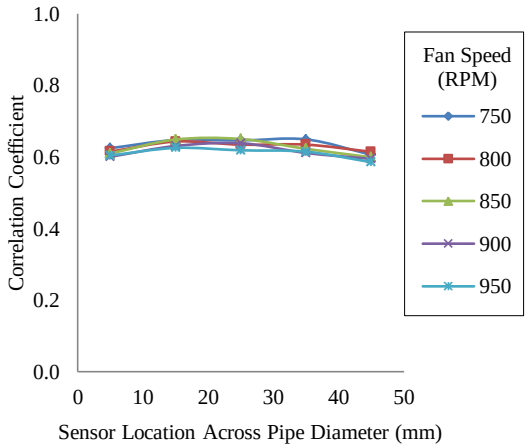

Fig. 6.163 Mean correlation coefficient profiles of pulverised coal on the X axis on a vertical pipe

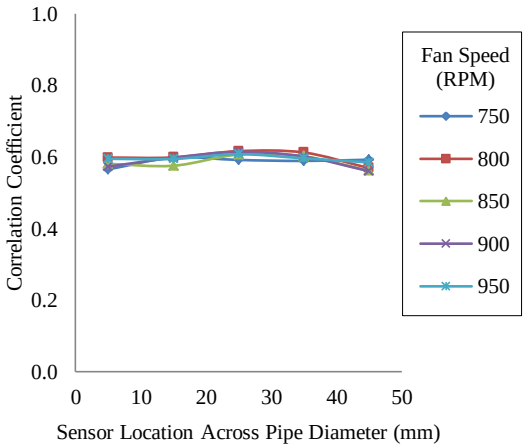

Fig. 6.164 Mean correlation coefficient profiles of pulverised coal on the Y axis on a vertical pipe

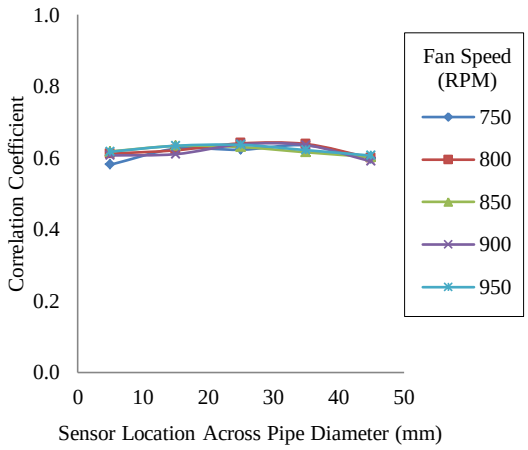

Fig. 6.165 Mean correlation coefficient profiles of pulverised coal/biomass (95%/5% blend) on the X axis on a vertical pipe

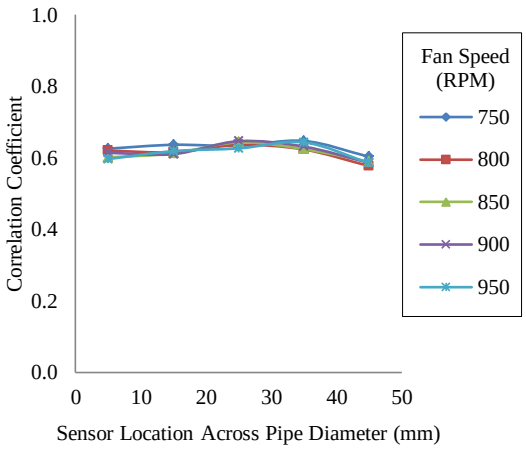

Fig. 6.166 Mean correlation coefficient profiles of pulverised coal/biomass (95%/5% blend) on the Y axis on a vertical pipe

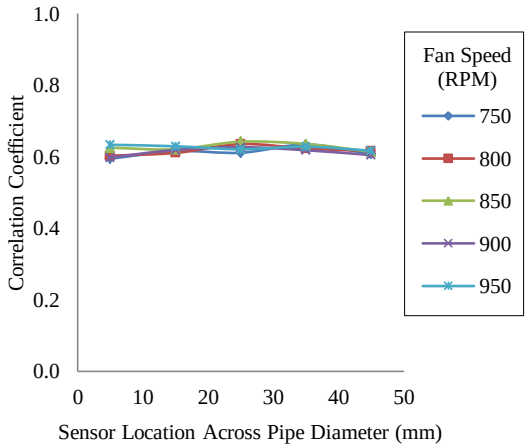

Fig. 6.167 Mean correlation coefficient profiles of pulverised coal/biomass (90%/10% blend) on the X axis on a vertical pipe

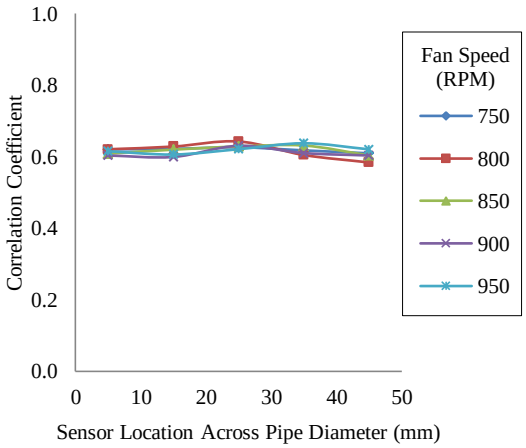

Fig. 6.168 Mean correlation coefficient profiles of pulverised coal/biomass (90%/10% blend) on the Y axis on a vertical pipe

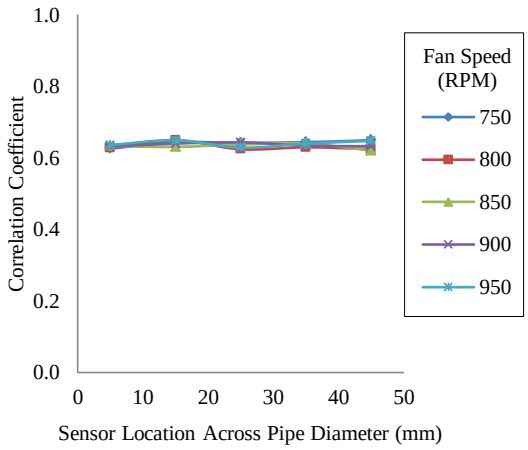

Fig. 6.169 Mean correlation coefficient profiles of pulverised coal/biomass (85%/15% blend) on the X axis on a vertical pipe

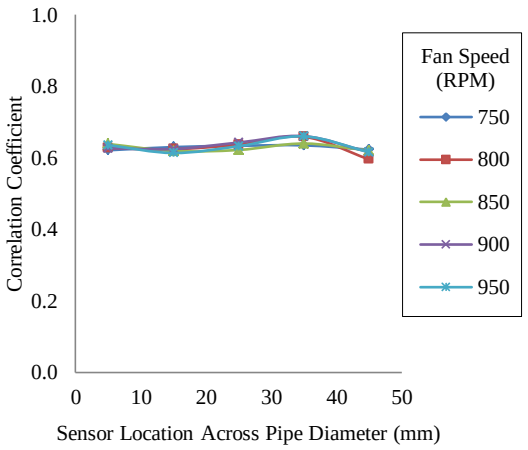

Fig. 6.170 Mean correlation coefficient profiles of pulverised coal/biomass (85%/15% blend) on the Y axis on a vertical pipe

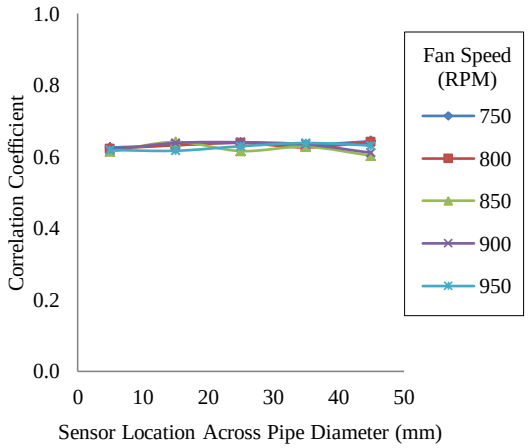

Fig. 6.171 Mean correlation coefficient profiles of pulverised coal/biomass (80%/20% blend) on the X axis on a vertical pipe

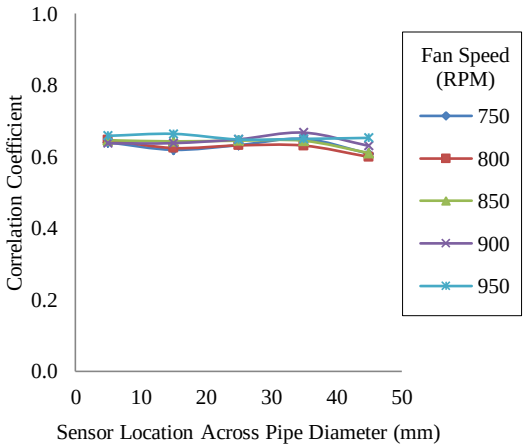

Fig. 6.172 Mean correlation coefficient profiles of pulverised coal/biomass (80%/20% blend) on the Y axis on a vertical pipe

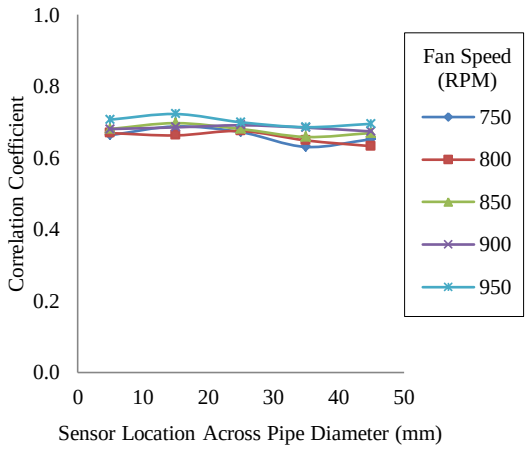

Fig. 6.173 Mean correlation coefficient profiles of pulverised biomass on the X axis on a vertical pipe

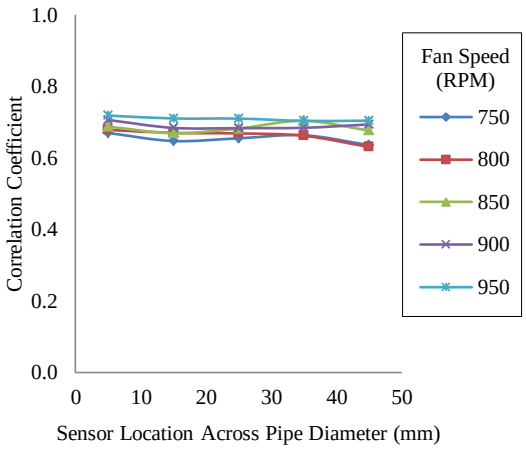

Fig. 6.174 Mean correlation coefficient profiles of pulverised biomass on the Y axis on a vertical pipe

The shapes of the normalised standard deviation profiles for correlation coefficient for the vertical particle flow (Fig. 6.175 – Fig. 6.186) are similar in shape to the normalised standard deviation profiles for the horizontal particle flow (Fig. 6.151 – Fig. 6.162). However the parabola shape of the profile is not as pronounced on the vertical flow compared to the horizontal flow. This is possibly due to the fact the particle flow is still in the process of developing due to the sensor location in relation to the right-angle pipe bend.

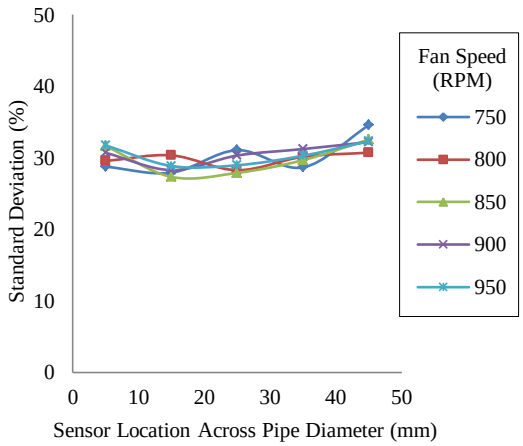

Fig. 6.175 Normalised standard deviation profiles of the correlation coefficient of pulverised coal on the X axis on a vertical pipe

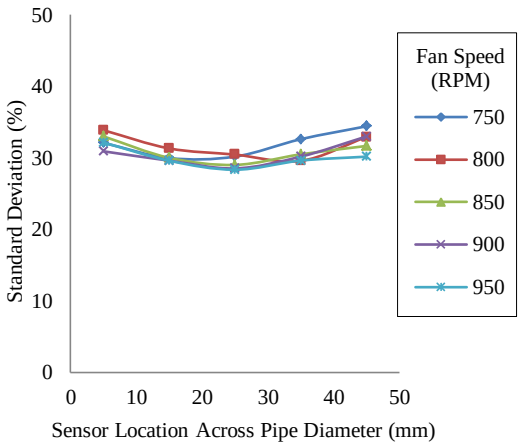

Fig. 6.176 Normalised standard deviation profiles of the correlation coefficient of pulverised coal on the Y axis on a vertical pipe

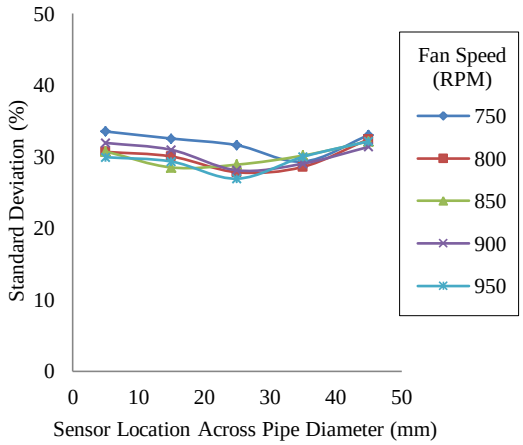

Fig. 6.177 Normalised standard deviation profiles of the correlation coefficient of pulverised coal/biomass (95%/5% blend) on the X axis on a vertical pipe

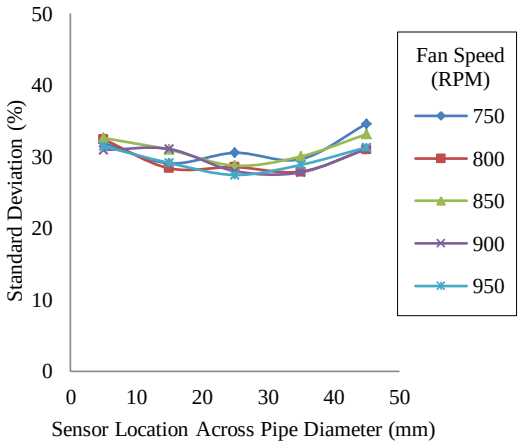

Fig. 6.178 Normalised standard deviation profiles of the correlation coefficient of pulverised coal/biomass (95%/5% blend) on the Y axis on a vertical pipe

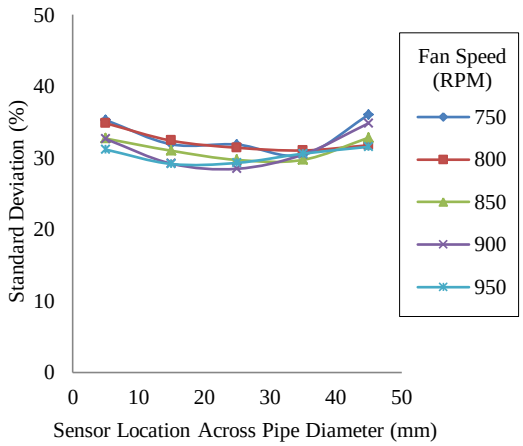

Fig. 6.179 Normalised standard deviation profiles of the correlation coefficient of pulverised coal/biomass (90%/10% blend) on the X axis on a vertical pipe

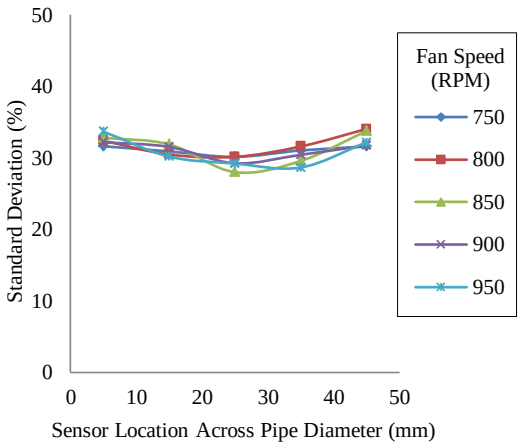

Fig. 6.180 Normalised standard deviation profiles of the correlation coefficient of pulverised coal/biomass (90%/10% blend) on the Y axis on a vertical pipe

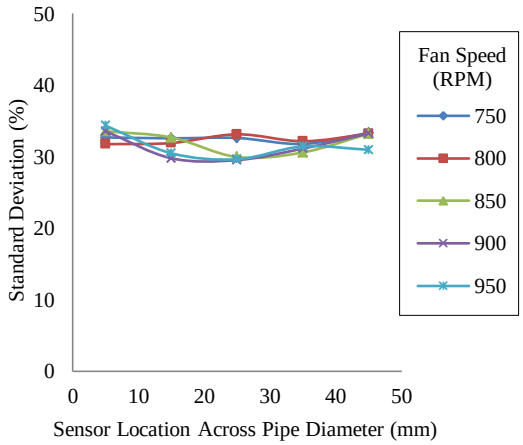

Fig. 6.181 Normalised standard deviation profiles of the correlation coefficient of pulverised coal/biomass (85%/15% blend) on the X axis on a vertical pipe

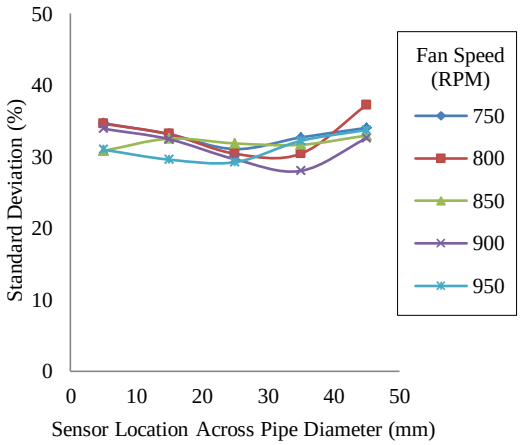

Fig. 6.182 Normalised standard deviation profiles of the correlation coefficient of pulverised coal/biomass (85%/15% blend) on the Y axis on a vertical pipe

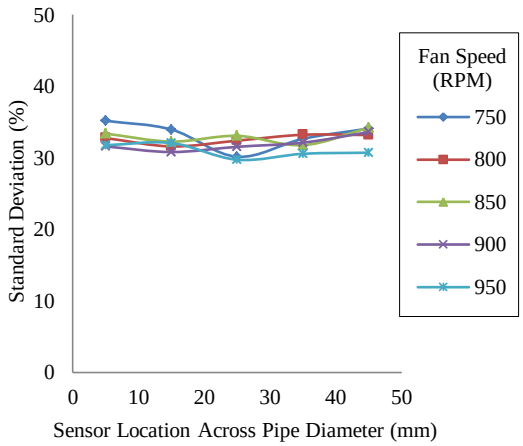

Fig. 6.183 Normalised standard deviation profiles of the correlation coefficient of pulverised coal/biomass (80%/20% blend) on the X axis on a vertical pipe

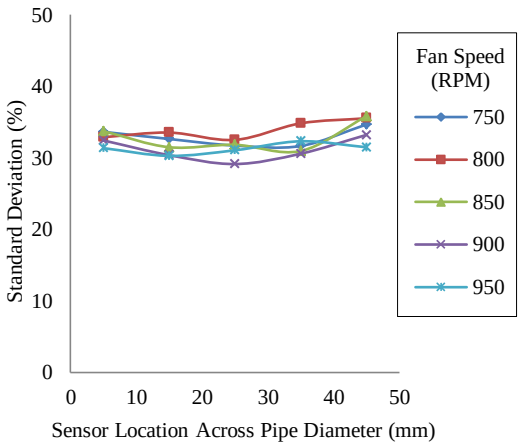

Fig. 6.184 Normalised standard deviation profiles of the correlation coefficient of pulverised coal/biomass (80%/20% blend) on the Y axis on a vertical pipe

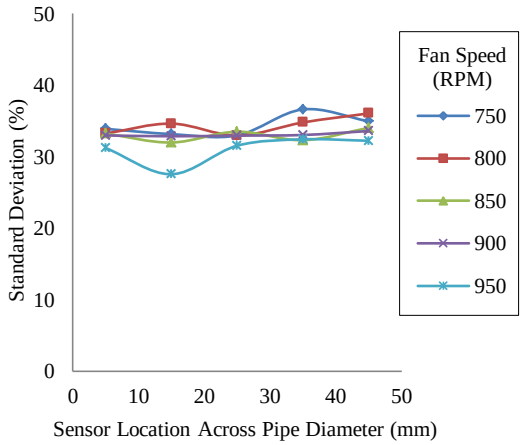

Fig. 6.185 Normalised standard deviation profiles of the correlation coefficient of pulverised biomass on the X axis on a vertical pipe

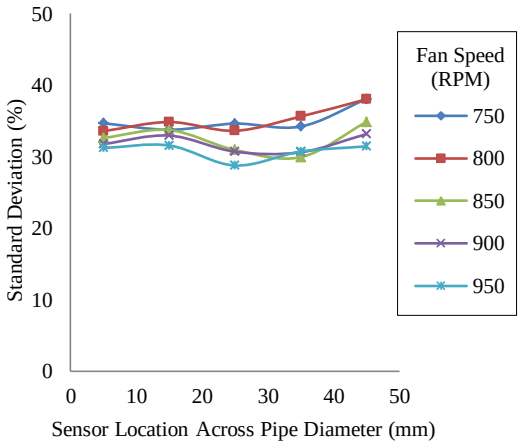

Fig. 6.186 Normalised standard deviation profiles of the correlation coefficient of pulverised biomass on the Y axis on a vertical pipe

6.2.3.5 Discussion on the Flow Characteristics of Pneumatically Conveyed Coal/Biomass Blends

The electrostatic sensor array is capable of determining the particle velocity and concentration profiles of positive pressure conveyed coal, biomass and coal biomass blends on both horizontal and vertical pipe sections. The measured velocity profiles for the horizontal particle flow illustrate that they are fully developed. Conversely the velocity profiles on the vertical pipe are still in the process of developing as seen by their underdeveloped curved shapes due to the position of the electrostatic sensor array in relation to a right-angle pipe bend. The effect of gravity can be seen in the measured particle concentration profiles with higher particle concentration at the bottom of the pipe. The particle concentration profiles at the very bottom of the pipe for pure coal and low ratios of biomass have reduced measured particle concentration. However for pure biomass and coal/biomass blends (> 15% biomass by weight) this phenomenon of reduced particle concentration does not occur. This is conceivably due to turbulence caused by the sensor array blade in relation to the pipe wall which would prevent the smaller particles (coal) from entering the space between the sensor blade and the pipe wall or the Magnus effect. Larger biomass particles, however, do not suffer from this effect due to the pulverised biomass having a larger particle size consequently a higher particle mass allowing them to overcome the turbulence or Magnus effect. Through analysis of the correlation coefficient profiles as well as analysis of the standard deviation of the velocity profiles on the horizontal developed particle flow, it is clear that the flow is more stable in the centre of the pipe compared to along the pipe wall.

6.3 The Piezoelectric Sensor Array

The piezoelectric sensor array is designed to determine the particle concentration and particle size distribution profiles in dilute multi-phase flow. The piezoelectric sensor array achieves this by having an array of piezoelectric impact sensors along the leading edge of the sensor blade. In order to determine the effectiveness of the piezoelectric sensor array a series of experiments were carried out both on-line and off-line and compared to the theoretical system model.

6.3.1 Off-Line Experimentation Using the Piezoelectric Sensor (Single Sensor Element)

In order to compare the developed system model for the piezoelectric impact sensor to experimental data off-line experimentation was carried out using the off-line impact test rig. The off-line test rig was used to ensure as many experimental conditions as possible were known, thus ensuring accurate comparison to the developed system model.

6.3.1.1 Experimental Conditions

For off-line experimentation three sizes of ball bearings were used with the off-line test rig (2.5 mm, 3 mm and 3.5 mm diameter) each with a mass of 11.62 mg, 20.08 mg and 31.88 mg respectively. The ball bearings are made from Delrin which is a high strength engineering polymer. The Delrin ball bearings have a Poisson Ratio of 0.35 and Young's Modulus of $3.1_{x10}{}^{9}$ N/m^2 [111]. The impacted surface (impact waveguide) is manufactured out of engineering brass which has a Poisson Ratio of 0.331 [112] and Young's Modulus of $102_{x10}{}^{9}$ N/m^2 [113]. The mass for the impact target is assumed to be sufficiently large making it insignificant for the effective mass calculation (4.14) [114]. The impact velocity was independently measured by the optical sensor on the off-line impact test rig.

6.3.1.2 Unfiltered Impact Analysis

The impact sensor was first tested without the bandpass filter in order to examine the frequency component of the ball bearing impact. A total of 200 impact reading were taken for each size of ball bearings. Fig. 6.187 shows the peak amplitude of the impact signals. The magnitude of the unfiltered impact signals shows a high level of deviation, especially on 2.5 mm diameter ball bearing. The impact signals for the 3 mm ball bearing also show a large number of impact signals that are at the supply voltage (1.65V) indicating that the preamplifier has saturated for the impacts.

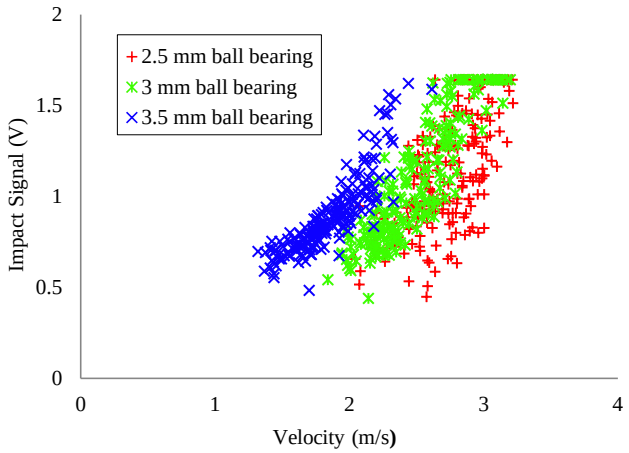

Fig. 6.187 Magnitude of dominant peak of ball bearing impact (unfiltered)

Power spectral analysis of impacts of all three sizes of ball bearings is carried out for 2.0 m/s, 2.2 m/s, 2.4 m/s and 2.6 m/s, as shown in Fig. 6.188 – Fig. 6.191 respectively. The power spectra in Fig. 6.188 – Fig. 6.191 indicate that the smaller diameter ball bearings have higher frequency components. This higher frequency component is conceivably related to the impact duration. Fig. 6.192 shows the theoretical impact duration calculated using (4.15). Illustrating that impact duration decreases for smaller diameter ball bearings, thus introducing a higher frequency (lower period) into the particle impact. Additionally, for larger diameter ball bearings at higher velocity there is a large DC component in the signal indicating that the signal has saturated to the supply voltage.

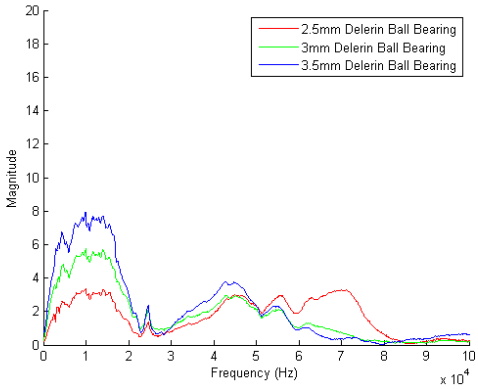

Fig. 6.188 Power spectra of the ball bearing impacts at 2.0 m/s

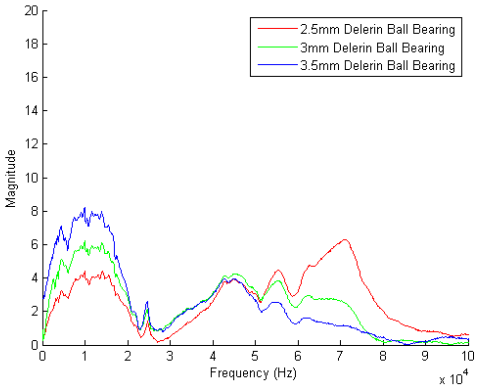

Fig. 6.189 Power spectra of the ball bearing impacts at 2.2 m/s

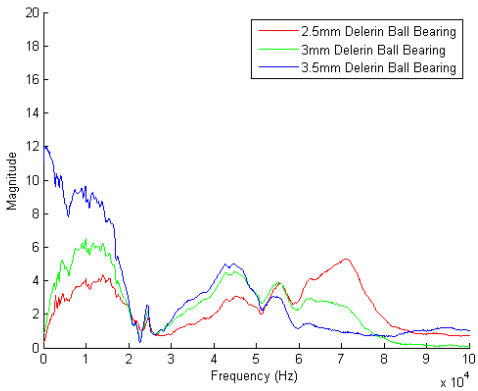

Fig. 6.190 Power spectra of the ball bearing impacts at 2.4 m/s

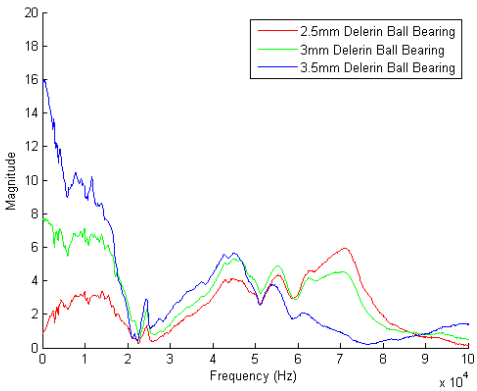

Fig. 6.191 Power spectra of the ball bearing impacts at 2.6 m/s

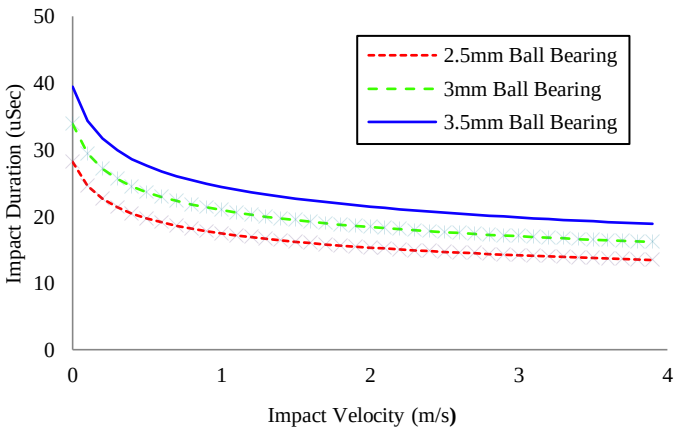

Fig. 6.192 Impact duration for 2.5 mm, 3 mm and 3.5 mm Delrin ball bearings calculated using (4.15)

Fig. 6.193 – Fig. 6.195 shows the power spectra for the ball bearing with different impact velocities. They too show an increase in magnitude for higher frequency components which also corresponds to the theoretical impact durations shown in Fig. 6.192. Likewise, Fig. 6.193 – Fig. 6.195 show a higher DC component for the higher impact velocities for 3 mm and 3.5 mm ball bearing impacts illustrating that the impact sensor signal has saturated to the supply voltage for higher impact forces.

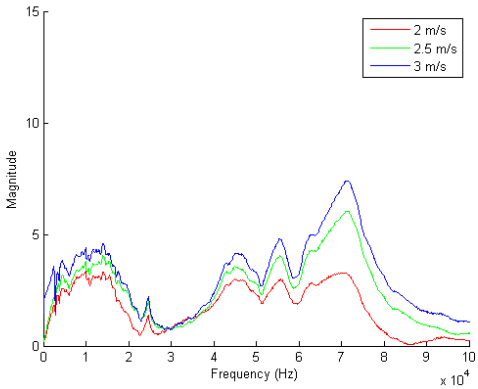

Fig. 6.193 Power spectra of 2.5 mm ball bearing impact signal

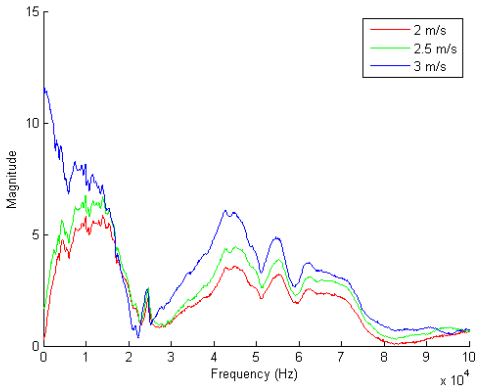

Fig. 6.194 Power spectra of 3 mm ball bearing impact signal

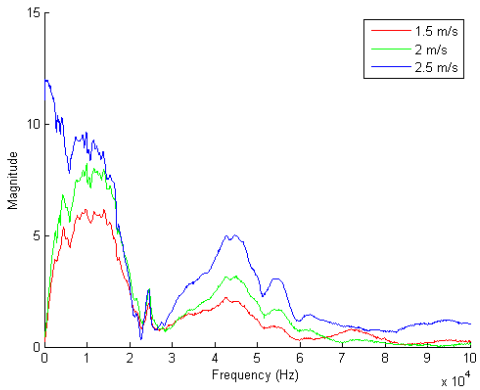

Fig. 6.195 Power spectra of 3.5 mm ball bearing impact signal

For Fig. 6.188 – Fig. 6.191 and Fig. 6.193 – Fig. 6.195 there is a common frequency range (approximately between 5 kHz and 15 kHz) that is consistently proportional to the impact force due to a higher impact velocity or larger mass of the ball bearing.

6.3.1.3 Filtered Impact Analysis

A second order bandpass filter with a low cut-off frequency of 5 kHz and an upper cut-off frequency of 15 kHz was placed between the impact sensor's output and the ADC. This was done to remove the DC component caused by saturation as well as the high frequency components and only use the frequencies that were shown to be proportional to the impact force as seen in Fig. 6.188 – Fig. 6.191 and Fig. 6.193 – Fig. 6.195. The filtered power spectra analysis of the filtered impact signals (Fig. 6.196 – Fig. 6.201) illustrate that magnitude of the frequency component between 5 kHz – 15 kHz increases proportionally for higher impact force caused by larger particle mass or impact velocity.

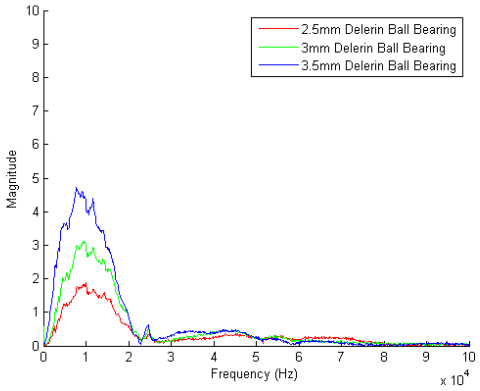

Fig. 6.196 Power spectra of the ball bearing impacts at 2.2 m/s (filtered)

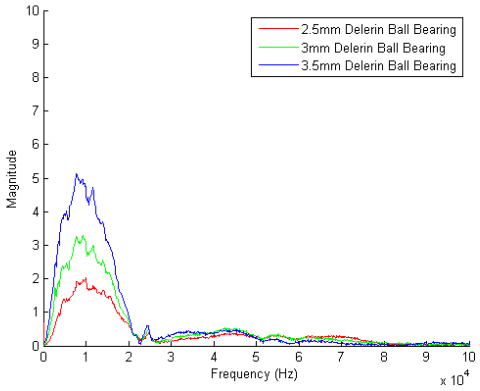

Fig. 6.197 Power spectra of the ball bearing impacts at 2.4 m/s (filtered)

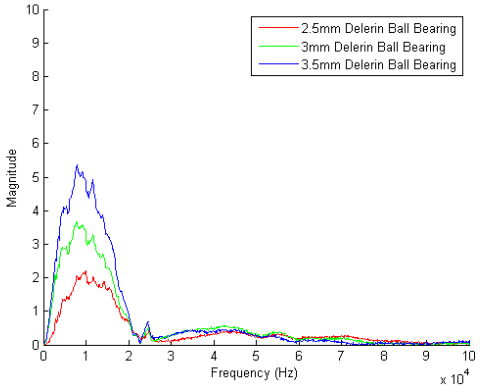

Fig. 6.198 Power spectra of the ball bearing impacts at 2.6 m/s (filtered)

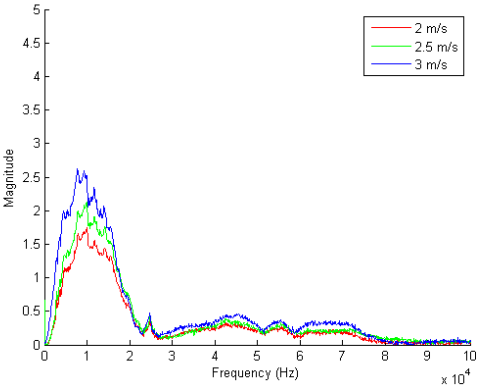

Fig. 6.199 Power spectra of 2.5 mm ball bearing impact signal (filtered)

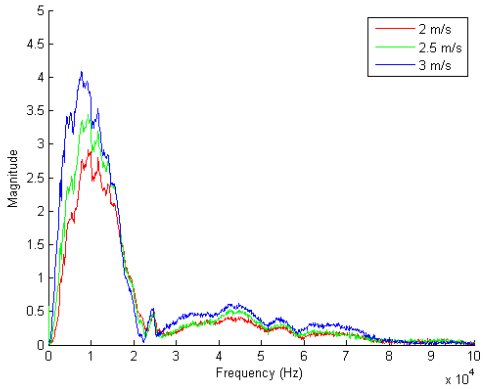

Fig. 6.200 Power spectra of 3 mm ball bearing impact signal (filtered)

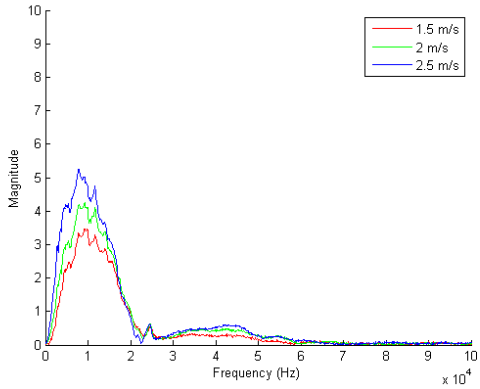

Fig. 6.201 Power spectra of 3.5 mm ball bearing impact signal (filtered)

The same experiment was repeated again 200 times for all three ball bearing diameters using the bandpass filter. Fig. 6.202 shows the peak amplitude of the filtered impact signals. Fig. 6.202 also shows the calculated signal magnitude using the mechanical characteristics of the waveguide and the Delrin ball bearings and a range of impact velocities using (4.18).

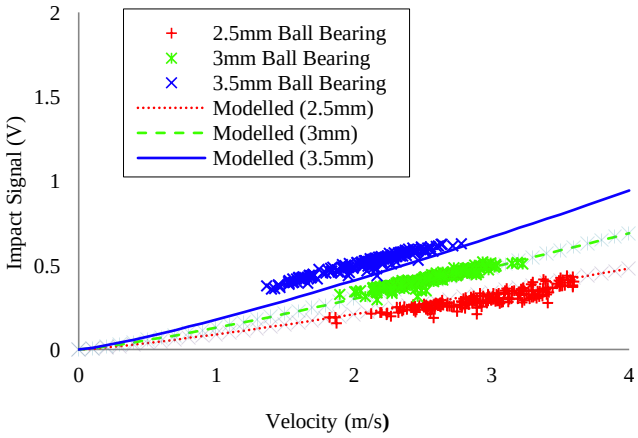

Fig. 6.202 Magnitude of dominant peak of ball bearing impact (with bandpass filter)

The signal output from the impact sensor agrees well with the calculated values using (4.18). However, the results from the 2.5 mm impacts show a higher deviation compared to the other two. This is believed to be due to the fact that, even though the guiding tube is centred above impact sensor waveguide, some of the 2.5mm ball

bearings may not be impacting the centre of the waveguide. Furthermore, for higher impact forces the impact sensor output is greater than the calculated values (3.5 mm ball bearing impacts); this is possibly due to the higher impact force being able to overcome the adhesive effect between the rubber and the waveguide [106]. This indicates that for a spherical particle, if the particle velocity is known as well as the mechanical characteristic of the particle, particle size can be determined via impact analysis using the piezoelectric impact sensor.

6.3.1.4 Discussion on the Off-Line Experimentation Using the Piezoelectric Sensor

The piezoelectric impact sensor has been capable of determining the particle size through analysis of the magnitude of the particle impact signal. Through analysis of the frequency component of the sensor output during impact, it has been determined that selective filtering of frequency components of the impact signal has an effect on reducing the deviation of the peak magnitude of the impact signal. The comparison between the calculated output signal values and the sensor outputs obtained during the experimentation agree well. This outcome indicates that, for a spherical particle, the piezoelectric impact sensor is capable of determining the size of the particle through impact analysis, assuming that the mechanical properties of the particle and particle impact velocity are known. The impact sensor has a very small active sensing area, making it ideal for online particle size measurement on a pneumatic conveying system since the small active sensing area reduces the chance of simultaneous impacts of multiple particles occurring.

6.3.2 On-Line Experimentation Using the Piezoelectric Sensor (Single Sensor Element)

Before the piezoelectric sensor array was fully constructed a single piezoelectric impact sensor was constructed inside the sensor blade. This was done to ensure the sensor design was viable before full construction of the piezoelectric sensor array was carried out. The single piezoelectric impact sensor was placed in the centre of the sensor blade (centre of the pipe).

6.3.2.1 Measuring the Performance of the Anti-Vibration Shielding

The drawback of previous sensors (impact bar sensor designs) that determined particle size through impact analysis was the relatively large surface area of the impact bar. This design feature caused a problem that even in dilute phase particle flow multiple impacts may occur simultaneously which would lead to measurement errors. In contrast, this design of impact sensor has the novel feature that only a small particle of the sensor blade is active due to specific anti-vibration shielding on the leading edge of the sensor. In order to test the effectiveness of this anti-vibration shielding a series of off-line tests were carried out. These tests utilised the off-line test rig and involved impacting Delrin ball bearings at a specific impact velocity (2 m/s) and size of ball bearing (3.5 mm) on both the active sensor area and non-active sensor area to measure the impact attenuation caused by the anti-vibration shielding. Fig. 6.203 and Fig. 6.204 show the impact signal of a Delrin ball bearing impacting the active (unfiltered) and non-active (filtered) sensor areas respectively. The attenuation of particle impacts caused by the combination of the anti-vibration shielding and the band-pass filter is approximately -28 dB.

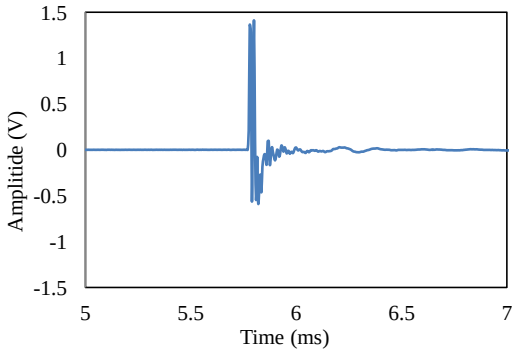

Fig. 6.203 Unfiltered impact signal of a 3.5 mm Delrin ball bearing with an impact velocity of 2 m/s impacting the active sensor area

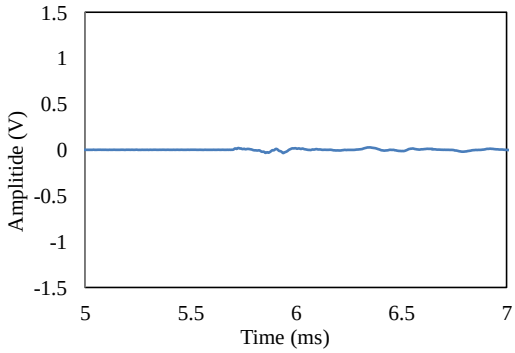

Fig. 6.204 Filtered impact signal of a 3.5 mm Delrin ball bearing with an impact velocity of 2 m/s impacting the non-active sensor area

6.3.2.2 Experimental Conditions

Testing was carried out using the positive pressure test rig with the sensor mounted on a horizontal pipe sections. The impact sensor was mounted on a horizontal pipe section after a 6400 mm straight horizontal pipe section ensuring measurement of a developed

flow. During the experiments, temperature (21 °C average) and relative humidity (46.5% average) were monitored to ensure environmental test conditions were the same for each test.

The pulverised material used for this experimentation was plastic shot (Amino plastic blast media) which is used in industry for shot blasting when the substrate of the material must not be damaged [115]. This material was chosen over materials such as glass beads since the plastic shot will not fracture when it is being conveyed and consequently it is reusable. The plastic shot was first sieved between a 600 µm and a 700 µm sieve to reduce the particle size distribution. The shape of the plastic shot particles are semi cubical to angular; consequently the weight of the particles are estimated (estimated by assuming the particles are spherical and using the density of the plastic shot of 1.6 g/cm^3) at 0.18 mg (600 µm diameter particles) and 0.287 mg (700 µm diameter particles). Since the manufacture does not specify the exact mechanical properties of the plastic shot the estimated Poisson Ratio of 0.331 and Young's Modulus of $10_{x10}{}^9$ N/m^2 was taken from a similar material [116]. Particle size and shape distribution was independently measured using the off-line digital particle size imaging techniques. Fig. 6.205 and Fig. 6.206 shows the particle size and shape distribution of the sieved plastic shot.

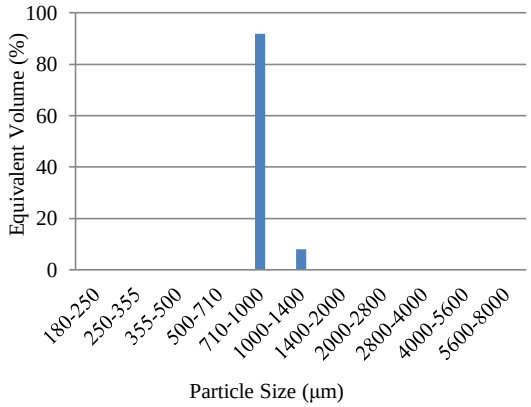

Fig. 6.205 Particle size distribution of plastic shot particles

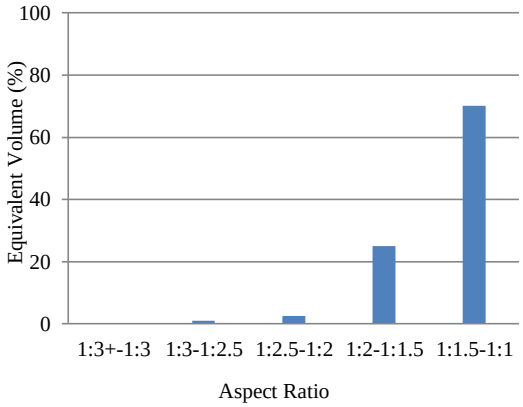

Fig. 6.206 Particle aspect ratio of plastic shot particles

Analysis of the particle size data show that the majority of the measured particles (90%) shown in Fig. 6.205 are within the range of 710-1000 μm which is slightly higher than the sieve mesh size. It has been documented that the digital imaging technique measures the particles to be slightly larger than their actual size [33]. The particle shape distribution shows that the majority of the particles have a an aspect ratio (Fig. 6.206) in the range of 1:1 – 1:1.5 indicating that most of the particles are close to being spherical.

Since the system model for determining the particle size requires the particle velocity to be known the electrostatic sensor array was used to determine the particle velocity at the centre of the pipe in the same location of the impact sensor. The experiment consisted of five different fan speeds were used to create five different particle velocities as shown in Table 6.4. This was done so the only variable that will affect the magnitude of the impact signal will be the particle velocity (since the plastic shot particles were sieved to have the same particle size).

Table 6.4

Plastic shot (single impact sensor) test condition matrix

Pulverised Material	Sensor Axis	Pipe Orientation	Fan Speed (RPM)
Plastic Shot	Z	Horizontal	750
Plastic Shot	Z	Horizontal	800
Plastic Shot	Z	Horizontal	850
Plastic Shot	Z	Horizontal	900
Plastic Shot	Z	Horizontal	950

Due to the small mass of the plastic shot particles compared to the Delrin ball bearings used in the off-line particle impact experiments a secondary amplifier was placed after the pre-amplifier. The secondary amplifier was set to have a gain of 1.5 to ensure the full range of the ADC on the data logger was used. Since the anti-vibration shielding on the leading edge of the sensor blade has creates an attenuation of approximately -28 dB a threshold signal magnitude was used to determine when a particle impact has occurred. This threshold signal voltage was set to 100 mV. This magnitude of threshold

ensured that only particles that impacted the active sensor area were categorised as a particle impact. Each individual experiment was carried out for approximately 10 minutes.

6.3.2.3 On-Line Experimentation Using the Piezoelectric Sensor (Single Sensor Element) Results

The measured particle impacts for the on-line experimentation indicate that the magnitude of the impacts increase with the higher particle velocities. Fig. 6.207 displays the average measured particle impacts for the five different particle velocities with the impact sensor being in the centre of the pipe. The measured average particle impact magnitudes for each of the five particle velocity appear to be slightly lower than the modelled data for the 600 μm plastic shot particles. This is conceivably due to some of the particles not impacting the active sensor area directly (glancing impacts); consequently not all the impact force is applied to the active sensor area. Another possibility is that the estimated mass of the individual particles is underestimated since the mass of the shot particles was estimated assuming the particles are spherical, however, according to the manufacturer the shape of the plastic shot are semi cubical to angular [115].

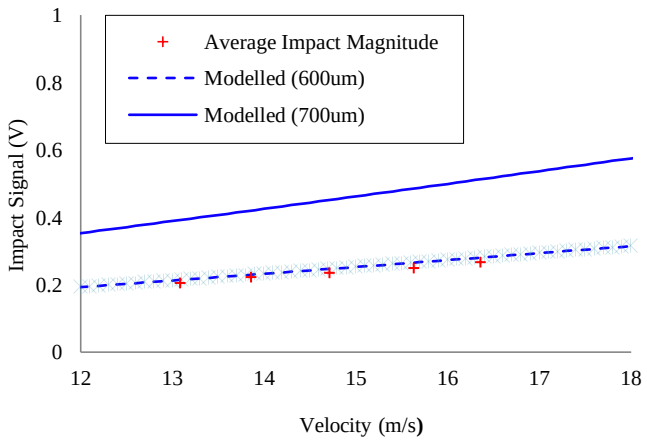

Fig. 6.207 Estimated and measured average magnitude of the particle impacts measured by the piezoelectric impact sensor mounted in the centre of the pipe

6.3.2.4 Discussion on the On-Line Experimentation Using the Piezoelectric Sensor (Single Sensor Element)

A single piezoelectric impact sensor has been successfully implemented in measuring the particle size of plastic shot through impact analysis in an on-line mode using a positive pressure bulk solid conveying test rig. It has been proven that if the mechanical properties of the conveyed material are known, as well as the particle velocity is independently measured (using an electrostatic sensor) the measured impact signal values show a close similarity to the calculated values using the derived system model. Through use of anti-vibration shielding a small active sensor area has been achieved on the leading edge of the sensor blade. This feature has ensured that the current design of the piezoelectric impact sensor does not suffer from measurement errors caused by multiple simultaneous impacts caused by large active sensor areas.

6.3.3 On-Line Experimentation Using the Piezoelectric Sensor Array

After successful on/off-line trials carried out using the single impact sensor on the sensor blade the full sensor array was constructed. The piezoelectric sensor array consists of five independent impact sensors on a sensor blade that spans the diameter of the pipe. The impact sensor elements are spaced out equally across the pipe diameter (10 mm apart). This design corresponds to the positions of the electrostatic sensor elements on the electrostatic sensor array. The purpose of this on-line experiment on the piezoelectric sensor array is to test the viability of the piezoelectric sensor array's ability to determine the particle size profiles as well as determining the particle concentration profiles across the diameter of the pipe. To this end the piezoelectric sensor array will be tested on a horizontal pipe on a developed dilute-phase particle flow with comparison made with measurements taken by the electrostatic sensor array.

6.3.3.1 Calibrating the Piezoelectric Sensor Array

Due to mechanical variations in the construction of each element of the piezoelectric sensor array, each impact sensor had to be calibrated to ensure consistent measurement of the particle size across the pipe diameter. The calibration process was carried out

using the off-line impact test rig and involved carrying out a series of 200 impacts per Delrin ball bearing diameter (2.5 mm, 3 mm and 3.5 mm). The secondary amplifiers on each piezoelectric impact sensor were then used to calibrate its respective impact sensor (fine adjustment was carried out using DSP). After the calibration process, the off-line test rig was used to verify each element was calibrated. Fig. 6.208 - Fig. 6.212 illustrate the off-line testing using the three sizes of Delrin ball bearings after calibration. The impact sensors were calibrated to the original impact values obtained from the off-line testing on the original impact sensor.

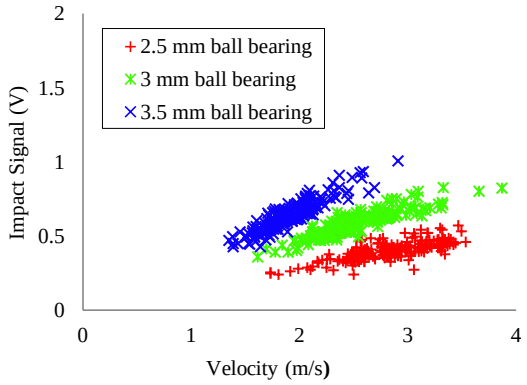

Fig. 6.208 Calibrated values of impacts measured on sensor 1 (5 mm) using Delrin ball bearings on the off-line impact test rig

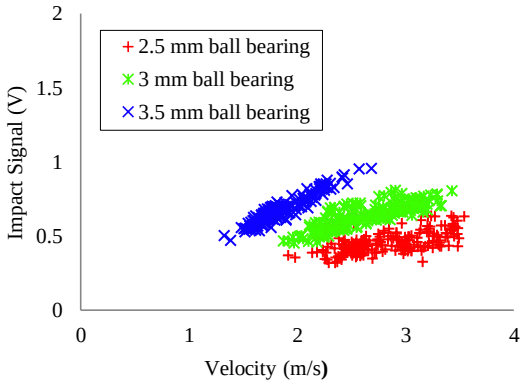

Fig. 6.209 Calibrated values of impacts measured on sensor 2 (15 mm) using Delrin ball bearings on the off-line impact test rig

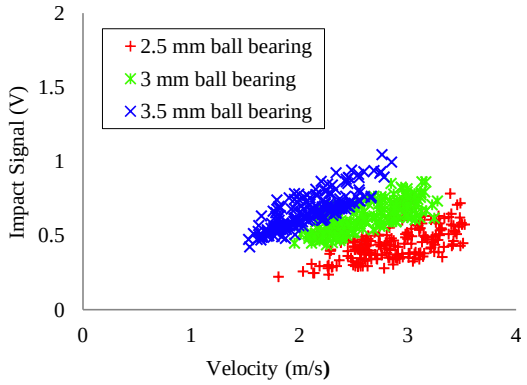

Fig. 6.210 Calibrated values of impacts measured on sensor 3 (25 mm) using Delrin ball bearings on the off-line impact test rig

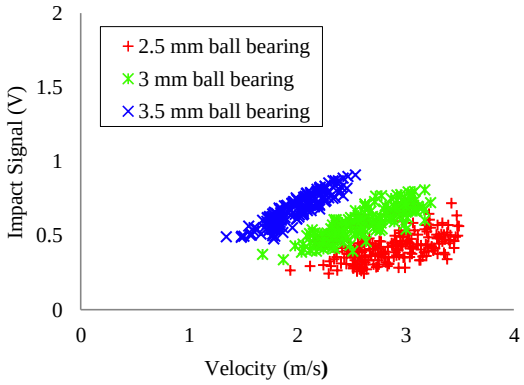

Fig. 6.211 Calibrated values of impacts measured on sensor 4 (35 mm) using Delrin ball bearings on the off-line impact test rig

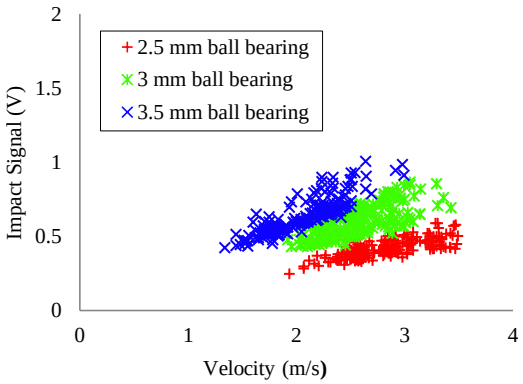

Fig. 6.212 Calibrated values of impacts measured on sensor 5 (45 mm) using Delrin ball bearings on the off-line impact test rig

6.3.3.2 Experimental Conditions

On-line experimentation on the piezoelectric sensor array was carried out on the positive pressure test rig. The impact sensor was mounted on a horizontal pipe section after a 6400 mm straight horizontal pipe section ensuring measurement of a developed flow. During the experiments, temperature (21 °C average) and relative humidity (45.5% average) were monitored to ensure environmental test conditions were the same for each test. The pulverised material used for this experimentation was the same plastic shot (Amino plastic blast media) which was used for the on-line experiment for the single piezoelectric impact sensor. Again the plastic shot was first sieved between a 600 µm and a 700 µm sieve to reduce the particle size distribution. Fig. 6.205 and Fig. 6.206 shows the particle size and shape distribution of the sieved plastic shot used for the on-line experiment for the piezoelectric sensor array.

The experiment consisted of five different fan speeds were used to create five different particle velocities with the piezoelectric sensor mounted in the Z and Y axis as shown in Table 6.5. This was done so the only variable that will affect the magnitude of the impact signal will be the particle velocity (since the plastic shot particles were sieved to have the same particle size).

Table 6.5

Plastic shot (array impact sensor) test condition matrix

Pulverised Material	Sensor Axis	Pipe Orientation	Fan Speed (RPM)
Plastic Shot	Z	Horizontal	750
Plastic Shot	Z	Horizontal	800
Plastic Shot	Z	Horizontal	850
Plastic Shot	Z	Horizontal	900
Plastic Shot	Z	Horizontal	950
Plastic Shot	Y	Horizontal	750
Plastic Shot	Y	Horizontal	800
Plastic Shot	Y	Horizontal	850
Plastic Shot	Y	Horizontal	900
Plastic Shot	Y	Horizontal	950

The electrostatic sensor array was used to measure the particle velocity profiles and the particle concentration profiles for both the Z and Y sensor axis and all particle velocities. During the experiments to measure the particle velocity and the concentration profiles of the pneumatically conveyed plastic shot it was found that the measured r.m.s. charge was considerably lower than the measured r.m.s. charge for the flour, biomass or coal. Consequently the gain of each of the secondary amplifies on the electrostatic sensor array had to be increased. A possible reason for this is that the plastic shot has an anti-static solution added to it during its manufacture [115] to reduce static charge build up during the shot blasting process. The measured particle velocity profiles presented in Fig. 6.213 and Fig. 6.214 show the typical velocity profiles of a developed particle flow on a horizontal pipe. This indicates that the particle velocity is higher in the centre of the pipe compared to the particle flow along the pipe wall. In addition the particle velocity measured on the Z axis (Fig. 6.213) shows that the particle velocity along the pipe wall at the bottom of the pipe (0 mm) is lower than the particle velocity along the pipe wall at the top of the pipe (45 mm). The reason for this is that gravity is causing the particles to come into contact with the bottom of the pipe more than the top of the pipe causing them to slow down more due to more friction with the pipe wall.

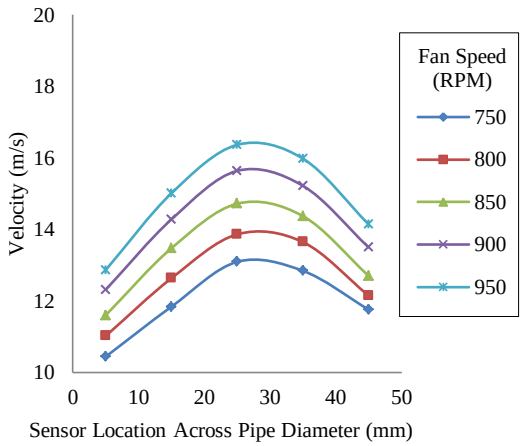

Fig. 6.213 Mean velocity profiles of plastic shot measured by the electrostatic sensor array on the Z axis on a horizontal pipe

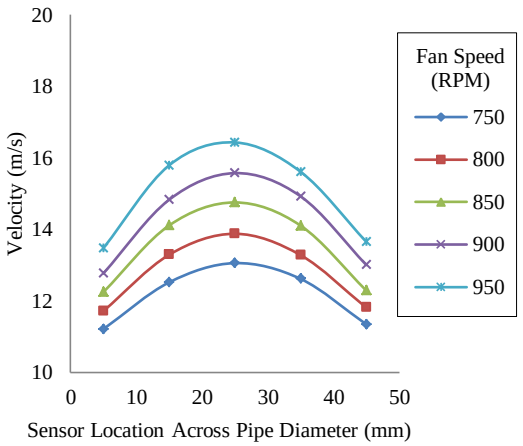

Fig. 6.214 Mean velocity profiles of plastic shot measured by the electrostatic sensor array on the Y axis on a horizontal pipe

The normalised standard deviation of the velocity profiles presented in Fig. 6.215 and Fig 6.216 illustrate that the particle velocity deviates less in the centre of the pipe compared to along the pipe wall.

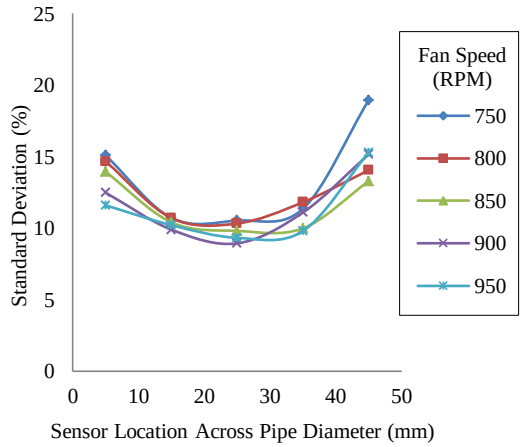

Fig. 6.215 Normalised standard deviation profiles of the velocities for plastic shot measured by the electrostatic array sensor on the Z axis on a horizontal pipe

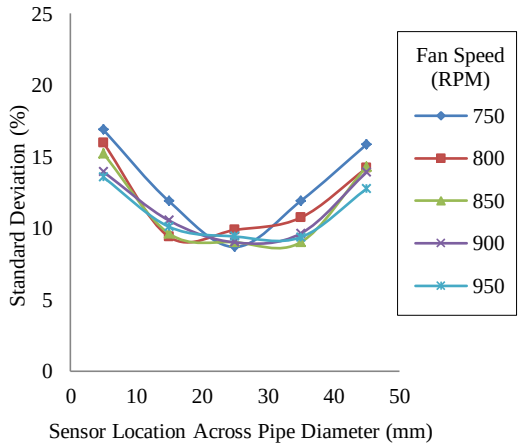

Fig. 6.216 Normalised standard deviation profiles of the velocities for plastic shot measured by the electrostatic array sensor on the Y axis on a horizontal pipe

The particle concentration profiles were also measured using the electrostatic sensor array for comparison purposes. Fig. 6.217 and Fig. 6.218 display the measured particle

concentration profiles measured by the electrostatic sensor array for the plastic shot on the horizontal pipe with the sensor in the Z and Y axis. The effect of gravity can be seen in the Z axis profiles (Fig. 6.217) which indicates that the particle concentration increases in the direction of gravity.

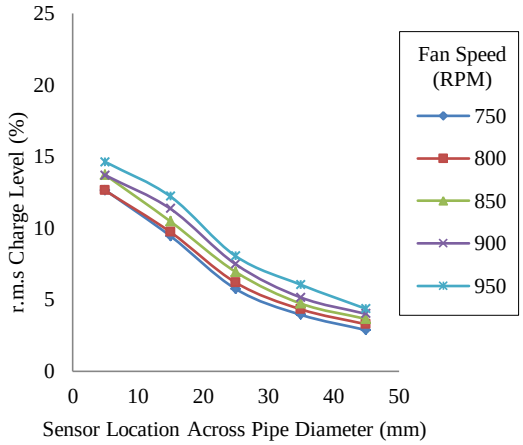

Fig. 6.217 Mean particle concentration profiles of plastic shot using normalised r.m.s. charge value to measure particle concentration on the Z axis on a horizontal pipe

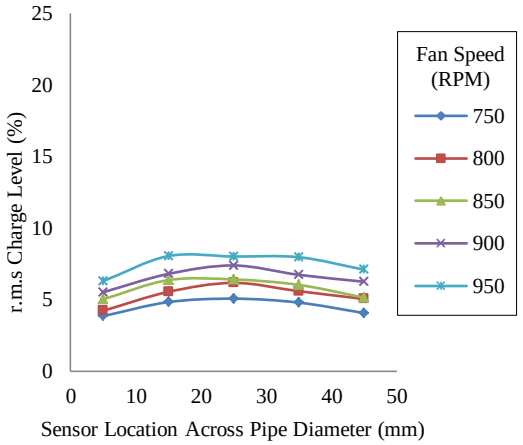

Fig. 6.218 Mean particle concentration profiles of plastic shot using normalised r.m.s. charge value to measure particle concentration on the Y axis on a horizontal pipe

The threshold signal voltage was set to 100 mV. This magnitude of threshold ensured that only particles that impacted the active sensor area were categorised as a particle impact. For each fan speed for the piezoelectric sensor array the experiment run time was approximately 50 minutes (approximately 10 minutes for each element of the piezoelectric sensor array).

6.3.3.3 Measured Particle Size Distribution Profiles

The particle size was determined by the magnitude of the measured particle impact signal on the active sensor area of each element of the piezoelectric sensor array (if the signal magnitude was over the threshold voltage). Fig. 6.219 and Fig. 6.220 show the average impact magnitude of detected impacts for the sensor mounting on the Z and Y axis (five particle velocities for each axis). Since the plastic shot particles were sieved to ensure a limited size distribution (sieved between a 600 μm and 700 μm sieves), the

only variable to affect the impact magnitude is the particle velocity. The displayed average impact magnitude profiles in. Fig. 6.219 and Fig. 6.220 clearly demonstrate that the measured impact force is proportional to the particle velocity. This illustrates that the piezoelectric sensor array is capable of determining the impact force of a particle impact and hence the particle size for the local area of the pipe. The analysis of the standard deviation of the profiles for the measured impacts on the piezoelectric impact array in Fig. 6.221 and Fig. 6.222 bare a close similarity to the standard deviation profiles of the velocity profiles measured by the electrostatic sensor array in Fig. 6.215 and Fig 6.216 in which the measured particle impacts deviate less in the centre of the pipe compared to the along the pipe wall. This analysis demonstrates that the particle velocity is the determining factor for the impact force when particle size and material are the same.

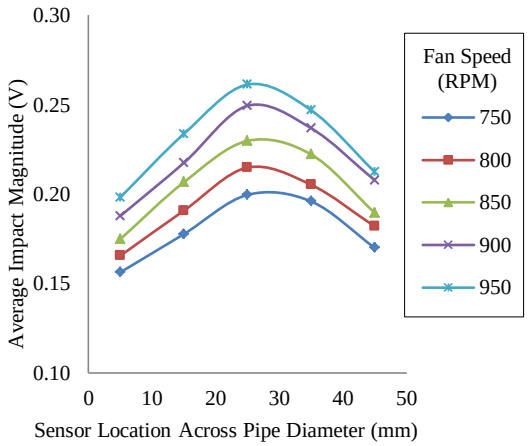

Fig. 6.219 Average impact magnitude profiles measured using the piezoelectric sensor array for plastic shot on the Z axis

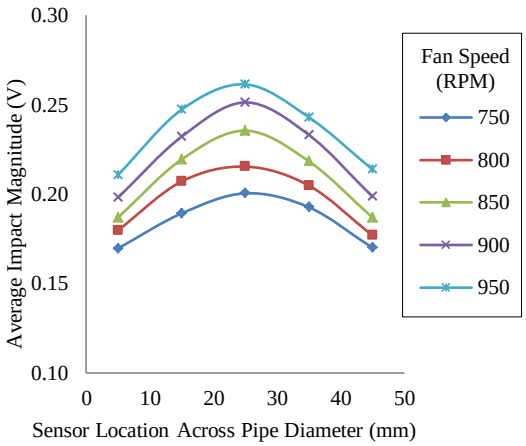

Fig. 6.220 Average impact magnitude profiles measured using the piezoelectric sensor array for plastic shot on the Y axis

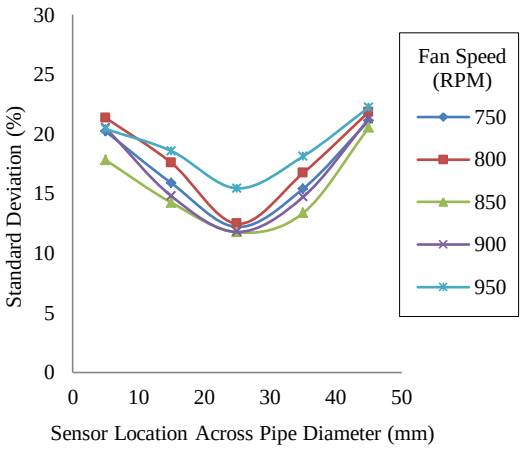

Fig. 6.221 Normalised standard deviation profiles of the impact magnitudes measured using the piezoelectric sensor array for plastic shot on the Z axis

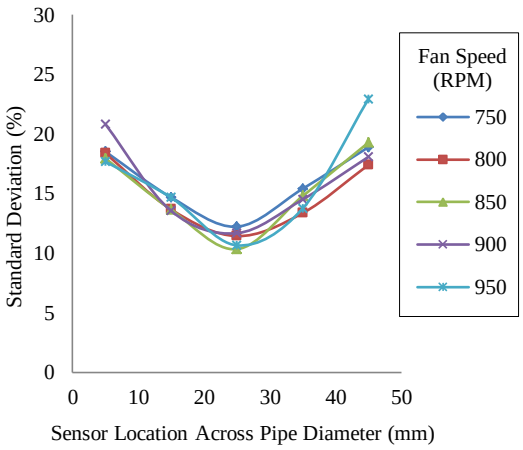

Fig. 6.222 Normalised standard deviation profiles of the impact magnitudes measured using the piezoelectric sensor array for plastic shot on the Y axis

6.3.3.4 Measured Particle Concentration Profiles

If the measured signal magnitude was higher than the set threshold voltage then a particle impact was registered to have occurred on the individual sensor element. The measured particle concentration measured by the piezoelectric sensor array was determined by the normalised number of particle impacts measured across the pipe diameter (on the five elements of the piezoelectric sensor array). The measured particle concentrations measured by the piezoelectric sensor array illustrated in Fig. 6.223 and Fig. 6.224 for the Z and Y sensor axis agree well with the measured particle concentration profiles measured with the electrostatic sensor array (Fig. 6.217 and Fig. 6.218). The effect of gravity can be seen with the sensor orientation on the Z axis with the particle concentration increasing in the direction of gravity (towards the bottom of the pipe).

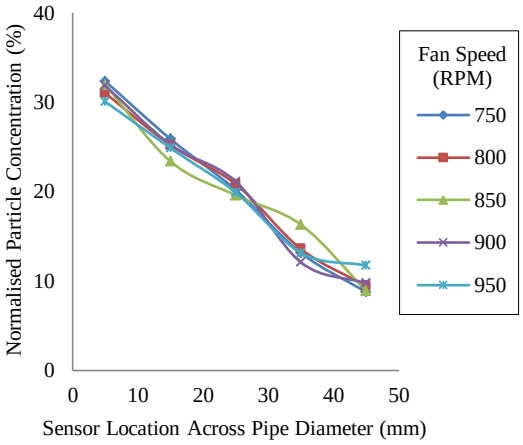

Fig. 6.223 Normalised particle concentration profiles measured by the piezoelectric sensor array on the Z axis for plastic shot

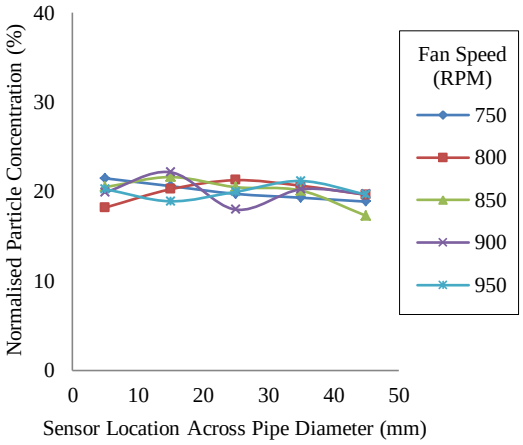

Fig. 6.224 Normalised particle concentration profiles measured by the piezoelectric sensor array on the Y axis for plastic shot

6.3.3.5 Discussion on the On-Line Experimentation Using the Piezoelectric Sensor Array

Calibration of each element of the piezoelectric sensor array using the off-line test rig has ensured that each sensor element gives the same output to each of the other elements in the piezoelectric sensor array. The use of anti-vibration shielding on the sensor blade and a threshold voltage to determine when a particle impact has occurred on the active sensor area demonstrates that the piezoelectric sensor array was capable of detecting particle impacts in specific areas of the pipe diameter. Through on-line experimentation using the positive pressure test rig and using plastic shot that has been sieved to ensure a similar particle size the piezoelectric has been shown to be able to detect increasing particle impact force when the particle velocity is increased. Consequently indicating that the piezoelectric sensor array is capable of determining the particle size (assuming the mechanical properties of the pulverised material are known and the particle velocity is independently measured). The piezoelectric sensor array has also been demonstrated to be capable of determining the particle concentration profiles across the pipe. This has been well documented in the experiments carried out with the piezoelectric sensor array and compared to particle concentrations measured using the electrostatic sensor array on both the Z and Y sensor axis. The effect of gravity can be

seen with the piezoelectric sensor array mounted in the Z axis in the horizontal pipe since the particle concentration increases in the direction of gravity.

6.4 Summary

The electrostatic sensor array has been demonstrated to be capable of determining the particle velocity and concentration profiles of dilute-phase pneumatically conveyed bulk solid materials in both developed and undeveloped flows (on horizontal and vertical pipe sections) in an on-line mode. This has been achieved on both positive and negative pressure laboratory scale pneumatic conveying test rigs. A wide variety of pulverised materials have been used in experimental work including: flour, biomass (of different particle sizes and materials), coal and coal/biomass blends. It has been shown that particle size and shape have a significant effect on particle flow stability. Through analysis of the standard deviation profiles of the velocity profiles as well as through analysis of the correlation coefficient profiles it has been demonstrated that different parts of the pipe cross section have more stable flow characteristics compared to others (more stable flow in the centre of the pipe). Experiments carried out on undeveloped particle flows have revealed that the electrostatic sensor array is capable of detecting specific flow regimes such as roping which was caused by the particle flow traveling through a right-angle bend.

Off-line experimentation using the off-line impact test rig on the piezoelectric sensor array has shown that for a spherical particle (ball bearing) the measured impact force agrees well with the developed system model (assuming the mechanical properties of the particles are known and the impact velocity is independently measured). It has also been found through spectral analysis of the impact signal that different parts of the frequency spectrum relate to aspects of a particle impact. Using the off-line impact test rig for calibrating each of the elements of the array it has been found that each impact

sensor element on the piezoelectric sensor array can give the same measurement for the same impact force.

Through a combination of the anti-vibration shielding and the selective frequency filtering, very small active sensing areas have been achieved. Consequently this has reduced the chances of measurement errors caused by simultaneous impacts and it has also allowed the impact force magnitude profiles to be measured across the diameter of the pipe. Consequently assuming the particle velocity is known as well as the mechanical properties of the particles being known the particle size can be determined. The piezoelectric sensor array has also demonstrated its capability of measuring the particle concentration profiles with comparisons made with the measured particle concentration profiles using the electrostatic sensor array with agree. This has been primarily demonstrated on the Z axis on a horizontal pipe where the particle concentration increases in the direction of gravity.

Chapter 7

Conclusions and Recommendations for Future Work

7.1 Research Contributions

A novel electrostatic sensor array and a piezoelectric impact sensor array have been designed, constructed and tested using a variety of pulverised materials on laboratory-scale pneumatic conveying systems. These sensor arrays span the diameter of the pipe and are capable of determining the particle velocity (electrostatic sensor array), particle concentration (electrostatic/piezoelectric sensor arrays) and particle size distribution (piezoelectric sensor array) profiles.

The electrostatic sensor array consists of five pairs of electrostatic electrodes (upstream and downstream) that span the diameter of the pipe with the pre-amplifiers constructed inside the sensor blade to improve signal to noise ratio. The particle velocity is determined using the cross correlation method and the particle concentration is determined by measuring the magnitude of the r.m.s charge value detected by the electrostatic sensors. Analysis of the particle velocity standard deviation as well as the correlation coefficient profiles has shown that different parts of the pipe cross section

have more stable flow compared to others (the centre of the pipe has a more stable flow compared to along the pipe wall). Measurements of undeveloped particle flow have shown that the electrostatic sensor array is also capable of determining specific particle flow regimes such as roping caused by particles going through a right angle pipe bend.

The piezoelectric sensor array consists of five individual impact waveguides (sensors) along the leading edge of the sensor blade. The impact waveguides only have a small active sensing area which allows them to achieve a very local area inside the pipe cross section as well as reducing the risk of simultaneous particle impacts. The waveguide is mechanically fixed to a piezoelectric transducer allowing the vibrations caused by particles impacting the waveguide to be detected. On-line and off-line experimentation was carried out using the piezoelectric sensor array which has shown that, using the developed system model, the particle size of spherical particles can be determined if the mechanical properties of the particle are known and the impact velocity is independently measured. On-line tests have also shown that the piezoelectric sensor array is capable of determining the particle concentration profile across the diameter of the pipe. The detected particle concentration profiles measured by the piezoelectric sensor array have been compared to concentration measurements taken by the electrostatic sensor array which show a close similarity.

This ability of the electrostatic and piezoelectric sensor arrays to measure the particle velocity, concentration and size distribution profiles is an improvement over previous sensor paradigms that are only capable of monitoring a small area of the pipe bore. This allows the developed sensor arrays to measure complex multi-phase flow characteristic that previous sensor technologies have been unable to achieve.

Both the electrostatic and piezoelectric sensor arrays would be of benefit to the coal/biomass power generation industries, allowing more accurate measurements of pulverised fuels entering the combustion furnace to be monitored and more advanced control systems to be developed and improve efficiency. The developed sensor arrays would also be of value to research in the area of computational fluid dynamics since

data collected from experiments using the electrostatic and piezoelectric sensor arrays can be compared to simulated flow patterns.

7.2 Conclusions from this Research

7.2.1 Electrostatic Sensor Array

An electrostatic sensor array has been designed, constructed and tested on a laboratory scale pneumatic conveying system using a variety of pulverised materials. The electrostatic sensor array consists of five pairs of electrostatic electrodes (upstream and downstream) that span the diameter of the pipe with the pre-amplifiers constructed inside the sensor blade to improve signal to noise ratio. The particle velocity is determined using the cross correlation method whereby the cross correlation algorithm is embedded inside a MBED microcontroller. Using the current MBED microcontroller, the particle velocity for each element of the array can be carried out in approximately 100ms (so the sensor has a refresh rate of 500ms for all five elements of the array). The particle concentration is determined by measuring the magnitude of the r.m.s of the electrostatic charge detected.

Experimental work with the electrostatic sensor array mounted on a laboratory scale pneumatic conveying systems has shown that the electrostatic sensor array is capable of determining both the particle velocity and concentration profiles. Analysis of the particle velocity standard deviation and the correlation coefficient profiles has shown that particle flow is more stable in the centre of the pipe compared to along the pipe wall. Experimental results for different particle sizes of biomass have shown that particle size has an effect on particle flow stability with smaller biomass particles having characteristics of more stable flow compared to larger biomass particles. Experiments using coal, biomass and coal/biomass blends have shown that coal and biomass have different flow characteristics. When coal-biomass is blended to 15% biomass or higher (by weight) the particle flow characteristic transitions from coal flow characteristics to biomass flow characteristics. Measurements of undeveloped particle

flow have shown that the electrostatic sensor array is likewise capable of determining specific particle flow regimes such as roping caused by particles going through a right angle pipe bend.

7.2.2 Piezoelectric Sensor Array

A piezoelectric impact sensor array has been designed, constructed and tested which is capable of determining both the particle concentration and particle size distribution profiles. The piezoelectric sensor array consists of individual impact sensors that span the diameter of the pipe. The piezoelectric sensor array uses custom piezoelectric transducers that have been fabricated from piezoelectric film (PVDF). The piezoelectric film transducers are mechanically interfaced with waveguides that protrude from the leading edge of the sensor blade which utilises anti-vibration shielding on the leading edge. This anti-vibration shielding has the effect of attenuating the vibration caused by any particle impacts that do not occur on the waveguide by -26 dB; consequently allowing each of the impact sensor elements to have a very small active sensing area (1 mm diameter) which reduces the chance of simultaneous impacts. This innovation solves the deficiency that other sensor technologies suffered from in previous impact sensor designs. The pre-amplifiers for the piezoelectric transducers are constructed inside the sensor blade to reduce the connection distance with the piezoelectric film to improve the signal to noise ratio.

The testing of the piezoelectric sensor array consisted of both off-line and on-line experimentation. Off-line experimentation was carried out using a custom built test rig that allowed ball bearings to be dropped onto the impact sensor and the impact velocity to be measured. The off-line testing allowed experiments to be carried out with controlled variables and allowed test data to be compared to the system model in order to determine particle size by measuring the magnitude of the particle impact. Analysis of the frequency spectrum of the impact signal using the off-line testing method has also found a link between the impact duration and frequency component of the impact signal; the shorter the impact duration the more higher frequency components are

present in the impact signal spectrum. Particle size was also determined by means of on-line experimentation on a positive pressure bulk solid conveying system using plastic shot. It was found that on-line and off-line experimental data show close similarities to the developed system model, assuming that the particles are spherical/close to being spherical, the mechanical properties of the particles are known and the particle impact velocity is independently measured. On-line testing has also shown that the piezoelectric sensor array is capable of determining the particle concentration profiles by measuring the number of particle impacts on each impact sensor element. The measured profiles using the piezoelectric sensor array were compared to particle concentration profiles that were measured using the electrostatic sensor array. The profiles from both sensor systems show close similarities.

7.3 Recommendations for Future Work

7.3.1 Combining the Electrostatic/Piezoelectric Sensor Arrays

Both the electrostatic and piezoelectric sensor arrays should be constructed inside a single sensor blade. With the electrostatic electrodes placed on the side of the sensor blade and the piezoelectric impact sensor array placed on the leading edge as shown in Fig. 7.1.

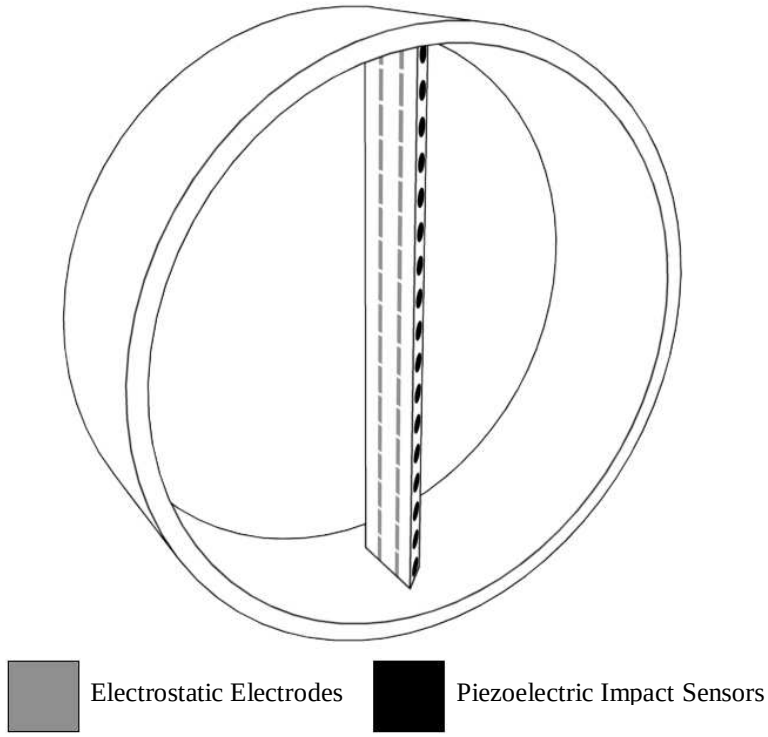

Fig. 7.1 Conceptual design of the combined electrostatic/piezoelectric sensor array

Each element of the electrostatic sensor array will consist of a pair of electrostatic electrodes in an upstream/downstream configuration using the cross correlation method to determine particle velocity. The pre-amplifier for the electrostatic sensor elements will be constructed inside the sensor blade to reduce the connection distance between the electrode and the pre-amplifier to improve signal to noise ratio. Subsequent signal conditioning elements for each element of the electrostatic sensor array will be constructed outside the sensor blade due to space constraints inside the sensor blade. The subsequent signal conditioning circuit for each element of the electrostatic sensor array will consist of:

- **Adjustable Amplifier** – this is to adjust the signal gain to allow the electrostatic sensor array to be configured for different particle flow conditions (different particle concentrations).
- **Low Pass Filter** – this is to remove any high frequency noise contamination.

- **MUX** – the multiplexer is controlled by the FPGA and used to select each element of the electrostatic sensor array.
- **ADC** – the analogue to digital converter is used to digitise the analogue signal for the FPGA.

Each element of the piezoelectric sensor array will consist of piezoelectric film transducers that will be fabricated using PVDF film with metallization layers on both sides of the PVDF film. The custom transducers are fabricated using chemical etching techniques in a similar way to how PCBs are fabricated. Using this method of construction the piezoelectric film transducer can be fabricated in such a way that only a specific area of the film is active (generates a signal output when mechanically stressed). The pre-amplifiers for each element of the piezoelectric sensor array will be constructed inside the sensor blade to reduce the connection distance to improve the signal to noise ratio. The subsequent signal conditioning circuit for each element of the piezoelectric sensor array will consist of:

- **Adjustable Amplifier** – this is used to calibrate each element of the piezoelectric sensor array to each of the other elements.
- **MUX** – the multiplexer is controlled by the FPGA and used to select each element of the electrostatic sensor array.
- **ADC** – the analogue to digital converter is used to digitise the analogue signal for the FPGA.

In order to allow the electronic sensor to analysis data in real time all signal processing will be performed by a FPGA (currently the electrostatic sensor array uses a MBED microcontroller to perform the cross correlation calculation with a refresh time of 100 ms for one element of the array). The use of a FPGA could allow the electrostatic/piezoelectric sensor arrays to be developed into a portable diagnostic tool much like a commercial hot wire anemometer.

7.3.2 Electrostatic Sensor Matrix

The use of a FPGA would not only allow more elements of the array to be added for larger diameter pipes (such as those used in power stations > 150 mm) to increase the resolution of the profile measurements but it also opens up the possibility of the implementation of an electrostatic matrix as shown in Fig. 7.2. The FPGA would be capable of using the cross correlation method to determine the particle velocity between adjacent electrostatic electrodes and thus be able to measure very complex flows (such as vortexes). The number of pre-amplifiers required for an electrostatic sensor matrix would need a much higher component density then in the current electrostatic sensor array design. For this reason either custom silicon would be needed to fabricate the pre-amplifiers or the pre-amplifiers could be implemented using PSoC (Programmable System on Chip) technology.

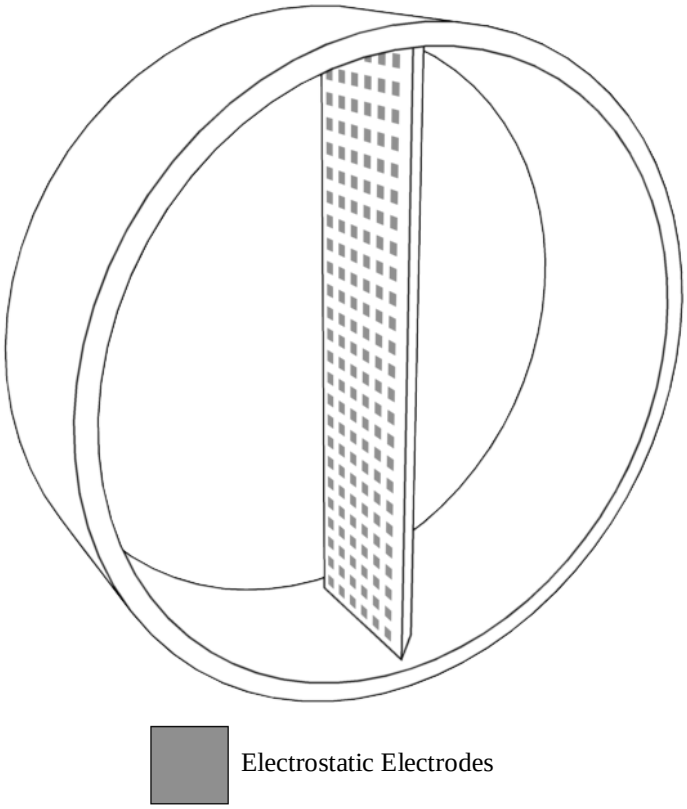

Fig. 7.2 Conceptual design of the electrostatic sensor matrix

The computational power of a FPGA would also allow frequency spectral analysis of the signal from the electrostatic sensor matrix to be processed in real time. This would allow the possibility of using spectral analysis to determine particle size distribution in real time.

References

[1] D. Mills, “Pneumatic Conveying Design Guide”, Second edition, Butterworth-Heinemann Publications, Oxford, UK, ISBN 0 7506 5471 6.

[2] Y. Yan, “Guide to the Flow Measurement of Particulate Solids in Pipelines”, Powder Handling & Processing, Vol. 13, No. 4, pp. 343 – 352, October/November 2001.

[3] H. Akillia, E. K Levyb and B. Sahina, ‘Gas–solid flow behavior in a horizontal pipe after a 90° vertical-to-horizontal elbow’, Powder Technology, vol. 116, issue 1, pp. 43 – 52, May 2001.

[4] S. Fokeer, S. Kingman, I. Lowndes and A. Reynolds, ‘Characterisation of the cross sectional particle concentration distribution in horizontal dilute flow conveying’, Chemical Engineering and Processing: Process Intensification, vol. 43, issue 6, pp. 677 – 691, June 2004.

[5] OECD (2014), “Electricity generation”, in OECD Factbook 2014: Economic, Environmental and Social Statistics, OECD Publishing, Paris.

[6] http://www.c2es.org/energy/source/coal (Centre for Climate and Energy Solutions) Accessed 21/04/2016.

[7] S. Penney, J. Bell and J. Balbus, ‘Estimating the Health Impacts of Coal-Fired Power Plants Receiving International Financing’, Environmental Defence Fund, https://www.edf.org/sites/default/files/9553_coal-plants-health-impacts.pdf, Accessed 21/04/2016.

[8] Drax Group plc, ‘A reliable, renewable future, today’, Annual report and accounts 2015,

http://www.drax.com/media/66479/24293_drax_ar15_web_v2.pdf, accessed 21/04/2016.

[9] Department of Energy & Climate Change, 'Energy Trends December 2015', https://www.gov.uk/government/statistics/energy-trends-december-2015 Accessed 21/04/2016.

[10] P. Teixeira, H. Lopes, I. Gulyurtlu, N. Lapa and P. Abelha, 'Evaluation of slagging and fouling tendency during biomass co-firing with coal in a fluidized bed', Biomass and Bioenergy, vol. 39, pp. 192 – 203, April 2012.

[11] N. Nikolopoulos, M. Agraniotis, I. Violidakis, E. Karampinis, A. Nikolopoulosa, P. Grammelis, Ch. Papapavlou, S. Tzivenis and E. Kakaras, 'Parametric investigation of a renewable alternative for utilities adopting the co-firing lignite/biomass concept' Fuel, vol. 113, pp. 873 – 897, November 2013.

[12] H. Cui and J. R. Grace, 'Pneumatic Conveying of Biomass Particles : A Review', China Particuology, vol. 4, issue 3 – 4, pp. 183 – 188, July 2006.

[13] John Bird, "Electrical Circuit Theory and Technology", Revised edition, Newnes, ISBN 0-7506-5784-7.

[14] H. L. Hu, T. M. Xu, S. E. Hui, Q. L. Zhou, 'A Novel Capacitive System for the Concentration Measurement of Pneumatically Conveyed Pulverized Fuel at Power Stations', Flow Measurement and Instrumentation, Vol. 17, pp. 87 – 92, April 2006.

[15] L. Xu, A. P. Weber, G. Kasper, 'Capacitance-Based Concentration Measurement for Gas-Particle System with Low Particles Loading', Flow Measurement and Instrumentation, Vol. 11, issue 3, pp. 185 – 194, September 2000.

[16] J. Zhang, H. Hu, J. Dong, Y. Yan, 'Concentration measurement of biomass/coal/air three-phase flow by integrating electrostatic and capacitive sensors', Flow Measurement and Instrumentation, Vol. 24, pp. 43 – 49, April 2012.

[17] A. Fuchs, H. Zangl, 'Single-Layer Measurement of Particle Velocity and Concentration in Pneumatic Dilute Phase Conveying', IEEE Sensors Conference, pp. 857 – 860, Irvine CA, October 30-November 3 2005.

[18] J. Li, H. Goa, C. Xu, S. Wang. 'A Dual Modality Tomography System for Particle Concentration and Charge Distribution Measurement in Dense-Phase Pneumatic Conveyor of Pulverized Coal', IEEE International Conference on Imaging Systems and Techniques (IST), pp. 450-455, Manchester UK, 16 – 17, July 2012.

[19] B. Zhou, J. Zhang, 'A Novel ECT-EST Combined Method for Gas-Solids Flow Pattern and Charge Distribution Visualization', IEEE International Conference on Imaging Systems and Techniques (IST), pp. 89 – 94, Manchester UK, 16 – 17 July 2012.

[20] X. X. Wang, J. B. Yan, H. L. Hu, Z. Y. Luo, 'An ECT Flow Regime Identification Technology for Gas/solid Two-phase Flow Phase Concentration Measurement', International Conference on Instrumentation, Measurement, Computer, Communication and Control (IMCCC), pp. 1318 – 1321, Harbin China, 8-10 December.

[21] Z. Cui, H. Wang, C. Yang, D. Zhang, Y. Geng, 'Development and Application of ECT Digital System for Online Flow Measurement', IEEE International Conference on Imaging Systems and Techniques (IST), pp. 599 – 604, Manchester UK, 16 – 17 July 2012.

[22] T. Zhao, M. Takel, D. H. Doh, 'ECT Measurement and CFD-DEM Simulation of Particle Distribution in a down-flow fluidized bed', Flow Measurement and Instrumentation, Vol. 21, issue 3, pp. 212 – 218, September 2010.

[23] S. Liu, Q. Chen, H. G. Wang, F. Jiang, I. Ismail, W. Q. Yang, 'Electrical Capacitance Tomography for Gas–Solids Flow Measurement for Circulating Fluidized Beds', Flow Measurement and Instrumentation, Vol. 16, issue 2-3, pp. 135 – 144, April-June 2005.

[24] H. Wang, G. Qiu, W. Yang, 'Investigation of the Gas-Solid flows in a circulating Fludisied Bed with Multi-Cyclone Separators by Electrical Capacitance tomography', IEEE International Conference on Imaging Systems and Techniques (IST), pp. 306 – 310, Beijing China, 22-23 October 2013.

[25] M. Taker, T. Zhao, K. Yamane, 'Measurement of Particle Concentration in Powder Coating Process Using Capacitance Computed Tomography and Wavelet Analysis' Powder Technology, Vol. 193, issue 1, pp. 93 – 100, July 2009.

[26] A. Fuchs, H. Zangl, G. Brasseur, E. M. Petriu, 'Flow-Velocity Measurement for Bulk Granular Solids in Pneumatic Conveyor Pipes Using Random-Data Correlator Architecture', IEEE Transactions on Instrumentation and Measurement, Vol. 55, Issue 4, pp. 1228 – 1234, August 2006.

[27] A. Fuchs, H. Zangl, 'A Capacitive Single-Layer Approach for Particle Velocity Estimation in Pneumatic Dilute Phase Conveying', IEEE Sensors Journal, Vol. 6, Issue 6, pp. 1722 – 1727, December 2006.

[28] L. Gao, Y. Yan, G. Lu, 'Contour-based Image Segmentation for On-line Size Distribution Measurement of Pneumatically Conveyed Particles', IEEE I2MTC Conference, pp. 1 – 5, Binjiang, 10-12 May, 2011.

[29] L. Wang, L. Zhang, Y. Yan, X. Huang, 'Imaging-based size measurement of fine particles from industrial stacks', 12th International Conference on Signal Processing, pp. 1099 – 1104, Hangzhou , 19 – 23 October, 2014.

[30] H. Chen, H. W. Tang, Y. Liu, H. Wang, G. P. Liu 'Measurement of particle size based on digital imaging technique', Journal of Hydrodynamics, Vol. 25, Issue 2, pp. 242 – 248, April 2013.

[31] L. Gao, Y. Yan, G. Lu, R. M. Carter, 'On-line measurement of particle size and shape distributions of pneumatically conveyed particles through multi-wavelength based digital imaging', Flow Measurement and Instrumentation, Vol. 27, pp. 20 – 28, October 2012.

[32] R. M. Carter, Y. Yan, S. D. Cameron, 'On-line Nonintrusive Measurement of Particle Size Distribution Through Digital Imaging', IEEE IMTC Conference, pp. 2044 – 2047, Ottawa, Ont, Canada, 16 - 19 May, 2005.

[33] R. M. Carter, Y. Yan. P. Lee, 'On-line Nonintrusive Measurement of Particle Size Distribution Through Digital Imaging', IEEE Transactions on Instrumentation and Measurement, Vol. 55 No. 6, pp. 2034 – 2038, December 2006.

[34] J. Shao, Y. Yan, Z. Lv, 'On-line Non-intrusive Measurements of the Velocity and Particle Size Distribution of Pulverised Fuel on a Full Scale Power Plant' IEEE I2MTC Conference, pp. 1 – 5, Binjiang, 10-12 May, 2011.

[35] Y. Yan, 'Recent Advances in Imaging Based Instrumentation for Combustion Plant Optimization', IEEE International Conference on Imaging Systems and Techniques, pp. 148 – 151, Thessaloniki, 1 – 2 July, 2010.

[36] X. Qian, Y. Yan, L. Wang, J. Shao, 'An integrated multi-channel electrostatic sensing and digital imaging system for the on-line measurement of biomass–coal particles in fuel injection pipelines', Fuel, Volume 151, pp. 2 – 10, July 2015.

[37] R. M. Carter, Y. Yan, 'A Novel Imaging System for Concurrent Measurement of Particle Velocity and Size Distribution in a Pneumatic Suspension' IEEE IMTC Conference, pp. 2050 – 2054, Victoria BC, Australia, 12-15 May, 2008.

[38] D. Song, L. Peng, G. Lu, S. Yang, Y. Yan, 'Digital image processing based mass flow rate measurement of gas/solid two-phase flow', The 6th International Symposiumon Measurement Techniques for Multiphase Flows, Journal of Physics: Conference Series, Vol. 147, no. 1, pp. 1 – 8, 2009.

[39] X. Chen, W. Zhou, X. Cai, M. Su, H. Liu, 'In-line imaging measurements of particle size, velocity and concentration in a particulate two-phase flow', Particuology, Vol. 13, pp. 106 – 113, April 2014.

[40] D. Song, L. Peng, G. Lu, S. Yang, Y. Yan, 'Velocity measurement of pneumatically conveyed particles through digital imaging', Sensors and Actuators, Vol. 149, Issue 2, pp. 180 – 188, February 2009.

[41] A. Fuchs, H. Zangl, D. Watzenig, P. Dollfuss, 'Vision-Based Particle Velocity Measurement in Granular Gas-Solid Flows with Special Focus on Knowledge Transfer', 3rd International Conference on Sensing Technology, pp. 158 – 161, Tainan, 30 November – 3 December, 2008.

[42] www.greenbankgroup.com/systems (MillMaster Particle Size Analyser) Accessed 24/02/2016.

[43] R. M. Carter and Y. Yan, 'On-line Particle Sizing of Pulverised and Granular Material Fuels using Digital Imaging Techniques', Measurement Science and Technology, Vol. 14, pp. 1099 – 1109, 2003.

[44] C. Xu, S. Wang, Y. Yan, 'Spatial selectivity of linear electrostatic sensor arrays for particle velocity measurement', IEEE Transactions on Instrumentation and Measurement, Vol. 62, Issue 1, pp. 167 – 176, January 2013.

[45] C. Xu, J. Li, S. Wang, 'A spatial filtering velocimeter for solid particle velocity measurement based on linear electrostatic sensor array', Flow Measurement and Instrumentation, Vol. 26, pp. 68 – 78, August 2013.

[46] J. Li, C. Xu, S. Wang, 'Spatial filtering characteristics of electrostatic sensor matrix for local velocity measurement of pneumatically conveyed particles', Measurement, Vol. 53, pp. 194 – 205, July 2014.

[47] J. Li, C. Xu, S. Wang, 'Local particle mean velocity measurement using electrostatic sensor matrix in gas–solid two-phase pipe flow', Flow Measurement and Instrumentation, Vol. 27, pp. 104 – 112, October 2012.

[48] J. Shao, J. Krabicka, Y. Yan, 'Velocity Measurement of Pneumatically Conveyed Particles Using Intrusive Electrostatic Sensors', IEEE Transactions on Instrumentation and Measurement, Vol. 59, Issue 5, pp. 1477 – 1484, May 2010.

[49] H. Seraj, M. F. Rahmat, M. Khalid, 'Measurement of velocity of solid/air two phase fluid using electrostatic sensors and cross correlation technique', Scientia Iranica, Vol. 20, Issue 3, pp. 786 – 792, June 2013.

[50] W. Zhang, C. Wang, Y. Wang, 'Parameter Selection in Cross-Correlation-Based Velocimetry Using Circular Electrostatic Sensors' IEEE Transactions on Instrumentation and Measurement, vol. 59, no. 5, pp. 1268 – 1275, May 2010.

[51] J. Krabicka, Y. Yan, 'Optimised Design of Intrusive Electrostatic Sensors for the Velocity Measurement of Pneumatically Conveyed Particles', Instrumentation and Measurement Technology conference, pp. 341 – 345, Singapore, 5-7 May, 2009.

[52] J. Shao, Y. Yan, Z. Lv, 'On-line Non-intrusive Measurements of the Velocity and Particle Size Distribution of Pulverised Fuel on a Full Scale Power Plant', Instrumentation and Measurement Technology conference, Binjiang, pp. 10 - 12 May, 2011.

[53] Y. Yan, L. Xu, P. Lee, 'Mass Flow Measurement of Fine Particles in a Pneumatic Suspension Using Electrostatic Sensing and Neural Network Techniques' IEEE Transactions on Instrumentation and Measurement, Vol. 55, Issue 6, pp. 2330 – 2334, December 2006.

[54] X. Qian and Y. Yan, 'Flow Measurement of Biomass and Blended Biomass Fuels in Pneumatic Conveying Pipelines Using Electrostatic Sensor-Arrays', IEEE Transactions on Instrumentation and Measurement, vol. 61, no. 5, pp. 1343 – 1352, May 2012.

[55] X. Qian, Y. Yan, J. Shao, L. Wang, H. Zhou, C. Wang, 'Quantitative characterization of pulverized coal and biomass–coal blends in pneumatic conveying pipelines using electrostatic sensor arrays and data fusion techniques', Measurement Science and Technology, Vol. 23, No. 8, pp. 1 – 13, June 2012.

[56] Y. Yan, B. Byrne, S. Woodhead, and J. Coulthard, 'Velocity Measurement of Pneumatically Conveyed Solid Using Electrodynamic Sensors', Measurement Science Technology, Vol. 6, No. 5, pp. 515 – 537, 1999.

[57] Y. Yan, 'Continuous measurement of particulate emissions', IEEE Instrumentation Measurement Magazine, Vol. 8, no. 4, pp. 35 – 39, October 2005.

[58] J. Q. Zhang, Y. Yan, 'On-line continuous measurement of particle size using electrostatic sensors', Powder Technology, Vol. 135 – 136, pp. 164 – 168, October 2003.

[59] J. Q. Zhang and Y. Yan, "On-line Continuous Measurement of Particle Size Using Electrostatic Sensors", IEEE Instrumentation and Measurement Conference, pp. 877 – 880, Vail, CO, USA, 20-22 May 2003.

[60] T. Tajdari, M. F. Rahmat, N. A. Wahab, 'New technique to measure particle size using electrostatic sensor', Journal of Electronics, Vol. 72, Issue 2, pp. 120 – 128, April 2014.

[61] Y. Yan, "Mass flow measurement of bulk solids in pneumatic pipelines," Measurement Science Technology, vol. 7, no. 12, pp. 1687–1706, 1996.

[62] J. Krabicka, Y. Yan, 'Finite-Element Modeling of Electrostatic Sensors for the Flow Measurement of Particles in Pneumatic Pipelines', IEEE Transactions on Instrumentation and Measurement, vol. 58, no. 8, pp. 2730 – 2736, August 2009.

[63] L. Peng, Y. Zhang, Y. Yan, 'Characterization of electrostatic sensors for flow measurement of particulate solids in square-shaped pneumatic conveying pipelines', Sensors and Actuators, Vol. 141, Issue 1, pp. January 2008.

[64] PfMaster Pulverised Fuel Monitoring System http://www.greenbankgroup.com/systems.htm Accessed 03-03-2016

[65] J. Krabicka, Y. Yan, 'Finite element modelling of intrusive electrostatic sensors for the measurement of Pulverised fuel flows', Instrumentation and Measurement Technology conference, pp. 1 – 4, Warsaw, 1 - 3 May, 2007.

[66] Y. Zheng, Q. Liu, 'Review of Techniques for the Mass Flow Rate Measurement of Pneumatically Conveyed Solids', Measurement, Vol. 44, Issue 4, pp. 589–604, May 2011

[67] J. Shao, Y. Yan, J. Krabicka, 'Comparative Studies of Electrostatic Sensors with Circular and Rod Electrodes for the Velocity Measurement of Pulverized Coal and Biomass Fuels', International Instrumentation and Measurement Technology conference, pp. 724 – 727, Singapore, 5-7 May, 2009.

[68] B. Jurjevčič, A. Senegačnik, B. Drobnič, I. Kuštrin, 'The Characterization of Pulverized-Coal Pneumatic Transport Using an Array of Intrusive Electrostatic Sensors', IEEE Transactions on Instrumentation and Measurement, Vol. 64, No. 12, pp. 3434 – 3443, December 2015

[69] L. Gao, Y. Yan, R. M. Carter, D. Sun, C. Xu, 'In-line Particle Sizing of Pneumatically Conveyed Particles Using a Piezo Film Sensor', IEEE International Instrumentation and Measurement Technology Conference, pp. 625 – 628, Minneapolis MN, 6 – 9 May.

[70] P. J. Coghill, 'Particle Size Determination by Impact Measurement in Pneumatically Conveyed Solids', Particle & Particle Systems Characterization, Vol. 18, Issue 3, pp. 114 – 119, October 2001.

[71] P. J. Coghill, 'Particle Size of Pneumatically Conveyed Powders Measured Using Impact Duration', Particle & Particle Systems Characterization, Vol. 24, Issue 6, pp. 464 – 469, December 2007.

[72] M. Uher, S. Šedivá, M. Havlíková, 'Comparison and cooperation of using camera and acoustic emission for solid particle flow measurement', 16th International Carpathian Control Conference, pp. 558 – 562, Szilvasvarad, 27 – 30 May.

[73] L. Goa, Y. Yan, R. M. Carter, D. Sun, P. Lee, C. Xu, 'On-line particle sizing of pneumatically conveyed biomass particles using piezoelectric sensors', Fuel, Vol. 113, pp. 810 – 816, November 2013.

[74] Y. Hu, L. Wang, X. Huang, X. Qian, L. Gao and Y. Yan, 'On-line Sizing of Pneumatically Conveyed Particles Through Acoustic Emission Detection and Signal Analysis', IEEE Transactions on Instrumentation and Measurement, Vol. 64, No. 5, pp. 1100 – 1109, May 2015.

[75] P. Müller, M. Trüe, R. Böttcher, J. Tomas, 'Acoustic evaluation of the impact of moist spherical granules and glass beads', Powder Technology, Volume 278, pp. 138 – 149, July 2015.

[76] G. P. Hancke and R. Malan, 'Modal Analysis Technique for the On-Line Particle Size Measurement of Pneumatically Conveyed Pulverized Coal' IEEE Transactions on Instrumentation and Measurement, Vol. 47, No. 1, pp. 114 – 122, February 1998.

[77] B. M. Meunier, P. M. Watts, J. S. Marshall, R. L. Dechene, W. Du, R. E. Newton, 'Vibration sensor for particle concentration measurement in pneumatic pipeline flows', Measurement Science and Technology, Vol. 21, pp. 1 – 10, 2010

[78] Z. Zhan, Z. Jing, 'Study on Grain Loss Detecting Sensor of Combine Harvester', International Conference on New Technology of Agricultural Engineering, pp. 109 – 112, Zibo, 27 – 29 May.

[79] K. Wang, Z. Liu, G. Liu, L. Yi, K. Yang, R. Li, M. Chen, S. Peng, 'Vibration sensor approaches for the sand detection in gas–sand two phases flow', Powder Technology, Vol. 288, pp. 221 – 227, January 2016.

[80] M. Mahmod, M. A, H. Liyana, E. J. Mohamad and O. M. F. Marwah, 'Velocity profile measurement of solid particles using LED as a light source', IEEE Student Conference on Research and Development, pp. 1 – 5, Batu Ferringhi, 16 – 17 December 2014.

[81] I.R. Barratt, Y. Yan, B, Byrne and M.S.A. Bradley, "Mass flow measurement of pneumatically conveyed solids using radiometric sensors", Flow Measurement and Instrumentation, Vol. 11, Issue 3, pp. 223 – 235, September 2000.

[82] Keven Conrad and Larry Lynnworth, “Fundamentals of Ultrasonic Flow Meters”, Proceedings, pp. 52 – 61, 2002. www.asgmt.com/wp-content/uploads/pdf-docs/2002/1/10.pdf (Accessed 05/04/2016).

[83] D.A. Abernethy, M.J. Millen and B.D. Sowerby “Plant Trial of an Ultrasonic Gauge for the On-Line Measurement of Pulverised Coal Mass Flow”, IEEE Instrumentation and Measurement Technology Conference, Brussels, pp. 667 – 670, 4 – 6 June 1996.

[84] AD8601/AD8602/AD8604 Precision CMOS, Single-Supply, Rail-to-Rail, Input/Output Wideband Operational Amplifiers Datasheet, Analog Devices, Rev. G.

[85] G. Clayton and S. Winder, ‘Operational Amplifiers’, Fifth Edition, Newnes Publications, Milton Keynes, UK, ISBN 978-0-7506-5914-7.

[86] How to Bias an Op-Amp, http://ocw.mit.edu/courses/media-arts-and-sciences/mas-836-sensor-technologies-for-interactive-environments-spring-2011/readings/MITMAS_836S11_read02_bias.pdf, Accessed 26/05/2016

[87] Sallen-Key Filter Design, http://sim.okawa-denshi.jp/en/OPseikiLowkeisan.htm, Accessed 26/05/2016

[88] Yong Yan, Shaun J Rodrigues and Zizhuo Xie, ‘Non-contact strip speed measurement using electrostatic sensing and correlation signal-processing techniques’, Measurement Science and Technology, vol. 22, no. 7, pp. 1 – 9, June 2011.

[89] BZA408B Quadruple Bidirectional ESD Transient Voltage Suppressor Datasheet, NXP Semiconductors, October 1998.

[90] SPX3819 500mA Low-Noise LDO Voltage Regulator Datasheet, EXAR, Rev. 2.0.2

[91] SP6203/SP6205 300mA/500mA Low Noise CMOS LDO Regulators Datasheet, EXAR, Rev. 2.0.0

[92] ADG706/ADG707 CMOS, +1.8 V to +5.5 V/2.5 V, 2.5Ω Low-Voltage, 8-/16-Channel Multiplexers Datasheet, Analog Devices, Rev. A.

[93] MBED ADC Input, https://developer.mbed.org/handbook/AnalogIn, Accessed 02/05/2016

[94] ADC Max Sampling Rate, https://developer.mbed.org/users/Sissors/code/FastAnalogIn, Accessed 02/05/2016

[95] ADC Spikes https://developer.mbed.org/users/chris/notebook/Getting-best-ADC-performance, Accessed 02/05/2016

[96] Ad7490 16-Channel, 1 MSPS, 12-Bit ADC with Sequencer in 28-Lead TSSOP Datasheet, Analog Devices, Rev. A.

[97] External MBED ADC Library, https://developer.mbed.org/users/ykuroda/code/AD7490/wiki/Homepage Accessed 25/05/2016

[98] MBED LPC1768 Specifications, https://developer.mbed.org/platforms/mbed-LPC1768/, Accessed 26/05/2016

[99] S. J. Rodrigues, Y. Yan, 'A Comparative Study of Rounded and Strip Electrostatic Sensors for Non-Contact Measurement of Cable Speed', IEEE International Instrumentation and Measurement Technology Conference, pp. 1159 – 1162, Graz, 13 – 16 May 2012.

[100] Measurement Specialties Inc. 'Piezo Film Sensors Technical Manual', REV B 02 APR 99

[101] Texas Instruments, 'Signal Conditioning Piezoelectric Sensors', Application Report SLOA033A - September 2000

[102] MBED SD Card Library, https://developer.mbed.org/cookbook/SD-Card-File-System Accessed 07/06/2016

[103] H. Hertz, Über die berührung fester elastischer Körper (On the contact of rigid elastic solids). In: Miscellaneous Papers. Jones and Schott, Editors, J. reine und

angewandte Mathematik 92, Macmillan, London (1896), p. 156 English translation: Hertz, H.

[104] S. Antonyuk, S. Heinrich, J. Tomas, N. G. Deen, M. S. van Buijtenen and J. A. M. Kuipers, "Energy absorption during compression and impact of dry elastic-plastic spherical granules", Granular Matter, vol. 12, no 1, pp. 15 – 47, 2010.

[105] K. Uchino, "Advance Piezoelectric Materials", Woodhead Publishing, Cambridge, UK, ISBN 978-1-84569-534-7.

[106] N.K. Myshkin, M.I. Petrokovets and A.V. Kovalev, "Tribology of polymers: Adhesion, Friction, Wear, and Mass-transfer", Tribology International, vol. 38, no 11, pp. 910 – 921, December 2006.

[107] http://www.free-instruction-manuals.com/pdf/pa_1049027.pdf Accessed 14/07/2016

[108] http://www.fansandblowers.com/uploads/pdfs/QZ_data_sheet_layout_v1.pdf Accessed 01/08/2016

[109] Magnus H (1983) On the Deviation of Projectiles; and on a Remarkable Phenomenon of Rotating Bodies. Memoirs of the Royal Academy, Berlin 1852. English translation in Scientific Memoirs London. p 210 Edited by Tyndall and Francis

[110] http://www.brites.eu/brites-wood-pellets-for-your-home/benefits-of-brites/#toggle-id-2 Accessed 18/05/2016

[111] http://www.dupont.com/content/dam/dupont/products-and-services/plastics-polymers-and-resins/thermoplastics/documents/Delrin/Delrin%20Design%20Guide%20Mod%203.pdf Accessed 29/05/2016

[112] http://www.engineeringtoolbox.com/poissons-ratio-d_1224.html Accessed 29/05/2016

[113] http://www.engineeringtoolbox.com/young-modulus-d_417.html Accessed 29/05/2016

[114] A. Cowell, D. McGlinchey, J.R. Pugh, M. Ibrahim, 'Investigation of the Parameters Important in the Measurement of Small Particle Impact Forces', Powder Technology, Vol. 269, pp. 267–274, January 2015.

[115] http://www.hodgeclemco.co.uk/wp-content/themes/Hodge%20Clemco/images/photos/TDS%2052%20Avialite%20Type%202%20Commercial.pdf 01/06/2016

[116] Urea formaldehyde (cellulose filled) http://www.engineeringtoolbox.com/polymer-properties-d_1222.html Plastic Shot Data Accessed 05/05/16

Appendix A

Circuit Schematics

This section contains the circuit schematics for the entire signal conditioning circuits for both the electrostatic and piezoelectric sensor arrays as well as the circuit schematics for the embedded microcontrollers used for signal processing and data logging.

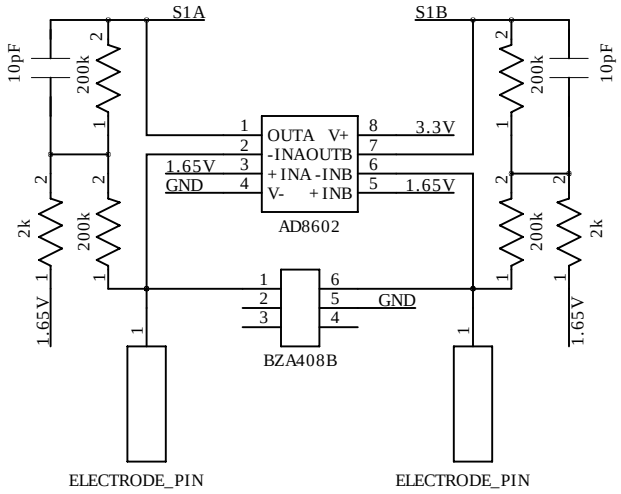

S1 Electrodes and Pre-Amps

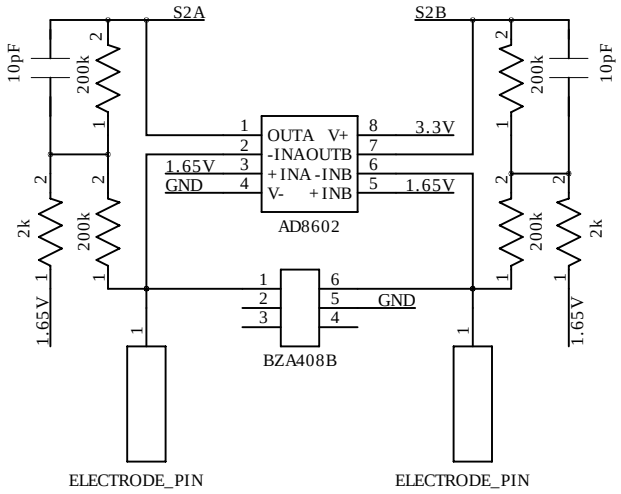

S2 Electrodes and Pre-Amps

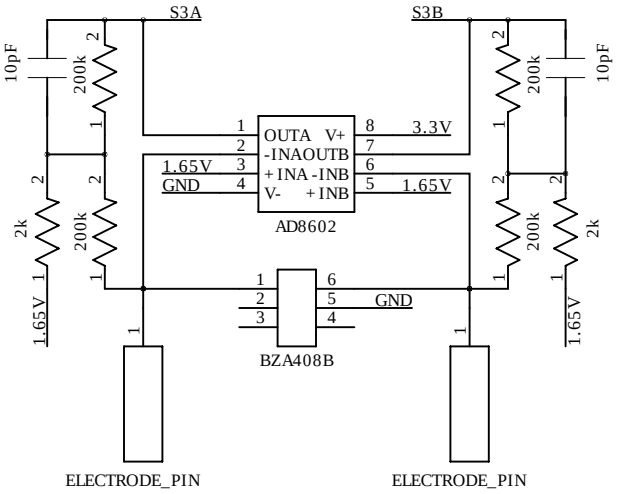

S3 Electrodes and Pre-Amps

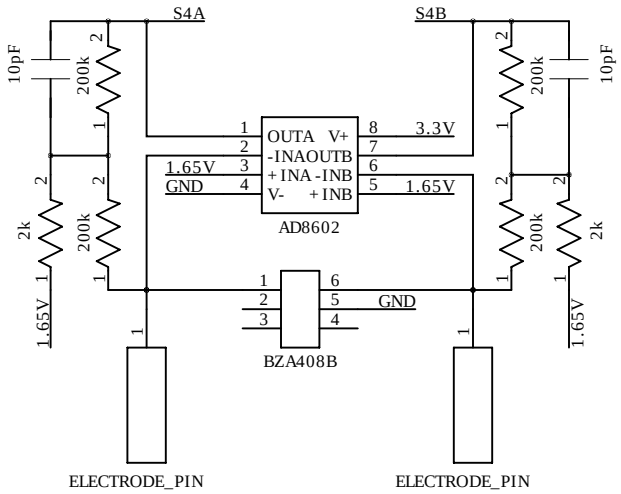

S4 Electrodes and Pre-Amps

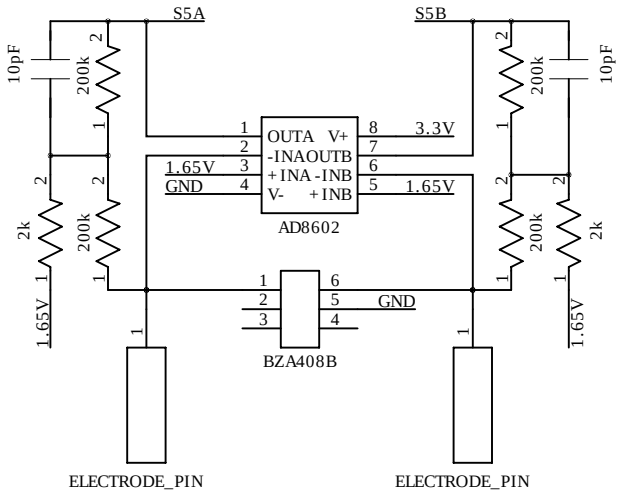

S5 Electrodes and Pre-Amps

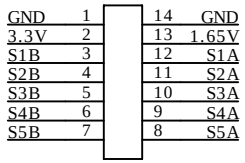

Sensor I/P Header

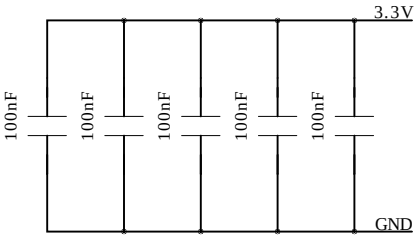

3.3V Decoupling Capacitors

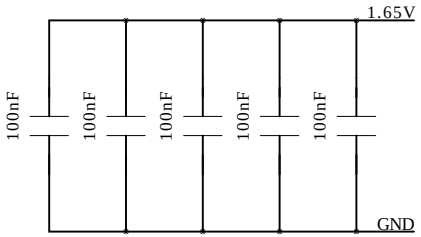

1.65V Decoupling Capacitors

COMPANY: **School of Engineering and Digital Arts**		
TITLE: Electrostatic Sensor Array Pre-Amps		
DRAWN BY: JRC55	LAST MODIFIED: 17/05/2016	REV: A
FILE NAME: Electrostatic Pre-Amps.sch	SHEET 1 OF 1	

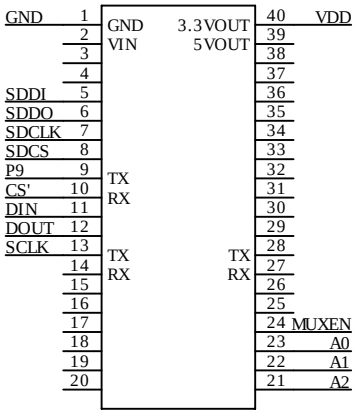

MBED Microcontroller

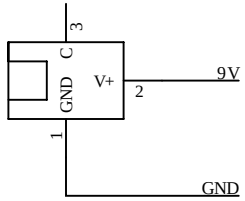

9V DC Supply Socket

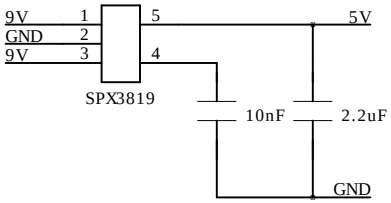

5V Power Supply

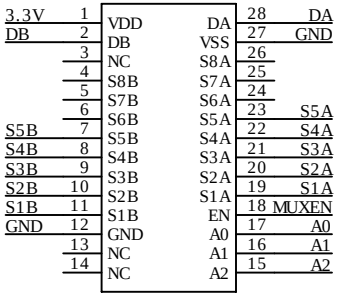

ADG707 MUX

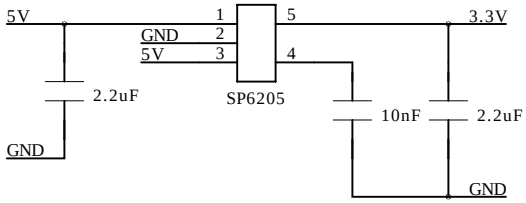

3.3V Power Supply

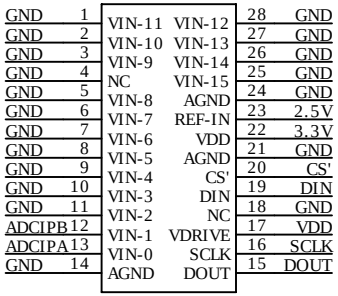

AD7490 ADC

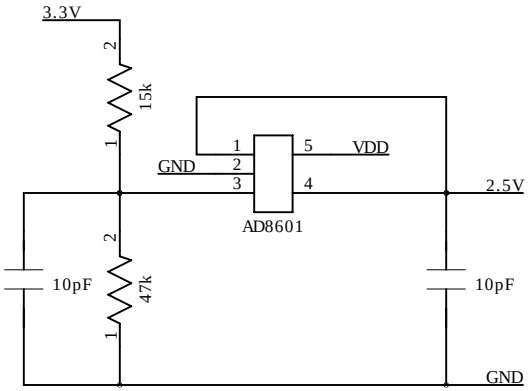

2.5V Reference Supply

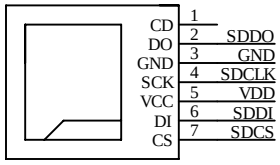

SD Card Interface

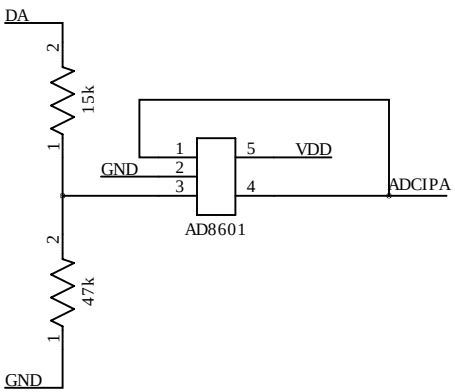

ADC Upstream (A) I/P Buffer

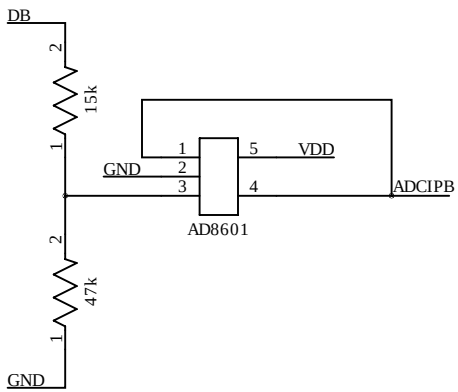

ADC Downstream (B) I/P Buffer

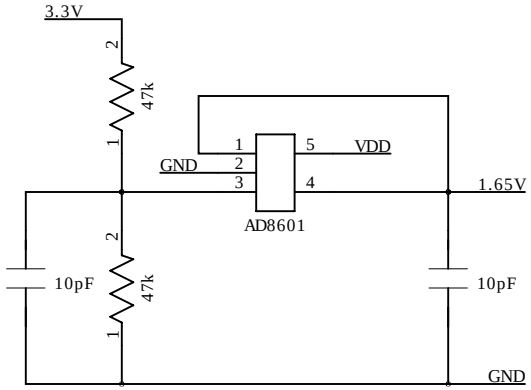

1.65V Reference Supply

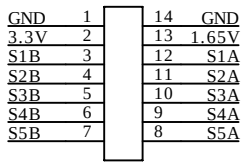

Sensor I/P Header

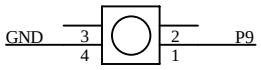

Push Button

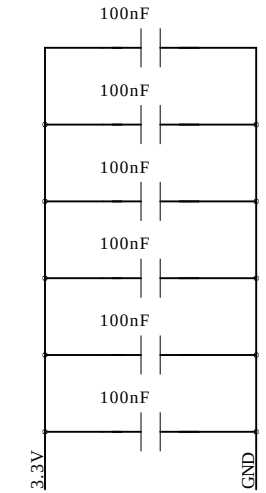

decoupling capacitors

COMPANY:	**School of Engineering and Digital Arts**
TITLE:	Electrostatic Data Logger
DRAWN BY: JRC55	LAST MODIFIED: 17/05/2016 — REV: A
FILE NAME: Electrostatic Data Logger.sch	SHEET 1 OF 1

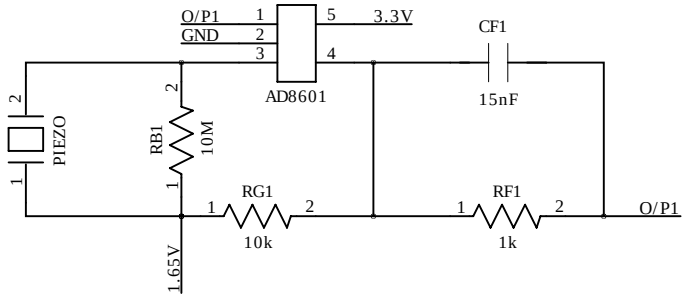

S1 Piezoelectric Film Transducer and Pre-Amps

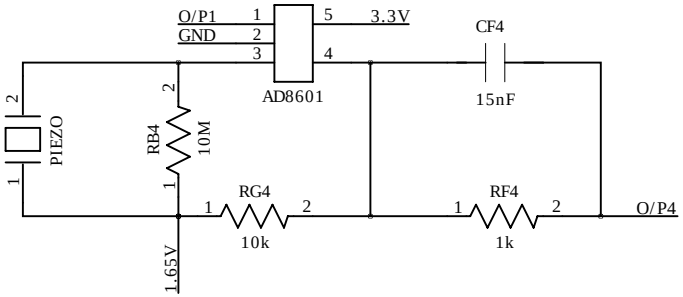

S4 Piezoelectric Film Transducer and Pre-Amps

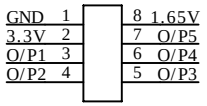

Sensor I/P Header

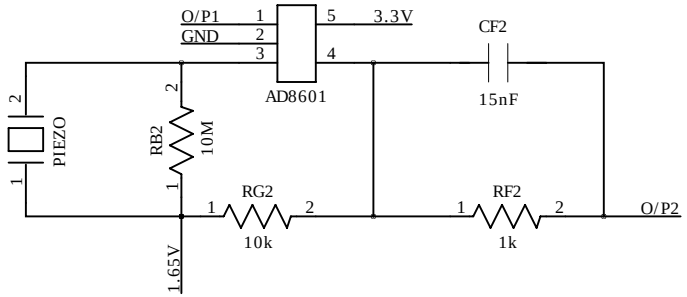

S2 Piezoelectric Film Transducer and Pre-Amps

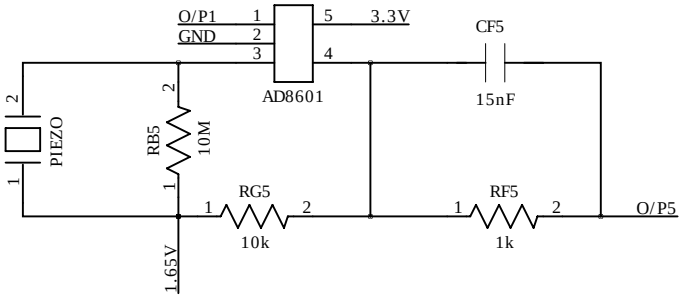

S5 Piezoelectric Film Transducer and Pre-Amps

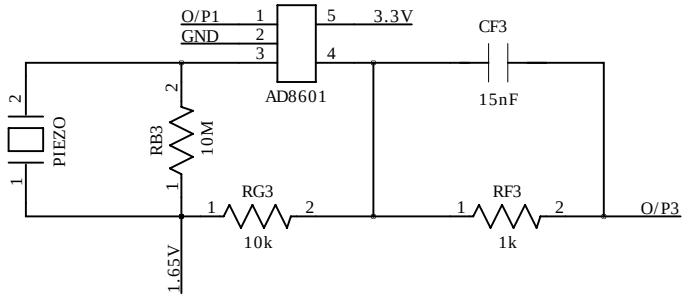

S3 Piezoelectric Film Transducer and Pre-Amps

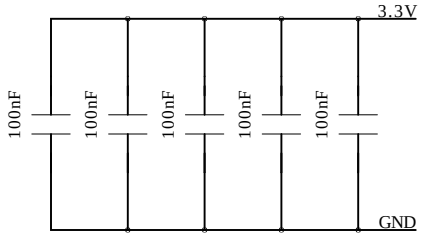

3.3V Decoupling Capacitors

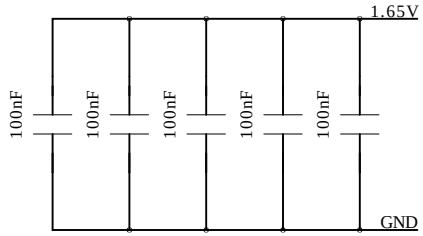

1.65V Decoupling Capacitors

COMPANY: **School of Engineering and Digital Arts**		
TITLE: Piezoelectric Sensor Pre-Amps		
DRAWN BY: JRC55	LAST MODIFIED: 10/06/2016	REV: A
FILE NAME: Piezoelectric Pre-Amps.sch	SHEET 1 OF 1	

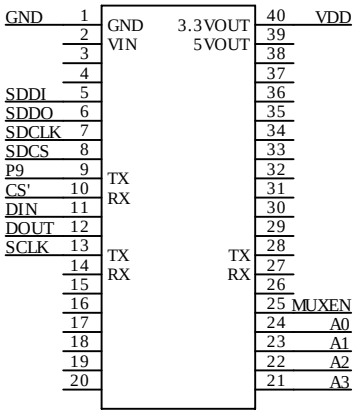

MBED Microcontroller

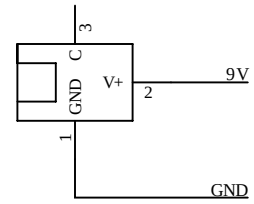

9V DC Supply Socket

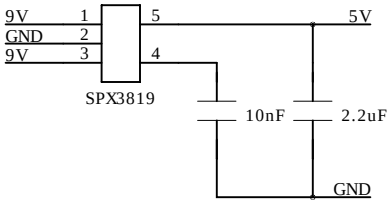

5V Power Supply

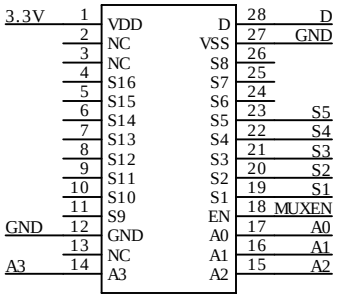

ADG706 MUX

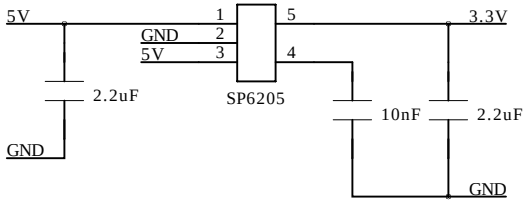

3.3V Power Supply

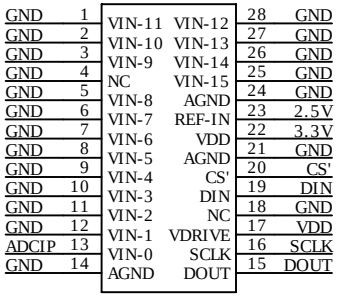

AD7490 ADC

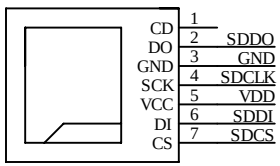

SD Card Interface

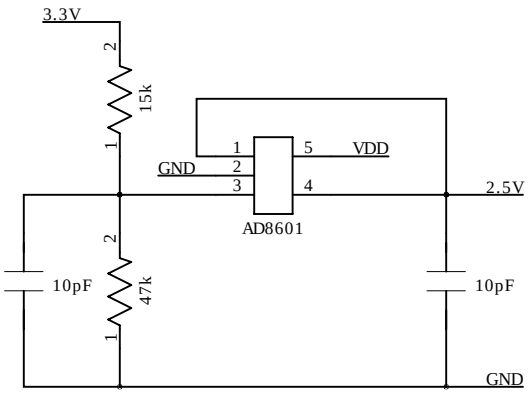

2.5V Reference Supply

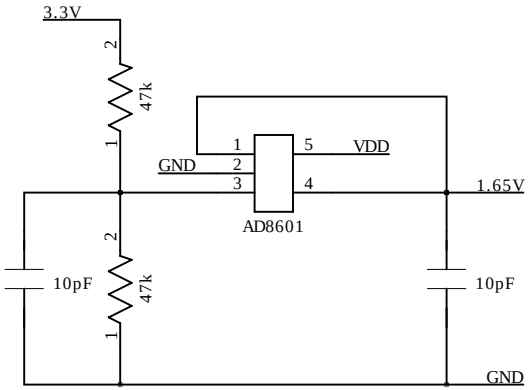

1.65V Reference Supply

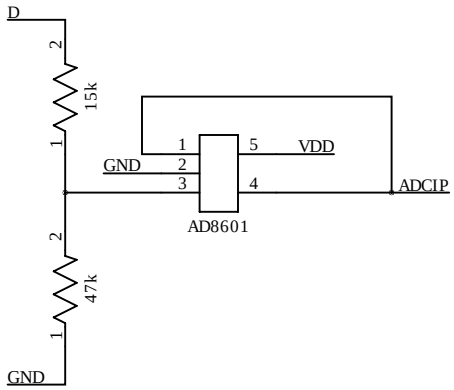

ADC I/P Buffer

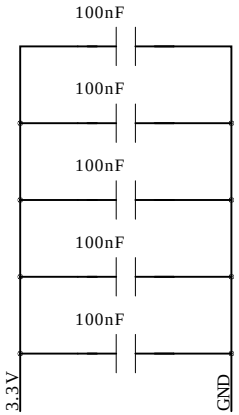

decoupling capacitors

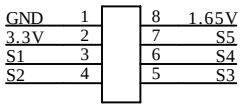

Sensor I/P Header

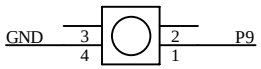

Push Button

COMPANY: **School of Engineering and Digital Arts**		
TITLE: Piezoelectric Data Logger		
DRAWN BY: JRC55	LAST MODIFIED: 17/05/2016	REV: A
FILE NAME: Piezoelectric Data Logger.sch	SHEET 1 OF 1	

Appendix B

MBED Embedded Software Code

This section contains the embedded software code used for both digital signal processing for the electrostatic sensor array and the software code for data logging the sensor output for the piezoelectric sensor array. The individual codes in this appendix are:

MBED Cross Correlation Code – this software code controls the analogue multiplexer that selects the elements on the electrostatic sensor array, interfaces the external ADC to the MBED through the SPI bus and calculates the particle velocity using a cross correlation algorithm

External AD7490 ADC.h Library – this is a modified code of an open source library that allowed the MBED to communicate with the AD7490 external ADC chip. The library was modified from its original configuration to increase the ADC sapling rate.

External AD7490 ADC.cpp Library – this is a modified code of an open source library that allowed the MBED to communicate with the AD7490 external ADC chip. The library was modified from its original configuration to increase the ADC sapling rate.

MBED On-line Piezoelectric Sensor Array Data Logging Code – this software code controls the analogue multiplexer that selects the elements on the piezoelectric sensor array, , interfaces the external ADC to the MBED through the SPI bus with the internal clock in the MBED controlling sapling period (200 kHz) and saves all sensor data to an SD card.

MBED Off-line Piezoelectric Sensor Data Logging Code - the software code interfaces with the off-line impact test rig and calculates the impact velocity of the ball bearings using the optical sensors on the off-line test rig. The software also data logs all sensor data from the impact sensor.

MBED Cross Correlation Code

```
#include "mbed.h"
#include "SDFileSystem.h"
#include "AD7490.h"

Serial pc(USBTX, USBRX);              // tx, rx
Timer t;                          // initiate timer function
//SDFileSystem sd(p5, p6, p7, p8, "sd");  // Set up the pinout on the SD card
SPI spi(p11,p12,p13);                 // Set up SPI for ADC interface
DigitalIn pb(p9);                   // Set Pin 9 to switch Input
DigitalOut ENled(LED1);               // Set LED 1
DigitalOut A0led(LED2);               // Set LED 2
DigitalOut A1led(LED3);               // Set LED 3
DigitalOut A2led(LED4);               // Set LED 4
DigitalOut ENmux(p21);
DigitalOut A0mux(p22);
DigitalOut A1mux(p23);
DigitalOut A2mux(p24);

int main() {

pb.mode(PullUp);       // Set to pullup mode for switch

int v;
int j;
int x;              // Raa0 and Rbb0 Loop Variable
int m;               // Zero r1 loop Variable
int n;              // r2 loop Variable
int p;              // Correlation Coeficent loop Variable
int samnum = 1024;      // Number of samples taken
int ccnum = samnum/2;   // Number of samples used for cross correlation
```

```
int counter;            // Correlation Counter Number
int a[samnum];          // Channel A (Upstream)
int b[samnum];          // Channel B (Downstream)
int muxl;
int muxlnum = 5;        // MUX Loop
int mainloop;
int mainloopnum = 500;
int sample_period_read[samnum];

float time_taken;
float Raa0;
float Rbb0;
float Rxx0;
float r1[ccnum];
float r2[ccnum];
float cc1_temp;
float velocity;
int Signal_a[samnum];
int Signal_b[samnum];
float RMS;
float PerRMS;
int cc_num;

for (;;)
{
//---------------------------Set up ADC pins---------------------------//
//-------------------------Push Button Control-------------------------//
      ENmux = 0;
      A0mux = 0;
      A1mux = 0;
      A2mux = 0;
```

```
      ENled = 0;
      A0led = 0;
      A1led = 0;
      A2led = 0;

   if (pb == 0)       // If push button is pressed
   {
//-------------------------Push Button Control-------------------------//
   for (mainloop = 0; mainloop < mainloopnum; mainloop++)
   {
      for (muxl = 0; muxl < muxlnum; muxl++)
      {
//------------------------------Set Mux------------------------------//

   if (muxl == 0)  // Set S1
   {
      ENmux = 1;  //ENled = 1;
      A0mux = 0;  //A0led = 0;
      A1mux = 0;  //A1led = 0;
      A2mux = 0;  //A2led = 0;
   }

   if (muxl == 1)  // Set S2
   {
      ENmux = 1;  ENled = 1;
      A0mux = 1;  A0led = 1;
      A1mux = 0;  A1led = 0;
      A2mux = 0;  A2led = 0;
   }

   if (muxl == 2)  // Set S3
```

```
  {
    ENmux = 1;  ENled = 1;
    A0mux = 0;  A0led = 0;
    A1mux = 1;  A1led = 1;
    A2mux = 0;  A2led = 0;
  }

  if (muxl == 3)  // Set S4
  {
    ENmux = 1;  ENled = 1;
    A0mux = 1;  A0led = 1;
    A1mux = 1;  A1led = 1;
    A2mux = 0;  A2led = 0;
  }

  if (muxl == 4)  // Set S5
  {
    ENmux = 1;  ENled = 1;
    A0mux = 0;  A0led = 0;
    A1mux = 0;  A1led = 0;
    A2mux = 1;  A2led = 1;
  }

    wait_ms(1);
//-------------------------------Set Mux-------------------------------//
//----------------------Set up ADC Parameters-------------------------//
  // set up SPI interface.
  spi.format(16,0);         // Set SPI format
  spi.frequency(12000000);   // Set SPI Clock Frequency

  // construct AD7490 instances
  AD7490 ad1(spi, p10);      // Set chip sellect for ADC on pin 10
```

```
   // start ADC conversion with sequential mode
   ad1.sequential(1);         // Sequential mode pin 0-1

   // Set up buffer size for SPI interface
   short ad_data[2];      // user buffer size
//-----------------------Set up ADC Parameters-------------------------//
//-----------------------------Sampling--------------------------------//
   t.reset();         // Reset timer t to zero
   t.start();         // Start timer t
      for(j=0; j < samnum; j++)
   {
      ad1.read(&ad_data[0]);  // save ADC data to buffer

      b[j] = ad_data[0];      // Assign ad_data[0] to a[j]
      a[j] = ad_data[1];      // Assign ad_data[1] to b[j]

     sample_period_read[j] = t.read_us();
   }
//-----------------------------Sampling--------------------------------//
//---------------------True Voltage Conversion-------------------------//
for (v = 0; v < samnum; v++)
{
Signal_a[v] = a[v] - 2048;
Signal_b[v] = b[v] - 2048;
}
//---------------------True Voltage Conversion-------------------------//
//----------------------Correlation Code Here--------------------------//
counter = 0;    // Reset counter to zero
cc1_temp = 0;   // Reset cc1 to zero
Raa0 = 0;       // Resets Raa0 to zero
Rbb0 = 0;       // Resets Raa0 to zero
```

```
cc_num = 0;
for (x=0; x < ccnum; x++)
{
Raa0 += (Signal_a[x] * Signal_a[x]);    // Calculates Raa0
Rbb0 += (Signal_b[x] * Signal_b[x]);    // Calculates Rbb0
}
Rxx0 = sqrt(Raa0*Rbb0);
   for (m=0; m < ccnum; m++)
   {
   r1[m] = 0;

      for (n=0; n < ccnum; n++)
      {
      r1[m] += (Signal_a[n] * Signal_b[(n + m) - 1]);
      }
      r2[m] = r1[m]/Rxx0;
      }

      for (p = 0; p < ccnum; p++)
      {
      counter++;
      if (r2[p] > cc1_temp)
      {


      cc1_temp = r2[p];

      cc_num = counter - 1;    //
      }
      }
//----------------------Correlation Code Here--------------------------//
//----------------------Velocity Calculation---------------------------//
```

```
   time_taken = sample_period_read[cc_num];
   velocity = 0.01 / (time_taken/1000000);
//----------------------Velocity Calculation---------------------------//
//-----------------------------RMS-----------------------------------//
  RMS = (sqrt(Raa0)) / 46341;
  PerRMS = RMS * 100;
//-----------------------------RMS-----------------------------------//
//------------------------Output Results-------------------------------//
   if (muxl < 4)
   {
   pc.printf("%.3f\t",velocity);
   pc.printf("%.3f\t",cc1_temp);
   pc.printf("%.3f\t",PerRMS);
   }
   if (muxl == 4)
   {
   pc.printf("%.3f\t",velocity);
   pc.printf("%.3f\t",cc1_temp);
   pc.printf("%.3f\t",PerRMS);
   pc.printf("%i\n",mainloop);
   }
//------------------------Output Results-------------------------------//

 }}}}}
```

External AD7490 ADC.h Library

```
//
//  AD7490 ... Analog Devices 16 channels, 1MSPS, 12bit ADC
//
//  2012.08.29 ... Originaly written by Yoji KURODA
//  2014.05.22 ... Modified by J R Coombes for fast sampling on inputs A1 and A2
//
#ifndef _AD7490_H
#define _AD7490_H
class AD7490 {
 protected:
   enum CREG {
      CREG_WRITE  = 0x800,
      CREG_SEQ    = 0x400,
      CREG_ADD3   = 0x200,
      CREG_ADD2   = 0x100,
      CREG_ADD1   = 0x080,
      CREG_ADD0   = 0x040,
      CREG_PM1    = 0x020,
      CREG_PM0    = 0x010,
      CREG_SHADOW = 0x008,
      CREG_WEAK   = 0x004,
      CREG_RANGE  = 0x002,
      CREG_CODING = 0x001
   };
   SPI spi;
   DigitalOut cs;
   unsigned short read(void);  // dummy read for triggering at sequential mode

 public:
   AD7490(SPI _spi, PinName _cs);
   virtual ~AD7490(){};

   unsigned short convert_single(int ch=0);      // one shot conversion at channel [ch]
   void convert(short data[]);           // convert all (16) channels with one short conv.

   unsigned short sequential(int ch=15);   // start sequential mode from channel [0] to [ch]
   void read(short data[]);              // read [0] to [ch], and copy to user area
};

#endif  // _AD7490_H
```

External AD7490 ADC.cpp Library

```
//
//  AD7490 ... Analog Devices 16 channels, 1MSPS, 12bit ADC
//
//  2012.08.29 ... Originaly written by Yoji KURODA
//  2014.05.22 ... Modified by J R Coombes for fast sampling on inputs A1 and A2
//
#include "mbed.h"
#include "AD7490.h"

AD7490::AD7490(SPI _spi, PinName _cs)
:  spi(_spi),
   cs(_cs)
{
   unsigned short x = 0;

   for(int i=0; i<3; i++){

      x = 0;
      x |= CREG_WRITE;
   //    x |= CREG_SEQ;
   //    x |= CREG_SHADOW;
      x |= CREG_ADD3;
      x |= CREG_ADD2;
      x |= CREG_ADD1;
      x |= CREG_ADD0;
      x |= CREG_PM1;
      x |= CREG_PM0;
      x |= CREG_RANGE;
      x |= CREG_CODING;

      cs = 0;
      unsigned short ret = spi.write(x<<4);
      cs = 1;

//       printf("INIT: send = 0x%X, ret = 0x%X\n", x, ret);
   }
}

unsigned short
AD7490::convert_single(int ch)
```

```
{
   unsigned short x = 0;

   x |= CREG_WRITE;
//   x |= CREG_SEQ;
//   x |= CREG_SHADOW;
//   x |= CREG_ADD3;
//   x |= CREG_ADD2;
//   x |= CREG_ADD1;
   x |= (CREG_ADD0|CREG_ADD1|CREG_ADD2|CREG_ADD3) & (ch<<6);

   x |= CREG_PM1;
   x |= CREG_PM0;
   x |= CREG_RANGE;
   x |= CREG_CODING;

   cs = 0;
   unsigned short ret = spi.write(x<<4);
   cs = 1;

//   printf("send = 0x%X, ch = %2d, ret = %d\n", x, (ret>>12)&0xF, ret&0xFFF);

   return ret;
}

void
AD7490::convert(short data[])
{
   for(int ch=0; ch<16; ch++) data[ch]=0;
   for(int ch=0; ch<16; ch++){
      unsigned short ret = convert_single(ch);

      data[ ret>>12&0xF ] = ret&0xFFF;
   }
}


unsigned short
AD7490::sequential(int ch)
{
   unsigned short x = 0;
```

```
    x |= CREG_WRITE;
    x |= CREG_SEQ;
    x |= CREG_SHADOW;
//  x |= CREG_ADD3;
//  x |= CREG_ADD2;
//  x |= CREG_ADD1;
    x |= (CREG_ADD0|CREG_ADD1|CREG_ADD2|CREG_ADD3) & (ch<<6);

    x |= CREG_PM1;
    x |= CREG_PM0;
    x |= CREG_RANGE;
    x |= CREG_CODING;

    cs = 0;
    unsigned short ret = spi.write(x<<4);
    cs = 1;

    return ret;
}



unsigned short
AD7490::read(void)
{
    unsigned short x = 0;

//  x |= CREG_WRITE;
//  x |= CREG_SEQ;
//  x |= CREG_SHADOW;
//  x |= CREG_ADD3;
//  x |= CREG_ADD2;
//  x |= CREG_ADD1;
//  x |= (CREG_ADD0|CREG_ADD1|CREG_ADD2|CREG_ADD3) & (ch<<6);

//  x |= CREG_PM1;
//  x |= CREG_PM0;
//  x |= CREG_RANGE;
//  x |= CREG_CODING;
```

```
   cs = 0;
   unsigned short ret = spi.write(x<<4);
   cs = 1;

//    printf("send = 0x%X, ch = %2d, ret = %d\n", x, (ret>>12)&0xF, ret&0xFFF);

   return ret;
}

void
AD7490::read(short data[])
{
   for(int ch=0; ch<2; ch++) data[ch]=0;  //     for(int ch=0; ch<16; ch++) data[ch]=0;
   for(int ch=0; ch<2; ch++){            //     for(int ch=0; ch<16; ch++){
      unsigned short ret = read();

      data[ ret>>12&0xF ] = ret&0xFFF;
   }
}
```

MBED On-line Piezoelectric Sensor Array Data Logging Code

```
#include "mbed.h"
#include "AD7490.h"
#include "SDFileSystem.h"
DigitalOut ENled(LED1);              // Set LED 1
DigitalOut A0led(LED2);              // Set LED 2
DigitalOut A1led(LED3);              // Set LED 3
DigitalOut A2led(LED4);              // Set LED 4
DigitalOut ENmux(p25);
DigitalOut A0mux(p24);
DigitalOut A1mux(p23);
DigitalOut A2mux(p22);
DigitalOut A3mux(p21);
SPI spi(p11,p12,p13);    // Set SPI interface pins
DigitalIn pb(p9);       // Set Pin 9 to switch Input
Timer t1;              // initiate timer function
SDFileSystem sd(p5, p6, p7, p8, "sd");  // Set up the pinout on the SD card
int main()
{
Serial pc(USBTX, USBRX); // tx, rx
int n = 4000;   // Number of Samples per Cycle
int time_sample_delay; // ADC Period
int time_sample_read; // Read Clock for ADC Period
int adc0_data[n]; // ADC Data
int mainloop; // Main Loop Variable
int mainloopnum = 100;  // Number of Data Capture Cycles
int muxl;  // Array Loop Variable
int muxlnum = 5;  // Number of array elements
float abs_adc0_data; // Peak Impact Value
float impact_peak_temp; // Impact Signal Peak Temp Value
float square_adc0_data; // Absolute ADC Value
float no_ref_adc0; // Removes Vref from ADC Signal
```

```
pb.mode(PullUp);       // Set to pullup mode for switch

for (;;)
{
//-------------------------Push Button Control-------------------------//
      ENmux = 0;
      A0mux = 0;
      A1mux = 0;
      A2mux = 0;
      A3mux = 0;

      ENled = 0;
      A0led = 0;
      A1led = 0;
      A2led = 0;
  if (pb == 0)       // If push button is pressed
  {
//-------------------------Push Button Control-------------------------//
      for (mainloop = 0; mainloop < mainloopnum; mainloop++)
      {

        for (muxl = 0; muxl < muxlnum; muxl++)
        {
//-------------------------------Set Mux-------------------------------//

//-------------------------------Set Mux-------------------------------//
   if (muxl == 0)  // Set S1
  {
      ENmux = 1;  ENled = 1;
      A0mux = 0;  A0led = 0;
      A1mux = 0;  A1led = 0;
      A2mux = 0;  A2led = 0;
```

```
    A3mux = 0;
  }
  if (muxl == 1)  // Set S2
  {
    ENmux = 1;  ENled = 1;
    A0mux = 1;  A0led = 1;
    A1mux = 0;  A1led = 0;
    A2mux = 0;  A2led = 0;
    A3mux = 0;
  }
  if (muxl == 2)  // Set S3
  {
    ENmux = 1;  ENled = 1;
    A0mux = 0;  A0led = 0;
    A1mux = 1;  A1led = 1;
    A2mux = 0;  A2led = 0;
    A3mux = 0;
  }
  if (muxl == 3)  // Set S4
  {
    ENmux = 1;  ENled = 1;
    A0mux = 1;  A0led = 1;
    A1mux = 1;  A1led = 1;
    A2mux = 0;  A2led = 0;
    A3mux = 0;
  }
  if (muxl == 4)  // Set S5
  {
    ENmux = 1;  ENled = 1;
    A0mux = 0;  A0led = 0;
    A1mux = 0;  A1led = 0;
    A2mux = 1;  A2led = 1;
```

```
      A3mux = 0;
   }
      wait_ms(1);
//------------------------------Set Mux------------------------------//
//-----------------------Set up ADC Parameters-------------------------//
// should be set before call AD7490 constructer
spi.format(16,0);
spi.frequency(12000000);

// construct AD7490 instances
AD7490 ad1(spi, p10);   // ADC chip Sellect Pin 10

// start ad conversion with sequential mode
ad1.convert_single(0);
//-----------------------Set up ADC Parameters-------------------------//
//-----------------------------Sampling--------------------------------//
   short ad_data[1];     // user buffer area
   t1.reset();         // Reset timer t to zero
   t1.start();         // Start timer t
   time_sample_delay = 0;
      for(int j=0; j<n; j++)
      {
      time_sample_read = t1.read_us();
         if (time_sample_read >= time_sample_delay)
         {
         ad1.read(&ad_data[0]);  // save the first ADC data to buffer
         adc0_data[j] = ad_data[0];
         time_sample_delay = (time_sample_delay + 5); // Sample Period 5us (200KHz)
         }
            else if (time_sample_read < time_sample_delay)
            {
            j--;
```

```
            }
        }
//------------------------------Sampling--------------------------------//

//--------------------Find the Peak of Impact signal--------------------//
impact_peak_temp = 0;    // Reset impact_peak_temp to zero
square_adc0_data = 0;
abs_adc0_data = 0;
no_ref_adc0 = 0;
   for (int p = 0; p < n; p++)
   {
   no_ref_adc0 = (adc0_data[p] - 2047); // Removes DC Reference Voltage
   square_adc0_data = (no_ref_adc0 * no_ref_adc0); // Square value of adc0_data
   abs_adc0_data = sqrt(square_adc0_data); // Normallises ADC Signal
      if (abs_adc0_data > impact_peak_temp)
      {
      impact_peak_temp = abs_adc0_data;
      }
   }
//--------------------Find the Peak of Impact signal--------------------//
//-------------------------Save to SD Card-------------------------------//

   if (muxl == 0)  // Save S1 Data
   {
FILE *impact_file_open_data = fopen("/sd/ImpactArrayData/S1ImpactData.txt", "a");
   if(impact_file_open_data == NULL)
   {
   error("Could not open file S1ImpactData\n");
   }
for(int i=0; i<n; i++)
   {
   fprintf(impact_file_open_data,"%i\t", adc0_data[i]);
```

```
  }
fclose(impact_file_open_data);

FILE *impact_file_open_newline = fopen("/sd/ImpactArrayData/S1ImpactData.txt", "a");
  if(impact_file_open_newline == NULL)
  {
  error("Could not open file S1ImpactData\n");
  }
fprintf(impact_file_open_newline,"\r\n");
fclose(impact_file_open_newline);
  }

  if (muxl == 1)  // Save S2 Data
  {
FILE *impact_file_open_data = fopen("/sd/ImpactArrayData/S2ImpactData.txt", "a");
  if(impact_file_open_data == NULL)
  {
  error("Could not open file S2ImpactData\n");
  }
for(int i=0; i<n; i++)
  {
  fprintf(impact_file_open_data,"%i\t", adc0_data[i]);
  }
fclose(impact_file_open_data);

FILE *impact_file_open_newline = fopen("/sd/ImpactArrayData/S2ImpactData.txt", "a");
  if(impact_file_open_newline == NULL)
  {
  error("Could not open file S2ImpactData\n");
  }
fprintf(impact_file_open_newline,"\r\n");
fclose(impact_file_open_newline);
```

```
  }

  if (muxl == 2)  // Save S3 Data
  {
FILE *impact_file_open_data = fopen("/sd/ImpactArrayData/S3ImpactData.txt", "a");
  if(impact_file_open_data == NULL)
  {
  error("Could not open file S3ImpactData\n");
  }
for(int i=0; i<n; i++)
  {
  fprintf(impact_file_open_data,"%i\t", adc0_data[i]);
  }
fclose(impact_file_open_data);

FILE *impact_file_open_newline = fopen("/sd/ImpactArrayData/S3ImpactData.txt", "a");
  if(impact_file_open_newline == NULL)
  {
  error("Could not open file S3ImpactData\n");
  }
fprintf(impact_file_open_newline,"\r\n");
fclose(impact_file_open_newline);
  }

  if (muxl == 3)  // Save S4 Data
  {
FILE *impact_file_open_data = fopen("/sd/ImpactArrayData/S4ImpactData.txt", "a");
  if(impact_file_open_data == NULL)
  {
  error("Could not open file S4ImpactData\n");
  }
for(int i=0; i<n; i++)
```

```
  {
  fprintf(impact_file_open_data,"%i\t", adc0_data[i]);
  }
fclose(impact_file_open_data);

FILE *impact_file_open_newline = fopen("/sd/ImpactArrayData/S4ImpactData.txt", "a");
  if(impact_file_open_newline == NULL)
  {
  error("Could not open file S4ImpactData\n");
  }
fprintf(impact_file_open_newline,"\r\n");
fclose(impact_file_open_newline);
  }

  if (muxl == 4)  // Save S5 Data
  {
FILE *impact_file_open_data = fopen("/sd/ImpactArrayData/S5ImpactData.txt", "a");
  if(impact_file_open_data == NULL)
  {
  error("Could not open file S5ImpactData\n");
  }
for(int i=0; i<n; i++)
  {
  fprintf(impact_file_open_data,"%i\t", adc0_data[i]);
  }
fclose(impact_file_open_data);

FILE *impact_file_open_newline = fopen("/sd/ImpactArrayData/S5ImpactData.txt", "a");
  if(impact_file_open_newline == NULL)
  {
  error("Could not open file S5ImpactData\n");
  }
```

```
fprintf(impact_file_open_newline,"\r\n");
fclose(impact_file_open_newline);
   }
//-----------------------Save to SD Card-----------------------------//
//-----------------------Output Peak Value-----------------------------//

   if (muxl < 4)
   {
   pc.printf("%.3f\t",impact_peak_temp);
   }
   if (muxl == 4)
   {
   pc.printf("%.3f\t",impact_peak_temp);
   pc.printf("%i\n",mainloop);
   }

//-----------------------Output Peak Value-----------------------------//
          }
       }
 }
 }
 }
```

MBED Off-line Piezoelectric Sensor Data Logging Code

```
#include "mbed.h"
#include "AD7490.h"
#include "SDFileSystem.h"
DigitalIn pd1(p19);     // Set Pin 19 to digital Input (upstream)
DigitalIn pd2(p20);     // Set Pin 20 to digital Input (downstream)
DigitalOut myled1(LED1); // Set myled1 to LED1
DigitalOut myled4(LED4); // Set myled4 to LED4
SPI spi(p11,p12,p13);    // Set SPI interface
Timer t1;               // initiate timer function
Timer t2;               // initiate timer function
SDFileSystem sd(p5, p6, p7, p8, "sd");  // Set up the pinout on the SD card
int main() {
Serial pc(USBTX, USBRX);              // tx, rx
float time_read;
int WL;
int n = 2000;   //Number of samples
int time_sample_delay;
int time_sample_read;
int adc0_data[n];
float abs_adc0_data;
float impact_peak_temp;
float square_adc0_data;
float no_ref_adc0;
//float impact_peak_true;
float real_time;
float velocity;
wait(0.5);

for (;;)
{
```

```
// set up SPI interface.
// should be set before call AD7490 constructer
spi.format(16,0);
spi.frequency(12000000);

// construct AD7490 instances
AD7490 ad1(spi, p10);   // ADC chip Sellect Pin 10

// start ad conversion with sequential mode
ad1.convert_single(0);

myled1 = 0;
myled4 = 1;
  if (pd1 == 0)       //
  {
  t1.reset();         // Reset timer t to zero
  t1.start();         // Start timer t
  myled1 = 1;
  myled4 = 0;
  WL=1;
    while (WL == 1)
    {
      if (pd2 == 0)       //
      {
      time_read = t1.read_us();
      real_time = time_read / 1000000;
      velocity = 0.025 / real_time;
      pc.printf("%f\t",velocity);
      WL=0;
      /////////Sample Impact Data///////////
            short ad_data[1];     // user buffer area
```

```
        t2.reset();         // Reset timer t to zero
        t2.start();         // Start timer t
        time_sample_delay = 0;
        for(int j=0; j<n; j++)
        {
        time_sample_read = t2.read_us();
        if (time_sample_read >= time_sample_delay)
          {
          ad1.read(&ad_data[0]);  // save the first ADC data to buffer
          adc0_data[j] = ad_data[0];
          time_sample_delay = (time_sample_delay + 5);
          }
            else if (time_sample_read < time_sample_delay)
            {
            j--;
            }
        }
    ////////Sample Impact Data///////////
    /////Record Impact Data to SD Card/////
      FILE *impact_file_open_data = fopen("/sd/Impactdata/ImpactSignalData.txt", "a");
      if(impact_file_open_data == NULL)
      {
      error("Could not open file ImpactSignalData\n");
      }
      for(int i=0; i<n; i++)
      {
      fprintf(impact_file_open_data,"%i\t", adc0_data[i]);
      }
      fclose(impact_file_open_data);

      FILE *impact_file_open_newline = fopen("/sd/Impactdata/ImpactSignalData.txt", "a");
      if(impact_file_open_newline == NULL)
```

```
    {
    error("Could not open file ImpactSignalData\n");
    }
    fprintf(impact_file_open_newline,"\r\n");
    fclose(impact_file_open_newline);
/////Record Impact Data to SD Card/////
////Record Velocity Data to SD Card////
    FILE *velocity_file_open_data = fopen("/sd/Impactdata/VelocityData.txt", "a");
    if(velocity_file_open_data == NULL)
    {
    error("Could not open file VelocityData\n");
    }
    fprintf(velocity_file_open_data,"%f\r\n", velocity);
    fclose(velocity_file_open_data);
////Record Velocity Data to SD Card////
//////Find the Peak Impact Signal//////
    impact_peak_temp = 0;    // Reset impact_peak_temp to zero
    square_adc0_data = 0;
    abs_adc0_data = 0;
    no_ref_adc0 = 0;
    for (int p = 0; p < n; p++)
    {
    no_ref_adc0 = (adc0_data[p] - 2047); // Removes DC Reference Voltage
    square_adc0_data = (no_ref_adc0 * no_ref_adc0); // Square value of adc0_data
    abs_adc0_data = sqrt(square_adc0_data);
        if (abs_adc0_data > impact_peak_temp)
        {
            impact_peak_temp = abs_adc0_data;
        }
    }
//////Find the Peak Impact Signal//////
///Record Impact Peak Data to SD Card//
```

```
            FILE *Impact_Peak_file_open_data = fopen("/sd/Impactdata/ImpactPeakData.txt", "a");
            if(Impact_Peak_file_open_data == NULL)
            {
            error("Could not open file ImpactPeakData\n");
            }
            fprintf(Impact_Peak_file_open_data,"%f\r\n", impact_peak_temp);
            fclose(Impact_Peak_file_open_data);
          ///Record Impact Peak Data to SD Card//
          pc.printf("%f\n",impact_peak_temp);
          }
       }
    }
}
}
```

Appendix C

Matlab Code

This Matlab code is used to analysis data from a .txt file containing the impact sensor data and applies digital filtering to examine the effect filtering has on the impact magnitude. A threshold voltage of 100 mV is used to determine when an impact has occurred.

Impact Analysis with Bandpass Filter and Threshold Voltage

```
clear all;
close all;
clc;

%% load data
[fname,pname] = uigetfile('*.txt','Select a file');

if (any(pname ~= 0) && any(fname ~=0))
    data = load([pname fname]);
else
    disp('Flie selection has been cancelled');
    return;
end
arraynum = 3000;

for i = 1:1:arraynum

   fs = 200000;
    Sample_Lengh = 0.02;
    N = fs*Sample_Lengh;
    fnyquist = fs/2;


    S1 = data(i:arraynum:arraynum-(arraynum - i),:);

    S1Norm = (S1-2050)*0.00080586;  % True signal voltage

    %   Design filter (butterworth)
    [b a] = butter(1, [0.05,0.15], 'bandpass');

    %   Filter signal
    S1_filtered = filter(b,a,S1Norm);

    S1abs = abs(S1_filtered);

    S1Max = max(S1abs);


if (S1Max > 0.1)
    fprintf('%f\n',S1Max);
end
end
fprintf('end');
```

Publications from this Research

[1] J. R. Coombes and Y. Yan, 'Experimental Investigations into the Use of Piezoelectric Film Transducers to Determine Particle Size through Impact Analysis', Proceedings of IEEE International Instrumentation and Measurement Technology Conference (I2MTC), pp. 780 – 785, Taipei, Taiwan, 23 - 26 May, 2016. DOI: 10.1109/I2MTC.2016.7520464

[2] J. R Coombes and Y. Yan, 'Measurement of Velocity and Concentration Profiles of Pneumatically Conveyed Particles using an Electrostatic Sensor Array', IEEE Transactions on Instrumentation and Measurement, vol. 65, no. 5, pp. 1139 – 1148, November 2015 DOI: 10.1109/TIM.2015.2494620

[3] J. R Coombes and Y. Yan, 'Experimental Investigations into the Flow Characteristics of Pneumatically Conveyed Biomass using an Electrostatic Cross Sectional Sensor Array', Fuel, vol.151, pp.11 - 20, July 2015. DOI: 10.1016/j.fuel.2014.11.048

[4] J. R Coombes and Y. Yan, 'Development of an Electrostatic Array Sensor for Measuring the Velocity and Concentration Profiles of Pneumatically Conveyed Particles', Proceedings of IEEE I2MTC, pp. 138 – 143, Pisa, Italy, 11 - 14 May, Pisa Italy, 2015. DOI: 10.1109/I2MTC.2015.7151254

This full text paper was peer-reviewed at the direction of IEEE Instrumentation and Measurement Society prior to the acceptance and publication.

Experimental Investigations into the Use of Piezoelectric Film Transducers to Determine Particle Size through Impact Analysis

James Robert Coombes
School of Engineering and Digital Arts, University of Kent
Canterbury, Kent CT2 7NT, UK
jrc55@kent.ac.uk

Yong Yan
School of Engineering and Digital Arts, University of Kent
Canterbury, Kent CT2 7NT, UK
y.yan@kent.ac.uk

***Abstract* – Sensors are required to determine the particle size of granular materials in a variety of industries such as energy, chemical manufacturing and food processing. The importance of accurately monitoring the particle size is essential in quality control in these industrial sectors. This paper presents the use of a custom made piezoelectric PVDF film transducer that is capable of determining the particle size of granular material through impact analysis. Experiments were carried out using a purpose-built test rig using ball bearings of different sizes traveling at different velocities. Through power spectral analysis of the impact signal it has been determined that different components of the signal spectrum may relate to different characteristics of the particle itself such as particle impact velocity and particle size. A comparison between the experimental data and system modelling results using the known mechanical characteristics of the test particles shows close similarities.**

Keywords - piezoelectric film, impact, PVDF, particle size, particle velocity

I. INTRODUCTION

The ability to determine the particle size in granular materials is important in many industrial sectors such as energy, chemical manufacturing and food processing. The importance of accurately determining the particle size is vital for quality control.

One of the main areas of interest is an online method for monitoring particle size distribution during the transport of granular materials. One of the most common ways granular materials are transported is through the use of bulk solid pneumatic conveying systems. This type of system uses high velocity air to convey pulverised material along a pipe using either positive or negative pressure [1].

Many sensing methods have been researched such as optical [2 and 3], electrostatic [4] and impact/acoustic [5 and 6] to determine particle size in bulk solid pneumatic conveying systems. The optical method uses a transparent window and a camera to capture an image of the conveyed particles, a laser screen is used to illuminate the particles as they travel past the camera's view. This method has the disadvantage that the transparent window is susceptible to contamination by the fine dust in the material. However, this problem was addressed by the use of an air purging system to prevent particles coming into contact with the window [3].

Electrostatic sensors have also been deployed to determine particle size. The principle of using electrostatic sensors is that as the particles travel down the pipe they pick up an electrostatic charge due to friction with each other and the air [1]. The use of electrostatic sensors to determine particle size is based on the idea that a larger particle carries more electrostatic charge on its surface than that of a smaller one of the same type [4]. However, Coombes and Yan [7] found that smaller particles had a higher level of electrostatic charge compared to larger ones of the same type for the same mass flow rate.

Particle size has also been determined by measuring the vibrations caused by particle impacts. These sensors have used accelerometers to measure the vibrations [5], piezoelectric materials [6] and piezoelectric acoustic emission sensors [8]. All these methods use an impact bar that comes into contact with the particle flow. This method has the disadvantage of the sensor being intrusive, however, in dilute phase flow (particle concentration less than 0.1% by volume [1]) this does not cause a significant problem. However, the design of the impact bar used in these sensing methods is quite large so even in a dilute phase flow multiple impacts may occur at the same time. Also the design of the impact bar and position of the sensor means that the same sized particles travelling at the same speed could impact the bar at different locations and the sensor output would be different. Off-line experimentation has also been carried out using a piezoelectric sensor to measure the impact characteristics of spherical particles [9]. This work used a large impact plate with a piezoelectric sensor mounted on the reverse side of the plate. This sensor arrangement would be unsuitable for measuring particle size in dilute phase flow since the large plate would suffer from simultaneous impacts by many particles.

This research aims to illustrate the feasibility of using a piezoelectric film sensor that is capable to determine particle size which can be adapted for online measurement of pneumatically conveyed particles. This sensor would have the

novel feature in that it will have a very small active sensing area, thus reducing the chance of multiple impacts occurring at the same time.

II. Measurement Principle

When a moving particle collides with a fixed solid surface the kinetic energy of the moving particle is converted into an impact force. Hertz was the first to pioneer this work [10]. In order to determine the impact force the particle is assumed to be a sphere. This is because many particles in industry such as coal particles in the energy industry or shot in manufacturing are close to being spherical in shape. In order to calculate the impact force the mechanical properties of the impact surface and particle have to be taken into account. The effective elastic modulus E^* can be determined by [11]:

$$E^* = 2\left(\frac{1-\nu_1^2}{E_1}+\frac{1-\nu_2^2}{E_2}\right)^{-1} \quad (1)$$

Where v_1 and v_2 is the Poisson's ratio of the particle and surface respectively and E_1 and E_2 Young's modulus of the particle and surface respectively. The size (radius) of the particle also has to be taken into account. The median radius R^* of the contact surfaces is defined as [11]:

$$R^* = \left(\frac{1}{R_1}+\frac{1}{R_2}\right)^{-1} \approx R_1 \quad (2)$$

Where R_1 and R_2 are the radius of the particle and surface respectively.

From the moment of collision occurs till the moment the particle velocity reduces to zero elastic deformations occur. The time (duration of impact) is determined by [11]:

$$s = \left(\frac{225}{64}\frac{m^2V^2}{E^{*2}R^*}\right)^{1/5} \quad (3)$$

Where m is the mass of the particle, V is the velocity of the particle. The maximum impact force is defined by [11]:

$$F_{max} = \left(\frac{225\,m^3\,E^{*2}\,R^*\,V^6}{144}\right)^{1/5} \quad (4)$$

To measure the impact force of the colliding particle a piezoelectric transducer is used to measure the vibrations caused by the particle impact. Piezoelectric materials convert mechanical stress and strain into voltage or charge [12].

PVDF (Polyvinylidene Fluoride) film is a piezoelectric material which was chosen as the transducer for the impact sensor because it has: a wide frequency range (0.001 Hz – 10^9 Hz), high mechanical strength and impact resistance, high voltage output (10 times higher than piezo ceramics) and it can be manufactured into complex shapes [13].

The PVDF transducer is fabricated by having a layer of PVDF film sandwiched between two metal surfaces. The metal surfaces are applied to the PVDF surface by evaporatively deposited metals such as copper, nickel, silver or gold with the metal layer being between 500 – 1000 Å thick [13]. The active area on the PVDF transducer is determined by where the metal surfaces overlap to form an electrode as shown in Fig. 1. These electrode shapes can be fabricated using chemical etching techniques [13].

When stress is applied to the active area on the PVDF transducer the deformation changes the charge density of the material, this change causes a voltage to be generated between the two electrodes. The output voltage is directly proportional to the magnitude and frequency of the applied stress [13].

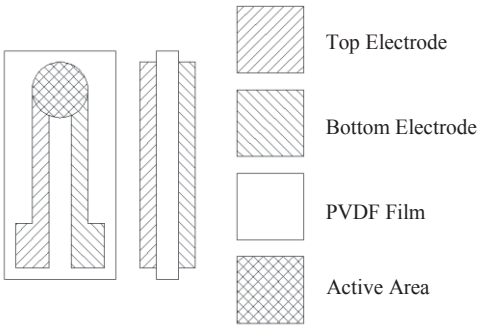

Fig. 1 Diagram of PVDF transducer

PVDF film is anisotropic which means the voltage output is dependent upon which axis the mechanical stress is applied. These piezo coefficients are most commonly used in either charge or voltage modes (d_{3n} or g_{3n} respectively). The output of the PVDF film can be either charge or voltage. The output charge in charge mode is represented by [13]:

$$D = \frac{Q}{A} = d_{3n}\,F_n \quad (5)$$

Where D is the charge density developed, Q is the charge developed A is the conductive area of the electrodes, d_{3n} is the axis of the applied stress or strain and F_n is the applied stress in the specified direction. When configured in voltage mode the output voltage is represented by [13]:

$$V_o = g_{3n}\,X_n\,t \quad (6)$$

Where V_o is the output voltage, g_{3n} is the axis of the applied stress or strain, X_n is the applied stress in the specified direction and t is the thickness of the PVDF film. The mechanical stress X_n is calculated by:

$$X_n = \frac{F_{max}}{A} \quad (7)$$

III. Impact Sensor Design

The impact sensor and data logger consists of the impact waveguide, a PVDF film transducer (illustrated in Fig. 2), a signal conditioning circuit and a microcontroller controlled analogue to digital converter (ADC) which outputs the impact sensor data to a PC or an SD memory card is shown in Fig. 3.

The waveguide primary function is to act as a conduit for the vibrations caused by the particle impact. The waveguide is secured using tightly fitting rubber washers which limits the directional axis of movement to one direction (one dimension of movement). By doing this the rubber washer also applies friction to this dimension of movement and this would reduce

to amount of stress applied to the piezo transducer during impact. For this the output voltage is calculated by:

$$V_o = \frac{g_{3n} X_n t}{f_f} \quad (8)$$

Where f_f is the frictional force acting against the waveguide from the rubber washer during the ball bearing impact. However it is difficult to quantify the frictional force between the rubber washer due to the complexity of the surface texture of the waveguide, rubber washer and the force between the washer and waveguide [14]. For this reason the value f_f is an estimate.

The waveguide also has a very small active sensing area (1 mm diameter). The advantage of this is, if the impact sensor was to be mounted in a 50 mm bore pipe to measure particle size on a pneumatic conveyor system, the active sensing area would be less than 0.001% of the pipe bore. This would reduce the possibility of simultaneous impacts of multiple particles. The waveguide also protects the piezo transducer from possible damage caused by particle impacts. The current sensor housing is 6 mm thick meaning that if the impact sensor was to be mounted inside a 50 mm pipe bore the non-active sensor cross section would take up approximately 15% of the pipe bore. However, for larger bore pipes such as those in the power industry (150 mm and greater) this would be less of a problem.

The piezo transducer consists of a layer of PVDF film of 110 μm thick with nickel copper alloy electrodes. The electrodes were fabricated via a chemical etching process using ferric chloride [13]. The piezo transducer is insulated with a layer of silicone to prevent short circuiting between the electrode and waveguide. The silicone insulation also protects the delicate electrodes. The piezo transducer is glued to the waveguide and fixed surface using a specialist adhesive for gluing silicone based rubbers as shown in Fig. 2.

The first stage of the signal conditioning circuit is a preamplifier. The preamplifier is a non-inverting amplifier (voltage mode) with the electrodes directly connected to the amplifier to reduce connection distance and maintain high signal-to-noise ratio [13]. The first stage of the signal conditioning circuit is also contained inside a shielded casing for noise protection. Having the pre-amplifier in voltage mode also has the advantage that changes in temperature have little effect on the voltage sensitivity [13].

The output of the preamplifier is then passed through an optional second-order active bandpass filter. This bandpass filter is adjustable to change the lower and upper limits of frequencies.

The signal is then digitised in an ADC. The ADC is controlled by a microcontroller using a serial peripheral interface (SPI) bus. The ADC has a 12-bit resolution and a sampling frequency of 200 kHz (since the highest frequency expected from a PVDF film transducer in 1 directional axis will output a frequency of less than 100 kHz [13]). Data is transmitted to a PC or saved on an SD card.

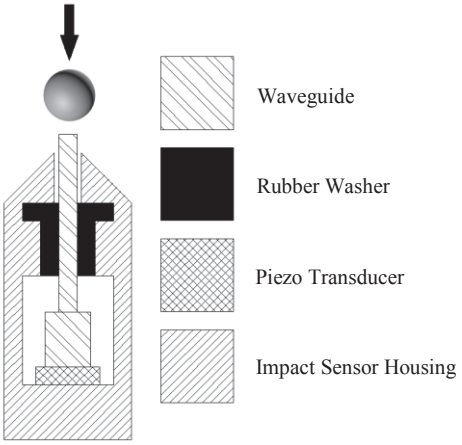

Fig. 2 Cut away view of the piezo impact sensor

IV. Experimental Setup

In order to compare the impact force measured by the impact sensor to the theoretical impact force ball bearings were used as test particles. The ball bearings are made of Delrin which is a high strength engineering polymer. Three different sizes of Delrin ball bearings were tested 2.5 mm, 3 mm and 3.5 mm in diameter (each with a mass of 11.62 mg, 20.08 mg and 31.88 mg respectively).

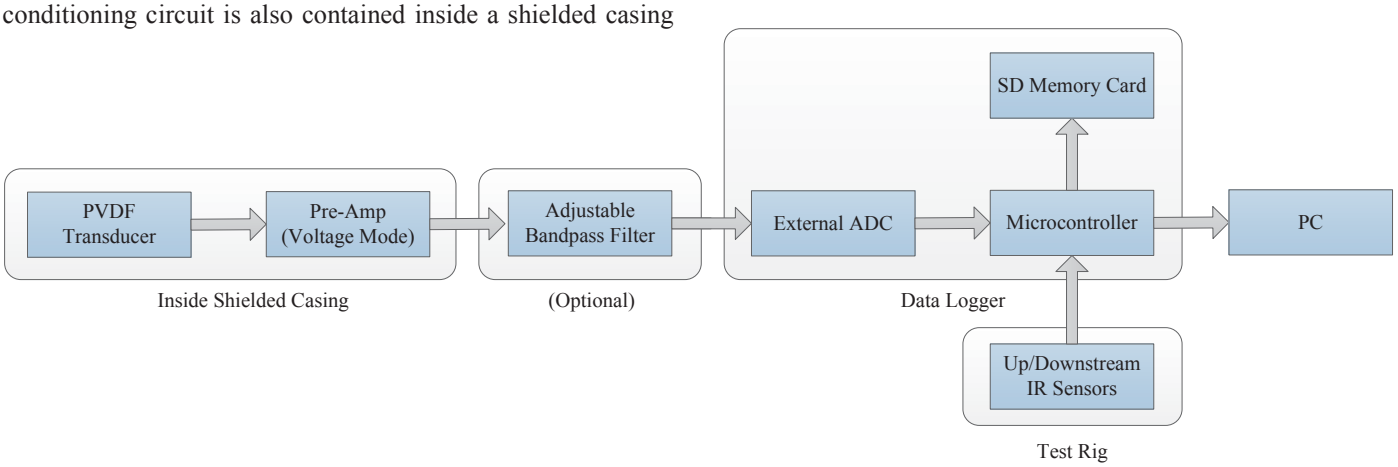

Fig. 3 Block diagram of the piezo impact sensor and data logger

Fig. 4 shows the experimental setup used in this study. The impact sensor is rigidly mounted in a vice to prevent movement. A guiding tube is centred above the impact sensor to guide the ball bearing onto the impact sensor. The guiding tube can be adjusted to different lengths (500 mm, 750 mm, 1000 mm and 1250 mm), allowing the ball bearing under test to be dropped from different heights for different impact velocities.

To independently measure the impact velocity of the ball bearing before impact at the end of the guiding tube (just before the impact sensor) optical sensors are set 25 mm apart as shown in Fig. 4. The optical sensors consist of an IR (infra-red) emitter that creates an IR beam across the inside of the tube. This IR beam is detected by an IR receiver (IR photodiode). The two optical sensors are connected to the microcontroller as shown in Fig. 3. When the falling ball bearing breaks the upstream IR beam the microcontroller triggers the timer. When the falling ball bearing breaks the downstream IR beam the microcontroller reads the time taken for the ball bearing to travel from the upstream to the downstream sensor. The average velocity of the ball bearing is calculated from the spacing between the sensors and the measured time.

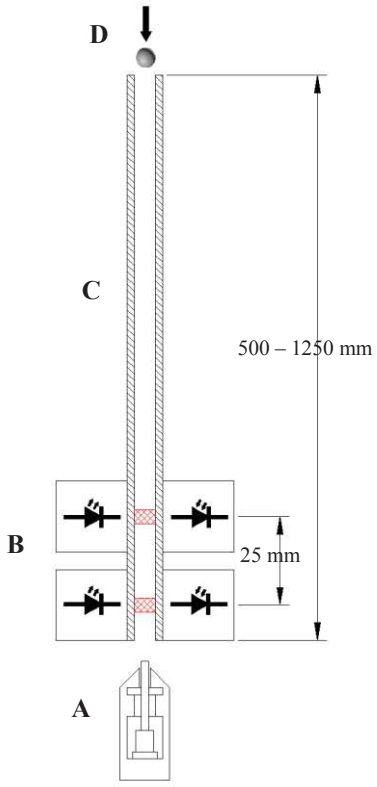

Fig. 4 Test rig (A) impact sensor, (B) upstream/downstream optical sensors, (C) guiding tube, (D) ball bearing entering guiding tube

After the downstream IR sensor has been triggered the microcontroller begins data logging from the ADC since an impact is imminent. All data from the impact sensor output is saved onto a SD memory card and an algorithm in the microcontroller determines the peak amplitude of the impact signal which is presented on the PC.

V. Results and Discussion

The impact sensor was first tested without the bandpass filter in order to examine the frequency component of the ball bearing impact. A total of 200 impact reading were taken for each size of ball bearings. Fig. 5 shows the peak amplitude of the impact signals. The magnitude of the unfiltered impact signals shows a high level of deviation, especially on 2.5 mm diameter ball bearing. The impact signals for the 3 mm ball bearing also show a large number of impact signals that are at the supply voltage (1.65V) indicating that the preamplifier has saturated for them impacts.

Power spectral analysis of impacts of all three sizes of ball bearings is carried out for 2.2 m/s, 2.4 m/s and 2.6 m/s, as shown in Fig. 6, 7 and 8 respectively.

The power spectra in Fig. 6 - 8 indicate that the smaller diameter ball bearings have higher frequency components. Also for larger diameter ball bearings at higher velocity there is a large DC component in the signal indicating the signal has saturated to the supply voltage.

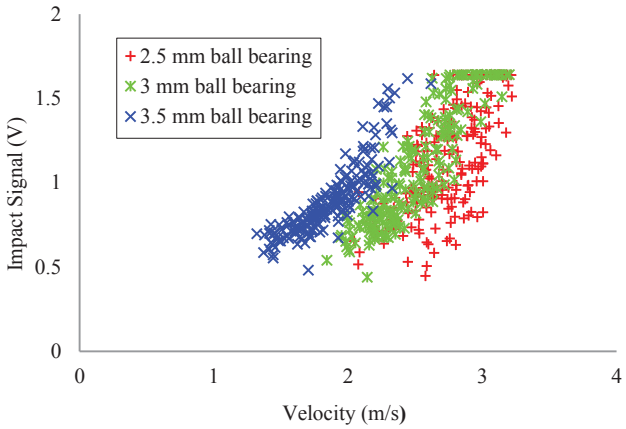

Fig. 5 Magnitude of dominant peak of ball bearing impact

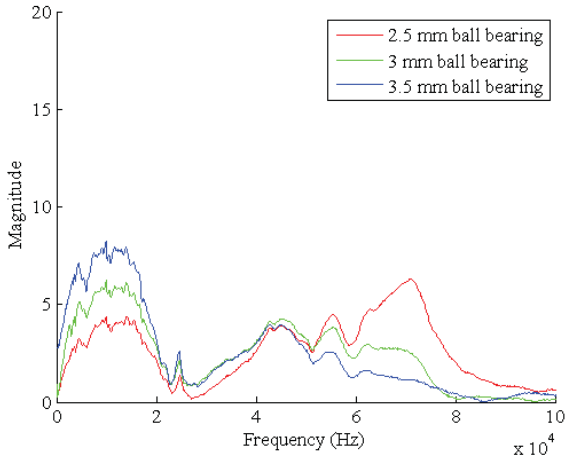

Fig. 6 Power spectra of the ball bearing impacts at 2.2 m/s

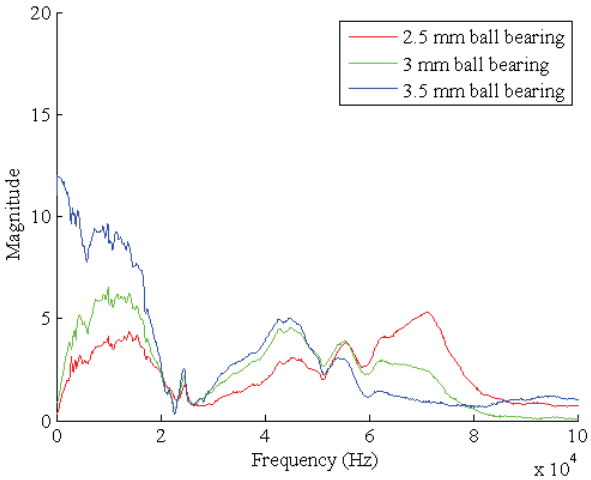

Fig. 7 Power spectra of the ball bearing impacts at 2.4 m/s

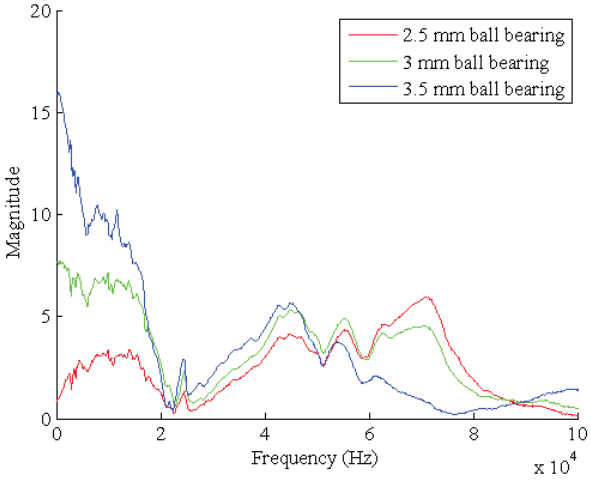

Fig. 8 Power spectra of the ball bearing impacts at 2.6 m/s

Fig. 9 - 11 shows the power spectra for the ball bearing with different impact velocities. They too show a high DC component for the higher impact velocities. For Fig. 6 – 11 there is a common frequency range (approximately between 5 kHz and 15 kHz) that is consistently proportional to the impact force due to a higher impact velocity or larger mass of the ball bearing.

A second order bandpass filter with a low cut-off frequency of 5 kHz and an upper cut-off frequency of 15 kHz was placed between the impact sensor's output and the ADC as shown in Fig. 3. This was done to remove the DC component caused by saturation and the high frequency components and only use the frequencies that were shown to be proportional to the impact force as seen in Fig. 6 – 11.

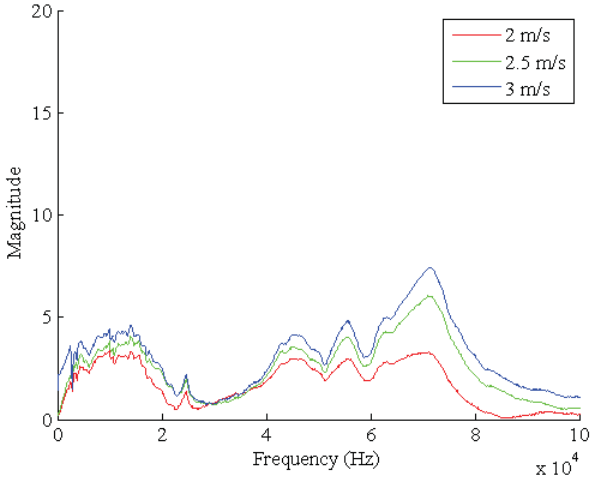

Fig. 9 Power spectra of 2.5 mm ball bearing impact signal

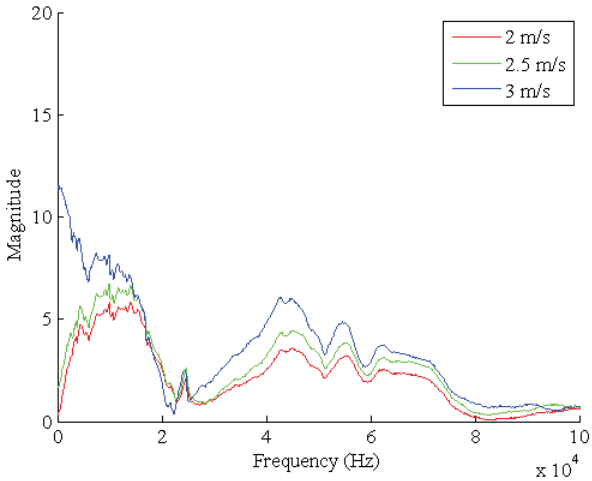

Fig. 10 Power spectra of 3 mm ball bearing impact signal

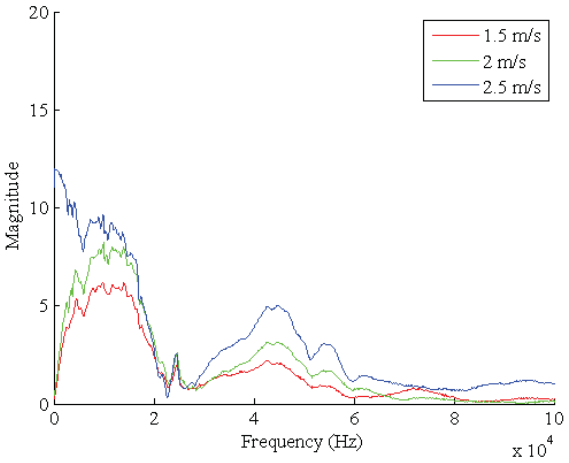

Fig. 11 Power spectra of 3.5 mm ball bearing impact signal

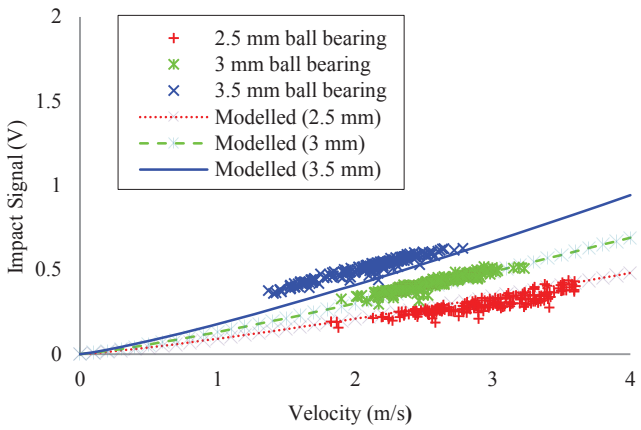

Fig. 12 Magnitude of dominant peak of ball bearing impact (with bandpass filter)

The same experiment was repeated again 200 times for all three ball bearing diameters using the bandpass filter. Fig. 12 shows the peak amplitude of the filtered impact signals. Fig. 12 also shows the calculated signal magnitude using the mechanical characteristics of the waveguide and the Delrin ball bearings and a range of impact velocities.

The signal output from the impact sensor agrees well with the calculated values using (8). However, the results from the 2.5 mm impacts show a higher deviation compared to the other two. This is believed to be due to the fact that, even though the guiding tube is centred above impact sensor waveguide, some of the 2.5mm ball bearings may not be impacting the centre of the waveguide. Also for higher impact forces the impact sensor output is greater than the calculated values (3.5 mm ball bearing impacts). This is possibly due to the higher impact force being able to overcome the adhesive effect between the rubber and the waveguide [14]. This indicates that for a spherical particle, if the particle velocity is known as well as the mechanical characteristic of the particle, particle size can be determined via impact analysis using the piezoelectric impact sensor.

VI. Conclusions

A new impact sensor using custom fabricated PVDF transducers has been designed, constructed and tested. Through analysis of the frequency component of the sensor output during impact it has been determined that selective filtering of frequency components of the impact signal has an effect on reducing the deviation of the peak magnitude of the impact signal.

The comparison between the calculated output signal values and the sensor outputs obtained during the experimentation agree well. This outcome indicates that, for a spherical particle, the piezoelectric impact sensor is capable of determining the size of the particle through impact analysis, assuming that the mechanical properties of the particle and particle velocity are known. For utilization of this sensor on a bulk solid conveying system the particle velocity would have to be independently measured using another sensing method such as electrostatic sensors [7].

The impact sensor proposed has a very small active sensing area, making it ideal for online particle size measurement on a pneumatic conveying system since the small active sensing area reduces the chance of simultaneous impacts of multiple particles occurring.

References

[1] Y. Yan, “Guide to the Flow Measurement of Particulate Solids in Pipelines”, Powder Handling & Processing, vol. 13, no. 4, October/November 2001.

[2] R. M. Carter, Y. Yan, P. Lee “On-line Nonintrusive Measurement of Particle Size Distribution through Digital Imaging”, IEEE Transactions on Instrumentation and Measurement, vol. 55, no. 6, pp. 2034 – 2038, 2006

[3] L. Gao, Y. Yan, G. Lu, “Contour-based Image Segmentation for On-line Size Distribution Measurement of Pneumatically Conveyed Particles”, Instrumentation and Measurement Technology Conference, pp. 285-289, Hangzhou, China, 10-12 May 2011.

[4] J. Q. Zhang and Y. Yan, “On-line Continuous Measurement of Particle Size Using Electrostatic Sensors”, Instrumentation and Measurement Conference, pp. 877-880, Vail, CO, USA, 20-22 May 2003.

[5] B. M. Meunier, P. M. Watts, J. S. Marshall, R. L. Dechene, W. Du, R. E. Newton, “Vibration Sensor for Particle Concentration Measurement in Pneumatic Pipeline Flows”, Measurement Science and Technology, vol. 2, no. 12, 2010.

[6] L. Gao, Y. Yan, R. M. Carter, D. Sun, P. Lee, C. Xu, “On-line Particle Sizing of Pneumatically Conveyed Biomass Particles Using Piezoelectric Sensors”, FUEL, vol. 113, pp. 810 – 816, November 2013.

[7] J. R. Coombes and Y. Yan, “Experimental investigations into the flow characteristics of pneumatically conveyed biomass using an electrostatic cross sectional sensor array”, FUEL, vol. 151, pp. 11 – 20, July 2015.

[8] Y. Hu, L. Wang, X. Huang, X. Qian, L. Gao, Y. Yan, “On-line Sizing of Pneumatically Conveyed Particles Through Acoustic Emission Detection and Signal Analysis”, IEEE Transactions on Instrumentation and Measurement, vol. 64, no 5, pp. 1100 – 1109, May 2015.

[9] P. Müller, M. Trüe, R. Böttcher, J. Tomas, “Acoustic evaluation of the impact of moist spherical granules and glass beads”, Powder Technology, vol. 278, pp. 138 – 149, July 2015.

[10] H. Hertz, Über die berührung fester elastischer Körper (On the contact of rigid elastic solids). In: Miscellaneous Papers. Jones and Schott, Editors, J. reine und angewandte Mathematik 92, Macmillan, London (1896), p. 156 English translation: Hertz, H.

[11] S. Antonyuk, S. Heinrich, J. Tomas, N. G. Deen, M. S. van Buijtenen and J. A. M. Kuipers, “Energy absorption during compression and impact of dry elastic-plastic spherical granules”, Granular Matter, vol. 12, no 1, pp. 15 – 47, 2010.

[12] K. Uchino, “Advance Piezoelectric Materials”, Woodhead Publishing, Cambridge, UK, ISBN 978-1-84569-534-7.

[13] Measurement Specialties Inc. “Piezo Film Sensors Technical Manual”, REV B 02 APR 99.

[14] N.K. Myshkin, M.I. Petrokovets and A.V. Kovalev, “Tribology of polymers: Adhesion, friction, wear, and mass-transfer”, Tribology International, vol. 38, no 11, pp. 910 – 921.

Measurement of Velocity and Concentration Profiles of Pneumatically Conveyed Particles Using an Electrostatic Sensor Array

James Robert Coombes and Yong Yan, *Fellow, IEEE*

***Abstract*— The ability to monitor the velocity and concentration profiles for the whole diameter of a pipe would allow the complex flow dynamics associated with particles in a pneumatic suspension to be measured. This paper presents a method of online monitoring of the particle velocity and particle concentration for the whole diameter of the pipe for a pneumatic bulk solid conveying system. This is achieved using an array structure of five electrostatic sensors across the whole diameter of the pipe to measure the particle velocity and concentration profiles. Experimental tests were carried out on a laboratory-scale test rig over a range of particle velocities. The results show that the electrostatic sensor array is capable of measuring the multiple velocities and concentrations that occur across the diameter of a pneumatic conveying pipe. Through the analysis of velocity and correlation coefficient data, flow across the diameter of the pipe including that along the pipe wall is determined to have more turbulence than the flow at the center of the pipe.**

***Index Terms*— Concentration profile, electrostatic sensor, mass flow rate, pulverized fuel, sensor array, velocity profile.**

I. Introduction

DILUTE gas–solid transport systems are used in a variety of industries such as chemical, steel, and energy. The concentration of solids in dilute gas–solid flow is less than 0.1% by volume, which presents a well-known measurement challenge [1]. Being able to monitor the velocity profile and particle concentration for the whole diameter of the pipe would allow the mass flow rate to be accurately monitored and achieve an in-depth understanding of gas–solid two-phase flows, allowing comparison and validation to be made between practical experiments and computational fluid dynamic simulations.

Nowhere is this more important than in the energy industry where accurately monitoring the mass flow rate of the fuel is important in improving burning efficiency and reducing slagging and emissions. Now that many coal fired power plants across the world are being converted to cofiring with a mixture biomass or 100% biomass fueling to increase the amount of renewable energy generated, the particle flow dynamics inside the pipe have become more complex due to the irregular shape and generally wider size range biomass particles.

To this end, a diverse range of sensor paradigms have been developed and proposed to monitor particle velocity and concentration in a bulk solid pneumatic conveying system; these include capacitive [2]–[6], radiometric [7], optical [8]–[11], acoustic/ultrasonic [12], microwave [13], and heat transfer method [14]. All of these types of sensors have the advantage of being nonintrusive and capable of monitoring both particle velocity and concentration. However, capacitive sensors are susceptible to moisture, which can affect the dielectric properties of the material being monitored [6]. Radiometric sensors have the drawbacks that they contain a radioactive material and their use is governed by administratively inconvenient health and safety regulations. Optical sensors have the shortcoming that they require a transparent window in the pipe that is susceptible to contamination and abrasion by the pulverized material. Nonetheless, this drawback can be addressed using an air purging system to reduce contamination [10]. Acoustic/ultrasonic sensors are susceptible to false signals that can result in error and the optimum frequency is linked to particle size distribution [15]. Microwave sensors have the disadvantage that they have a moderate accuracy and a relatively high cost [13]. The heat transfer method is mainly suited for dense-phase flow measurement [14]. However, electrostatic sensors due to their robustness and low cost have the advantage over other sensors. There are three main designs of electrodes used for electrostatic sensors: ring, arc, and probe electrodes [11], [16]–[19].

Ring electrodes are constructed within the pipe wall, and because of this, they have the advantage of being completely noninvasive since they do not impede the particle flow in the pipe. They do, however, have disadvantages in that they are more sensitive to particles in close proximity to the pipe wall [16]. Then again when ring electrodes are used to measure the particle velocity in a multiphase flow using the cross-correlation method, this will reduce the quality of the correlation coefficient between the upstream and downstream because different parts of the particle flow in the pipe cross section will be traveling at different velocities [16]. Particle velocity has also been determined using ring electrodes in a linear array configuration. Xu *et al.* [17] used a linear electrostatic sensor array to determine the particle velocity using the spatial filtering method. It was determined through experimentation and

Manuscript received June 19, 2015; revised September 1, 2015; accepted October 9, 2015. Date of publication November 9, 2015; date of current version April 5, 2016. The Associate Editor coordinating the review process was Dr. Huang-Chen Lee. *(Corresponding author: Yong Yan.)*

The authors are with the School of Engineering and Digital Arts, University of Kent, Canterbury CT2 7NT, U.K. (e-mail: y.yan@kent.ac.uk; jrc55@kent.ac.uk).

Color versions of one or more of the figures in this paper are available online at http://ieeexplore.ieee.org.

Digital Object Identifier 10.1109/TIM.2015.2494620

finite-element modeling (FEM) that the optimum number of electrodes should be between 4 and 10. It was also suggested that the ratio between the electrode spacing compared with the electrode width should be between 7 and 10, and the ratio of the electrode width to the pipe radius should be in the range 0.1–0.2.

Probe electrodes differ from ring and arc electrodes in that they have the disadvantage that they are an invasive sensor technology. However, in dilute phase flow, this does not cause a significant problem due to the very low particle concentration. Also the small cross-sectional area of the probe electrodes means that they obstruct a small proportion of the pipe cross section. Shao *et al*. [16] investigated this type of electrostatic sensor through a combination of practical online experimentation and offline FEM. One of the design aspects of the probe electrodes was the optimum depth of the probe. It was discovered that a probe depth of 0.3–0.5 of the pipe diameter would give a realistic approximation of the average particle velocity. Shao *et al.* [16] also compared the probe electrode with the ring electrode and found that using the cross-correlation method to determine the particle velocity, the probe electrode had a higher correlation coefficient (around 0.55–0.75) compared with the ring electrode (around 0.35–0.5).

The basic design of the electrostatic sensor array along with the preliminary experimental results was reported in [20]. This extended version of the paper presents in detail the design considerations, construction, and systematic assessment of the sensor array that were not covered in [20] and [21].

Electrostatic sensors have also been applied to measure the volumetric concentrations of the particles inside the pipe, as presented in [22]. The principle of using electrostatic sensors to determine particle concentration is that as the particle concentration increases, so does the magnitude of the electrostatic charge. Since the electrostatic sensors are designed to detect moving particles, the level of the charge is determined by measuring the magnitude of the change in the signal [22]. However, Yan [23] discusses that there are limitations to using electrostatic sensors to determine particle concentration in that the electrostatic signal is affected by particle variables such as particle size, how long the conveyed particles have had to precharge, and dielectric properties of the material being conveyed. Moreover, the environment inside the pipe, such as temperature and humidity, can be a factor. This paper presents an in-depth design and implementation of an electrostatic sensor array that is capable of measuring the particle flow dynamics that occur in the pipe that previous electrostatic sensors (probe [16], ring [16]–[18], and arc [18]) were unable to achieve.

II. Measurement Principle

An often unwanted phenomenon of pneumatic conveying systems (for safety reasons) is that as solid particles are conveyed down a pipe, they pick up electrostatic charge [24]. The level and distribution of this charge is random due to the nature of how it is generated inside the pipe through interaction and friction between air and other particles [24]. Using an electrostatic sensor the charge carried by the particles can be detected as the particles pass the sensor electrode. This is because a small amount of charge is induced on the sensor electrode [25].

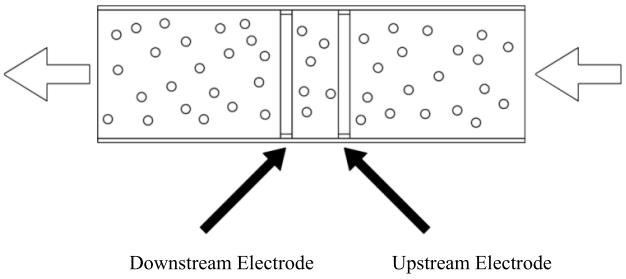

Fig. 1. Electrode configuration inside a pipe.

The electrostatic sensor consists of an insulated electrode and a signal conditioning circuit that takes the charge induced on the electrode and converts it into a voltage signal that can be digitized by an analog-to-digital converter (ADC).

There are two methods to determine particle velocity using electrostatic sensors: the spatial filtering method [17] and the cross-correlation method [23]. Since the spatial filtering method uses a linear array of electrodes, it was unsuitable for use with the electrostatic sensor array presented in this study due to space constraints on the sensor blade. Using the cross-correlation method to measure particle velocity of particles traveling inside the pneumatic conveying pipe involves the use of two electrodes arranged in a configuration as shown in Fig. 1 [25].

Since the distance between the upstream and downstream electrodes is known, particle velocity (V_c) can be calculated from

$$V_c = \frac{L}{\tau_m} \tag{1}$$

where L is the spacing between the upstream and downstream electrodes and τ_m is the time difference between the upstream and downstream signals. To determine τ_m, the upstream and downstream signals have to be digitized using an ADC. It is at this point that the resolution and sampling rate of the ADC have to be taken into account; the resolution of the ADC has to be sufficiently high enough to ensure minute changes in the charge picked up by the electrodes can be detected: the sampling rate of the ADC has to ensure that the resolution in the time domain is higher than the possible delay τ_m between the upstream and downstream signals. To determine τ_m, the cross-correlation method is used. The delay between the two signals is determined from the location of the dominant peak in the cross-correlation function [23]. The cross-correlation method in (2) is used since the cross correlation is carried out on an embedded microcontroller and computational resources are limited

$$Rxy[m] = \frac{1}{N}\sum_{n=1}^{N} x[n]y[n+m] \tag{2}$$

where $x[n]$ and $y[n]$ are the digitized signals from the upstream and downstream electrodes, respectively,

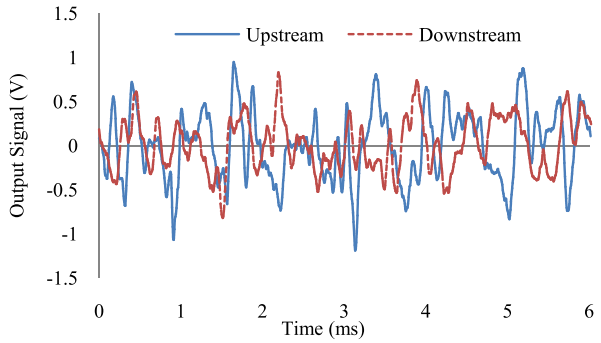

Fig. 2. Upstream and downstream signals from electrostatic sensors.

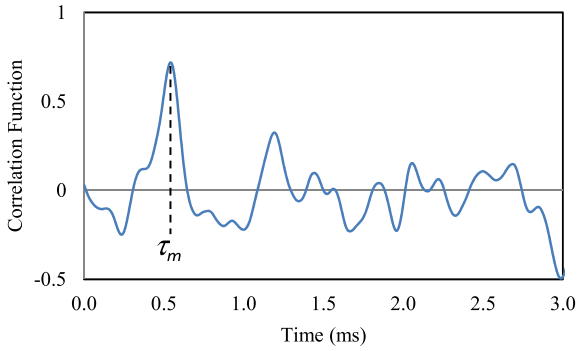

Fig. 3. Correlation function between the upstream and downstream sensor signals.

shown in Fig. 2. The position of the dominant peak for the resulting correlation function known as the correlation coefficient indicates the delay between the upstream and downstream signals, as shown in Fig. 3.

Since the resulting signal from the sensor is random [22], the particle concentration is determined and represented by the magnitude of the root-mean-square (rms) charge level of the electrostatic signal detected by the electrostatic sensor

$$V_{\text{rms}} = \sqrt{\frac{\sum_{n=1}^{N} x[n]^2}{N}} \tag{3}$$

where x is the signal from the electrostatic sensor electrode, n is the sample number, and N is the total number of samples. Conversely, the exact particle concentration cannot be determined via this method due to variables such as particle size, type of particles, and particle velocity [23].

III. Sensor Design

Like the probe electrode design, the electrostatic sensor array is an intrusive sensor that comes into contact with the particle flow. However, unlike the probe sensor, the sensor array spans the whole diameter of the pipe and is divided into five pairs of identical electrodes, as shown in Fig. 4. Due to the invasive nature of the sensor array design, all attempts have been made to reduce the thickness of the sensor, which is currently 2.5 mm thick. Each electrode has a width of 1 mm and a length of 8 mm and the electrode pairs (upstream/downstream) are set 10 mm apart. The sensor array is a blade design and has only electrodes on one side. The leading edge of the sensor array is a 45° knife edge intended to increase the aerodynamics of the sensor array. In addition, the 45° edge deflects most of the turbulence and velocity change caused by the sensor array behind the electrodes, as shown in Fig. 5. This design of the sensor array can be easily adopted for larger size ducting (150 mm in diameter and larger) as found in pulverized fuel-fired power stations. The use on larger diameter ducting would also allow more elements of the array to be added to increase the resolution of the measured velocity and concentration profiles.

The electrodes are fabricated out of copper and are etched onto the printed circuit board. The preamplifier for the electrostatic sensors is constructed inside the sensor array blade to reduce the connection distance between the electrode and the preamplifier, subsequently reducing unwanted noise. The outer casing of the sensor array blade is fabricated from a metal that is earthed to shield the preamplifier from unwanted noise. For practical versions of the electrostatic sensor array, the blade and electrodes can be coated with a durable material to improve abrasive resistance. The physical size of the electronics for the preamplifiers was the determining factor of the number of electrodes that could be constructed across the diameter of the pipe. The signal from the preamplifier is then passed through a variable secondary amplifier and an antialiasing low-pass filter with a cut off frequency of 15 kHz in order to remove high-frequency noise. Care was taken during the construction of the entire signal conditioning circuits to ensure that each was matched to each other. An analog multiplexer controlled from the microcontroller selects each element of the array. The analog signal is digitized in an external 12-bit ADC with a sampling rate of 150 kHz (10 times the highest frequency component of the signal), which is mounted near the signal conditioning circuit and is connected to the microcontroller via a serial peripheral interface bus. All analog parts of the signal conditioning circuit are shielded against external noise. The cross-correlation processing software is embedded into a 32-bit 100-MHz microcontroller, which outputs to a PC as shown in Fig. 6. The microcontroller is capable of calculating the velocity using the cross-correlation method for a single pair of electrodes in approximately 100 ms. Consequently, the system has a refresh rate for the measurement of the velocity, concentration, and correlation coefficient profiles of approximately 0.5 s.

IV. Experimental Setup

The sensor array is mounted inside a custom 50-mm bore spool piece that allows the sensor array to be rotated around the cross-sectional axes shown in Fig. 4. Experiments were carried out using flour in a dilute flow with a flow rate of 1.8 kg/h on a negative pressure bulk solid conveying test rig (Figs. 7 and 8). All pipework on the test rig is constructed from stainless steel for abrasive resistance and is grounded for safety. The lack of established standards and traceability in the field of particle flow measurement is one of the challenges

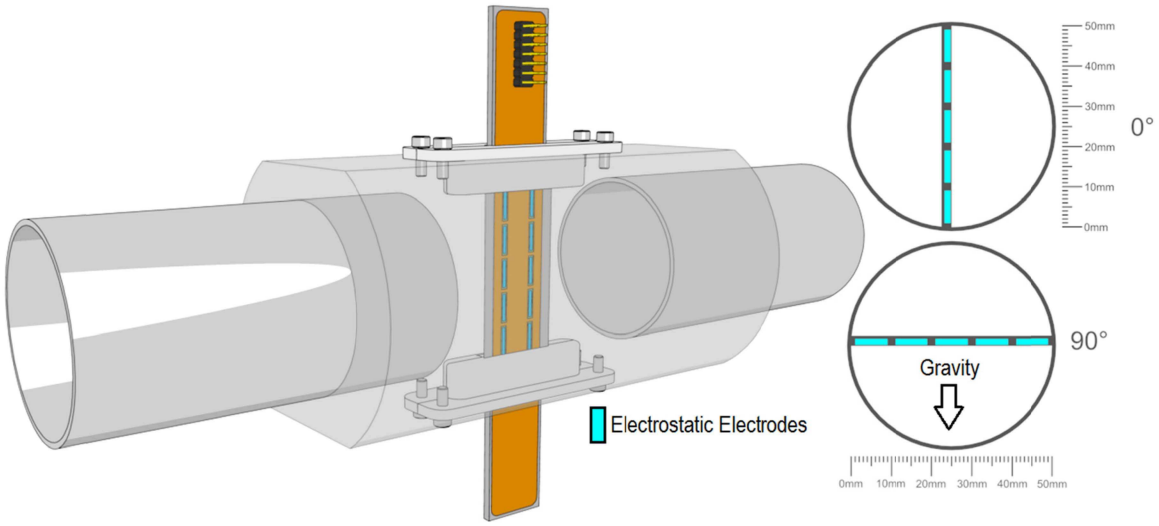

Fig. 4. Electrostatic array mounted inside a pipe spool with diagram of pipe cross section.

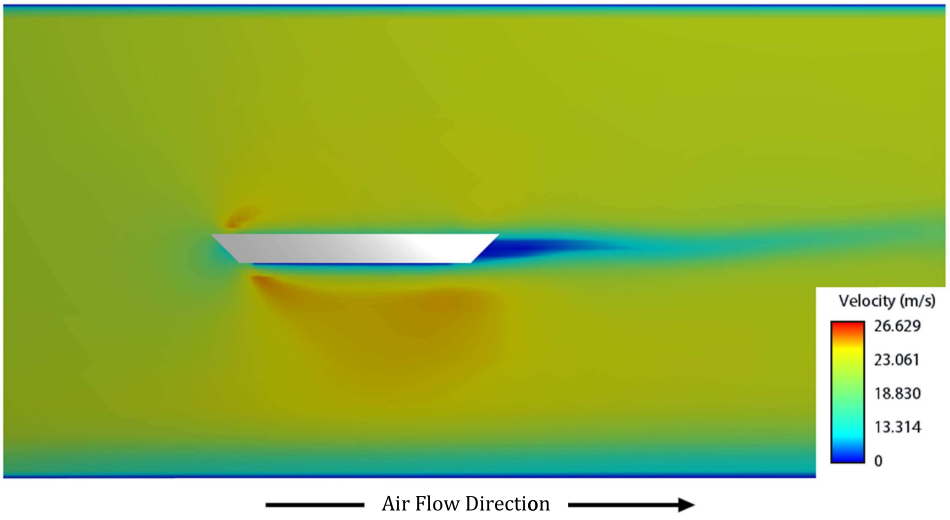

Fig. 5. Wind tunnel simulation of the effect of the sensor array on air velocity.

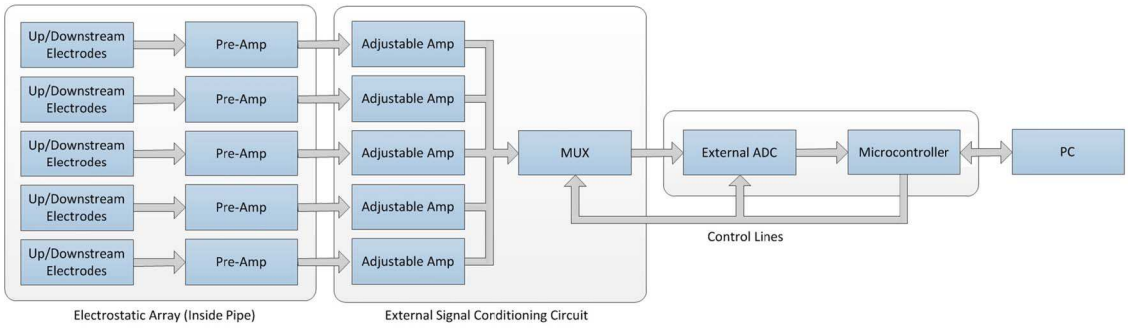

Fig. 6. Block diagram of the electrostatic-array-sensor-based particle measurement system.

researchers have to face when developing techniques to resolve the difficult industrial measurement problems [25]. In this paper, air velocity profiles were determined as a reference using a commercial hot-wire anemometer with readings taken from a pipe at the same location of the sensor array. During the experiments, ambient temperature (25.3 °C average) and relative humidity (47.5% average) were monitored to ensure that environmental test conditions were the same for each test.

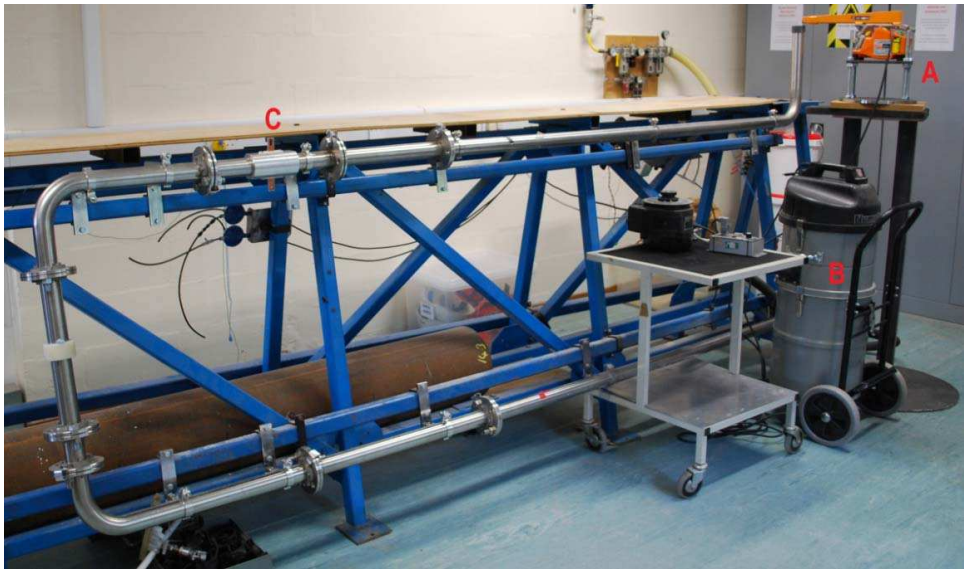

Fig. 7. Photo of the particle flow test rig. A: vibration feeder, B: variable vacuum unit, and C: sensor spool.

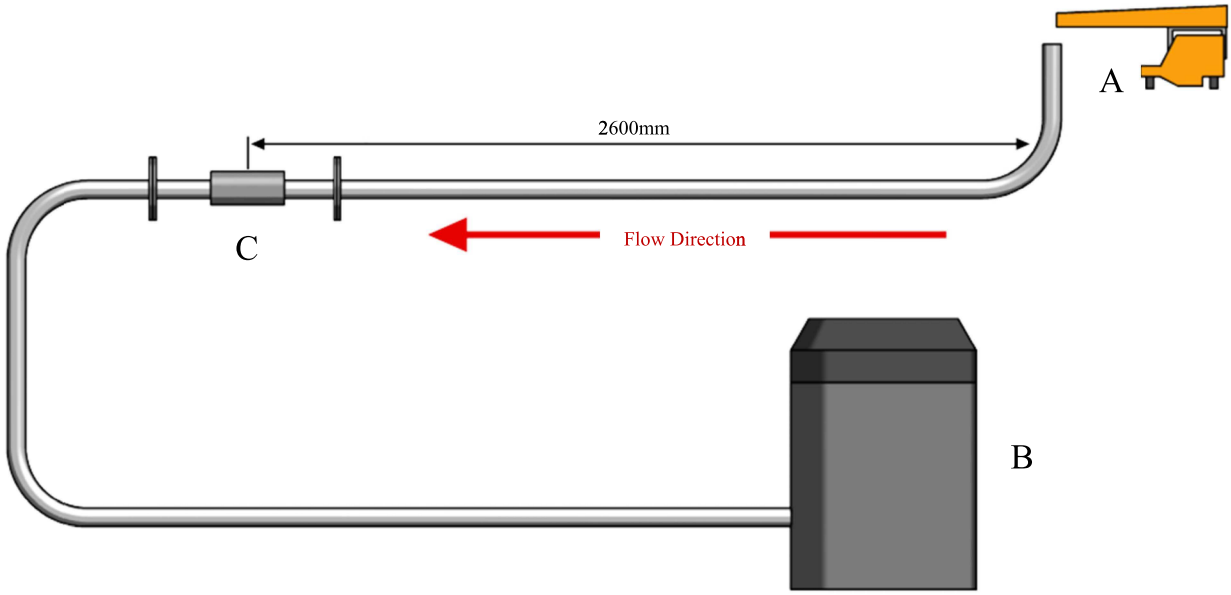

Fig. 8. Layout of particle flow test rig. A: vibration feeder, B: variable vacuum unit, and C: sensor spool.

Experiments were carried out with the sensor array mounted on a horizontal pipe section with the array mounted in two orientations 0° and 90°, as shown in Fig. 4. The electrostatic sensor array is mounted 2.6 m (52 pipe diameters) from the right angle pipe section on the feeder input to ensure the measurement of the developed flow. Tests were carried out with five different air velocities (reference air velocity measurements taken from the center of the pipe). After each experiment, the filter on the vacuum plant was cleaned to ensure consistency. For each pair of electrodes, the cross correlation used 1024 samples on both the upstream and downstream electrodes. A total of 500 velocity, concentration, and correlation coefficient readings were taken on each element of the array for each air velocity. It has been observed that the particle size and shape have an effect on particle flow stability [21]. In this study, the particle size and shape (Figs. 9–11) were measured using an in-house particle imager [26]. The particle shape was quantified by measuring the particle aspect ratio (shortest to the longest diameters across the particle). The aspect ratio distribution shown in Fig. 11 indicates that the majority of the flour particles are spherical in shape.

V. Results

The sensor array was able to determine the particle velocity and particle concentration for the diameter of the pipe. Figs. 12 and 13 show the mean velocity profile for a range of air velocities (20.3–24.3 m/s). The profiles clearly show

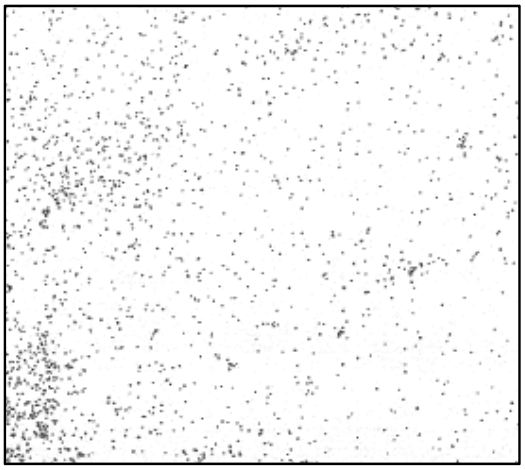

Fig. 9. Scan image of flour particles (not to scale).

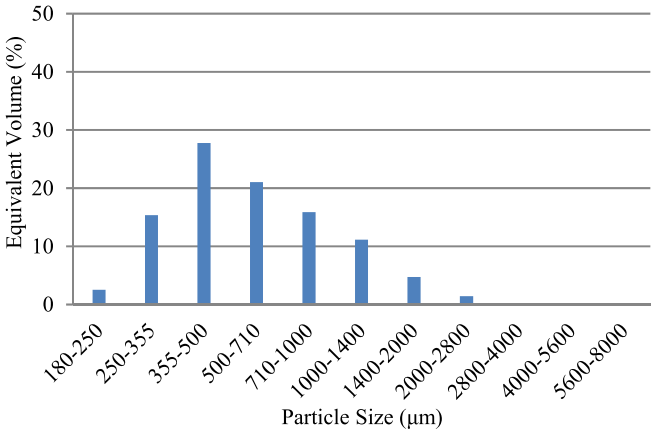

Fig. 10. Particle size distribution of flour particles.

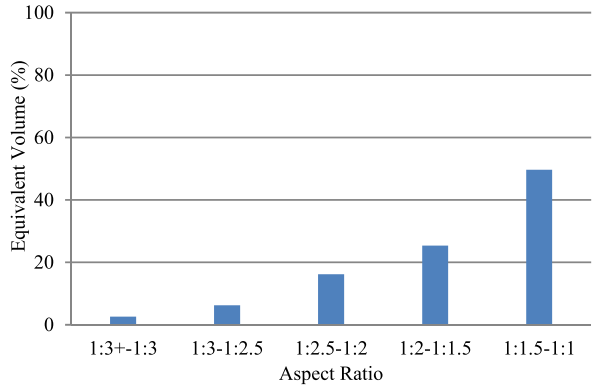

Fig. 11. Aspect ratio distribution of flour particles.

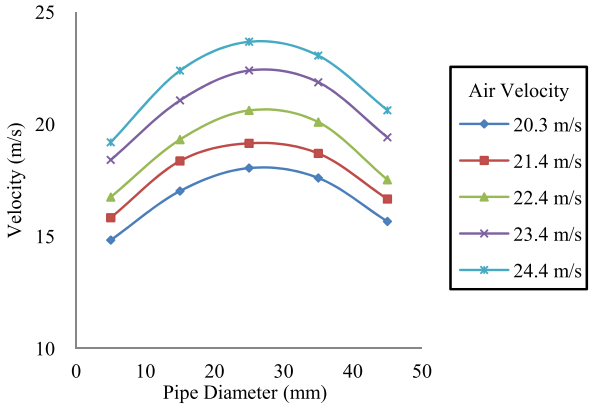

Fig. 12. Mean velocity profile measured by the sensor array at 0° (data points indicate the center of the electrode).

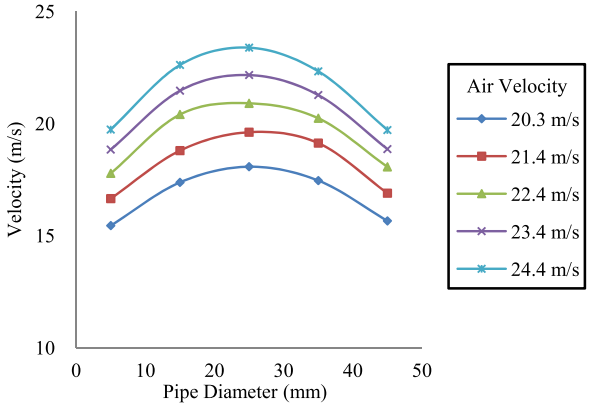

Fig. 13. Mean velocity profile measured by the sensor array at 90°.

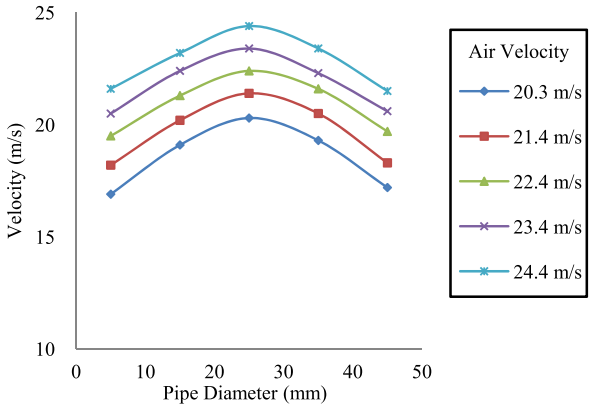

Fig. 14. Air velocity profiles measured using a hot-wire anemometer for the sensor array at 0°.

that particles traveling at the center of the pipe are moving at a higher velocity than those moving along the pipe wall due to the frictional force acting on the conveying air and particles caused by interaction with the pipe wall. The 0° velocity profile in Fig. 12 shows that the velocity at the bottom of the pipe (5 mm) is lower than the velocity at the top of the pipe (45 mm); this is due to gravity's effect on the particles forcing them to come into contact with the pipe wall at the bottom of the pipe. On the other hand, Fig. 13 shows the velocity profile for 90°, which is more symmetrical compared with the velocity profile for 0° since gravity is having a uniform effect over the whole diameter. Figs. 14 and 15 show the air velocity profiles as measured using a commercial hot-wire anemometer in both 0° and 90° orientations. Fig. 16 shows the particle velocity compared with the conveying air velocity at the center of the pipe. As expected, Figs. 14–16 show that the particle velocity is lower than the conveying

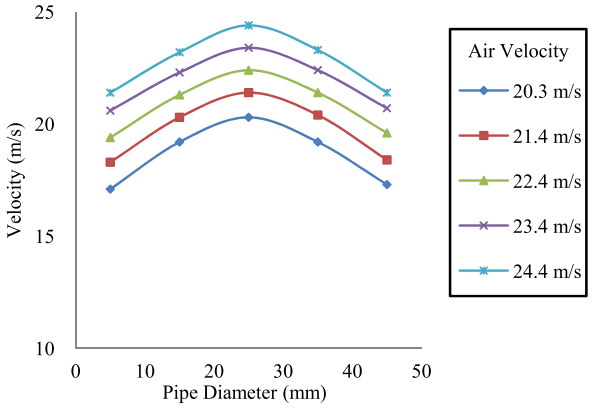

Fig. 15. Air velocity profiles measured using a hot-wire anemometer for the sensor array at 90°.

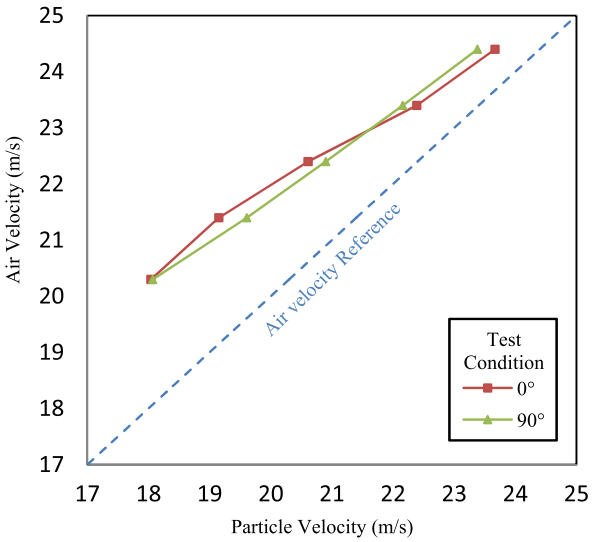

Fig. 16. Air velocity compared with particle velocity at the center of the pipe.

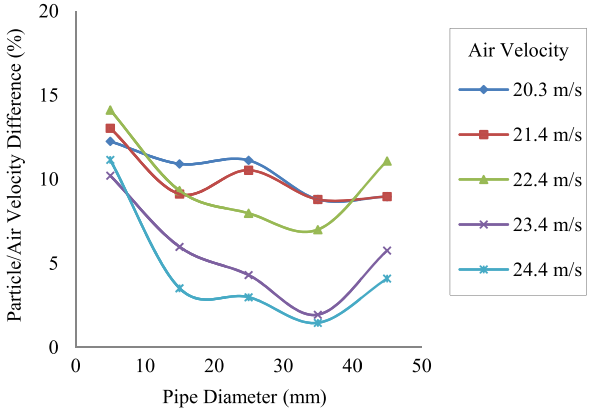

Fig. 17. Percentage difference between the air and particle velocity profiles for the sensor array at 0°.

air velocity. A detailed comparison of the particle and air velocity profiles, as shown in Figs. 17 and 18, shows that the difference between the particle and air velocities decreases for higher air velocities, indicating that higher air velocities are

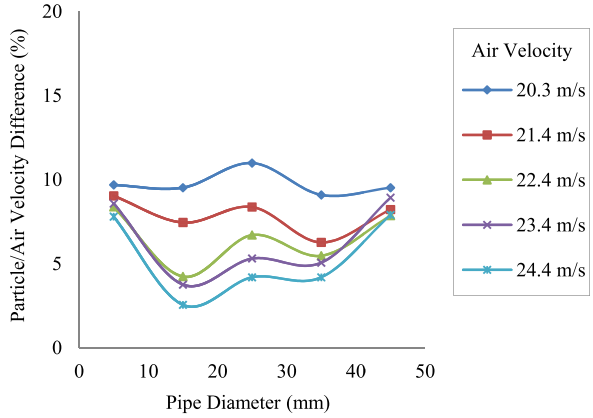

Fig. 18. Percentage difference between the air and particle velocity profiles for the sensor array at 90°.

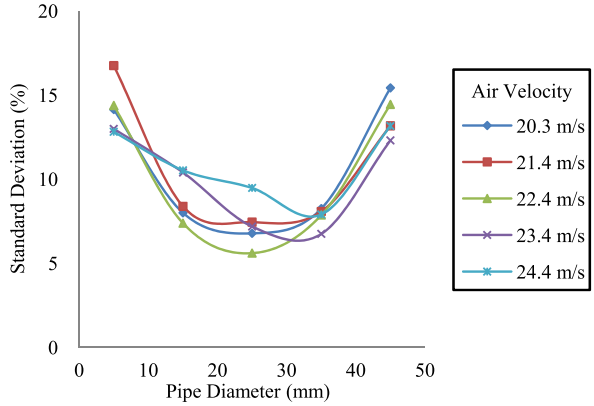

Fig. 19. Normalized standard deviation profile of the velocities measured by the electrostatic array sensor at 0°.

better at keeping the particles in a suspension. The reason for the difference between the conveying air velocity and particle velocity is because the process of conveying and suspending the particles is one of the drag forces, and hence, the particle velocity will be lower than the conveying air [24]. Typically in a horizontal pipe, the particle velocity is 80% of the conveying air velocity. However, this value can vary depending on the parameters such as particle size, shape, and density [24]. Conversely, the effect of friction between the pipe wall and particle flow can be observed in Figs. 17 and 18, where the difference between the particle and air velocities is higher at 5 and 45 mm (however, this observation only holds true at higher air velocities, and at lower air velocities 20.3 and 21.4 m/s, it has a more uniform profile since the particles may not be fully suspended). The effect of gravity can be observed in Fig. 17 where the difference between the measured air velocity and the particle velocity is higher the closer to the bottom of the pipe (5 mm) the measurement is taken.

The normalized velocity standard deviation profile shown in Figs. 19 and 20 shows that the particle velocities measured in the center of the pipe have a lower deviation compared with those along the pipe wall, indicating a more stable particle flow in the center of the pipe. These results are consistent with the previous investigations carried out using pulverized biomass in [21].

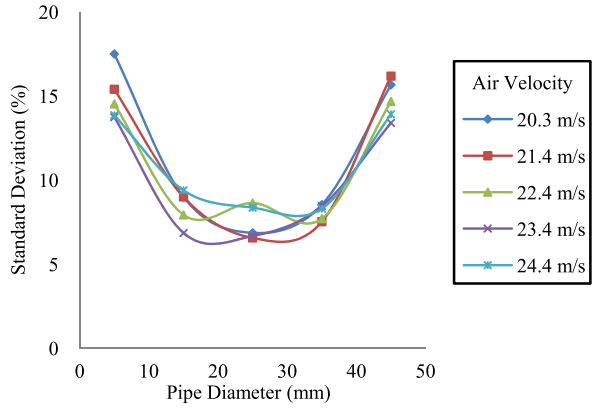

Fig. 20. Normalized standard deviation profile of the velocities measured by the electrostatic array sensor at 90°.

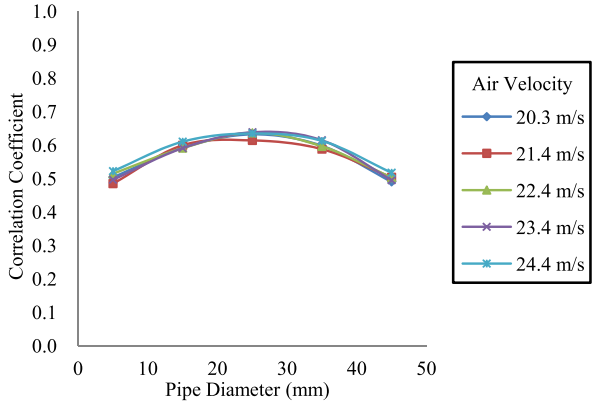

Fig. 23. Mean correlation coefficient profile for the pipe cross section at 0°.

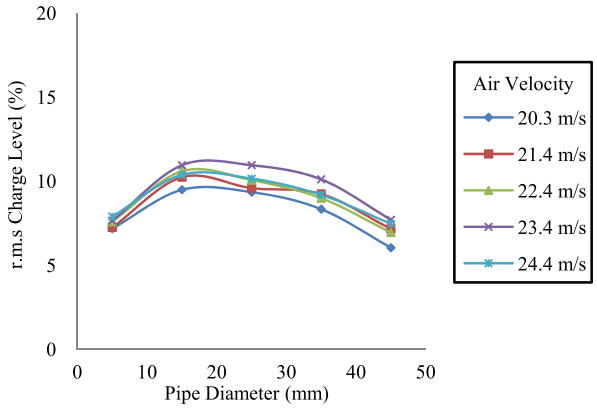

Fig. 21. Mean particle concentration profile using the normalized rms charge value to measure particle concentration at 0°.

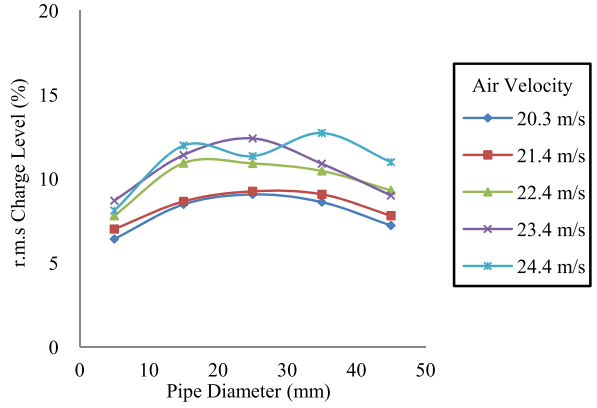

Fig. 22. Mean particle concentration profile using the normalized rms charge value to measure particle concentration at 90°.

The particle concentration shown in Fig. 21 shows that the concentration increases closer to the bottom of the pipe due to the effect of gravity. However, at the very bottom of the pipe (5 mm), the particle concentration is less than that measured on the above sensor element (15 mm). Similar experimentation carried out using different particle sizes of pulverized biomass [21] does not encounter this phenomenon. A possible reason for this is that the particle size of the flour used in this experiment is smaller than the willow biomass particles [21], as shown in Figs. 9–11. The smaller flour particles would have a lower mass than the larger biomass particles and would therefore be affected more by the turbulence caused by the proximity of the sensor blade and the pipe wall. This turbulence would mean that the smaller particles would be unable to enter the smaller volume of space at the bottom of the pipe between the sensor blade and pipe wall, thus causing less particles to be detected by the sensor. However, for larger pipe bores, this effect would be less dramatic since the pipe radius would be increased. The phenomenon of reduced particle concentration along the pipe wall can be seen on the 90° particle concentration profile (Fig. 22), which shows that the concentration in the center of the pipe is higher than that along the pipe wall. Another possibility is that smaller particles are affected more by the discharging effect of coming into contact with the pipe wall due to the steel pipe being earthed for safety reasons. Fig. 22 also shows that for the higher air velocities (22.4–24.4 m/s), the rms charge is increasing in the center of the pipe (with exception to the rms measured at the center of the pipe for 24.4 m/s. This is most likely due to a disruption of the particle input on the vibration feeder since it does not appear under other air velocity conditions). This is feasibly due to the fact that at higher air velocities, more particles are being suspended. Consequently, more particles are able to be detected by the sensor array in the 90° orientation.

The magnitude of the correlation coefficient is an indication of the stability of the particle flow [18] (the more closer to 1 the correlation coefficient is, the more stable the flow). Figs. 23 and 24 show the correlation coefficient profiles (0° and 90°, respectively). For the pipe diameter, it is clear that the correlation coefficient is higher in the center of the pipe compared with that along the pipe wall, demonstrating that the particle flow is more stable in the center of the pipe, which is consistent over all five air velocities.

The normalized standard deviation of the correlation coefficient with the sensor array in the 0° orientation shown in Fig. 25 agrees well with the standard deviation of the velocity in the same orientation (Fig. 19), with the correlation coefficient deviating less in the center of the pipe compared

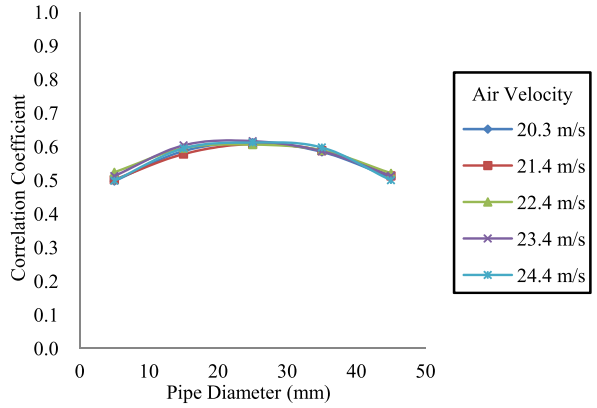

Fig. 24. Mean correlation coefficient profile for the pipe cross section at 90°.

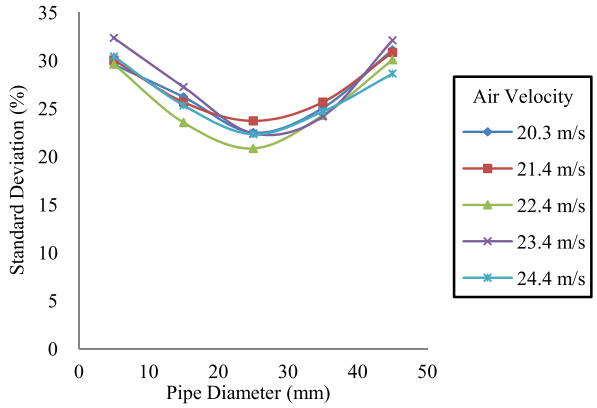

Fig. 25. Normalized standard deviation profile of the correlation coefficient measured by the electrostatic array sensor at 0°.

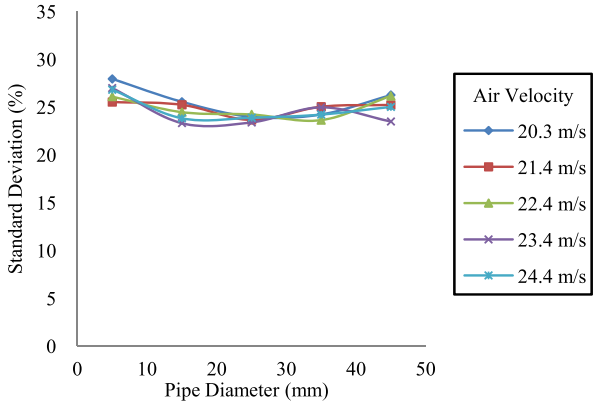

Fig. 26. Normalized standard deviation profile of the correlation coefficient measured by the electrostatic array sensor at 90°.

with that along the pipe wall. However, the normalized standard deviation of the correlation coefficient with the sensor array in the 90° orientation (Fig. 26) does not agree with the standard deviation of the velocity in the 90° orientation (Fig. 20). The normalized standard deviation shows that the correlation coefficient deviated more evenly over the pipe diameter with only a small reduction in the deviation in the center of the pipe. This effect is not fully understood. Reference [21] using fine pulverized biomass with the electrostatic sensor array in the 90° orientation on a horizontal pipe showed significantly less deviation in the center of the pipe. This is possibly an indication that a combination of turbulence (caused by the sensor array interacting with the particle flow), a smaller particle size/mass and gravity (since gravity is having a uniform effect), has a significant effect on the standard deviation of the correlation coefficient on a horizontal pipe at 90° orientation.

VI. Conclusion

An electrostatic sensor array has been designed, constructed, and tested, which is capable of monitoring the particle velocity and concentration profiles for the diameter of a pneumatic conveying pipe. The sensor array comprises five independent electrostatic sensing elements across the whole diameter of the pipe. Through the analysis of the velocity profiles as well as correlation coefficient profiles, it is clear that the performance of the electrostatic sensor array is in line with particle flow dynamics inside a pipe. It has been found that the particle flow in the center of the pipe is more stable than the particle flow along the pipe wall. A direct comparison between the air velocity profile (measured using a hot-wire anemometer) and the particle velocity profile (measured using the electrostatic sensor array) has shown that the interaction with the pipe wall results in velocity loss in the conveyed particles due to friction. The effect of gravity has also been observed on a horizontal pipe, since particles at the bottom of the pipe move slower than those at the top of the pipe.

References

[1] Y. Yan, "Guide to the flow measurement of particulate solids in pipelines—Part 1: Fundamentals and principles," *Powder Handling Process.*, vol. 13, no. 4, pp. 343–352, Oct./Nov. 2001.

[2] A. Fuchs and H. Zangl, "Single-layer measurement of particle velocity and concentration in pneumatic dilute phase conveying," in *Proc. IEEE Sensors Conf.*, Irvine, CA, USA, Oct./Nov. 2005, pp. 1–4.

[3] A. Fuchs, H. Zangl, G. Brasseur, and E. M. Petriu, "Flow-velocity measurement for bulk granular solids in pneumatic conveyor pipes using random-data correlator architecture," *IEEE Trans. Instrum. Meas.*, vol. 55, no. 4, pp. 1228–1234, Aug. 2006.

[4] A. Fuchs and H. Zangl, "A capacitive single-layer approach for particle velocity estimation in pneumatic dilute phase conveying," *IEEE Sensors J.*, vol. 6, no. 6, pp. 1722–1727, Dec. 2006.

[5] X. X. Wang, J. B. Yan, H. L. Hu, and Z. Y. Luo, "An ECT flow regime identification technology for gas/solid two-phase flow phase concentration measurement," in *Proc. 2nd Int. Conf. Instrum. Meas., Comput., Commun. Control*, Harbin, China, Dec. 2012, pp. 1318–1321.

[6] J. Zhang, H. Hu, J. Dong, and Y. Yan, "Concentration measurement of biomass/coal/air three-phase flow by integrating electrostatic and capacitive sensors," *Flow Meas. Instrum.*, vol. 24, pp. 43–49, Apr. 2012.

[7] I. R. Barratt, Y. Yan, B. Byrne, and M. S. A. Bradley, "Mass flow measurement of pneumatically conveyed solids using radiometric sensors," *Flow Meas. Instrum.*, vol. 11, no. 3, pp. 223–235, Sep. 2000.

[8] D. Song, L. Peng, G. Lu, S. Yang, and Y. Yan, "Velocity measurement of pneumatically conveyed particles through digital imaging," *Sens. Actuators A, Phys.*, vol. 149, no. 2, pp. 180–188, Feb. 2009.

[9] R. M. Carter, Y. Yan, and P. Lee, "On-line nonintrusive measurement of particle size distribution through digital imaging," *IEEE Trans. Instrum. Meas.*, vol. 55, no. 6, pp. 2034–2038, Dec. 2006.

[10] L. Gao, Y. Yan, and G. Lu, "Contour-based image segmentation for on-line size distribution measurement of pneumatically conveyed particles," in *Proc. IEEE Instrum. Meas. Technol. Conf.*, Hangzhou, China, May 2011, pp. 1–5.

[11] X. Qian, Y. Yan, L. Wang, and J. Shao, "An integrated multi-channel electrostatic sensing and digital imaging system for the on-line measurement of biomass–coal particles in fuel injection pipelines," *Fuel*, vol. 151, pp. 2–10, Jul. 2015.

[12] D. A. Abernethy, M. J. Millen, and B. D. Sowerby, "Plant trial of an ultrasonic gauge for the on-line measurement of pulverised coal mass flow," in *Proc. IEEE Instrum. Meas. Technol. Conf.*, Brussels, Belgium, Jun. 1996, pp. 667–670.
[13] A. Penirschke, A. Rijiranuwat, H. Maune, M. Schüßler, and R. Jakoby, "Microwave mass flow sensor for process monitoring applications," in *IEEE MTT-S Int. Microw. Symp. Dig.*, Atlanta, GA, USA, Jun. 2008, pp. 1195–1198.
[14] Y. Zheng, D. McGlinchey, J. Pugh, and Y. Li, "Experimental investigation on heat transfer mechanisms of pneumatically conveyed solids' plugs as a means to mass flow rate measurement," *Flow Meas. Instrum.*, vol. 40, pp. 232–237, Dec. 2014.
[15] Y. Zheng and Q. Liu, "Review of techniques for the mass flow rate measurement of pneumatically conveyed solids," *Measurement*, vol. 44, no. 4, pp. 589–604, May 2011.
[16] J. Shao, J. Krabicka, and Y. Yan, "Velocity measurement of pneumatically conveyed particles using intrusive electrostatic sensors," *IEEE Trans. Instrum. Meas.*, vol. 59, no. 5, pp. 1477–1484, May 2010.
[17] C. Xu, S. Wang, and Y. Yan, "Spatial selectivity of linear electrostatic sensor arrays for particle velocity measurement," *IEEE Trans. Instrum. Meas.*, vol. 62, no. 1, pp. 167–176, Jan. 2013.
[18] X. Qian and Y. Yan, "Flow measurement of biomass and blended biomass fuels in pneumatic conveying pipelines using electrostatic sensor-arrays," *IEEE Trans. Instrum. Meas.*, vol. 61, no. 5, pp. 1343–1352, May 2012.
[19] J. Krabicka and Y. Yan, "Finite-element modeling of electrostatic sensors for the flow measurement of particles in pneumatic pipelines," *IEEE Trans. Instrum. Meas.*, vol. 58, no. 8, pp. 2730–2736, Aug. 2009.
[20] J. R. Coombes and Y. Yan, "Development of an electrostatic array sensor for measuring the velocity and concentration profiles of pneumatically conveyed particles," in *Proc. IEEE Int. Instrum. Meas. Technol. Conf.*, Pisa, Italy, May 2015, pp. 138–143.
[21] J. R. Coombes and Y. Yan, "Experimental investigations into the flow characteristics of pneumatically conveyed biomass particles using an electrostatic sensor array," *Fuel*, vol. 151, pp. 11–20, Jul. 2015.
[22] Y. Yan, B. Byrne, S. Woodhead, and J. Coulthard, "Velocity measurement of pneumatically conveyed solids using electrodynamic sensors," *Meas. Sci. Technol.*, vol. 6, no. 5, pp. 515–537, 1995.
[23] Y. Yan, "Continuous measurement of particulate emissions," *IEEE Instrum. Meas. Mag.*, vol. 8, no. 4, pp. 35–39, Oct. 2005.
[24] D. Mills, *Pneumatic Conveying Design Guide*, 2nd ed. Oxford, U.K.: Butterworth-Heinemann Pub., 2004, pp. 6–584.
[25] Y. Yan, "Mass flow measurement of bulk solids in pneumatic pipelines," *Meas. Sci. Technol.*, vol. 7, no. 12, pp. 1687–1706, 1996.
[26] R. M. Carter and Y. Yan, "On-line particle sizing of pulverized and granular fuels using digital imaging techniques," *Meas. Sci. Technol.*, vol. 14, no. 7, pp. 1099–1109, 2003.

James Robert Coombes received the H.N.D. degree in electrical and electronic engineering from the University of Kent, Canterbury, U.K., in 2005, the H.N.D. degree in mechanical engineering from the University of Greenwich, Greenwich, U.K., in 2010, and the B.Eng. degree in electronic and communications engineering from the University of Kent, in 2012, where he is currently pursuing the Ph.D. degree in electronic instrumentation engineering.

He spent four years as a Production Engineer at a steel processing facility. His current research interests include particle flow measurement using electrostatic and piezoelectric sensors.

Yong Yan (M'04–SM'04–F'11) received the B.Eng. and M.Sc. degrees in instrumentation and control engineering from Tsinghua University, Beijing, China, in 1985 and 1988, respectively, and the Ph.D. degree in flow measurement and instrumentation from the University of Teesside, Middlesbrough, U.K., in 1992.

He was an Assistant Lecturer with Tsinghua University in 1988. In 1989, he joined the University of Teesside as a Research Assistant. After a short period of post-doctoral research, he was a Lecturer with the University of Teesside from 1993 to 1996, and then a Senior Lecturer, Reader, and Professor with the University of Greenwich, Greenwich, U.K., from 1996 to 2004. He is currently a Professor of Electronic Instrumentation, the Head of the Instrumentation, Control and Embedded Systems Research Group, and the Director of Research with the School of Engineering and Digital Arts, University of Kent, Canterbury, U.K. He has authored in excess of 300 research papers in journals and conference proceedings with an h-index of 33.

Fuel 151 (2015) 11–20

Contents lists available at ScienceDirect

Fuel

journal homepage: www.elsevier.com/locate/fuel

Experimental investigations into the flow characteristics of pneumatically conveyed biomass particles using an electrostatic sensor array

James Robert Coombes, Yong Yan *

Instrumentation, Control and Embedded Systems Research Group, School of Engineering and Digital Arts, University of Kent, Canterbury, Kent CT2 7NT, UK

HIGHLIGHTS

- Electrostatic sensors are constructed as an array across the diameter of the pipe.
- The sensor array is distributed along an intrusive blade across the pipe diameter.
- Both velocity and concentration profiles of biomass particles are measured.
- Experiments were conducted on a 50 mm bore pipeline with willow as a test fuel.
- Effects of particle size and shape on the flow characteristics are studied.

ARTICLE INFO

Article history:
Received 2 October 2014
Received in revised form 13 November 2014
Accepted 17 November 2014
Available online 3 December 2014

Keywords:
Biomass
Velocity profile
Concentration profile
Electrostatic sensor
Sensor array

ABSTRACT

As countries across the world are pushing towards the increased use of renewable sources of energy the burning of biomass fuels makes up an important part of this strategy. Many coal fired power stations have been converted to co-firing and in some cases are being completely biomass fuelled. However, due to their variability in size, shape and the complex nature of gas–solids two-phase flow the monitoring of biomass particles in a pneumatic conveying pipeline is difficult. This paper presents the results of experimental investigations carried out using a novel electrostatic sensor array that is capable of measuring the particle velocity and concentration profiles over the whole diameter of the pipe. Experimental tests were carried out on horizontal and vertical pipe sections with different particle sizes of a common biomass fuel – willow, over a range of flow conditions. Results from the experiments indicate that smaller biomass particles have more stable flow characteristics across the whole diameter of the pipe.

1. Introduction

The ability to accurately monitor the mass flow rate of pneumatically conveyed fuel is important in improving burning efficiency and reducing slagging and emissions. Power plants across the world have been converted to co-firing with a mixture of coal and biomass as well as solely biomass fuelling in order to increase the proportion of renewable energy generated.

There are several challenges in monitoring the complex flow characteristics of pulverised biomass inside a pneumatic conveying system. The first is that the pulverised fuel is conveyed in a dilute phase with particle concentration being less than 0.1% of the pipe volume [1], meaning that any sensor used to measure the particle flow will have to be sensitive enough to detect such low concentrations. Second is the shape of biomass particles which are elongated due to their fibrous structure meaning that the particle spin is more apparent compared to the spherical shape of pulverised coal. The third is that the particle size of pulverised biomass distributes over a much wider range than coal thus making particle flow in the pipe much more complex.

Various methods have been developed to monitor particle velocity and concentration in a pneumatic conveying pipeline. These include capacitive [2,3], radiometric [4], optical [5,6] and ultrasonic [7] sensing techniques. All of these sensor paradigms have the advantage of being nonintrusive and are capable of determining both particle velocity and concentration. Capacitive sensors, however, have a disadvantage in that they are sensitive to moisture in biomass, which can significantly change the dielectric properties of the fuel being monitored, leading to substantial errors in the concentration measurement. The radiometric method could outperform, in principle, all other techniques, but suffers from the

* Corresponding author.
E-mail addresses: jrc55@kent.ac.uk (J.R. Coombes), y.yan@kent.ac.uk (Y. Yan).

http://dx.doi.org/10.1016/j.fuel.2014.11.048
0016-2361/

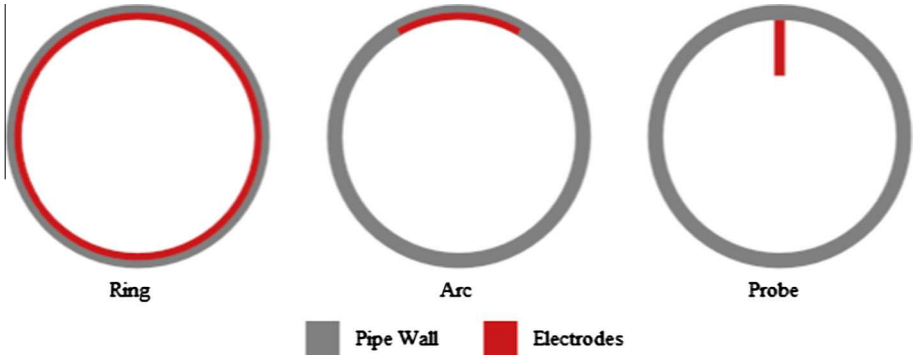

Fig. 1. Different designs of electrostatic electrodes.

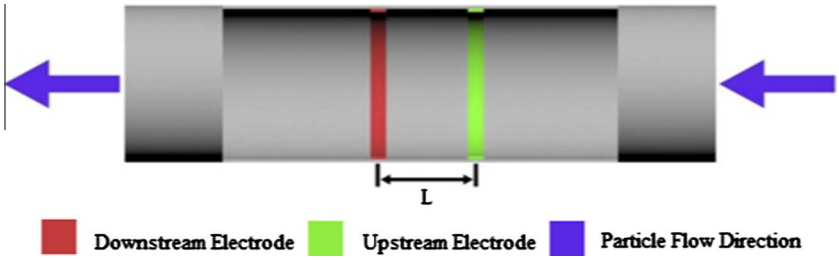

Fig. 2. Electrode configuration inside a pipe.

disadvantage of containing a radioactive material in the sensing system and associated administrative inconvenience dealing with stringent health and safety regulations. The drawback of using optical sensors lies in the requirement of a transparent window on the pipe to access the flow and the incorporation of an air purging mechanism to prevent the window from contamination due to fine dust accumulation. Electrostatic sensors, due to their simplicity, robustness and low cost, have the advantage over other sensors. Previous types of electrostatic sensors include ring, arc and probe electrodes [8–12], which are illustrated in Fig. 1. Electrostatic array sensors based on multiple ring and arc shaped electrodes have been used for the velocity measurement of pneumatically conveyed particles [10,11].

Ring electrodes are completely non-invasive since they lie flush with the pipe wall and consequently do not impede the particle flow in the pipe. They do, however, have disadvantages in that they are sensitive to particles close to the pipe wall. Nevertheless, when ring electrodes are used to measure the particle velocity through cross-correlation, the correlation coefficient between the upstream and downstream signals is limited because different parts of the pipe cross section can have different velocities depending upon the flow conditions [8]. Moreover, ring electrodes have a shortcoming that they are constructed inside pipe spool pieces, meaning that flanges are required to install the spool piece which is difficult to retrofit onto some existing systems.

Arc electrodes are very similar in design to ring electrodes except the latter are segmented individual sections of a ring which only cover a small portion of the circumference of the pipe wall [10,11]. Qian and Yan [10] used electrostatic sensor arrays with arc electrodes to monitor the local particle velocity of a flour/biomass mixture, making them much more able to accurately determine particle velocity. However, just like ring electrodes, arc electrodes are also built into pipe spools making installation difficult and costly.

Unlike ring and arc electrodes, probe electrodes are invasive in that they come into direct contact with the particle flow in the pipe. Nevertheless, this does not cause a problem in a dilute flow due to the low particle concentration (less than 0.1% by volume) coupled with the fact that the electrodes take up a very small proportion of the cross sectional area of the pipe. Shao et al. [8] assessed the performance of probe electrodes through a combination of practical on-line experimentation and off-line finite element modelling. It was found that a probe electrode with an electrode depth of 0.3–0.5 of the pipe diameter would give a

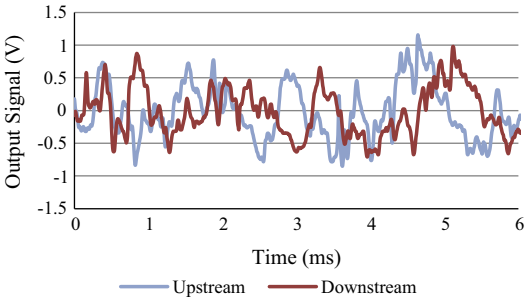

Fig. 3. Typical upstream and downstream signals from the electrostatic sensors.

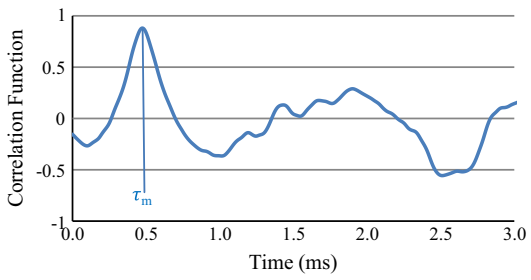

Fig. 4. Correlation function between the upstream and downstream signals.

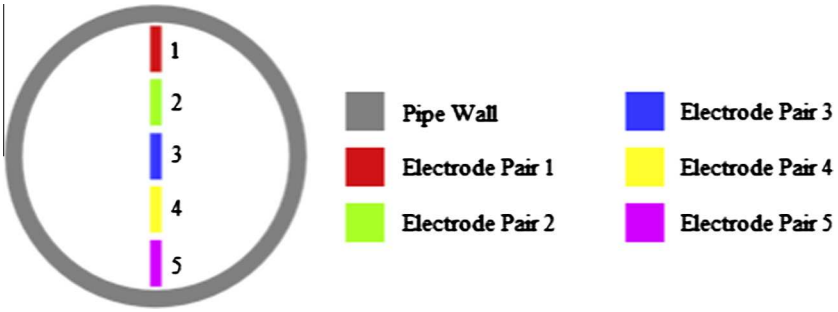

Fig. 5. Arrangement of the electrostatic sensor array.

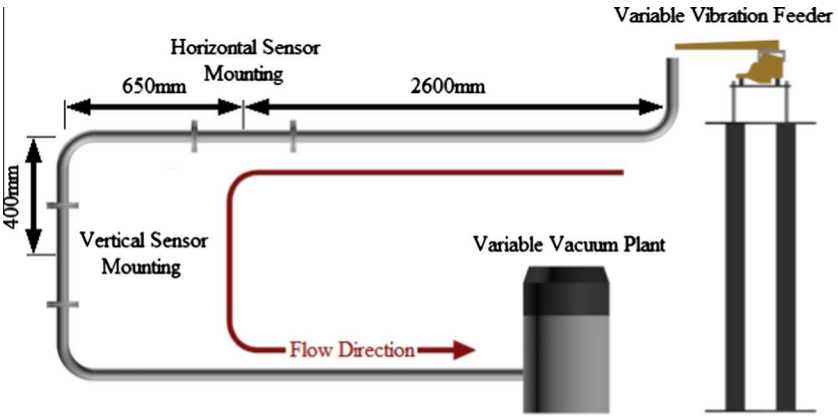

Fig. 6. Layout of the particle flow test rig (not to scale).

(a) Coarse willow (b) Fine willow

Fig. 7. Typical images of the willow particles (not to scale).

reasonable estimate of the true mean velocity for regular velocity profiles. In addition, it was found that the probe electrodes had a higher correlation coefficient compared to the traditional ring electrode design with the probe electrodes obtaining a correlation coefficient of around 0.55–0.75 compared to 0.35–0.50 for the ring electrodes under the conditions tested; this is due to the fact that the sensitivity of the probe electrodes is much more localised [12]. Furthermore, probe electrodes have an advantage over ring and arc electrodes in that they only require a tapped hole to be drilled in existing pipe work for installation, meaning lower installation and maintenance costs.

This paper presents a novel electrostatic sensor array that allows particle velocity profiles and particle concentration profiles to be measured for the whole diameter of the pipe. Experimental work was carried out on a laboratory-scale pneumatic conveyor system using willow, a common biomass fuel. It is expected that the electrostatic sensor array is capable of measuring the velocity and concentration profiles on a developed flow as well as detecting specific flow regimes such as roping [1].

2. Measurement principle

As the particles are conveyed down the pipe they pick up an electrostatic charge due to friction with the air and each other. The level of electrostatic charge on the particles is random because of the nature of how it is generated [13]. An electrostatic sensor consists of an insulated electrode connected to a suitable signal

conditioning circuit that amplifies the signal detected by the electrode to a level that can be digitised with an analogue to digital converter (ADC). As the charged particles travel past the electrode, a small amount of charge is induced on the electrode and hence a sensor signal generated. To measure the particle velocity through cross-correlation two identical electrostatic sensors are required in a configuration, as shown in Fig. 2.

As the particles travel past the electrode pair each electrode detects the electrostatic charge of the passing particles. Since the two electrodes are identical, the signal on the downstream electrode should be the very similar to that in the upstream except the time delay, as shown in Fig. 3. The time delay between the two signals, τ_m, can be determined using cross correlation:

$$Rxy(m) = \frac{1}{N}\sum x(n)y(n+m), \tag{1}$$

where $x(n)$ and $y(n)$ are the upstream and downstream signals, respectively. The location of the dominant peak of the resulting correlation function indicates the delay, as illustrated in Fig. 4 [14].

Since the distance between the electrodes, L, is known, the correlation velocity (V_c) can be derived from:

$$V_c = \frac{L}{\tau_m}. \tag{2}$$

It should be pointed out that the correlation velocity measured from Eq. (2) is not necessarily the expected "mean particle velocity" in the pipe, depending up the sensitivity profile of the sensor, particle velocity profile, particle distribution and algorithm of the correlation computation [14,15]. Particle concentration in this study is determined by measuring the rms (root-mean-square) magnitude of the sensor signal [15]:

$$V_{rms} = \sqrt{\frac{\sum_{n=1}^{N} x(n)^2}{N}} \tag{3}$$

where x is the voltage signal from the sensor, n is the sample number and N is the total number of samples. However, this method cannot be used to determine the exact particle concentration under practical flow conditions due to variations in particle size distribution, moisture content, and how long the particles have had to charge while being conveyed [16].

3. Electrostatic sensor array

The electrostatic sensor array developed in this study consists of five elements (five identical pairs of electrodes) mounted on a thin frame spanning the diameter of the pipe, as shown in Fig. 5.

The advantage of this sensor design compared to the previous designs is that it will be capable of observing internal flow dynamics under complex flow conditions (e.g. biomass/air and biomass/coal/air multiphase flows) and achieve more accurate measurements in the presence of complex flow profiles. Each electrode has a width of 1 mm and a length of 8 mm with each pair of electrodes being spaced 10 mm apart with a total of five pairs of electrodes in the array. Since the sensor array spans the diameter of the pipe (ID = 50 mm), all attempts have been made to ensure the sensor is as thin as possible to reduce its blockage effect on the particle flow. In the present study the sensor array is only 2.5 mm thick, which obstructs 6.4% of the pipe cross sectional area. The array can be made thinner in commercial versions.

The first stage of the signal conditioning circuit is a preamplifier, which is constructed inside the electrodes; this is to shorten the physical distance between the electrode and preamplifier to reduce unwanted noise entering the circuit. To amplify the signal from the preamplifier to a usable level a post-amplifier is used. The signal is then passed through an anti-aliasing filter with a cut-off frequency of 15 kHz to remove high frequency noise. The upstream and downstream signals are digitised using a 12-bit ADC with a sampling rate of 150 kHz. The cross correlation software is embedded into an ARM Cortex 32-bit microcontroller which outputs to a PC.

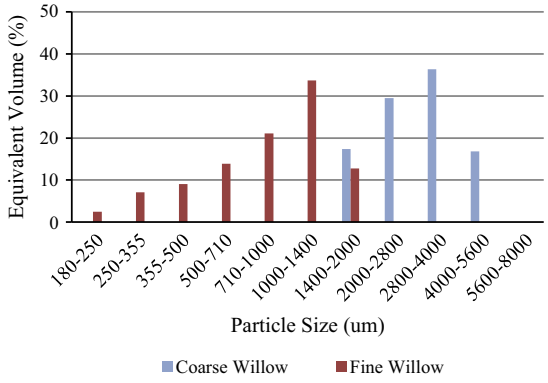

Fig. 8. Particle size distribution of coarse and fine willow.

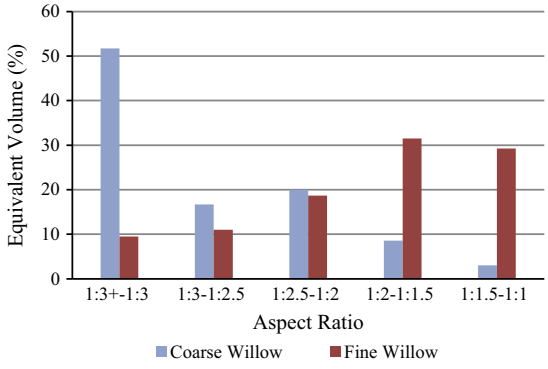

Fig. 9. Aspect ratio distribution of coarse and fine willow.

Table 1
Test condition matrix.

Particle size	Sensor mounting	Sensor orientation (plane)	Particle feed rate (kg/h)	Air velocities (m/s)
Coarse	Horizontal	*Z*	2.08	20.3–24.4
Fine	Horizontal	*Z*	1.48	20.3–24.4
Coarse	Horizontal	*Y*	2.08	20.3–24.4
Fine	Horizontal	*Y*	1.48	20.3–24.4
Coarse	Vertical	*X*	2.08	18.5–22.5
Fine	Vertical	*X*	1.48	18.5–22.5
Coarse	Vertical	*Y*	2.08	18.5–22.5
Fine	Vertical	*Y*	1.48	18.5–22.5

4. Test rig and experimental procedure

Experiments were carried out on a laboratory-scale pneumatic conveyor system with sensor mountings on horizontal (approximately 52 pipe diameters from input right-angle bend) and vertical (approximately 8 pipe diameters from right-angle bend) pipes as demonstrated in Fig. 6.

Willow, a common biomass fuel supplied from a power station, was used as a test fuel. The biomass sample was separated through filtering into two different particle size ranges: "fine" and "coarse" in order to investigate the effect of particle size on flow characteristics. Particle size was determined using an in-house particle ima-

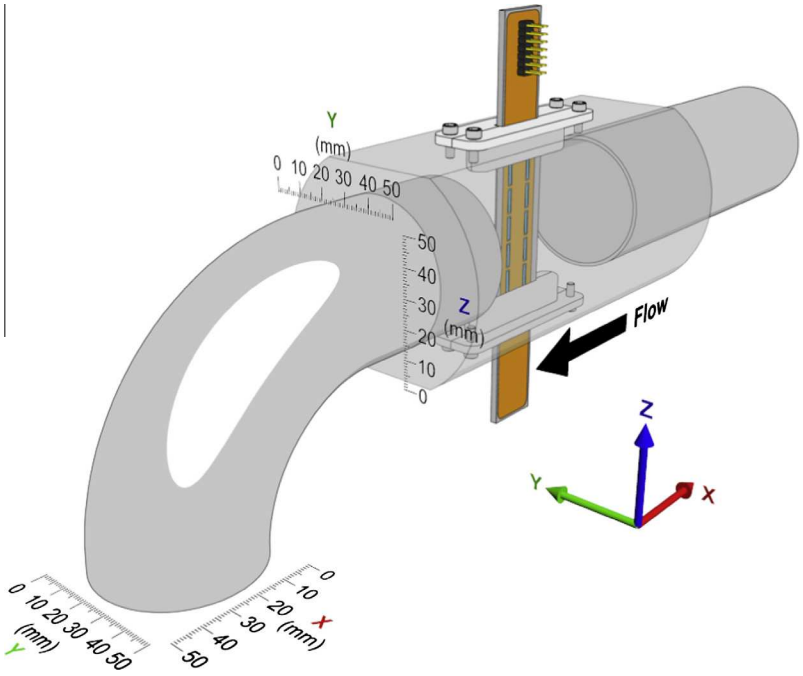

Fig. 10. Electrostatic sensor array mounted inside a pipe spool with orientation and pipe cross sectional measurements (not to scale).

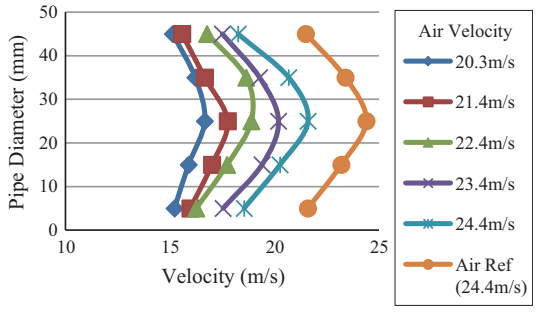

Fig. 11. Mean velocity profile on horizontal pipe section for coarse willow on the *Z* axis (data points indicate centre of the electrode).

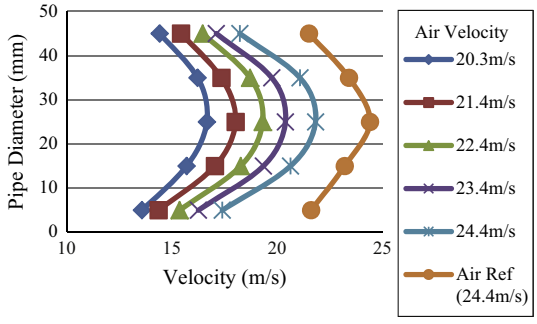

Fig. 12. Mean velocity profile on horizontal pipe section for fine willow on the *Z* axis.

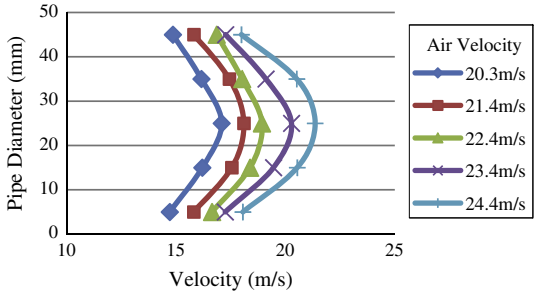

Fig. 13. Mean velocity profile on horizontal pipe section for coarse willow on the *Y* axis.

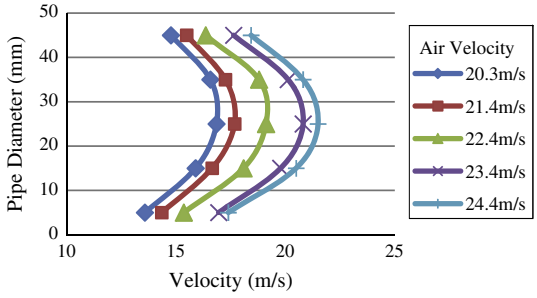

Fig. 14. Mean velocity profile on horizontal pipe section for fine willow on the *Y* axis.

ger [17]. Fig. 7 shows parts of typical images of the willow particles whereas Figs. 8 and 9 illustrate the corresponding particle size distribution and aspect ratio distribution.

Each set of tests was conducted on both horizontal and vertical pipe sections. For both particle size ranges five different air velocities (horizontal 20.3–24.4 m/s and vertical 18.5–22.5 m/s) were created. The air velocity was determined by using a hot wire anemometer with readings taken from the centre of the pipe at the same locations as the sensor array. The willow particles were metered into the system using a vibration feeder at material flow rates shown in Table 1.

The sensor array was mounted at different orientations across the pipe diameter on the *Y*–*Z* plane on the horizontal pipe and the *X*–*Y* plane on the vertical pipes, as shown in Fig. 10.

For each pair of electrodes on the sensor array the correlation computation used 1024 samples (150 kHz sampling rate) from

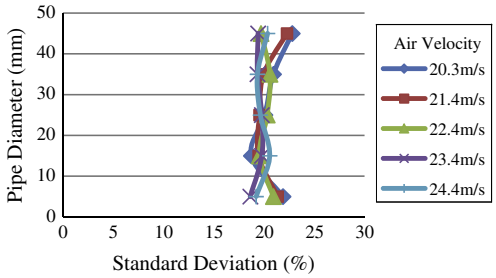

Fig. 15. Normalised standard deviation profile of the velocities on horizontal pipe section for coarse willow on the *Z* axis.

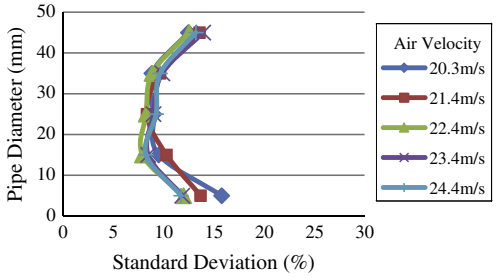

Fig. 16. Normalised standard deviation profile of the velocities on horizontal pipe section for fine willow on the *Z* axis.

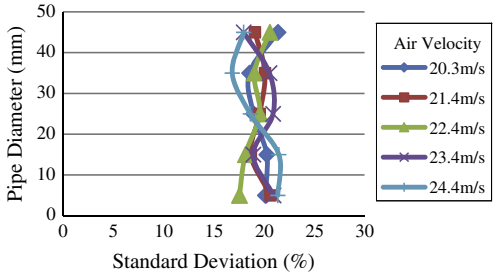

Fig. 17. Normalised standard profile of the velocities on horizontal pipe section for coarse willow on the *Y* axis.

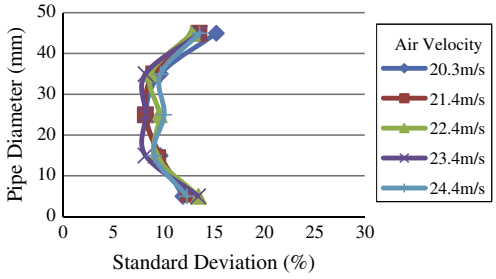

Fig. 18. Normalised standard deviation profile of the velocities on horizontal pipe section for fine willow on the *Y* axis.

both the upstream and downstream signals during each data processing cycle. A total of 500 velocity readings were taken on each element of the array for each air velocity (transitional readings were removed). Similarly, particle concentration and correlation coefficient data were also averaged over 500 readings, respectively. Standard deviations were also calculated to quantify the fluctuation of the measurements about the averages.

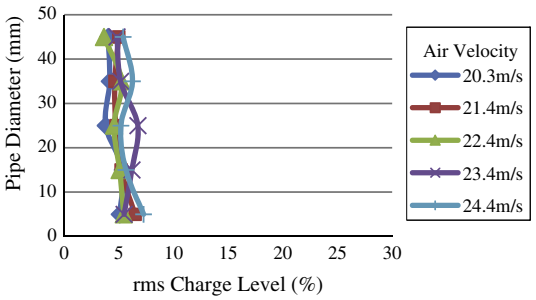

Fig. 19. Mean particle concentration profile on horizontal pipe section for coarse willow on the *Z* axis.

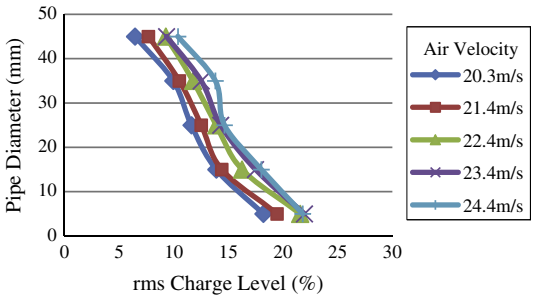

Fig. 20. Mean particle concentration profile on horizontal pipe section for fine willow on the *Z* axis.

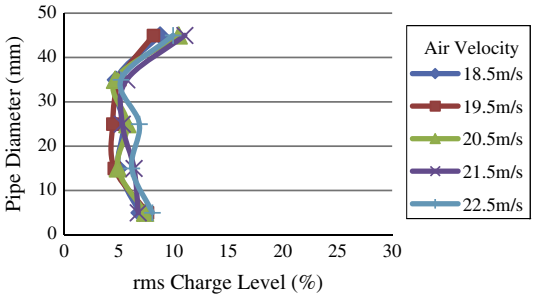

Fig. 21. Mean particle concentration profile on horizontal pipe section for coarse willow on the *Y* axis.

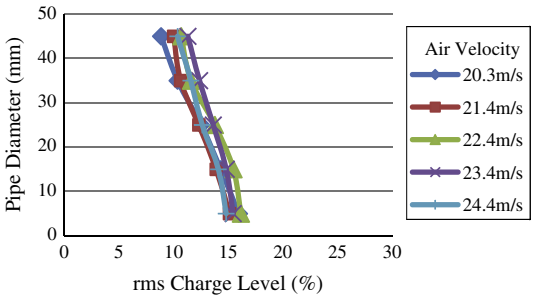

Fig. 22. Mean particle concentration profile on horizontal pipe section for fine willow on the *Y* axis.

5. Results and discussion

5.1. Horizontal flow

The electrostatic sensor array was able to measure the velocity across the whole diameter of the pipe. Figs. 11–14 show the velocity

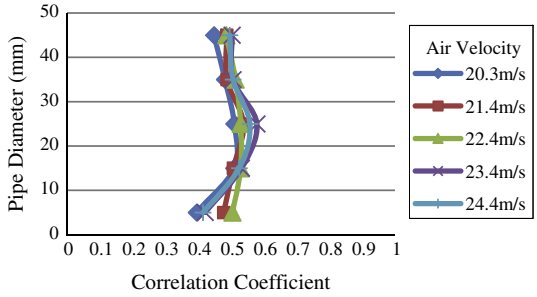

Fig. 23. Mean correlation coefficient profile across the pipe diameter on horizontal pipe section for coarse willow on the *Z* axis.

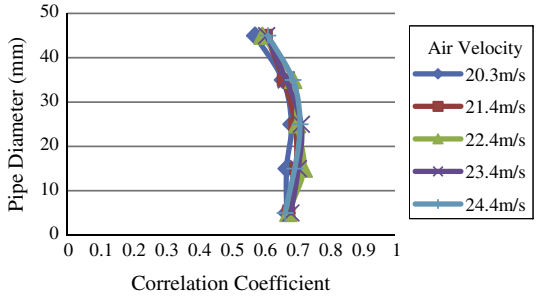

Fig. 24. Mean correlation coefficient profile across the pipe diameter on horizontal pipe section for fine willow on the *Z* axis.

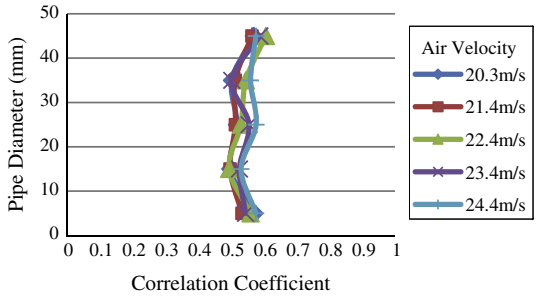

Fig. 25. Mean correlation coefficient profile across the pipe diameter on horizontal pipe section for coarse willow on the *Y* axis.

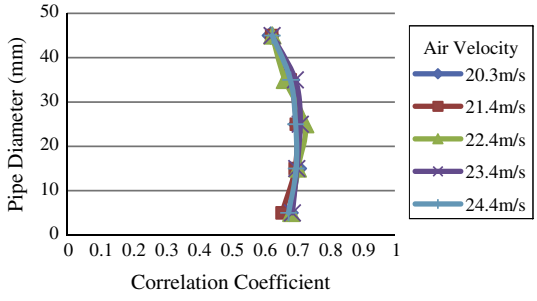

Fig. 26. Mean correlation coefficient profile across the pipe diameter on horizontal pipe section for fine willow on the *Y* axis.

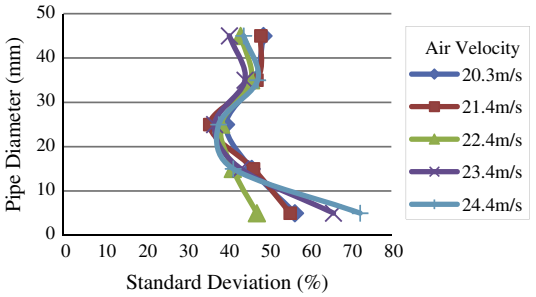

Fig. 27. Normalised standard deviation profile of the correlation coefficient on horizontal pipe section for coarse willow on the *Z* axis.

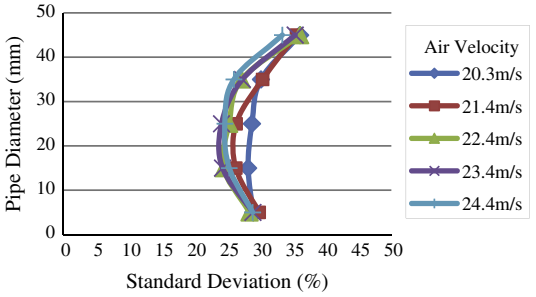

Fig. 28. Normalised standard deviation profile of the correlation coefficient on horizontal pipe section for fine willow on the *Z* axis.

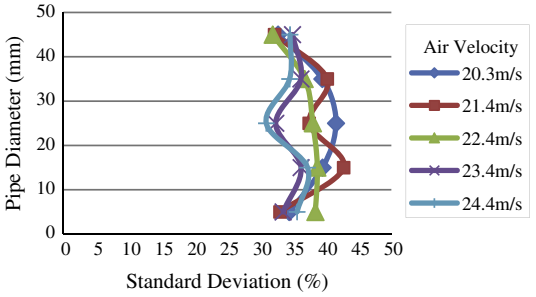

Fig. 29. Normalised standard deviation profile of the correlation coefficient on horizontal pipe section for coarse willow on the *Y* axis.

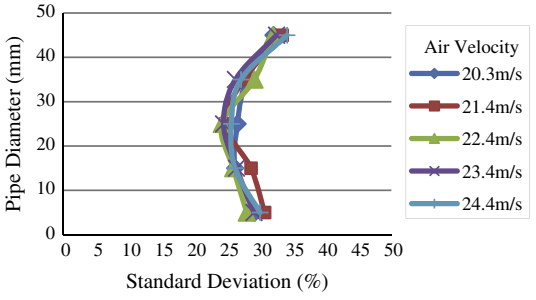

Fig. 30. Normalised standard deviation profile of the correlation coefficient on horizontal pipe section for fine willow on the *Y* axis.

profiles for the sensor array mounted on the *Z*–*Y* plane on the horizontal pipe (Fig. 10). The maximum air velocity profile shown in Figs. 11 and 12 indicates that the particles that are suspended in the air are travelling at a slower velocity then the conveying air (for presentation clarity, other air velocity profiles are not plotted in the figures). The particle velocity profiles indicate that the coarse and fine willow particles at the centre of the pipe travel faster than those near the pipe wall due to friction between the particles and the wall. The shape of the velocity profiles for the fine willow (Figs. 12 and 14) is much more homogeneous than the coarse willow

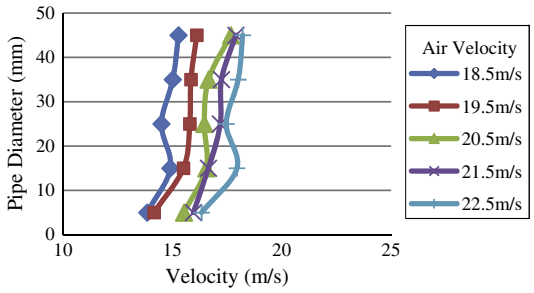

Fig. 31. Mean velocity profile on vertical pipe section for coarse willow on the *X* axis.

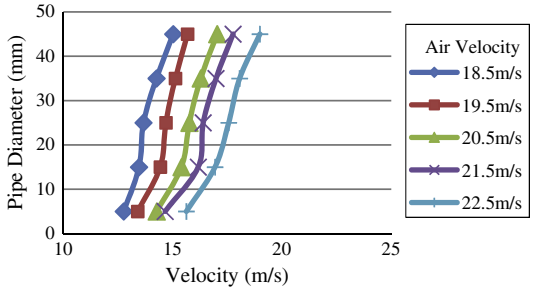

Fig. 32. Mean velocity profile on vertical pipe section for fine willow on the *X* axis.

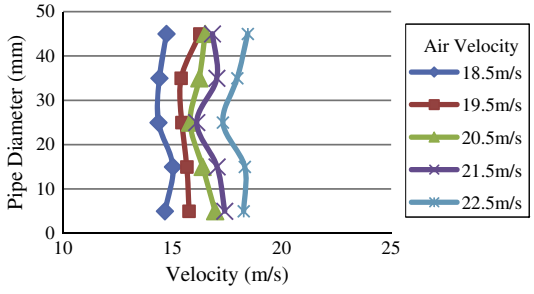

Fig. 33. Mean velocity profile on vertical pipe section for coarse willow on the *Y* axis.

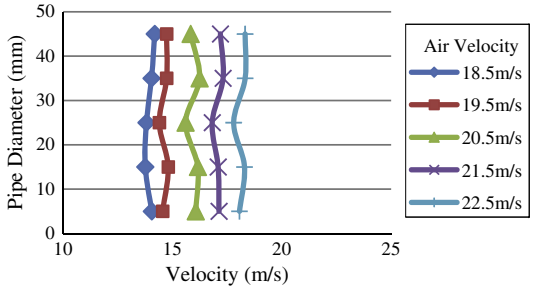

Fig. 34. Mean velocity profile on vertical pipe section for fine willow on the *Y* axis.

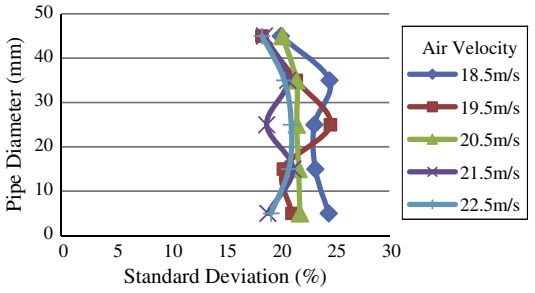

Fig. 35. Normalised standard deviation profile of the velocities on vertical pipe section for coarse willow on the *X* axis.

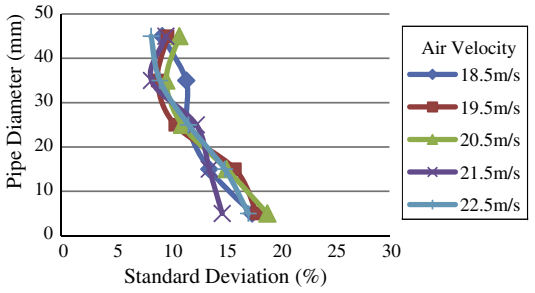

Fig. 36. Normalised standard deviation profile of the velocities on vertical pipe section for fine willow on the *X* axis.

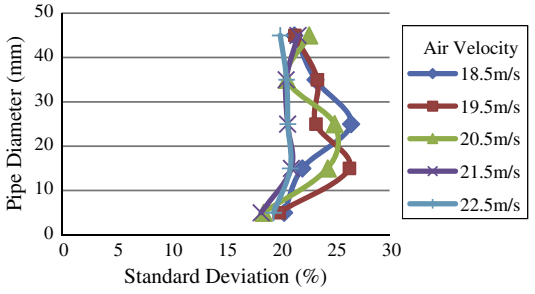

Fig. 37. Normalised standard deviation profile of the velocities on vertical pipe section for coarse willow on the *Y* axis.

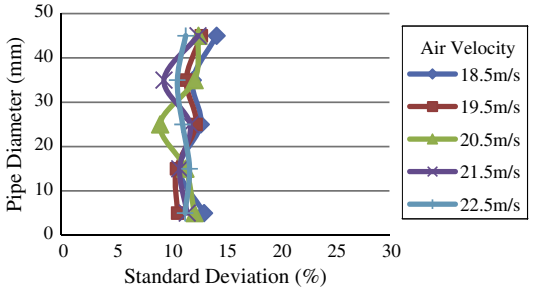

Fig. 38. Normalised standard deviation profile of the velocities on vertical pipe section for fine willow on the *Y* axis.

profiles (Figs. 11 and 13), indicating that smaller particles exhibit more stable flow characteristics.

The normalised standard deviation of the velocity profiles is an indication of flow stability. The coarse willow on the *Z*–*Y* plane shown in Figs. 15 and 17 illustrates that the velocity standard deviation is uniform across the whole diameter of the pipe. The velocity standard deviation profiles for the fine willow (Figs. 16 and 18) indicate that the particle velocity in the centre of the pipe deviates less than the particle flow along the pipe wall; this is an indication that the fine willow produces a more stable flow compared to the coarse willow. Moreover, the fine willow produces a standard deviation profile that is in line with flow dynamics; the flow along the pipe wall is more unstable than that at the centre of the pipe.

The use of the normalised rms magnitude to determine particle concentration can be seen in Figs. 19–22. From analysis of the rms

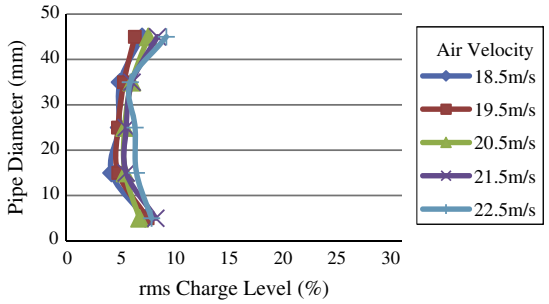

Fig. 39. Mean particle concentration profile on vertical pipe section for coarse willow on the *X* axis.

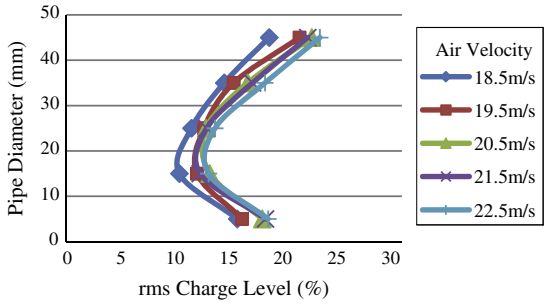

Fig. 40. Mean particle concentration profile on vertical pipe section for fine willow on the *X* axis.

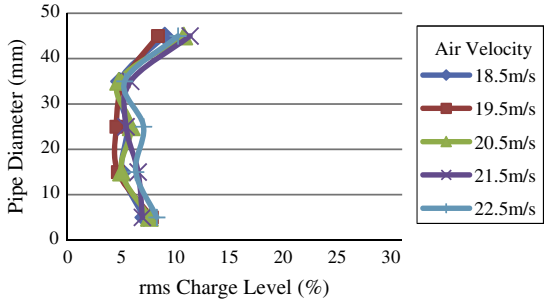

Fig. 41. Mean particle concentration profile on vertical pipe section for coarse willow on the *Y* axis.

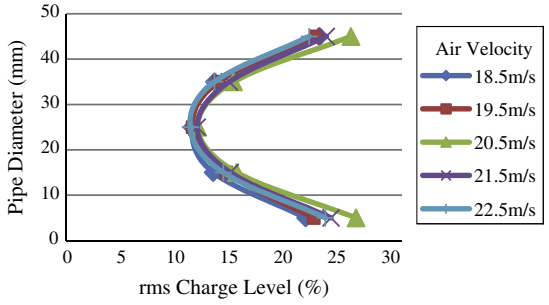

Fig. 42. Mean particle concentration profile on vertical pipe section for fine willow on the *Y* axis.

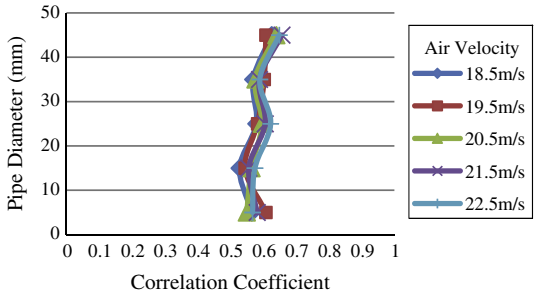

Fig. 43. Mean correlation coefficient profile on vertical pipe section for coarse willow on the *X* axis.

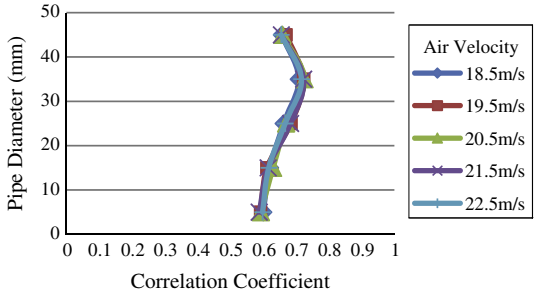

Fig. 44. Mean correlation coefficient profile on vertical pipe section for fine willow on the *X* axis.

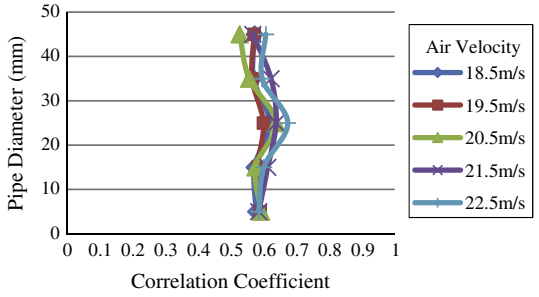

Fig. 45. Mean correlation coefficient profile on vertical pipe section for coarse willow on the *Y* plane.

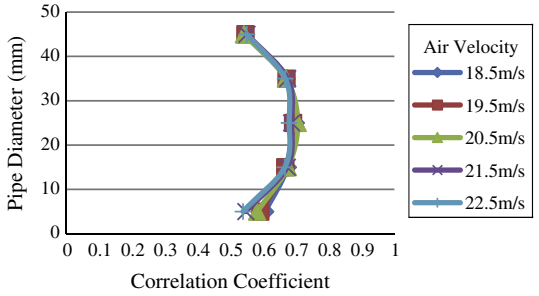

Fig. 46. Mean correlation coefficient profile on vertical pipe section for fine willow on the *Y* plane.

profiles it is clear that the fine willow (Figs. 20 and 22) has a higher rms charge magnitude than that of the coarse willow (Figs. 19 and 21). This result indicates that a high volume of smaller particles carry a higher electrostatic charge compared to smaller concentrations of larger particles (even though the coarse willow has a higher mass flow rate than the fine willow). This is due to the fact that many smaller particles have a larger surface area when compared to the surface area created by fewer large particles.

The effect of gravity can be seen in the rms profile for the fine willow particles (Fig. 20) where the rms charge magnitude is higher at the bottom of the pipe (0 mm) compared to the top of

the pipe (45 mm). The increased concentration shown in Fig. 22 on the 0 mm side of the pipe could possibly be down to the vibration feeder unevenly distributing particles in the input pipe.

The value of the correlation coefficient is also an indication of flow stability [10], i.e. the closer to 1 the correlation coefficient, the more stable the flow. The fine willow shown in Figs. 24 and 26 has a higher correlation coefficient compared to the coarse willow shown in Figs. 23 and 25, indicating that the fine willow has a more stable flow compared to the coarse willow; this is consistent with the velocity standard deviation results. The correlation coefficient profiles for the fine willow in Figs. 24 and 26 also show that the correlation coefficient is higher in the centre of the pipe than that along the pipe wall, indicating that the particle flow along the pipe wall is more unstable than those in the centre of the pipe.

Analysis of the standard deviation of the correlation coefficient shows that the fine willow (Figs. 28 and 30) deviates less than the coarse willow (Figs. 27 and 29). The shape of the profiles for the fine willow (Figs. 28 and 30) likewise indicates that the correlation coefficient deviates less in the centre of the pipe compared to along the pipe wall, indicating that the flow along the pipe wall is more unstable than that at the centre of the pipe.

5.2. Vertical flow

The velocity profile measured using the electrostatic sensor array mounted on the *X*–*Y* plane on the vertical pipe (Fig. 10) is not an atypical velocity profile (Figs. 31–34). This is because the velocity profile has yet to develop from when it has left the right-angle bend. However, the shape of the velocity profiles (Figs. 31 and 32) indicates that the particle flow along the outer radius (45 mm) travels faster than that along the inner radius as the particles leave the right-angle bend.

The normalised standard deviation velocity profiles in Figs. 35–38 show that the fine willow (Figs. 36 and 38) deviates less than the coarse willow (Figs. 35 and 37), suggesting that the fine willow flow is more stable than the coarse willow when mounted on the vertical pipe section.

The normalised rms profile measured by the sensor array mounted on the vertical pipe section indicates that the smaller particles of the fine willow (Figs. 40 and 42) carry more electrostatic charge than the coarse willow biomass (Figs. 39 and 41). The shape of the profiles also indicates that the highest particle concentration is along the pipe wall. This result shows that the particles are forced along the outer wall due to the centrifugal force caused by the particles travelling along the right-angle bend. Moreover, this demonstrates that the sensor array is capable of detecting roping flow regime inside a pneumatic conveying pipeline.

The correlation coefficient profile for the coarse willow shown in Figs. 43 and 45 is consistent across the whole pipe diameter. However, the correlation coefficient profile for the fine willow, as shown in Figs. 44 and 46, increases towards the centre of the pipe. This can especially be seen in Fig. 46 where the correlation coefficient is around 0.6 along the pipe wall and 0.7 at the centre of the pipe, suggesting that the flow in the centre of the pipe is more stable than that along the pipe wall.

6. Conclusions

An electrostatic sensor array has been successfully used to measure the velocity and concentration profiles of biomass particles in a pneumatic conveying pipeline. The velocity profiles have clearly shown that the particles along the pipe wall travel at a slower velocity than those in the centre of the pipe. The use of the electrostatic sensor array to measure the particle concentration profile has been well demonstrated on the vertical pipe sections. This is because the centrifugal force due to the particle flow exiting the right angle bend forces the particles against the pipe wall, which also demonstrates that the sensor array is capable of detecting roping flow regimes in a pipeline.

Through analysis of the normalised standard deviation of the velocity profiles, as well as the correlation coefficient profiles, it can be seen that the flow at the centre of the pipe is more stable than that along the pipe wall on developed flow. The comparison between the fine and coarse willow particles has shown that the fine willow produces characteristics of more stable flow compared to the coarse willow. Moreover, the rms profiles have demonstrated that the fine willow generates a sensor signal of a higher magnitude than that of the coarse willow, despite the lower feed rate of the fine willow.

Acknowledgments

This work is supported by the Research Councils UK's Energy Programme (EP/F061307/1), but the views expressed are those of the authors and not necessarily those of the funding body. The Energy Program is an RCUK cross-council initiative led by the Engineering and Physical Sciences Research Council and contributed to by the Economic and Social Research Council, Natural Environment Research Council, Biotechnology and Biological Sciences Research Council, and Science and Technology Facilities Council.

References

[1] Yan Y. Guide to the flow measurement of particulate solids in pipelines. Powder Handling Process 2001;13(4).
[2] Fuchs A, Zangl H. Single-layer measurement of particle velocity and concentration in pneumatic dilute phase conveying. Proc IEEE Conf Sens 2005;30(3):857–60 (Irvine CA, USA).
[3] Zangl H, Fuchs A, Brasseur G, Petriu EM. Random-data cross-correlation for flow measurement of bulk solids in pneumatic conveyor pipes. In: Proceedings of the IEEE international instrumentation and measurement technology conference, Ottawa, Canada, 16–19, May 2005.
[4] Barratt IR, Yan Y, Byrne B, Bradley MSA. Mass flow measurement of pneumatically conveyed solids using radiometric sensors. Flow Meas Instrum 2000;11(3):223–35.
[5] Song D, Peng L, Lu G, Yang S, Yan Y. Velocity measurement of pneumatically conveyed particles through digital imaging. Sens Actuators A: Phys 2009;149(2):180–8.
[6] Carter RM, Yan Y, Lee P. On-line nonintrusive measurement of particle size distribution through digital imaging. IEEE Trans Instrum Meas 2006;55(6):2034–8.
[7] Abernethy DA, Millen MJ, Sowerby BD. Plant trial of an ultrasonic gauge for the on-line measurement of pulverised coal mass flow. In: Proceedings of the IEEE international instrumentation and measurement technology conference, Brussels, Belgium, 4–6, June 1996.
[8] Shao J, Krabicka J, Yan Y. Velocity measurement of pneumatically conveyed particles using intrusive electrostatic sensors. IEEE Trans Instrum Meas 2010;59(5):1477–84.
[9] Xu C, Li J, Wang S. A spatial filtering velocimeter for solid particle velocity measurement based on linear electrostatic sensor array. Flow Meas Instrum 2012;26(8):68–78.
[10] Qian X, Yan Y. Flow measurement of biomass and blended biomass fuels in pneumatic conveying pipelines using electrostatic sensor-array. IEEE Trans Instrum Meas 2012;61(5):1343–52.
[11] Li J, Xu C, Wang S. Local particle mean velocity measurement using electrostatic sensor matrix in gas–solid two-phase pipe flow. Flow Meas Instrum 2012;27(10):104–12.
[12] Krabicka J, Yan Y. Finite element modelling of electrostatic sensors for the flow measurement of particles in pneumatic pipelines. IEEE Trans Instrum Meas 2009;58(8):2730–6.
[13] Mills D. Pneumatic conveying design guide. 2nd ed. Oxford, UK: Butterworth-Heinemann Publications; 2004. ISBN 0 7506 5471 6.
[14] Yan Y. Mass flow measurement of bulk solids in pneumatic pipelines. Meas Sci Technol 1996;7(7):1687–706.
[15] Yan Y, Byrne B, Woodhead S, Coulthard J. Velocity measurement of pneumatic conveyed solids using electrodynamic sensors. Meas Sci Technol 1995;6(5):515–37.
[16] Yan Y. Continuous measurement of particulate emissions. IEEE Instrum Meas Magaz 2005;8(4):35–9.
[17] Carter RM, Yan Y. On-line particle sizing of pulverized and granular fuels using digital imaging techniques. Meas Sci Technol 2003;14(7):1099–109.

This full text paper was peer-reviewed at the direction of IEEE Instrumentation and Measurement Society prior to the acceptance and publication.

Development of an Electrostatic Array Sensor for Measuring the Velocity and Concentration Profiles of Pneumatically Conveyed Particles

James Robert Coombes
Instrumentation, Control and Embedded Systems Group
School of Engineering and Digital Arts, University of Kent
Canterbury, Kent CT2 7NT, UK
jrc55@kent.ac.uk

Yong Yan
Instrumentation, Control and Embedded Systems Group
School of Engineering and Digital Arts, University of Kent
Canterbury, Kent CT2 7NT, UK
y.yan@kent.ac.uk

Abstract **– The ability to monitor the velocity and concentration profiles for the whole diameter of a pipe would allow the complex flow dynamics associated with particles in a pneumatic suspension to be measured. This paper presents a method of online monitoring of the particle velocity and particle concentration for the whole diameter of the pipe for a pneumatic bulk solid conveying system. This is achieved by using an array structure of five electrostatic sensors across the whole diameter of the pipe to measure the particle velocity and concentration profiles. Experimental tests were carried out on a laboratory-scale test rig over a range of particle velocities and concentrations. Results show that the electrostatic sensor array is capable of measuring the multiple velocities and concentrations that occur across the diameter of a pneumatic conveying pipe. Through analysis of velocity and correlation coefficient data different parts of the pipe diameter are determined to have more turbulence then others.**

Keywords - pulverized fuel; velocity profile; concentration profile; mass flow rate; electrostatic sensor; sensor array

I. INTRODUCTION

Dilute gas-solid transport systems are used in a variety of industries such as chemical, steel and energy. Being able to monitor the velocity profile and particle concentration for the whole diameter of the pipe would allow the mass flow rate to be accurately monitored and achieve an in-depth understanding of gas/solid two phase flows.

Nowhere is this more important than in the energy industry where accurately monitoring the mass flow rate of the fuel is important in improving burning efficiency and reducing slagging and emissions. Now that many coal fired power plants across the world are being converted to co-firing with a mixture biomass or 100% biomass fuelling to increase the amount of renewable energy generated, the particle flow dynamics inside the pipe have become more complex due to the irregular shape and generally wider size range biomass particles.

Various methods have been developed to monitor particle velocity and concentration in a bulk solid pneumatic conveying system; these include capacitive [1,2], radiometric [3], optical [4-6], and ultrasonic [7]. All these types of sensors have the advantage of being nonintrusive and capable of monitoring both particle velocity and concentration. However capacitive sensors are susceptible to moisture which can affect the dielectric properties of the material being monitored. Radiometric sensors have the drawbacks that they contain a radioactive material and their use is governed by administratively inconvenient health and safety regulations. Optical sensors have the shortcoming that they require a transparent window in the pipe which is susceptible to contamination by the pulverised material. Nonetheless, this drawback can be addressed by using an air purging system to reduce contamination [6]. However electrostatic sensors due to their robustness and low cost have the advantage over other sensors. There are three main designs of electrodes used for electrostatic sensors: ring, arc and probe electrodes [8-10]

Ring electrodes are completely non-invasive since they are flush with the pipe wall so they do not impede the particle flow in the pipe. They do, however, have disadvantages in that they are only sensitive to particles close to the pipe wall. Then again when ring electrodes are used to measure the particle velocity in a multi-phase flow using the cross-correlation method this will reduce the correlation coefficient between the upstream and downstream because different parts of the pipe cross section will be traveling at different velocities [8].

Arc electrodes are very similar in design to ring electrodes except each arc electrode only covers a small section of the outer circumference of the pipe. Qian and Yan [9] used multi-channel arc electrostatic sensors to monitor the local particle velocity of a flour/biomass mixture.

Unlike the ring and arc electrodes, probe electrodes are invasive in that they come into direct contact with the particle flow in the pipe. Nevertheless, this does not cause a problem in a dilute flow due to the low particle concentration coupled with the fact that the electrodes take up very little of the cross sectional area of the pipe. Shao *et al.* [8] investigated this through a combination of practical online experimentation and offline finite element modelling. It was found that an electrode depth of 0.3-0.5 of the pipe diameter would give a reasonable

estimate of the true mean velocity. In addition, it was found that the probe electrodes had a higher correlation coefficient compared to the traditional ring electrode design with the probe electrodes obtaining a correlation coefficient of around 0.55-0.75 compared to 0.35-0.5 for the ring electrodes [10].

Electrostatic sensors have also been applied to measure the volumetric concentrations of the particles inside the pipe as presented by Yan *et al.* [13]. The principle of using electrostatic sensors to determine particle concentration is that as the particle concentration increases so does the magnitude of the electrostatic charge. However, Yan [14] discusses that there are limitations to using electrostatic sensors to determine particle concentration in that the electrostatic signal is affected by particle variables such as: particle size; how long the conveyed particles have had to pre-charge; and dielectric properties of the material being conveyed. Moreover, the environment inside the pipe, such as temperature and humidity, can be a factor.

This research aims to develop an electrostatic sensor array that is capable of measuring the particle flow dynamics in the pipe that previous electrostatic sensors were unable to achieve.

II. Measurement Principle

As solid particles are conveyed down the pipe in a pneumatic conveying system they pick up electrostatic charge. The level of this charge is random due to the nature of how it is generated inside the pipe through friction between the air and other particles [11]. Using an electrostatic sensor the charge carried by the particles can be detected as the particles pass the sensor since a small amount of charge is induced on the electrode [12].

The electrostatic sensor consists of an insulated electrode and a signal conditioning circuit that takes the charge induced on the electrode and converts it into a voltage signal that can be digitised by an analogue to digital converter (ADC).

Using electrostatic sensors to measure particle velocity of particles traveling inside the pneumatic conveying pipe involves the use of two electrodes arranged in a configuration as shown in Fig. 1 [12].

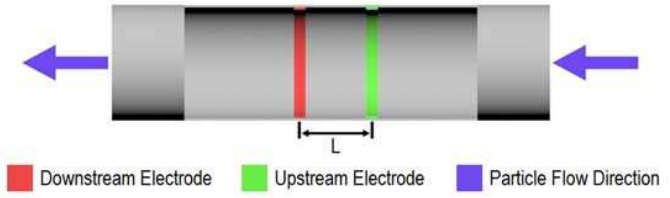

Fig. 1. Electrode configuration inside a pipe

As the particles travel past the electrodes their charge is detected by the electrodes. If both electrodes and signal conditioning circuits are identical the signal from the upstream electrode will be the same as the signal on the downstream electrode except the signal on the downstream will be time delayed. Since the distance between the upstream and downstream electrodes is known, particle velocity (V_c) can be calculated from.

$$V_c = \frac{L}{\tau_m} \quad (1)$$

Where L is the spacing between the upstream and downstream electrodes and τ_m is the time difference between the upstream and downstream signals. To determine τ_m the upstream and downstream signals have to be digitised using an ADC. It is at this point that resolution and sampling rate of the ADC has to be taken into account; the resolution has to be sufficiently high enough to ensure minute changes in the charge picked up from the electrodes can be detected. To determine τ_m the cross-correlation method is used. The delay between the two signals is determined from the location of the dominant peak in the cross correlation function [12].

Particle concentration is determined and represented by the magnitude of the r.m.s. (root-mean-square) charge level of the electrostatic signal detected by the electrostatic sensor. Conversely the exact particle concentration cannot be determined via this method due to variables such as particle size, type of particles and particle velocity [14].

III. Sensor Array Design

Like the probe electrode design the electrostatic sensor array is an intrusive sensor that comes into contact with the particle flow. However, unlike the probe sensor, the sensor array covers the whole diameter of the pipe and is divided into five pairs of identical electrodes as shown in Fig. 2. Due to the invasive nature of the sensor array design all attempts have been made to reduce the thickness of the sensor which is currently 2.5 mm thick. Each electrode has a width of 1mm and a length of 8 mm and these are set 10 mm apart. The sensor array is a blade design and only has electrodes on one side. The leading edge of the sensor array is a 45° knife edge intended to increase the aerodynamics of the sensor array. In addition, the 45° degree edge deflects most of the turbulence and velocity change caused by the sensor array behind the electrodes as illustrated in Fig. 3.

The preamplifier for the electrostatic sensors is constructed inside the sensor array blade to reduce the connection distance between the electrode and the preamplifier, subsequently reducing unwanted noise. The outer casing of the sensor array blade is fabricated from metal which is earthed to shield the preamplifier from unwanted noise. The physical size of the electronics for the preamplifiers was the determining factor of the number of electrodes that could be constructed across the diameter of the pipe. The signal from the preamplifier is then passed through a variable secondary amplifier and an anti-aliasing low pass filter to remove high frequency noise. Care was taken during the construction of the entire signal conditioning circuits to ensure each was matched to each other. An analogue multiplexer controlled from the microcontroller selects each element of the array. The analogue signal is digitised in an external 12-bit ADC with a sampling rate of 150 kHz. All analogue parts of the signal conditioning circuit are shielded against external noise. The cross correlation processing software is embedded into a 32 bit microcontroller which outputs to a PC as shown in Fig. 4.

IV. Experimental Setup

The sensor array is mounted inside a custom 50mm bore spool piece that allows the sensor array to be rotated around the cross sectional axes shown in Fig. 2. Experiments were carried out using flour in a dilute flow with a flow rate of 1.8 kg/hour on a negative pressure bulk solid conveying test rig (Fig. 5). Lack of established standards and traceability in the field of particle flow measurement is one of the challenges researchers have to face when developing techniques to resolve the difficult industrial measurement problems [12]. In the present study air velocity was determined as a reference by using a commercial hot wire anemometer with readings taken from the centre of the pipe at the same location of the sensor array. During the experiments, temperature (25.3°C average) and relative humidity (47.5% average) were monitored to ensure environmental test conditions were the same for each test. Experiments were carried out with the sensor array mounted on a horizontal pipe section with the array mounted in two orientations 0° and 90° as shown in Fig. 2. Tests were carried out with five different air velocities. For each pair of electrodes the cross correlation used 1024 samples on both the upstream and downstream electrodes. A total of 500 velocity readings were taken on each element of the array for each air velocity.

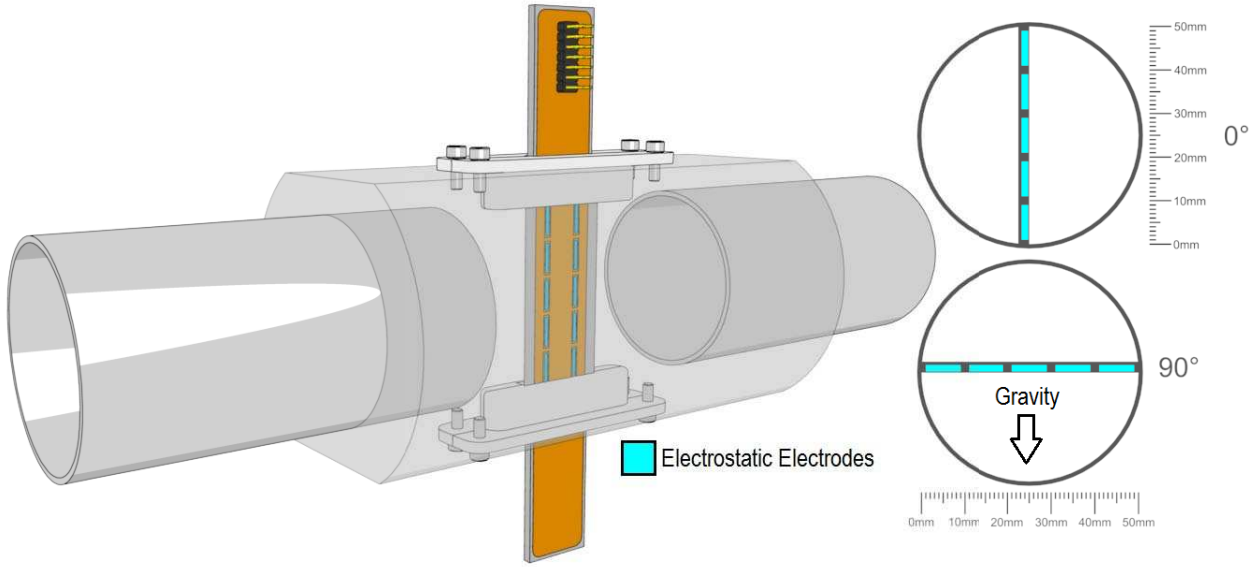

Fig. 2. Electrostatic array mounted inside a pipe spool with pipe cross section diagram

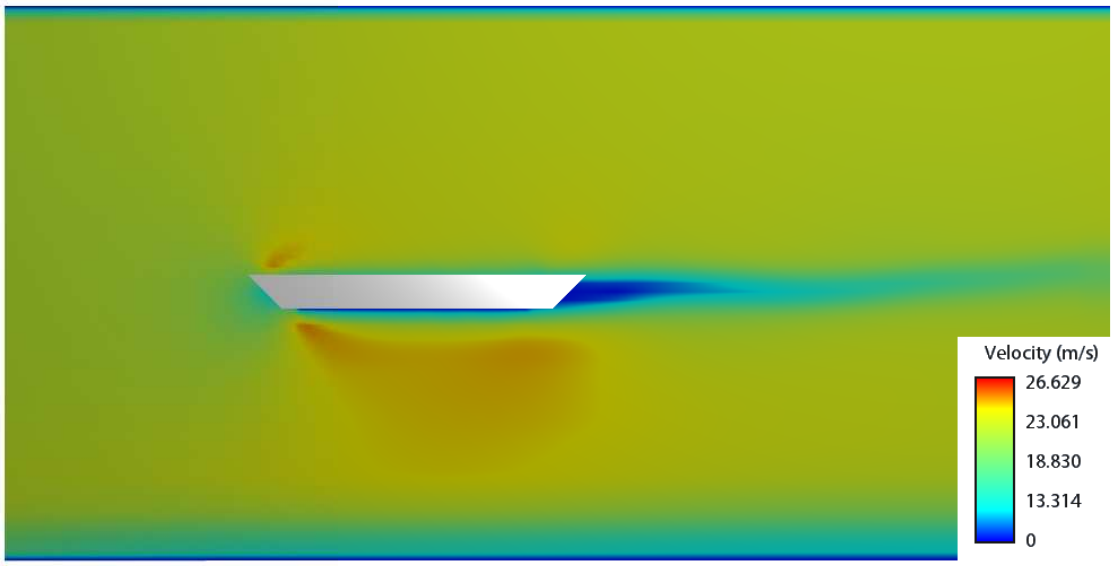

Fig. 3. Wind tunnel simulation of the effect of the sensor array's cross section on air velocity

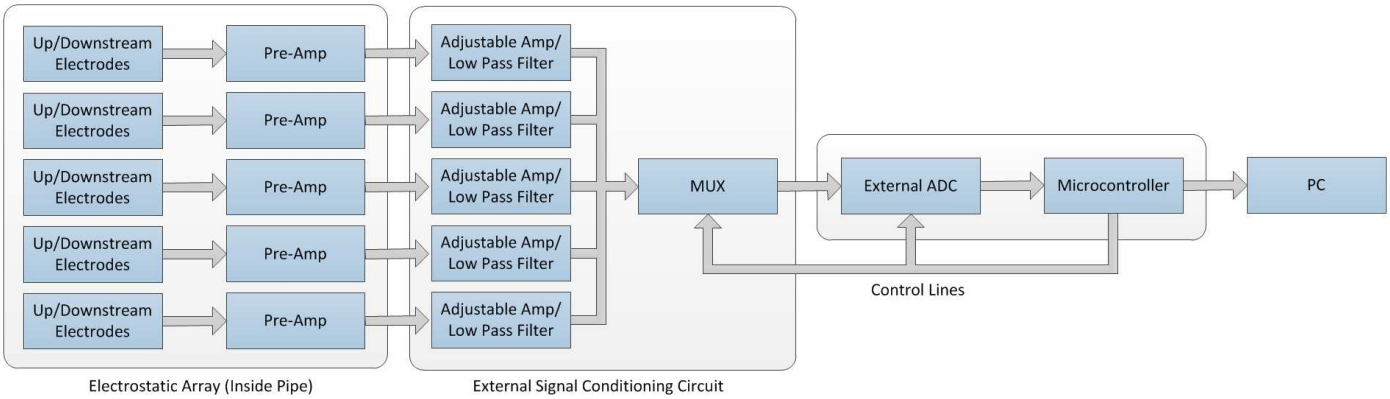

Fig. 4. Block diagram of the electrostatic array sensor based particle measurement system

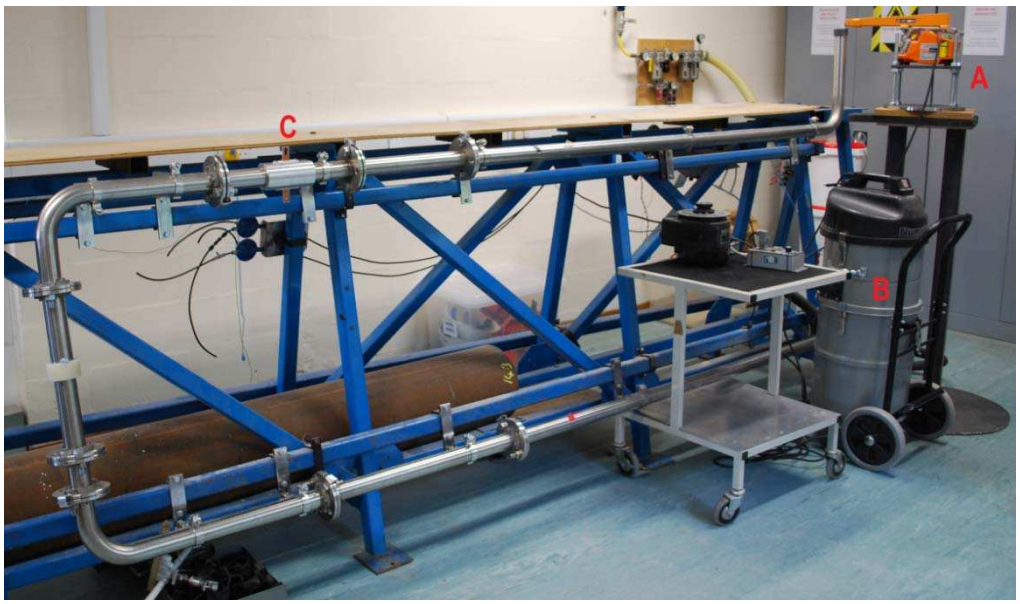

Fig. 5. Photo of the particle flow test rig, (A) vibration feeder, (B) vacuum plant, (C) array sensor spool on horizon

V. Results and Discussion

The sensor array was able to determine the particle velocity and particle concentration for the diameter of the pipe. Fig. 6 and Fig. 7 show the mean velocity profile for a range of air velocities (20.3-24.3 m/s). The profiles clearly show that particles traveling at the centre of the pipe are moving at a faster velocity then those moving along the pipe wall due to the friction of the particle interacting with the pipe wall. The 0° velocity profile in Fig. 6 shows that the velocity at the bottom of the pipe (5 mm) is slower than the velocity at the top of the pipe (45 mm); this is due to gravity's effect on the particles forcing them to come into contact with the pipe wall at the bottom of the pipe. Whereas Fig. 7 shows the velocity profile for 90° which is more symmetrical compared to 0° since gravity is having a uniform effect over the whole diameter. Fig. 8 illustrates particle velocity compared to the conveying air velocity at the centre of the pipe. As expected, the particle velocity is slower than the conveying air due to the drag force. Conversely, at lower air velocities the difference between the conveying air velocity and particle velocity is larger; this could be because the particles are not fully suspended in the conveying air at lower air velocities. The normalised velocity standard deviation profile shown in Fig. 9 and Fig. 10 shows that the particle velocities measured in the centre of the pipe have a lower deviation compared to those along the pipe wall indicating a more stable particle flow in the centre of the pipe.

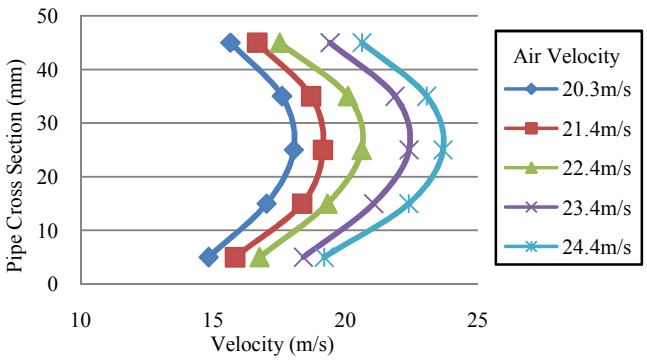

Fig. 6. Mean velocity profile measured by the electrostatic sensor array at 0° (data points indicate centre of the electrode)

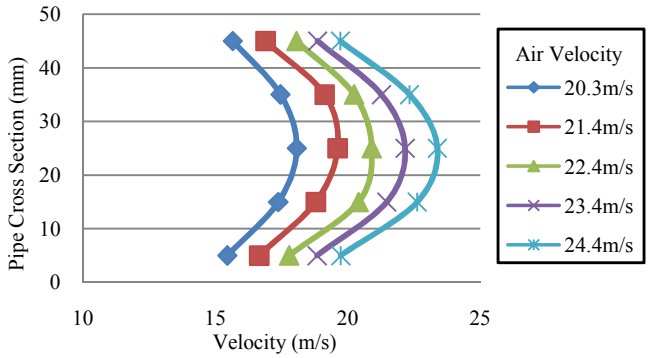

Fig. 7. Mean velocity profile measured by the electrostatic sensor array at 90°

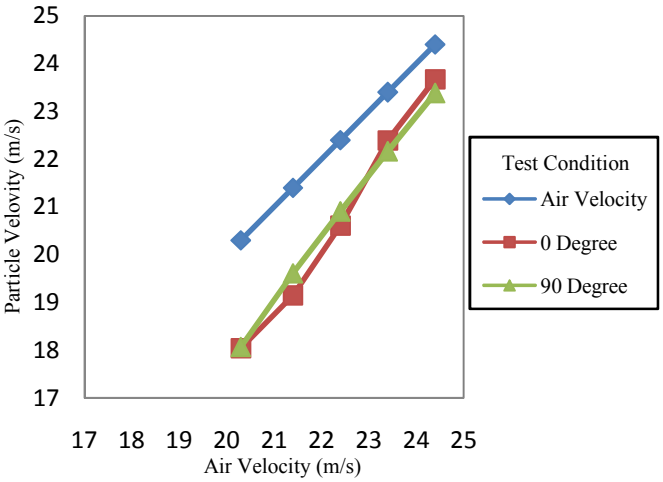

Fig. 8. Air velocity compared to particle velocity at the centre of the pipe

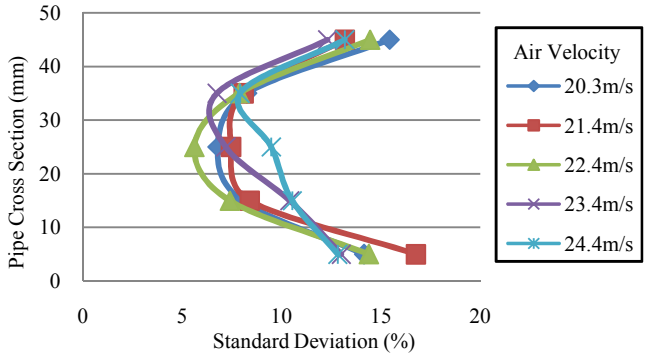

Fig. 9. Normalised standard deviation profile of the velocities measured by the electrostatic array sensor at 0°

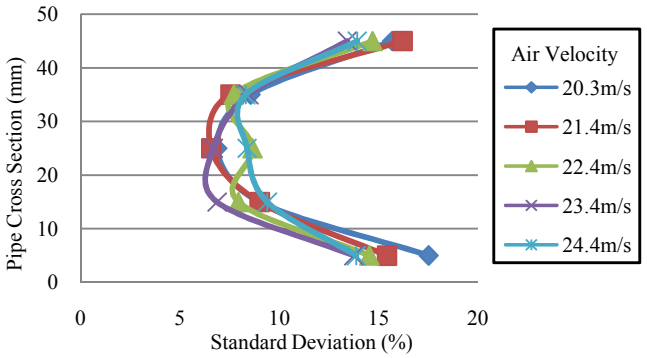

Fig. 10. Normalised standard deviation profile of the velocities measured by the electrostatic array sensor at 90°

The particle concentration shown in Fig. 11 shows that the concentration increases the closer to the bottom of the pipe due to the effect of gravity. However at the very bottom of the pipe (5 mm) the particle concentration is less; this is possibly due to the proximity of the electrode to the pipe wall caused by the pipe radius which would reduce the volume of space in the sensing area of the electrodes.

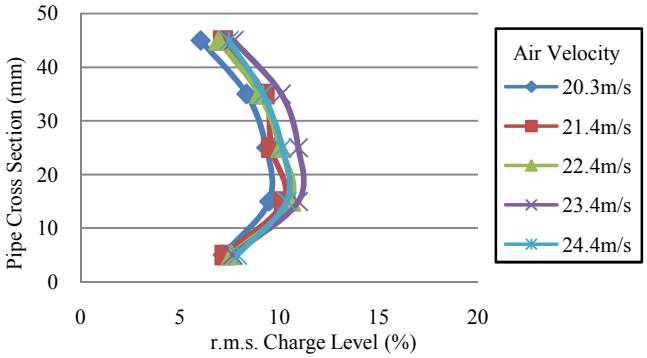

Fig. 11. Mean particle concentration profile using normalised r.m.s. charge value to measure particle concentration at 0°

The effect of reduced sensing area can be seen on the 90° particle concentration profile shown in Fig. 12, which shows that the concentration in the centre of the pipe is higher than along the pipe wall. Another possibility is that the particles that are coming into contact with the pipe wall are discharging due to the steel pipe being earthed. Fig. 12 also shows that for the higher air velocities (22.4-24.4m/s) the r.m.s charge is increasing in the centre of the pipe. This is feasibly due to the fact that at higher air velocities more particles are being suspended. Consequently more particles are able to be detected by the sensor array in the 90° orientation.

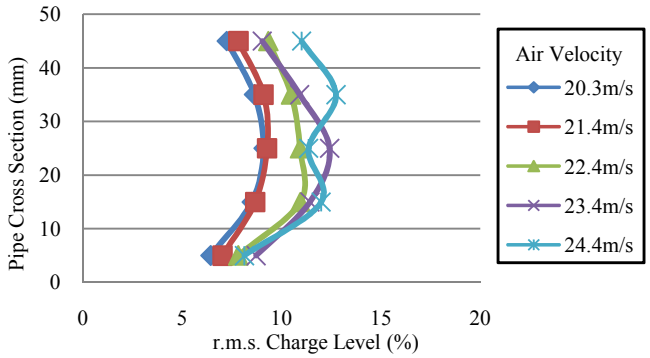

Fig. 12. Mean particle concentration profile using normalised r.m.s. charge value to measure particle concentration at 90°

The magnitude of the correlation coefficient is an indication of the stability of the particle flow [9] (the closer to 1 the correlation coefficient is, the more stable the flow). Fig. 13 and Fig. 14 show the correlation coefficient profiles (0° and 90° respectively).

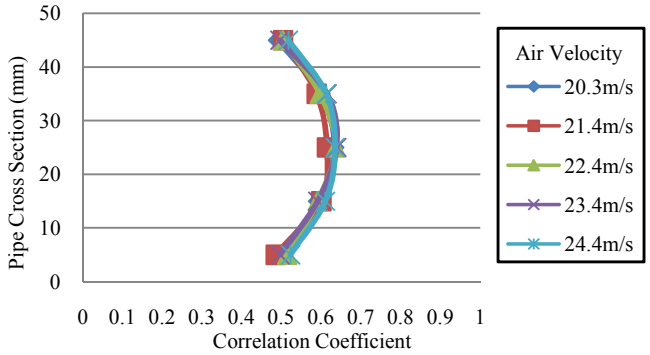

Fig. 13. Mean correlation coefficient profile for the pipe cross section at 0°

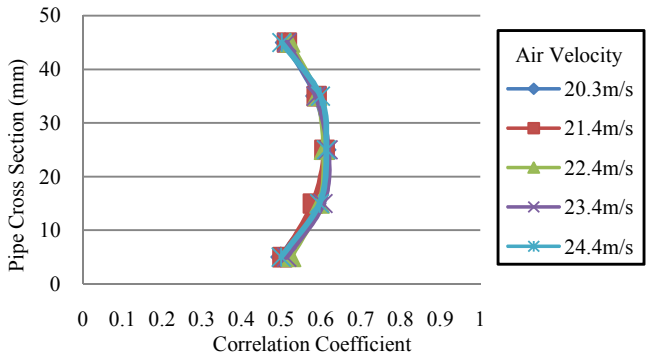

Fig. 14. Mean correlation coefficient profile for the pipe cross section at 90°

For the pipe cross section it is clear that the correlation coefficient is higher in the centre of the pipe compared to that along the pipe wall, demonstrating that the particle flow is more stable in the centre of the pipe which is consistent over all five air velocities.

VI. Conclusions

A new electrostatic sensor array has been designed, constructed and tested that is capable of monitoring the particle velocity and concentration profiles for the diameter of a pneumatic conveying pipe. The sensor array comprises of five independent electrostatic sensing elements across the whole diameter of the pipe.

Through analysis of the velocity profiles as well as correlation coefficients the performance of the electrostatic sensor array is in line with particle flow dynamics inside a pipe. With the particle flow in the centre of the pipe being more stable than the particle flow along the pipe wall

References

[1] A. Fuchs and H. Zangl, "Single-Layer Measurement of Particle Velocity and Concentration in Pneumatic Dilute Phase Conveying" IEEE Conference, Irvine CA, October 30-November 3 2005.

[2] X. X. Wang, J. B. Yan, H. L. Hu, Z. Y. Luo, "An ECT Flow Regime Identification Technology for Gas/Solid Two-Phase Flow Phase Concentration Measurement", Second International Conference on Instrumentation & Measurement, Computer, Communications and Control, Harbin China, 8-12 December 2012, pp. 1318-1321.

[3] I. R. Barratt, Y. Yan, B, Byrne and M.S.A. Bradley, "Mass flow measurement of pneumatically conveyed solids using radiometric sensors", Flow Measurement and Instrumentation 11, September 2000, pp. 223 - 235.

[4] D. Song, L. Peng, G. Lu, S. Yang, Y. Yan, "Velocity measurement of pneumatically conveyed particles through digital imaging", Sensors and Actuators A 149, pp. 180 – 188, 2009

[5] R. M. Carter, Y. Yan, P. Lee "On-line Nonintrusive Measurement of Particle Size Distribution through Digital Imaging", IEEE Transactions on Instrumentation and Measurement, Vol. 55, Issue 6, pp. 2034 – 2038, 2006

[6] L. Gao, Y. Yan, G. Lu, "Contour-based Image Segmentation for On-line Size Distribution Measurement of Pneumatically Conveyed Particles", Instrumentation and Measurement Technology Conference, Hangzhou China, May 10-12 2011, pp. 285-289.

[7] D. A. Abernethy, M.J. Millen and B.D. Sowerby "Plant Trial of an Ultrasonic Gauge for the On-Line Measurement of Pulverised Coal Mass Flow", IEEE Instrumentation and Measurement Technology Conference, Brussels, June 4 - 6 1996.

[8] J. Shao, J. Krabicka and Y. Yan, "Velocity Measurement of Pneumatically Conveyed Particles Using Intrusive Electrostatic Sensors", Instrumentation and Measurement, Vol. 59, Issue 5, pp. 1477 – 1484, 2010.

[9] X. Qian, Y. Yan, "Flow Measurement of Biomass and Blended Biomass Fuels in Pneumatic Conveying Pipelines Using Electrostatic Sensor-Array", IEEE Transactions on Instrumentation and Measurement, Vol. 61, Issue 5, pp. 1343 – 1352, 2012

[10] J. Krabicka and Y. Yan, "Finite Element Modelling of Electrostatic Sensors for the Flow Measurement of Particles in Pneumatic Pipelines", IEEE Transactions on Instrumentation and Measurement, Vol 58, Issue 8, pp 2730 – 2736, 2009.

[11] D. Mills, "Pneumatic Conveying Design Guide", Second edition, Butterworth-Heinemann Publications, Oxford, UK, ISBN 0 7506 5471 6, Page 584.

[12] Y. Yan, "Mass flow measurement of bulk solids in pneumatic pipelines", Measurement Science and Technology, Vol. 7, Issue 7, pp. 1687 – 1706, 1996.

[13] Y. Yan, B. Byrne, S. Woodhead and J. Coulthard, "Velocity Measurement of Pneumatic Conveyed Solids Using Electrodynamic Sensors", Measurement Science and Technology Vol. 6, pp. 515 – 537, 1995.

[14] Y. Yan, "Continuous Measurement of Particulate Emissions", IEEE Instrumentation & Measurement Magazine, pp. 35 – 39, October 2005.